Development of Homogeneous Manganese Catalysts for

Organic Transformations and Inorganic Polymerizations

by

Thu Thao Nguyen

A Dissertation Presented in Partial Fulfillment
of the Requirements for the Degree
Doctor of Philosophy

Approved October 2022 by the
Graduate Supervisory Committee:

Ryan J. Trovitch, Chair
Anne Katherine Jones
Laura K. G. Ackerman-Biegasiewicz

ARIZONA STATE UNIVERSITY

December 2022

ABSTRACT

The development of sustainable catalysts that exhibit exceptional activity has become a major goal of organometallic chemists. Considering their low cost and environmentally benign nature, the use of base metals in catalysis has recently been explored. This dissertation is focused on the development of manganese catalysts for organic transformations and inorganic polymerizations. Previous advances in Mn-based hydrosilylation and hydroboration catalysis are reviewed in Chapter 1 and set the stage for the experimental work described herein.

In Chapter 2, the electronic structure of $[(^{2,6-iPr_2Ph}BDI)Mn(\mu\text{-}H)]_2$ is explored. This compound was evaluated by density functional theory calculations, SQUID magnetometry and EPR spectroscopy at low temperature. Single crystal X-ray diffraction data was collected for related compounds that feature bridging X-type ligands. The data revealed how bridging ligands impact the Mayer bond order between the two Mn atoms and explained why $[(^{2,6-iPr_2Ph}BDI)Mn(\mu\text{-}H)]_2$ is an active catalyst for organic transformations.

Chapter 3 spotlights the first study to systematically demonstrate commercial aminosilane CVD precursor synthesis by way of SiH_4 and amine dehydrocoupling using $[(^{2,6-iPr_2Ph}BDI)Mn(\mu\text{-}H)]_2$. In addition, the study provided an efficient and halogen-free preparation of highly cross-linked polycarbosilazanes under ambient conditions. Furthermore, exceptionally pure perhydropolysilazane was directly prepared from ammonia and silane at room temperature through dehydrogenative coupling. These are also the first reported examples of Mn-catalyzed Si–N dehydrocoupling.

This research was then extended to the Mn-catalyzed dehydrogenative coupling of NH_3 and diamines to organic silanes. Organic polysilazanes and polycarbosilazanes were

synthesized and the structures were characterized by NMR, FT-IR, and MALDI-TOF spectroscopy. The thermal properties and coating applications of the products were evaluated by TGA, DSC, X-ray powder diffraction, SEM and EDX. A turnover frequency (TOF) experiment using 0.01 mol% of [($^{2,6-iPr_2Ph}$BDI)Mn(μ-H)]$_2$ revealed a maximum TOF of 300 s^{-1}, which is the highest activity ever reported for this transformation.

The last chapter highlights the first examples of nitrile dihydroboration mediated by a manganese catalyst. Using 0.5 mol% of [($^{2,6-iPr_2Ph}$BDI)Mn(μ-H)]$_2$, 14 nitriles were reduced with HBPin at 80 °C to afford *N,N*-diborylamines after 24 h. A mechanism was proposed based on the isolation of [($^{2,6-iPr_2Ph}$BDI)Mn(NCHPh)]$_2$ as an intermediate and further substantiated by DFT.

What you GET by achieving your goals is not as important as
what you BECOME by achieving your goals.

~Henry David Thoreau~

ACKNOWLEDGMENTS

First and foremost, I want to express my unconditional gratefulness to my advisor Prof. Ryan J. Trovitch. While anyone would consider a research advisor a boss and a mentor, my lab mates and I have grown to love and respect him as much more. All throughout my four years, there have been countless times, despite his busy schedule, that Dr. Trovitch has welcomed questions, ideas, and discussions from my group and I whether it be related to a current project or our daily difficulties. His knowledge and passion for research motivates me to work to the best of my abilities. I am personally thankful for his kindness, understanding, and support. I would not have made it through my studies without him.

I would like to thank Prof. Anne Katherine Jones and Prof. Laura K. G. Ackerman-Biegasiewicz for serving on my dissertation committee on top of their demanding schedules. They have remained supportive and considerate throughout my doctoral research and have provided insightful discussions regarding my projects.

There is a list of talented and enthusiastic scientists who have made significant contributions to my research. I would like to thank all the collaborators who contributed to my projects and helped me tell insightful stories in each publication. I am grateful to Dr. Thomas L. Groy for the single crystal X-ray data collection. I especially thank Dr. Marco Flores for his input on EPR experiments and simulations, along with his willingness to learn and run the XRD facility after Dr. Thomas retired. I have truly enjoyed working with him and listening to his stories. I would like to thank Dr. Brian Cherry, who helped our group when we faced any problems using instruments at the NMR facility. I would also like to thank Prof. Mu-Hyun Baik (KAIST) and his talented students for the computational

iv

input to my research. I appreciate the supportive collaboration of Tam Nguyen from Dr. Seo's group, who contributed to the solid-state characterization of my polycarbosilazanes. This thesis would not have been completed without the expertise of E-Jay Christopher who resurrected this document after my laptop crashed.

Four years may seem like a long time, but it passed by much faster than I could ever imagine. I am thankful for my time spent in the Trovitch group because I was able to meet so many precious colleagues. I would like to acknowledge my first labmate, Matthew. He is a great graduate student and an even better friend. I want to especially acknowledge Anuja, my best labmate and friend. Her positive energy recharges me, her kindness and her great moral support gives me the strength to overcome many daily life problems. I would also like to thank other members of the Trovitch team including Brock, Elizabeth, Veronica, Riley, Yichen and Michael. Each member of the group is very friendly and cooperative, which helps me open-up and makes the lab my second home. I will cherish all the up and down moments and the precious experiences that I have gained here forever.

Last but not least, I would like to dedicate this thesis to my family – my dear mother and sisters. My mother has filled the place of both a mother and a father, she devoted her entire life to raise us. Her presence has shaped me through every stage in my life to who I am today. Her unconditional love and support are what motivates me to strive for success. Although we are million miles apart, just thinking about my family keeps my heart at peace. I want to spend the last sentences to thank my soulmate and husband, Nguyen. He is the best listener and the most reliable partner, with whom I can truly be myself. Thanks to him, I have a mini me, my little Celine. This precious, energetic girl lightens up our day with just a smile and completes my day with a tight hug.

TABLE OF CONTENTS

LIST OF TABLES

LIST OF FIGURES

LIST OF SCHEMES

CHAPTER 1

INTRODUCTION

1.1. Overview

The utilization of manganese catalysts for hydrofunctionalization reactions has grown at a rapid pace in recent years. Early efforts to develop manganese catalysts for carbonyl hydrosilylation have been followed up with considerable improvements in activity and substrate reduction scope. Efficient manganese catalysts for carbonyl, formate, ester, and alkene hydrosilylation have been discovered. Furthermore, recent reports have demonstrated deoxygenative amide reduction, carbon dioxide reduction, and even the formation of silicones that are traditionally prepared using platinum catalysts. Manganese catalysts have also been shown to catalyze asymmetric ketone hydrosilylation and hydroboration with excellent enantioselectivity. A considerable amount of mechanistic information has been gathered throughout these contributions, which will undoubtedly guide the development of next generation manganese catalysts.

1.2. Inspiration

Hydrofunctionalization, which involves H—X bond addition across an unsaturated carbon-carbon or carbon-heteroatom bond, unlocks possibilities for atom-economical synthesis. Metal catalysts play a crucial role in this transformation in terms of achieving regio-, stereo-, and enantioselectivity. This chapter covers two important manganese catalyzed hydrofunctionalization reactions, hydrosilylation and hydroboration, parts of which have been covered in recent reviews.[1–4]

Hydrosilylation, the addition of a Si—H bond across an unsaturated bond, has attracted widespread interest for its industrial and laboratory-scale applications. The hydrosilylation of olefins to prepare silicones still relies on catalysts derived from platinum. Speier first reported using $[H_2PtCl_6] \cdot H_2O$ to mediate alkene hydrosilylation with high selectivity in 1957,[5] and a significant advance was made by Karstedt in 1973, who developed a soluble platinum(0) catalyst that exhibits desirable activity and selectivity for olefin hydrosilylation (Figure 1.1, a).[6] The hydrosilylation of carbonyl containing compounds has become a popular way to prepare alcohols on a small scale. In 1972, Ojima's group first reported that Wilkinson's rhodium(I) catalyst (Figure 1.2, b) mediates carbonyl hydrosilylation under mild conditions to give silyl ethers in high yield.[7]
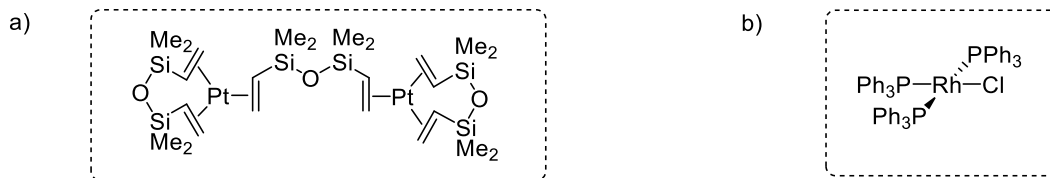
Figure 1.1. Karstedt's and Wilkinson's catalysts.

Hydroboration, the process of adding a B—H bond across a carbon-heteroatom double or triple bond, also provides useful reagents for organic synthesis. Herbert C. Brown

was recognized with a Nobel Prize in Chemistry for the synthesis of organoboranes, and he also discovered a convenient route to prepare alcohols following direct alkene hydroboration.[8] This method involved the use of pyrophoric boranes such as BH_3 and B_2H_6; therefore, metal catalyzed routes that use milder boranes have been targeted. In 1975, Kono and co-workers found that Wilkinson's catalyst oxidatively adds catecholborane,[9] and a decade later, Männig and Nöth reported the first metal-catalyzed alkene hydroboration using Wilkinson's catalyst under mild conditions (0.05 mol% cat., 20 °C, 25 min).[10] Interestingly, the Rh-catalyzed hydroboration of 5-hexene-2-one using catecholborane resulted in selective C=C bond hydroboration (Scheme 1.1).
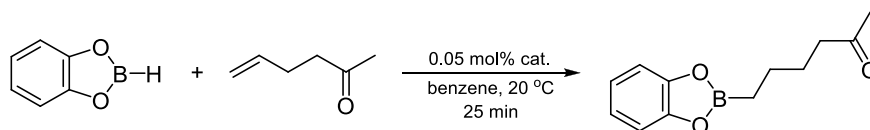
Scheme 1.1. Selective alkene hydroboration catalyzed by Wilkinson's catalyst.

Although precious metal catalysts exhibit distinctive reactivity and stability, the evaluation of non-toxic, environmentally benign, and economical alternatives that feature base metals is critical for sustainable catalyst development. Manganese is a promising alternative to precious metals in hydrofunctionalization catalysis due to its low cost, Earth-abundance, and lack of toxicity. Considering that its common oxidation states vary from 0 to +7, manganese has immense potential to generate useful catalysts. In particular, this chapter highlights the recent development of manganese-based hydrosilylation and hydroboration catalysts. In addition to catalytic activity, mechanistic insight is discussed.

1.3. Background Literature

1.3.1. Hydrosilylation

Hydrosilylation of Carbonyls and Carboxylates

The first manganese-catalyzed hydrosilylation of a ketone was reported in 1982 by Yates under UV irradiation (Scheme 1.2); however, $Mn_2(CO)_{10}$ turned out to be a poor photocatalyst for acetone and 2-heptanone hydrosilylation, with just 5% yield of silyl ether product obtained after acetone photolysis (Scheme 1.2).[11]
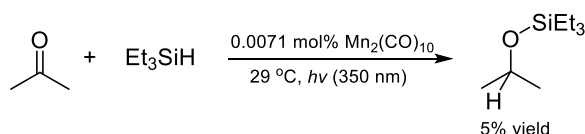
Scheme 1.2. Hydrosilylation of acetone catalyzed by $Mn_2(CO)_{10}$.

In the 1990's, the Cutler group made significant advances in the use of manganese-acyl complexes for the hydrosilylation of C=O bonds, including the ketones and esters of organoiron carbonyl complexes. In 1991, they evaluated the hydrosilylation of FpC(O)R compounds [R = CH_3, Ph; Fp = $Fe(CO)_2(\eta^5\text{-}C_5H_5)$] with mono-, di-, and trihydrosilanes to yield the corresponding Fp(α-siloxyalkyl) complexes. Eighteen examples were demonstrated using a series of manganese complexes including $Mn_2(CO)_{10}$, $(CO)_5MnR$ (R = CH_3, $SiMe_3$, and CHPh(OSiHR'$_2$), and $L(CO)_4MnC(O)R$ as the precatalysts [L = CO, R = CH_3, Ph; L = PPh_3, PEt_3, R = CH_3] (Scheme 1.3, a).[12] All of these catalysts were effective for the hydrosilylation of FpC(O)CH_3 with near complete conversion observed, and the hydrosilylation of FpC(O)Ph with Ph_2SiH_2 was achieved using 2.4 mol% of $(Ph_3P)(CO)_4MnC(O)CH_3$ to afford FpCH(Ph)OSiHPh$_2$ after 0.5 hours.

This method was extended to the hydrosilylation of the methoxycarbonyl complex, FpC(O)OCH$_3$, with PhSiH$_3$ or Ph$_2$SiH$_2$ in the presence of 2-3 mol%

4

$(Ph_3P)(CO)_4MnC(O)CH_3$ (**1**) to afford $(\eta^4\text{-}C_5H_6)Fe(CO)_3$, which features an η^4-cyclopentadiene ligand. The silane moiety was determined to be a mixture of unreacted $PhSiH_3$ and methoxysilanes (Scheme 1.3, b). Note that a longer reaction time was required when using Ph_2SiH_2 (3 h compared to 20 minutes when using $PhSiH_3$).[13] Interestingly, the acyl manganese catalysts were able to mediate deoxygenative iron acyl hydrosilylation to afford the corresponding alkyl compounds (Scheme 1.3, c).[14]
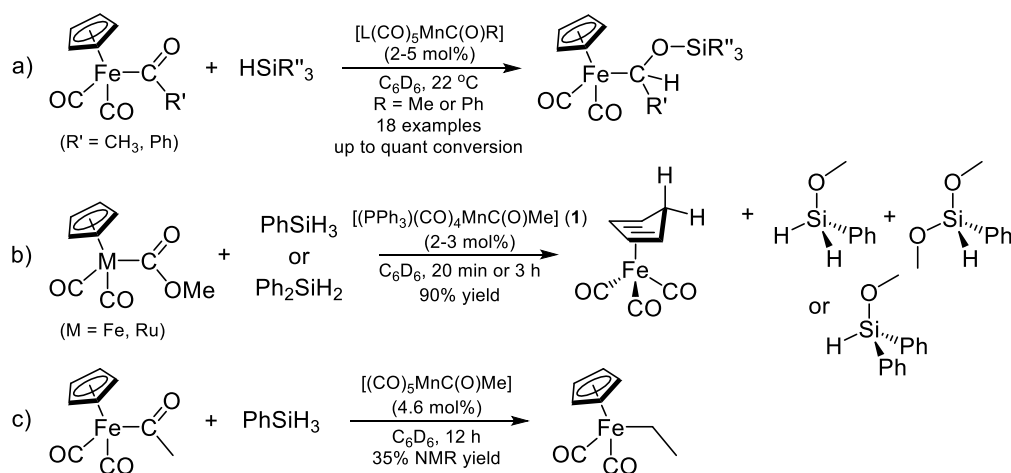
Scheme 1.3. Hydrosilylation of organoiron complexes mediated by $L(CO)_4MnC(O)R$.

The manganese acetyl complexes were also utilized for the hydrosilylation of organic ketones and esters. The activity of **1** for the hydrosilylation of acetone with $PhMe_2SiH$ was much higher than what was achieved using $(PPh_3)_3RhCl$, with turnover frequencies (TOFs) of 27.2 ± 5.0 min^{-1} (Scheme 1.4, a).[15] The hydrosilylation of other ketones including acetophenone, cyclohexanone, and 2-cyclohexene-1-one was also evaluated with $PhMe_2SiH$ and Ph_2SiH_2 using 2.4 mol% of **1**, which resulted in up to >95% NMR yield after 4 minutes. The proposed mechanism for ketone hydrosilylation (Scheme 1.4, b) begins with the generation of active catalyst **2** from manganese acyl complex **1** *via* σ-bond metathesis with phenylsilane. Next, alkyl complex **4** forms following C=O bond

5

coordination and insertion into the Mn—Si bond. Catalysis continued with Si—H oxidative addition and reductive elimination of the silyl ether product to regenerate **2**.
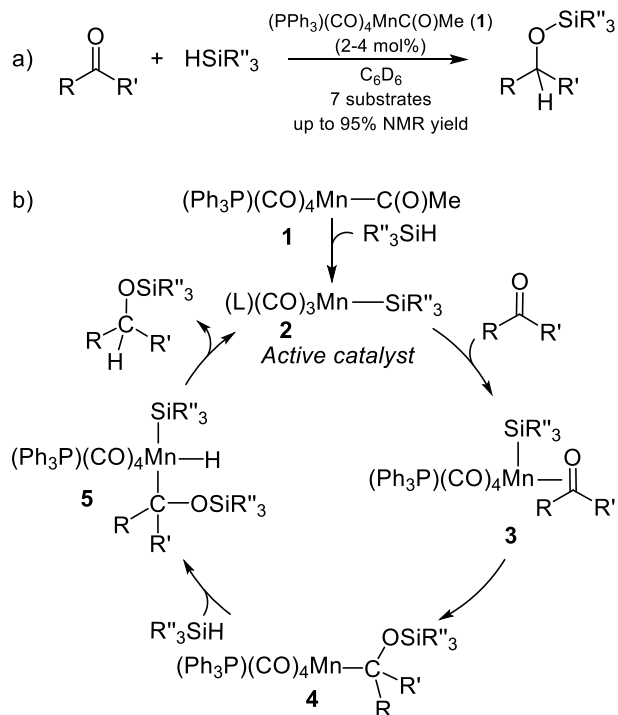
Scheme 1.4. Hydrosilylation of ketones catalyzed by **1**. b) Mechanism of hydrosilylation catalyzed by **1**.

A large scope of 13 ester substrates was also evaluated for hydrosilylation to yield ether or alkoxysilane products (Scheme 1.5, a).[16] Deoxygenation was proposed to proceed through two successive hydrosilylation events that are catalyzed by manganese (Scheme 1.5, b). In particular, the hydrosilylation process was similar to that of ketone hydrosilylation, but the silyl ether product is reduced by intermediate **6** to afford the corresponding ether and siloxane.
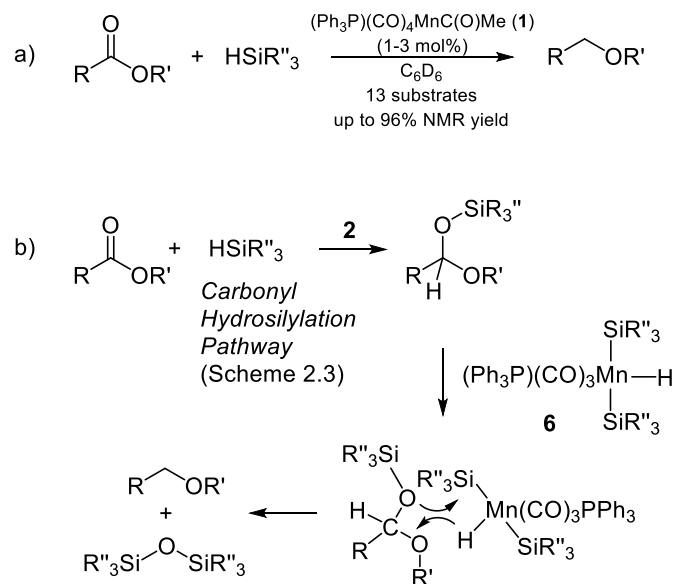
Scheme 1.5. a) Ester hydrosilylation catalyzed by **1**. b) Mechanism of ester hydrosilylation mediated by active catalyst **2**.

In 1999, Chung's group found that the naphthalene derived manganese complexes, $(\eta^5\text{-}C_{10}H_9)Mn(CO)_3$ (**7**) and $[(\eta^6\text{-}C_{10}H_8)Mn(CO)_3][BF_4]$ (**8**), catalyze ketone hydrosilylation to give alcohols with high yields following hydrolysis.[17] In both cases, facile ring slippage was believed to play a vital role in the catalytic activity of the catalysts (Scheme 1.6, left). A scope of 10 substrates was evaluated for ketone hydrosilylation using 5 mol% of **7** under ambient temperature to give up to 99% NMR yield after 3 hours. Substitution patterns were found to significantly affect the conversion of aryl ketones. In fact, no transformation was observed for acetophenones containing electron-withdrawing cyano and nitro groups, while 4-methoxyacetophenone reached 28% yield after 7 hours due to competing methoxy group coordination. The η^6-coordinated cation was found to be more reactive for ketone hydrosilylation than the neutral η^5-coordinated complex (Scheme 1.6).[17,18]

7
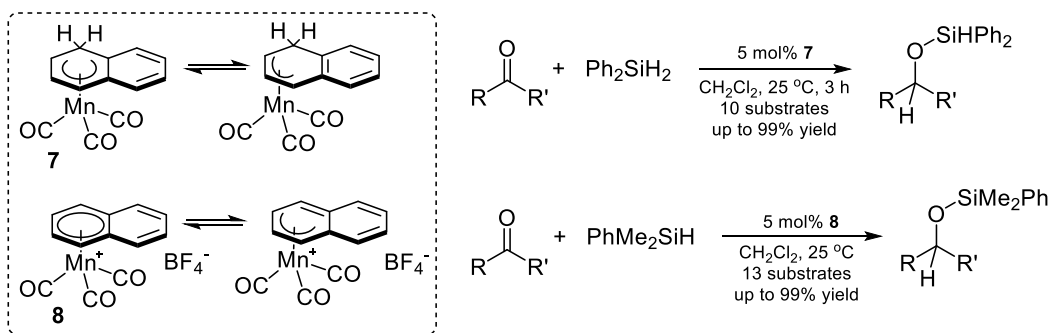
Scheme 1.6. Ring slippage and ketone hydrosilylation catalyzed by **7** and **8**.
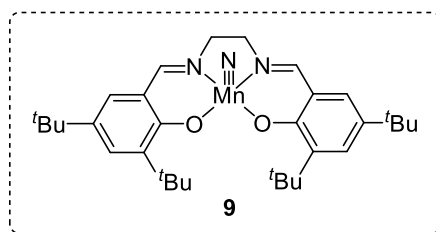
Figure 1.2. Structure of catalyst **9**.

In 2013, Du and co-workers developed an air-stable manganese catalyst featuring a salen ligand framework.[19] Their catalyst, (salen-3,5-^{t}Bu$_2$)MnN (**9**, Figure 1.2), was able to mediate the hydrosilylation of aldehydes and ketones with impressive activity (maximum TOF of 11,760 h^{-1}) at 80 °C. The hydrosilylation of 14 aliphatic and aromatic carbonyl substrates with phenylsilane was evaluated using 0.5 mol% of **9** (Scheme 1.7, a). This catalyst was found to exhibit good functional group tolerance, yielding a diverse set of primary and secondary alcohols following hydrolysis. Most aldehyde substrates were completely reduced after 20 minutes, while more time was required for ketones (up to 3 hours). However, substitution did have a significant impact on the hydrosilylation of aryl carbonyl compounds. In particular, the electron-withdrawing nitro group of *p*-nitrobenzylaldehyde accelerated the hydrosilylation compared to benzaldehydes featuring electron-donating substituents such as *p*-OCH$_3$ or *p*-Cl. Nitro substitution was unfavorable

for ketone hydrosilylation; complete reduction was not achieved for *p*-nitroacetophenone even after 2 days. In addition, ring-opened products were not observed during the reduction of cyclic ketones. Notably, 1,3-diphenylpropan-1-one was obtained for the hydrosilylation of chalcone (an α,β-unsaturated ketone), which was believed to go through a silyl enol ether intermediate. The proposed mechanism involves the reduction of catalyst **9** with silane to form a manganese(III) hydride that participates in carbonyl insertion to generate the desired silyl ether product (Scheme 1.7, b).
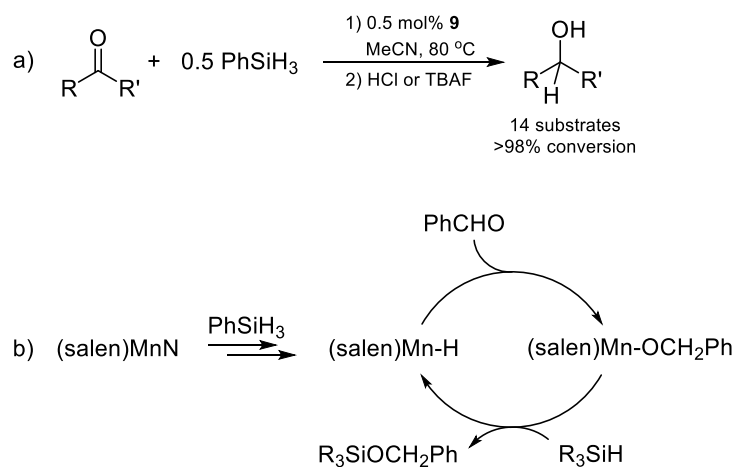
Scheme 1.7. a) Carbonyl hydrosilylation catalyzed by **9**. b) Proposed mechanism for **9**-catalyzed carbonyl hydrosilylation.

With an interest in preparing renewable materials to replace plastic, recent studies from Du, Sibi, and co-workers demonstrated that **9** can enable the polymerization of diols, dicarbonyls, and cellulosic furans to prepare poly(silylether)s (PSEs) following dehydrogenative coupling and carbonyl hydrosilylation.[20,21] Note that PSEs are promising alternative materials since their Si-O-C linkages can be easily degraded through hydrolysis. Using hydrosilanes to produce PSEs can overcome the disadvantages of using chlorosilanes, including air and moisture sensitivity and the formation of byproducts such as HCl. Several diols and dicarbonyl compounds including bio renewable furans such as
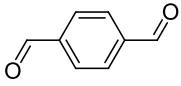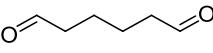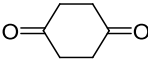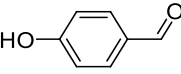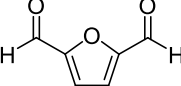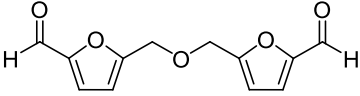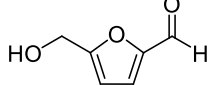
2,5-diformylfuran (DFF), 5,5′-[oxybis(methylene)]di(2-furaldehyde) (OBMF), 5-(hydroxymethyl)furfural (HMF), and 2,5-bishydroxymethylfuran (BHMF) were evaluated for manganese-catalyzed polymerization.

The reaction conditions were optimized to use toluene as the solvent, refluxing temperature (110 °C), and a catalyst loading of 1 mol% **9**. Polymerization of dialdehydes (terephthalaldehyde, 1,6-hexanedial) with Ph_2SiH_2 took 24 hours to reach 90% conversion, while 1,4-cyclohexandione took up to 48 hours. However, the isolated yield and molecular weight of the corresponding polymers were lower than those prepared from the dehydrogenative coupling of diols and silanes (yield = 40-58%, M_n = 1800-2400, Table 1.1). This result was explained by the stronger nucleophilic properties of hydroxyls than carbonyls in the reaction with silanes. Silyl ether polymers with varying connectivity were observed when using *p*-hydroxybenzaldehyde, which possesses both alcohol and aldehyde functional groups. This protocol was extended to the hydrosilylation of DFF, OBMF, and HMF under the same catalytic conditions (Scheme 1.8), and the corresponding high molar-weight PSE polymers were collected after 40 hours in modest yield (Table 1.1). The mechanism of **9**-catalyzed polymer formation was proposed to start with the reduction of **9** by Ph_2SiH_2 to form a low-valent complex [either Mn(II) or Mn(III)]. Then Si-H coordination to the metal center in an η^1- or η^2-fashion affords a silane complex that undergoes nucleophilic attack by a carbonyl group to form an Si─O bond.
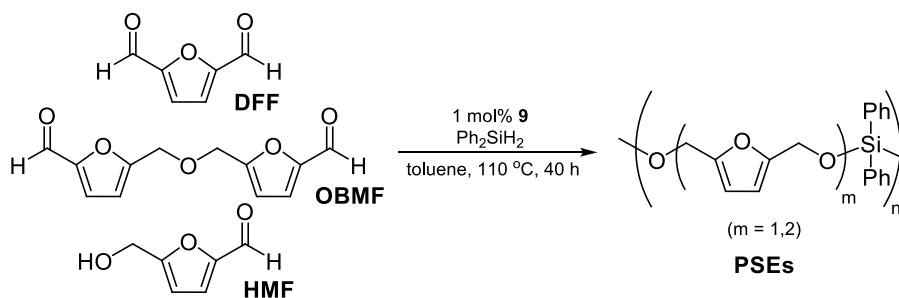
Scheme 1.8. PSE preparation by way of carbonyl hydrosilylation catalyzed by **9**.

Table 1.1. Polymerization of carbonyl compounds with Ph_2SiH_2.

Substrate	t (h)	M_n (g/mol)	Yield (%)
	24	2400	58
	24	1800	40
	48	2100	49
	18	3800	69
	40	5500	76
	40	6400	78
	40	8000	74

The groups of Darcel and Sortais reported the selective reduction of carboxylic acids with Et_3SiH under UV irradiation followed by acidic hydrolysis to yield aldehydes using $Mn_2(CO)_{10}$ (Scheme 1.9).[22] The catalytic conditions were optimized (5 mol% catalyst, 3.3 eq. of Et_3SiH, toluene or Et_2O, UV irradiation at 350 nm, 25 °C), and

conversion was determined after 3 hours. In particular, the electronic properties and positions of aryl substituents had a considerable effect on the catalytic activity. Most *para*-substituted phenylacetic acids including *p*-alkyl, *p*-halide, and *p*-methoxy variants underwent reduction in good to excellent yield (>97% conversion observed). The amine group of *p*-aminophenylacetic acid did not inhibit hydrosilylation, affording the corresponding amino aldehyde in good isolated yield (85%). Extra considerations were required for some substrates. For example, 5 equivalents of silane were required for 4-hydroxyphenylacetic acid due to silylation of the hydroxyl group, while halide substituted substrates took up to 24 hours to reach up to 91% conversion. However, nitrobenzene was believed to form an adduct with $Mn_2(CO)_{10}$ under catalytic conditions; therefore, it did not undergo hydrosilylation. Both *meta*- and *ortho*-methyl substitution was found to hinder hydrosilylation (89% and 61% conversion, respectively). Notably, carboxylic acids featuring heteroaryl groups were also reduced successfully. In the case of saturated aliphatic substrates, the long chain did not influence the reduction of palmitic and tetradecanoic acids and the C=C bond in oleic acid was retained following reduction. The terminal double bond in hept-6-enoic acid was observed to participate in the hydrosilylation, which resulted in mixture of products. Finally, formic acid and acetic acid were hydrosilylated in good yield, while trifluoroacetic acid was not successfully reduced.
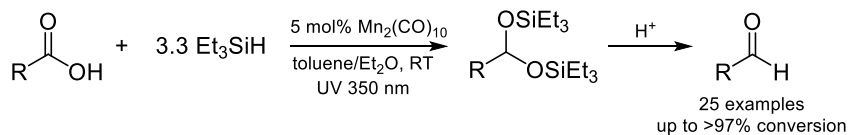
Scheme 1.9. Carboxylic acid hydrosilylation mediated by $Mn_2(CO)_{10}$.

In subsequent papers, several half-sandwich Mn(I) complexes featuring an *N*-heterocyclic carbene (NHC) ligand were synthesized and evaluated for photocatalyzed carbonyl hydrosilylation (Scheme 1.10, a).[23,24] Among six $Cp(CO)_2Mn(NHC)$ derivatives, $Cp(CO)_2Mn(IMes)$ (**10**) was found to exhibit the highest photocatalytic activity for carbonyl hydrosilylation (maximum TON of 960).[24] Aldehyde hydrosilylation was carried out under mild conditions (25 °C in toluene) for 13 substrates in the presence of 1 mol% **10** under 350 nm irradiation (Scheme 1.10, b).[23] Good to excellent conversion was observed for most substrates including aliphatic, aromatic, and heterocyclic aldehydes after 1 hour and the corresponding primary alcohols were collected following hydrolysis with NaOH (2 M) solution and extraction into MeOH. The electronic properties of the *para*-substituent did not affect the transformation of aromatic aldehydes. However, *m*-fluoro substitution was found to reduce the catalytic activity, requiring 8 hours to reach 92% conversion. Importantly, **10** selectively catalyzed the hydrosilylation of alkenyl and alkynyl substrates with >97% conversion, without reduction or polymerization of the unsaturated C—C bonds. In the case of ketone hydrosilylation, a scope of 13 substrates was effectively reduced under identical catalytic conditions. Many aliphatic and substituted aromatic ketones were hydrosilylated within 4 hours; however, less active ketones such as *o*-methylacetophenone, acetylferrocene, dialkyl, and cyclic substrates required up to 24 hours to be fully converted. Chloro- and bromo-substituents contributed to the decomposition of **10** under UV irradiation, hence, no conversion was observed for these substrates.
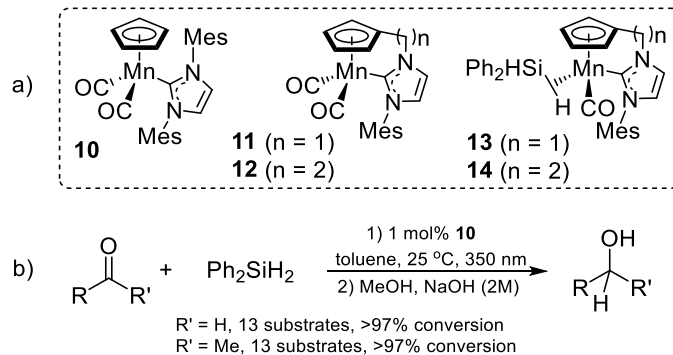
Scheme 1.10. a) Structures of **10-14**. b) Carbonyl hydrosilylation mediated by **10**.

The synthesis of piano-stool Mn(I) complexes, (Cp(CH₂)ₙNHCMes)Mn(CO)₂ (**11, 12**; n = 1, 2; Scheme 1.10, a), was then reported and their hydrosilylation activity was compared to **10** by hydrosilylating 2-acetonaphthone with Ph_2SiH_2.[24] Under identical conditions, **11** and **12** exhibited less activity with just 56% and 66% NMR yield observed in the presence of 1 mol% catalyst, respectively. However, the synthesis and characterization of these complexes gave access to the monocarbonyl η^2-silane intermediates, (Cp(CH₂)ₙNHC^{Mes})Mn(CO)(η^2-H−SiHPh₂) (**13, 14**; n = 1, 2; Scheme 1.10, a), suggesting that the catalytic mechanism is consistent with traditional Ojima ketone hydrosilylation.[25]

In 2018, Royo's group reported the development of a manganese complex featuring a bis-NHC ligand, (bis-NHC^{Me})Mn(CO)₃Br (**15**), which is not only air-stable but is also an effective catalyst for ketone hydrosilylation.[26] Compound **16**, which was prepared by treating **15** with AgBF₄, was also found to be stable in air (Scheme 1.11, a). To compare the catalytic activity of these complexes, 14 ketones were separately evaluated for hydrosilylation using phenylsilane in the presence of either **15** or **16** at elevated temperature under air (Scheme 1.11, b). In particular, aromatic substrates were effectively reduced except for *p*-iodobenzaldehyde, which afforded the dehalogenated product 1-

phenylethanol. Aliphatic ketones, including alkyl, alkenyl, and cyclic substrates also underwent hydrosilylation and *trans*-4-phenyl-3-buten-2-one was selectively reduced without reduction or polymerization of the C=C bond. The silyl ether products were collected following hydrolysis with NaOH (2 M) solution and extraction with dichloromethane to afford the corresponding secondary alcohol in good yield. It was determined that **16** is more active than **15** since the former hydrosilylated all substrates within 5 hours, whereas more time was required using **15** under identical conditions. In fact, the maximum TON observed using 0.1 mol% **16** for the hydrosilylation of acetophenone and phenylsilane was 1000 (TOFs of up to 320 h^{-1}). Surprisingly, when polymethylhydrosiloxane (PMHS) was employed as the silane source instead of $PhSiH_3$, **15** was found to be significantly more effective. Therefore, ketone hydrosilylation using PMHS was evaluated for a large scope of aliphatic and aromatic ketones under identical conditions. Except for substrates featuring iodo substitution, hydrosilylation occurred in 56-91% NMR yield after 8 hours.

For $PhSiH_3$, 14 substrates, up to 99% NMR yield
For PMHS, 14 substrates, up to 91% NMR yield
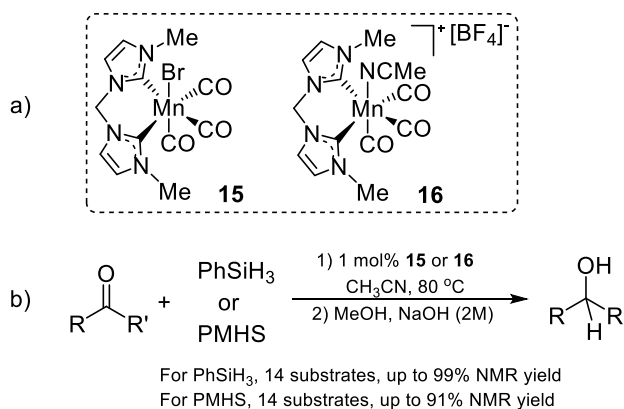
Scheme 1.11. a) Structures of **15** and **16**. b) Carbonyl hydrosilylation mediated by **15** or **16**.

The same group recently employed **15** to achieve the hydrosilylation of esters to yield alcohols.[27] A scope of 14 esters featuring a variety of functional groups was screened for hydrosilylation in the presence of PhSiH$_3$. Excellent conversions and yields were observed; however, significant limitations were found in the hydrosilylation of benzoates featuring NO$_2$, NH$_2$, and CN groups. Notably, this study presented the first examples of Mn-catalyzed ester hydrosilylation that utilize cheap and readily available PMHS as the silane source. In the presence of this reagent, **15** was found to catalyze methyl and ethyl ester hydrosilylation to yield the corresponding high molecular weight alcohol in moderate to excellent yields, except the case of NO$_2$- and NH$_2$- functionalized benzoates.

Very recently, Bagh and co-workers described a Mn(I) catalyst for ester hydrosilylation under neat conditions at 100 °C.[28] Loadings of *fac*-[Mn-(xantphos)(CO)$_3$Br] as low as 1 mol% were used for the hydrosilylation of 17 different esters to yield the corresponding alcohols in up to 97% isolated yield after basic workup. The substrate scope was expanded to include popular industrial alcohols; 11 fatty acid esters were hydrosilylated under neat conditions to generate the desired alcohols (up to 97% isolated yield).

Since 2014, our group has been working to develop manganese hydrosilylation catalysts featuring pyridine diimine (PDI) and pyridine bis(eneamide) (PDEA) ligands (Scheme 1.12, **17**-**20**). Hydrosilylation has not only been evaluated for ketones,[29–31] but has also been extended to a considerable substrate scope of esters,[29] aldehydes,[30–32] and formates[31,32] under mild conditions with low catalyst loadings (Scheme 1.12). Note that (^{Ph_2PPr}PDI)Mn (**17**),[29] (^{PyEt}PDEA)Mn (**19**),[30] and [(^{Ph_2PEt}PDI)Mn]$_2$ (**20**)[31] show extraordinary reactivity for aldehyde hydrosilylation with respective TOFs of up to 4,900 min^{-1}, 2,475

min^{-1}, and 4,950 min^{-1}. Notably, catalysts **17** and **20** were the leading transition metal catalysts for carbonyl hydrosilylation under ambient conditions when published. Although the hydride complex (^{Ph_2PPr}PDI)MnH (**18**)[32] is slightly less active for aldehyde and ketone hydrosilylation, it turned out to be highly effective for formate dihydrosilylation with a maximum observed TOF of 330 min^{-1}. This activity is orders of magnitude higher than what had been reported for carboxylate dihydrosilylation catalysts prior to 2017.

The mechanism of **17**-catalyzed carbonyl hydrosilylation was proposed to follow the modified Ojima mechanism shown in Scheme 1.13.[32] The catalytic process begins with phosphine dissociation and the reversible oxidative addition of a Si─H bond to generate **21**. Next, carbonyl substrates reversibly coordinate to the metal center to afford intermediate **22** and then insert into the Mn─H bond to generate **23**. Insertion was believed to be the rate determining step (RDS) due to kinetic studies. For carbonyl ketone hydrosilylation, **23** undergoes fast reductive elimination to release the desired hydrosilylated product and regenerate catalyst **17**. In the case of di- and trihydrosilanes, the remaining Si─H bonds can participate in hydrosilylation to form doubly- and triply-condensed products. Regarding formate and ester dihydrosilylation, **23** undergoes fast β-alkoxide elimination to form **24**, followed by reductive elimination of silyl ether and loss of aldehyde to regenerate **17**. Interestingly, the redox non-innocent ^{Ph_2PPr}PDI ligand stabilizes the intermediates, allowing Mn(II) to remain throughout the catalytic process.
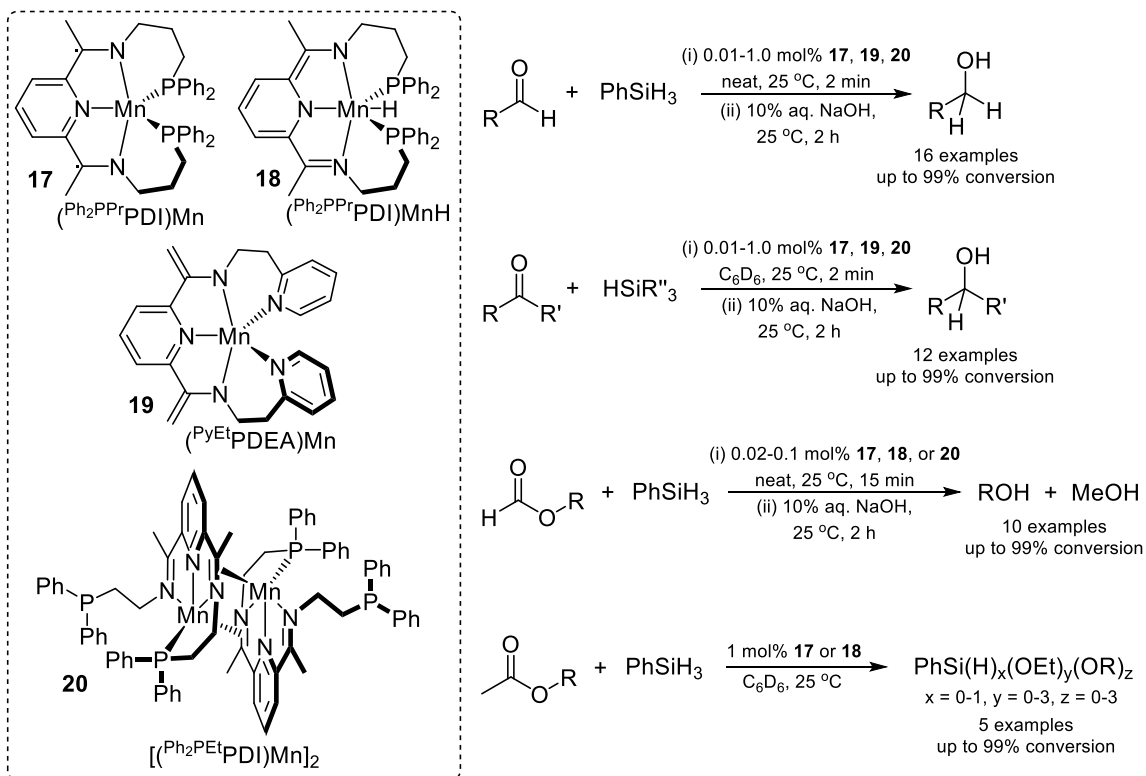
Scheme 1.12. Structures of **17**-**20**, carbonyl hydrosilylation and carboxylate dihydrosilylation catalyzed by **17**-**20**.
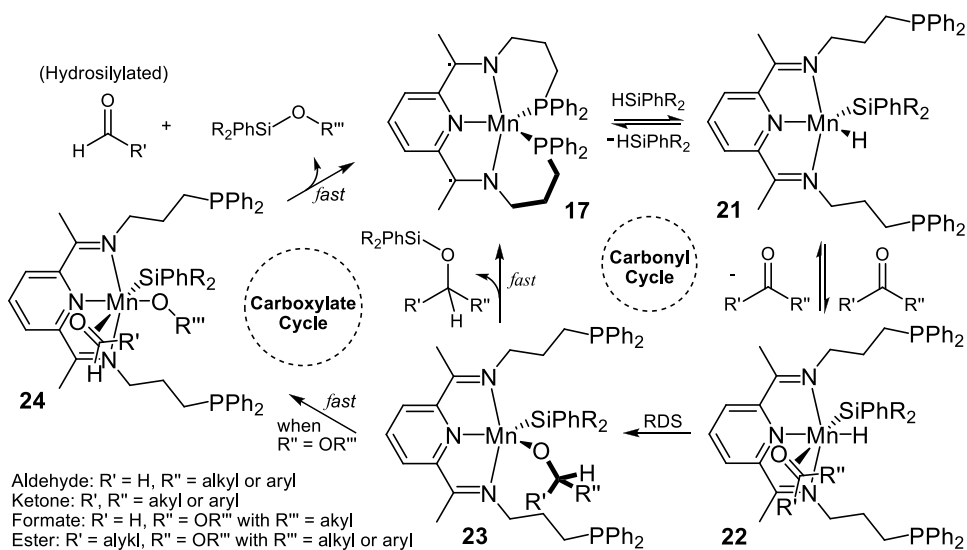
Scheme 1.13. Modified Ojima mechanism for aldehyde, ketone, formate, and ester hydrosilylation catalyzed by **17**.

Although **18** showed lower activity than **17** for carbonyl hydrosilylation, its activity for carboxylate dihydrosilylation was higher, and the proposed mechanism for **18**-catalyzed transformations is shown in Scheme 1.14.[32] For carbonyl hydrosilylation, coordination of the substrate C=O bond to Mn is followed by insertion to form **26**. The RDS was proposed to be the σ-bond metathesis reaction between **26** and silane to release the hydrosilylated product and regenerate catalyst **18**. In the case of carboxylate dihydrosilylation, **26** undergoes fast β-alkoxide elimination to afford **28**. Then σ-bond metathesis between the Mn─O bond of **28** and Si─H yields the silyl ether product, aldehyde, and **18**. Note that the aldehyde released in both mechanisms (Scheme 1.13 and 1.14) was believed to be hydrosilylated during the catalytic reaction to form the corresponding silyl ether.

Aldehyde: R' = H, R" = alkyl or aryl
Ketone: R', R" = akyl or aryl
Formate: R' = H, R" = OR''' with R''' = akyl
Ester: R' = alykl, R" = OR''' with R''' = alkyl or aryl
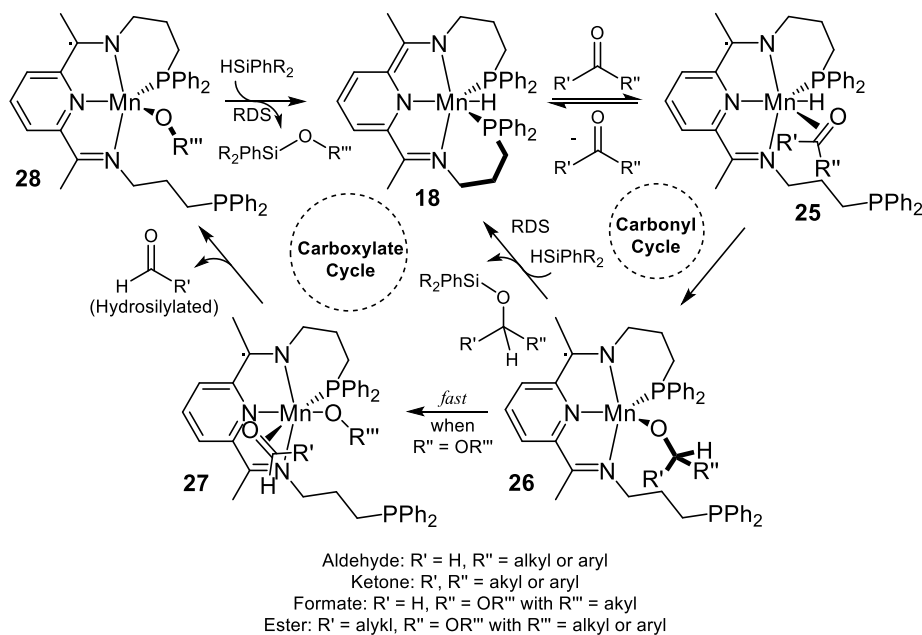
Scheme 1.14. Mechanism for aldehyde, ketone, formate, and ester hydrosilylation catalyzed by **18**.

In 2017, Huang's group synthesized of a series of Mn(II) complexes featuring chiral iminopyridine oxazoline (IPO) ligands that were found to mediate the asymmetric hydrosilylation of aryl ketones (**29**-**32**, Scheme 1.14, a, left).[33] Interestingly, the catalyst possessing the bulkiest IPO ligand (**32**) was found to exhibit the highest activity for ketone hydrosilylation. Catalysis required the use of NaBHEt$_3$ as an activating reagent and the reactions were conducted with 0.1 M ketone since concentration was found to significantly influence the rate of hydrosilylation (Scheme 1.15, a). A broad scope of aromatic ketones was selectively hydrosilylated to obtain secondary alcohols in excellent yield and enantioselectivity following hydrolysis of the corresponding silyl ethers. Substrate substitution patterns had a considerable influence on the conversion and enantioselectivity of the transformation. For example, acetophenones featuring *o*-chloro or *o*-methoxy groups required heating to 60 °C for selective conversion. *m*-Methoxyacetophenone underwent hydrosilylation with higher enantioselectivity than *p*-methoxyacetophenone, while different positions of chloro substitution did not affect the results.

In 2017, Gade and co-workers developed manganese catalysts bearing [2,5-bis(2-oxazolinyldimethylmethyl)pyrrole] pincer ligands (PdmBOX).[34] In comparison to iron and cobalt sources; the addition of ligand **33** and **34** to Mn(CH$_2$TMS)$_2$ allowed for efficient acetophenone hydrosilylation using (Et$_2$O)$_2$SiMeH. Greater than 95% conversion was observed for both catalysts; however, the products were obtained with only modest enantioselectivity [(*ee* = 9% (*R*) and 50% (*R*), respectively] (Scheme 1.15, b).
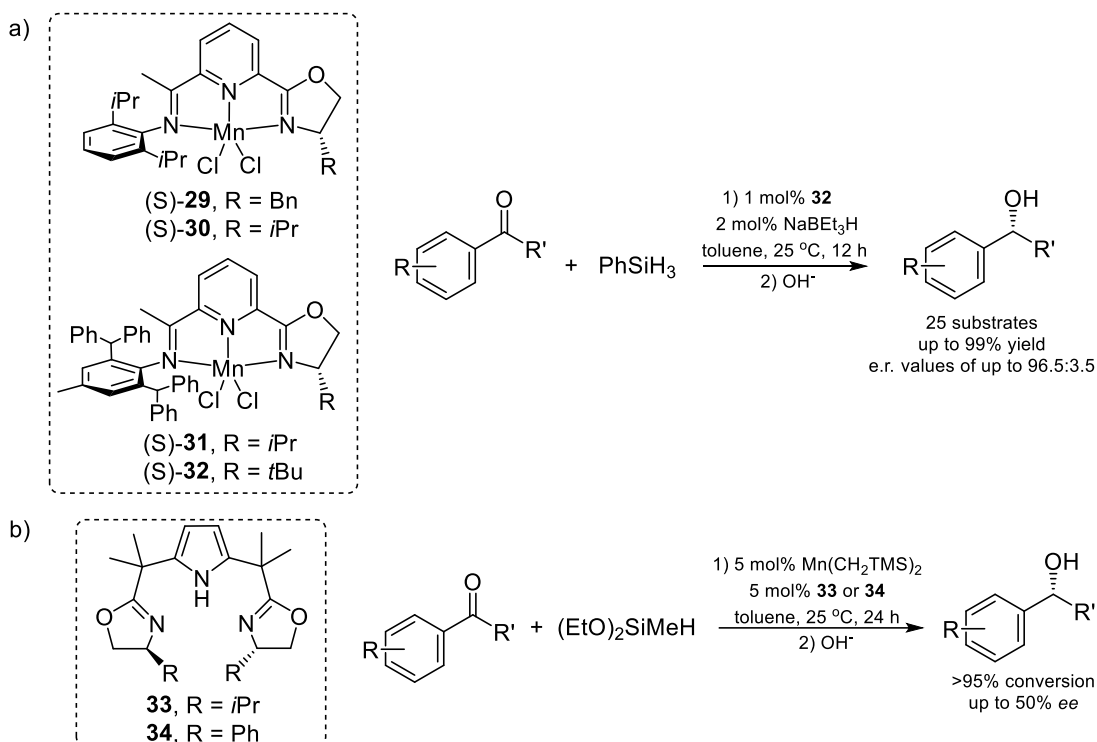
Scheme 1.15. Asymmetric ketone hydrosilylation mediated by manganese catalysts.

The Werlé and Leitner groups recently found that Mn(I) complexes bearing triazole ligands[35] are active for the hydrosilylation of carbonyl and carboxyl groups. Of the evaluated catalysts, **35** and **36** exhibited the best performance (Scheme 1.16).[36] In particular, 19 ketones were screened for hydrosilylation catalyzed by 0.25–1 mol% **35** at 80 °C (Scheme 1.16, a). Moderate to high yield was observed for most substrates, with the notable exceptions of 2-acetylanisole and 2-acetylfuran. Interestingly, cationic complex **36** exhibited activity for carbonyl hydrosilylation and the hydrosilylative reduction of carboxyl groups. Using 2 mol% **36**, a variety of esters underwent hydrosilylation with phenyl silane, and hydrolysis yielded the corresponding alcohols and ethers (Scheme 1.16, b). Notably, **36** represents the first manganese catalyst capable of hydrosilylating

carboxylic acids to generate alcohols (Scheme 1.16, c). The independent reaction of **36** with PhSiH$_3$ supported the formation of a catalytically relevant hydride species.
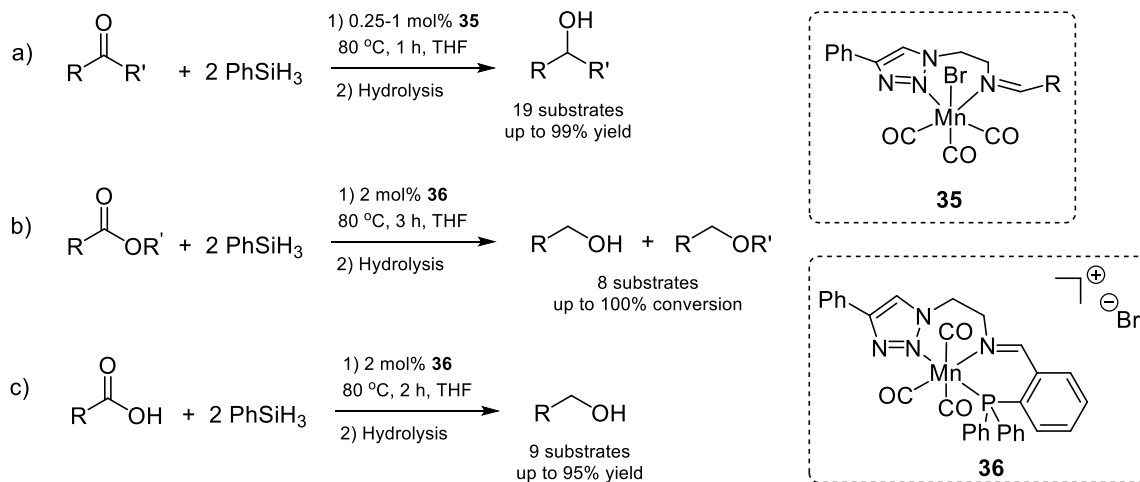
Scheme 1.16. a) Ketone hydrosilylation mediated by **35**. b) Ester hydrosilylation mediated by **36**. c) Carboxylic acid hydrosilylation mediated by **36**.

Solid-phase Mn catalysts have recently been shown to mediate carbonyl hydrosilylation. Copéret and co-workers described silica-supported Mn(II) sites for the reduction of carbonyl compounds and transesterification.[37] Their catalysts, Mn$_2$[OSi(O^{t}Bu)$_3$]$_4$@SiO$_{2-400}$ and Mn{N(SiMe$_3$)$_2$}$_2$·THF@SiO$_{2-400}$, were well-defined and the latter was found to effectively mediate benzaldehyde hydrosilylation using either PhSiH$_3$ (>99% NMR yield after 10 min) or triethoxysilane (97% NMR yield after 1 h) under mild conditions (0.5 mol% cat., 25 °C). Very recently, the groups of Zhang and Zheng described the synthesis of an air-stable 1-D Mn(II) coordination polymer featuring a 4′-pyridyl-2,2′;6′,2″-terpyridine (pytpy) ligand, which is an effective pre-catalyst for hydrofunctionalization reactions including hydroboration and hydrosilylation.[38] Using KO^{t}Bu as an activator and PhSiH$_3$, 10 aldehydes and ketones were successfully reduced

and worked up to yield the corresponding alcohols (complete carbonyl reduction was noted and isolated yields of up to 95% were achieved).

Hydrosilylation of Amides

So far, relatively few examples of manganese-catalyzed amide reduction have been reported. In 2001, the reduction of amides with hydrosilanes using a number of transition-metal complexes was reported by Fuchikami's group.[39] In the presence of $Mn_2(CO)_{10}$ and Et_2NH, *N*-acetylpiperidine was reduced to *N*-ethylpiperidine in good yield (Scheme 1.17, a). In 2012, Pannell and co-workers reported the photocatalytic activity of $CpMn(CO)_3$ for the reduction of DMF and *N,N*-diethylformamide under UV irradiation (Scheme 1.18, b). They also found this catalyst to be active for the same reactions at 120 °C.[40]
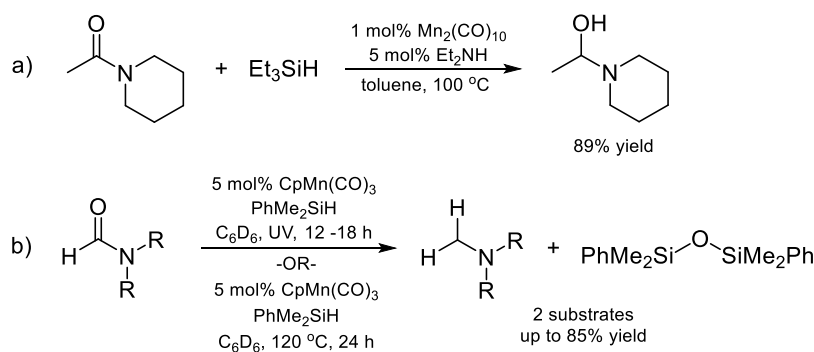
Scheme 1.17. Amide hydrosilylation catalyzed by manganese catalysts.

In 2017, Sydora, Stradiotto, Turculet and co-workers developed a Mn pre-catalyst $[(\kappa^2\text{-P,N})Mn(N(SiMe_3)_2)]$ that deoxygenates tertiary amides to give the corresponding amines in the presence of silane reductant (Figure 1.3).[41] A large scope of aliphatic and aromatic tertiary amides was reduced with phenylsilane under mild conditions (Scheme 1.18, a). Using 5 mol% **37** and heating to 75 °C allowed amide hydrosilylation to reach completion after 1 hour. The reduction of substituted benzyl amides, as well as sterically bulky tertiary dibenzyl amides containing (hetero)benzyl and even *N*-benzylpiperidine

23

functionalities were effectively deoxygenated with >90% conversion observed. Aliphatic substrates were also reduced to tertiary alkyl amines; however, lower catalyst loadings and temperature (2 mol% **37**, 25 °C) reduced the rate of the reaction (18 hours needed for completion). In addition, this catalyst was found to mediate the reduction of aldehydes, ketones (Scheme 1.18, b), and esters (Scheme 1.18, c) using phenylsilane under mild conditions (1 mol% **37**, benzene, 25 °C).
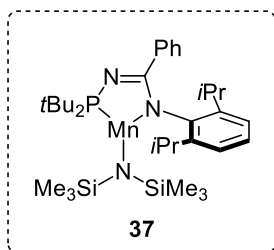
Figure 1.3. Structure of **37**.
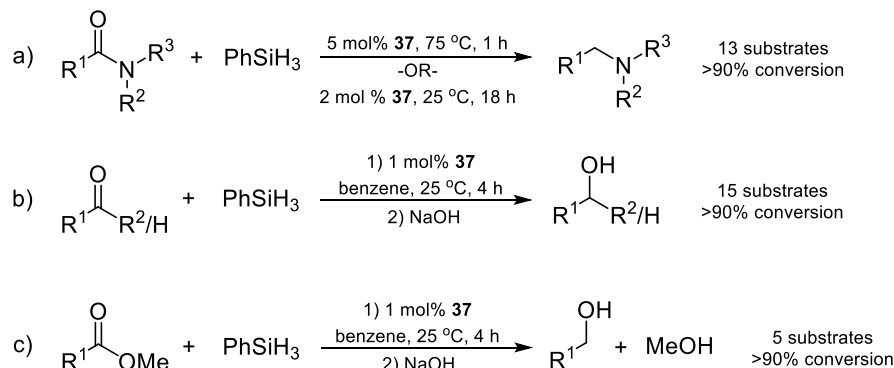
Scheme 1.18. Hydrosilylation of a) amides, b) ketones/aldehydes, and c) esters using **37**.

Acetophenones and benzaldehydes featuring electron-donating and -withdrawing groups underwent hydrosilylation (>90% conversion observed after 4 hours, Scheme 1.18, b) and afforded the corresponding alcohols. Saturated and unsaturated aliphatic ketones were also selectively hydrosilylated under the catalytic conditions. A maximum TON of 400 and TOFs of up to 200 min^{-1} were achieved upon evaluating the reduction of 4-

heptanone at low catalyst loading (0.25 mol%). The hydrosilylation of esters using **37** was assessed under the same conditions as carbonyl hydrosilylation. Methyl benzoates featuring varied substitution and methyl heptanoate were successfully reduced to obtain the corresponding primary alcohols and MeOH upon hydrolysis.
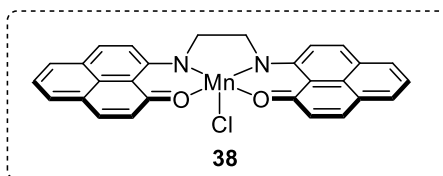
Figure 1.4. Structure of **38**.

Mandal's group recently reported a Mn(III) complex featuring a phenalenyl ligand (**38**, Figure 1.4) that converts primary amides to either amines or nitriles following hydrosilylation (Scheme 1.19, a).[42] In the presence of KO^{t}Bu and PhSiH$_3$ at 50 °C, 5 mol% of **38** enabled the hydrosilylation of aryl, hetero-aryl, and aliphatic amides to yield primary amines as their hydrochloride salts in moderate to excellent yield (61-95%). In particular, benzylamides with varied substitution were reduced and worked up to afford benzylamine salts in moderate to excellent yield (64-95%), while aromatic amides with hetero rings such as 3-pyridine-carboxamide and 2-thiophenecarboxamide underwent the transformation in moderate yield (61-63%). Aliphatic amides were successfully converted to the corresponding aliphatic amine salts in good yield. In addition, the protocol was extended to yield nitriles under identical conditions in the presence of 20 mol% of *N*-methylbenzamide as the inhibitor to prevent the nitrile from further reduction. A scope of 16 substrates with various aryl and aliphatic amides were assessed for deoxygenation under these conditions (Scheme 1.19, b). Benzylamides were converted to the corresponding nitriles in good to excellent yield (74-96%), as were heteroaryl and aliphatic substrates.

Interestingly, selective reduction of the primary amides in 4-cyanobenzamide and *N*-(4-carbamoylphenyl)benzamide afforded the corresponding nitrile products, with the existing nitrile or secondary amide groups retained.
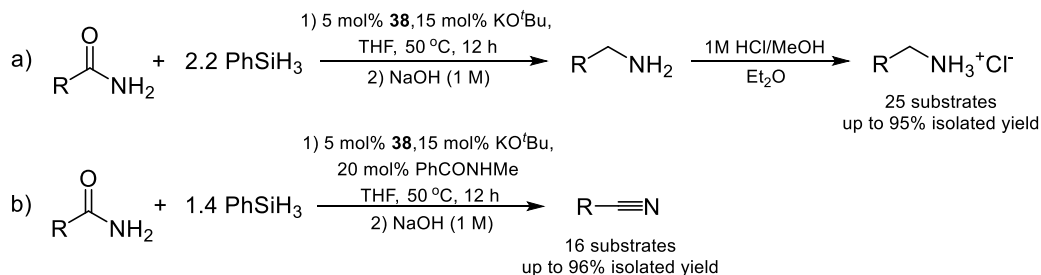
Scheme 1.19. a) Amide hydrosilylation to amines catalyzed by **38**. b) Amide hydrosilylation to nitriles catalyzed by **38**.

Hydrosilylation of Carbon Dioxide

Carbon dioxide, an abundant greenhouse gas, is also a convenient C_1 source for small-scale synthetic chemistry. Recently, Gonsalvi, Kirchner, and co-workers reported that their Mn(I) PNP pincer complexes, $(PNP^{NR}-iPr)Mn(CO)_2H$ (**39**: R = H, **40**: R = Me; Figure 1.5), effectively enabled CO_2 hydrosilylation under mild conditions (1 bar CO_2) to form methoxysilyl products and MeOH upon simple hydrolysis.[43] Screening experiments indicated that **39** exhibits higher CO_2 hydrosilylation activity than catalyst **40**. The activity of **39** for CO_2 reduction was evaluated using $PhSiH_3$ (5 equiv. with respect to CO_2) and 2 mol% catalyst (with respect to Si−H) at 25 and 80 °C in DMSO-d_6 (Scheme 1.20), and product formation was monitored by NMR spectroscopy. Reactions at room temperature took up to 24 hours to reach the methoxysilyl product, while CO_2 hydrosilylation at elevated temperature afforded reduced products in high yield (89%) after just 1 hour. Note that the formation of methane was not observed in this work. Hydrosilylation using an excess amount of CO_2 (1:1 molar ratio vs. Si−H) was also conducted at 80 °C. Complete

reduction of CO_2 to the methoxysilyl product was observed after 24 hours without the presence of any byproducts. A maximum TON of 100 was achieved by lowering the catalyst loading to 1 mol% under identical conditions.
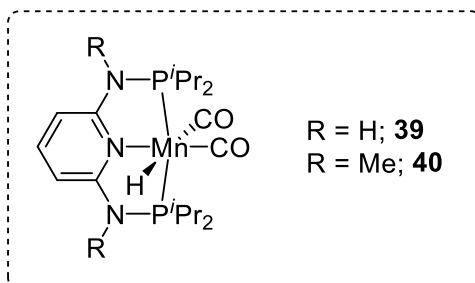
Figure 1.5. Structure of **39**, **40**.

The mechanism for **39**-catalyzed CO_2 hydrosilylation was proposed based on NMR experiments, DFT calculations, and the isolation of key intermediates (Scheme 1.20, b). The first step involves the insertion of CO_2 into the Mn─H bond to generate intermediate **41**. Next, σ-bond metathesis between **41** and an incoming Si─H bond yields **39** and silylformate, which undergoes insertion to afford **42**. Subsequent σ-bond metathesis between another Si─H equivalent and the pendant C─O bond yields intermediate **43** and liberates siloxane. The final step also involves σ-bond metathesis between Si─H and Mn─O to regenerate **39** and afford the methoxyphenylsilane.
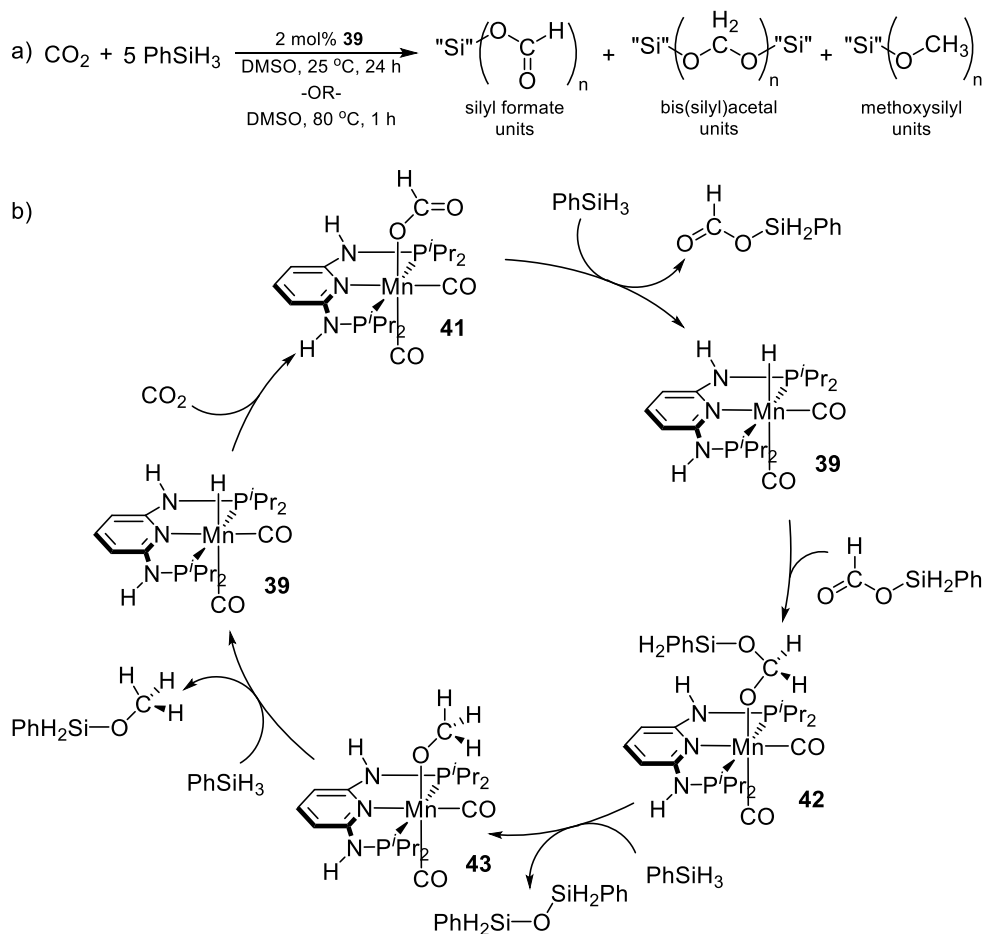
Scheme 1.20. a) Hydrosilylation of CO_2 catalyzed by **39**. b) Proposed mechanism for **39**-catalyzed CO_2 hydrosilylation.

Hydrosilylation of C=C and C≡C bonds

In comparison with carbonyl hydrosilylation, the development of manganese catalysts for alkene and alkyne hydrosilylation has remained under investigated. The chemo selectivity of C=C and C≡C multiple bond hydrosilylation is readily complicated by side reactions such as isomerization, hydrogenation, dehydrogenative silylation as well as dihydrosilylation. Given the lower polarity of C=C and C≡C bonds compared to C=O bonds, only a few examples of manganese-based alkene and alkyne hydrosilylation have been reported.

28

Olefin Hydrosilylation

In 1983, an early investigation by Faltynek utilized the triphenylsilyl complex, $(CO)_5MnSiPh_3$ (Figure 1.6, **44**), for the hydrosilylation of terminal alkenes following both thermal and photochemical activation.[44] The reactions were carried out using heptamethylcyclotetrasiloxane (HMCTS-H) and 1-pentene. Interestingly, heating at 180 °C afforded a mixture of products including the desired alkylsilane and byproducts arising from dehydrogenative silylation and alkene isomerization. In contrast, activation of **44** with UV light allowed for sole preparation of the hydrosilylation product in high yield (Scheme 1.21).
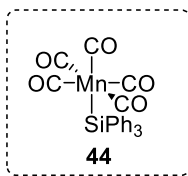
Figure 1.6. Structure of **44**.
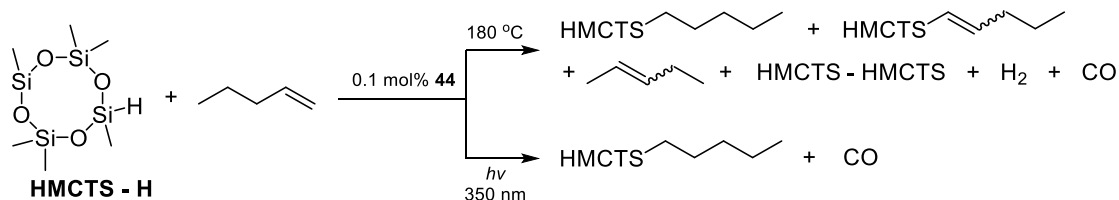
Scheme 1.21. Hydrosilylation of 1-pentene with HMCTS-H catalyzed by **44**.

In 1987, Hilal and co-workers reported the use of $Mn_2(CO)_{10}$ to hydrosilylate 1-hexene with Et_3SiH or $(EtO)_3SiH$.[45] The reaction catalyzed by $Mn_2(CO)_{10}$ was slightly slower than that using $Co_2(CO)_8$; however, the manganese complex was found to exhibit better selectivity for alkene hydrosilylation despite the low yield observed (Scheme 1.22, a). In 1999, they developed a protocol to mediate the hydrosilylation of 1-octene using

triethoxysilane and $Mn_2(CO)_{10}$ supported by an aminated poly(siloxane) surface (Figure 1.7). The alkylsilane product was collected in high yield with no evidence of byproduct formation due to alkene isomerization (Scheme 1.22, b).[46] Continuing work on the development of supported manganese catalysts, Hilal studied the activity of tetra(4-pyridyl)porphyrinato-manganese(III) cation $[Mn^{III}(TPyP)]^+$ for alkene hydrosilylation from three different sources; homogeneous $[Mn(TPyP)]^+$ ions, the micro-particle supported catalyst, MnTPyP@Micro-Clay, and the nano-particle supported catalyst, MnTPyP@Nano-Clay.[47] Comparison was made by evaluating the hydrosilylation of 1-octene with triethoxysilane (Scheme 1.22, c). Interestingly, intercalation was believed to enhance both the activity and selectivity of the catalyst, especially in the case of the nanoparticle supported system, for which conversion of 85% and TOFs of up to 1200 min^{-1} were observed. However, the activity decreased as leaching out of $MnTPyP^+$ occurred.
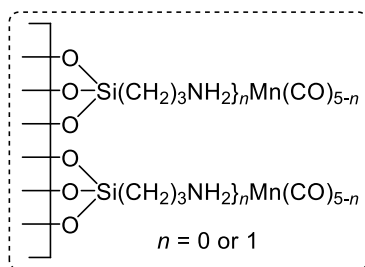
Figure 1.7. Structure of supported $Mn_2(CO)_{10}$ catalyst.
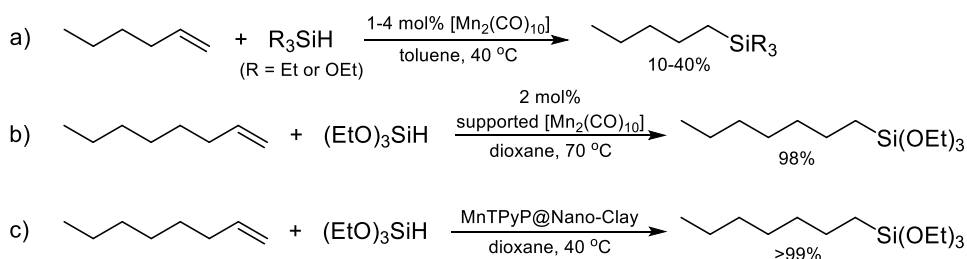
Scheme 1.22. a) Hydrosilylation of 1-hexene catalyzed by $Mn_2(CO)_{10}$. b) Hydrosilylation of 1-octene catalyzed by supported $Mn_2(CO)_{10}$. c) Hydrosilylation of 1-octene catalyzed by MnTPyP@Nano-Clay.

In 2017, Thomas's group made a significant contribution by evaluating base metal catalyst activation in the presence of sodium *tert*-butoxide for a series of reactions including hydrosilylation, hydroboration, hydrovinylation, hydrogenation, and $[2\pi+2\pi]$ alkene cycloaddition.[48] This study included the related iron and cobalt complexes; however, the manganese precatalyst, ($^{2,6\text{-Et}_2\text{Ph}}$PDI)MnBr$_2$ (**45**) was also evaluated for alkene hydrosilylation and found to exhibit moderate activity (Scheme 1.23, a). After reporting this preliminary result, they sought to develop improved alkene hydrosilylation catalysts by employing different ligand frameworks, alternating the steric bulk of the ligand, and screening the activators.[49] The combination of ($^{2,6\text{-}i\text{Pr}_2\text{Ph}}$PDI)MnBr$_2$ (**46**) and NaO^{t}Bu in 1:3 molar ratio was found to exhibit the best reactivity and a wide scope of alkenes were hydrosilylated under mild conditions. Three different silane reductants were used (HSi(OEt)$_3$, HSiMe(OEt)$_2$, and PhSiH$_3$) and high yields of the linear silane products were obtained with excellent regioselectivity (Scheme 1.23, b). Concurrently, Emslie and co-workers reported the synthesis of several manganese hydride complexes derived from (dmpe)$_2$MnH(C$_2$H$_4$).[50] Preliminary results showed that 2 mol% of *cis*-[(dmpe)$_2$MnH(Et$_2$Si=CHMe)] mediated ethylene hydrosilylation using diethylsilane at 60 °C to give triethylsilane with 60% conversion after 24 h, suggesting that compounds of this type can also be used as precatalysts for future alkene hydrosilylation studies.
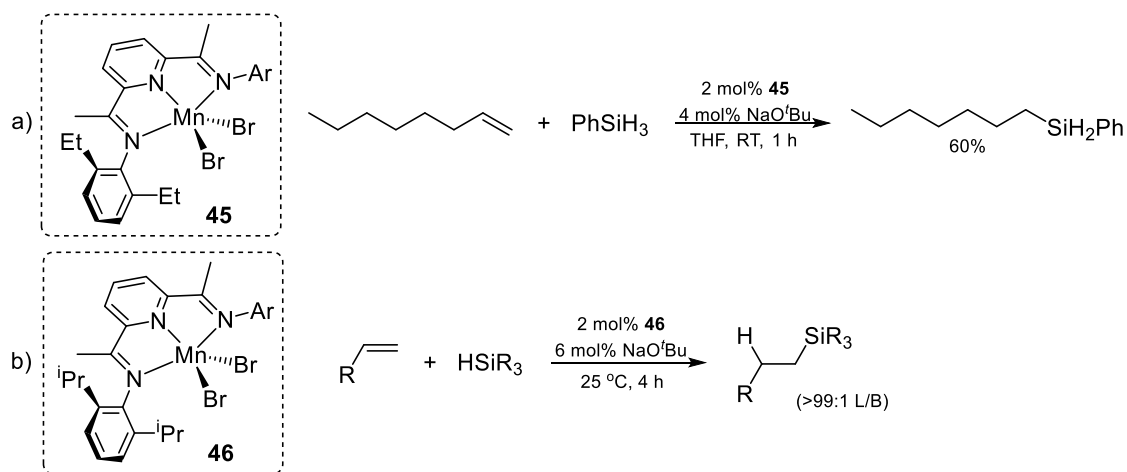
Scheme 1.23. a) Hydrosilylation of 1-octene with phenylsilane catalyzed by **45** and NaO^{t}Bu. b) Regioselective hydrosilylation of alkenes catalyzed by **46** and NaO^{t}Bu.
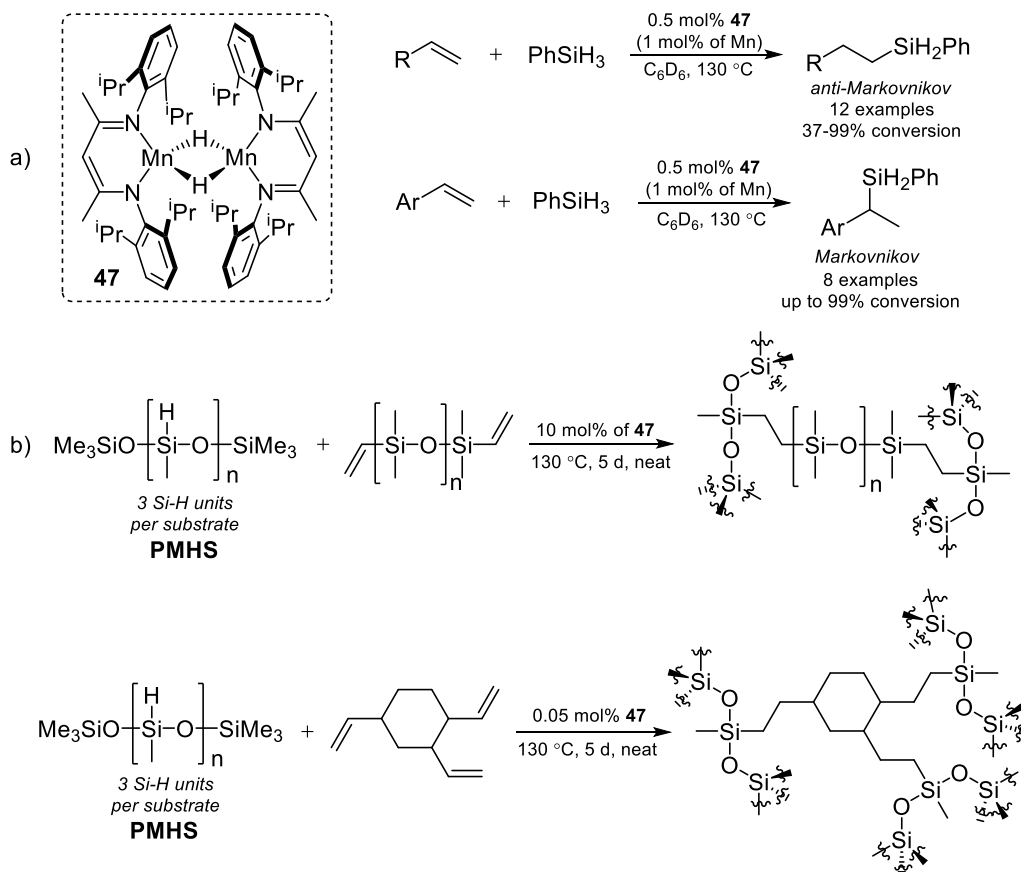
Scheme 1.24. a) Hydrosilylation of alkenes and styrenes catalyzed by **47**. b) Silicone preparation by **47**.

In 2018, our group reported the synthesis of a dimeric manganese compound featuring β-diketiminate ligands, [($^{2,6-iPr_2Ph}$BDI)Mn(μ-H)]$_2$ (**47**), which was found to mediate olefin hydrosilylation at 130 °C.[51] In particular, aliphatic alkenes underwent hydrosilylation with phenylsilane to yield *anti*-Markovnikov products, while styrenes were found to participate in Markovnikov hydrosilylation (Scheme 1.24, a). Despite the non-ideal conditions required for alkene hydrosilylation, the hydride complex was found to catalyze the cross-linking of PMHS with vinyl-terminated poly(dimethylsiloxane) to prepare silicones that are commonly used as coatings and in household consumer products. A silicone used for oxygen permeable contact lenses and transparent LED screen coatings was also prepared by hydrosilylating 1,2,4-trivinylcyclohexane with PMHS in the presence of **47** (Scheme 1.24, b). Notably, these are the first silicones featuring non-hydrolysable Si-C bonds prepared by a Mn-catalyst.

The mechanisms for aliphatic and aromatic alkene hydrosilylation were proposed and are shown in Scheme 1.25. Notice that these transformations do not to follow the commonly involved Chalk-Harrod mechanism for alkene hydrosilylation, which involves Si─H oxidative addition.[52] Instead, the hydrosilylation of aliphatic alkenes begins with alkene insertion into the Mn─H bond and concurrent dimer dissociation to generate primary alkyl intermediate **48**. Then σ-bond metathesis between the Si─H and Mn─C bonds releases the linear silane product and regenerates **47** (Scheme 1.25, a). In contrast, styrenes other than α-methylstyrene underwent insertion to form the secondary alkyl intermediate **49**, which results in preparation of the *anti*-Markovnikov product.
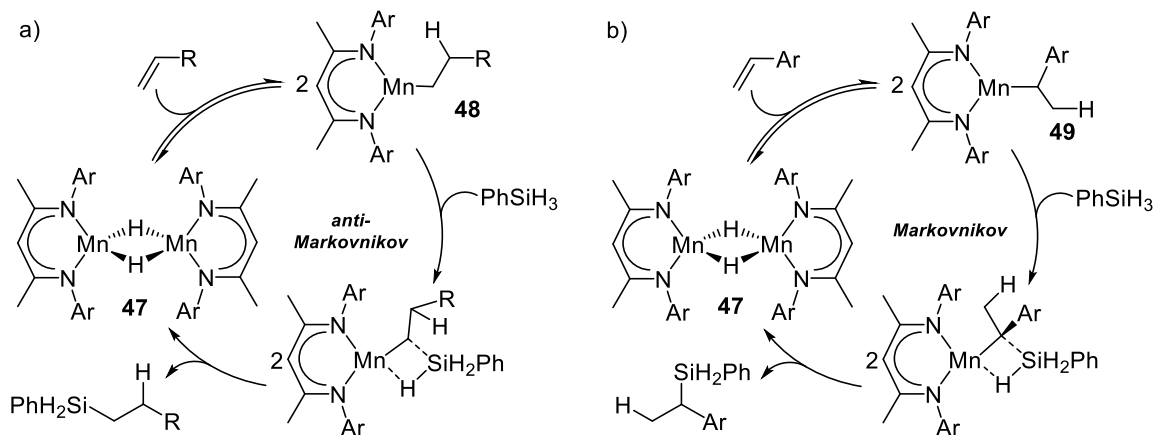
Scheme 1.25. Proposed mechanisms of alkene hydrosilylation catalyzed by **47**: a) *anti*-Markovnikov pathway and b) Markovnikov pathway.

Soon after, Yang and Wang reported chemo- and regio-selective olefin hydrosilylation using $Mn(CO)_5Br$.[53] Hydrosilylation was evaluated for a wide substrate scope including functionalized styrenes and aliphatic alkenes (Scheme 1.26, a). Most substrates were effectively hydrosilylated using benzyldimethylsilane under the optimized conditions (5 mol% cat., hexane, 60 °C, 4 hours) to give the corresponding *anti*-Markovnikov product with good to excellent isolated yield. In particular, styrene substitution did not affect the transformation and aryl derivatives such as 2-naphthalyl and 2-pyridyl underwent hydrosilylation in modest yield at 100 °C). Interestingly, $Mn_2(CO)_{10}$ was also found to be active for alkene hydrosilylation under UV irradiation. Mechanistic insight was gained by conducting deuterium labeling experiments and isolating key intermediates, which implicated a radical pathway for *anti*-Markovnikov hydrosilylation. The proposed mechanism for $Mn(CO)_5Br$-catalyzed alkene hydrosilylation is shown in Scheme 1.26, b, which begins with the formation of $HMn(CO)_5$ *via* σ-bond metathesis between $Mn(CO)_5Br$ and silane, followed by the generation of $(CO)_5Mn\bullet$ (**50**). The reaction of **50** and silane affords $HMn(CO)_5$ and silyl radical **51**, which then reacts with

34

alkene to yield the β-silyl alkyl radical **52**. Hydrogen atom transfer between HMn(CO)$_5$ and **52** releases the desired *anti*-Markovnikov product and regenerates **50**.
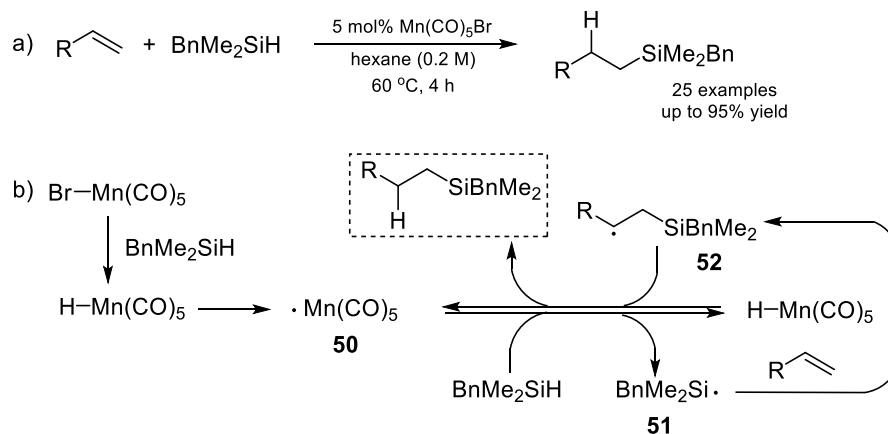
Scheme 1.26. a) Alkene hydrosilylation catalyzed by Mn(CO)$_5$Br. b) Proposed mechanism for *anti*-Markovnikov alkene hydrosilylation.

Wang's group also reported the dehydrogenative silylation of alkenes using Mn$_2$(CO)$_{10}$.[53] Using 1,1'-biphenyl-2-dimethylsilane, dehydrogenative silylation was performed for 9 styrene substrates using 10 mol% catalyst at 150 °C and good isolated yields were collected after 12 hours (Scheme 1.27). However, Mn$_2$(CO)$_{10}$ was unable to mediate this transformation for aliphatic alkenes. Dehydrogenative silylation was proposed to occur through a radical pathway in which *β*-silyl manganese intermediates undergo *β*-H elimination to generate the corresponding vinyl silane.
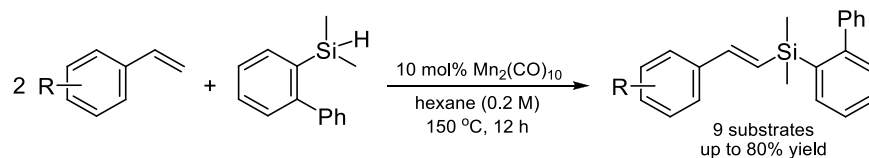
Scheme 1.27. Dehydrogenative silylation of styrenes catalyzed by Mn$_2$(CO)$_{10}$.

As part of Zhang and co-workers recent demonstration of carbonyl hydrosilylation using 1-D Mn(II) coordination polymers, KO^{t}Bu activation was also found to enable ambient temperature alkene hydrosilylation.[38] The preliminary screening of 5 aromatic alkenes indicated that the catalyst system effectively and regioselectively hydrosilylates styrene to yield the branched product in 90% isolated yield, while the reductions of other functionalized styrenes were modestly successful (up to 58% isolated yield was found). Notably, these results were achieved using 0.1 mol% of catalyst under neat conditions.

Alkyne Hydrosilylation

It was not until 2018 that Wang and co-workers reported the first examples of alkyne hydrosilylation mediated by a manganese complex.[54] A variety of alkynes were evaluated for hydrosilylation with mono-, di-, and tri-substituted aliphatic and aromatic silanes. In particular, the use of mononuclear MnBr(CO)$_5$ in the presence of AsPh$_3$ afforded the *E*-products in moderate to good yields (Scheme 1.28, a). In contrast, dinuclear Mn$_2$(CO)$_{10}$ in the presence of dilauroyl peroxide (LPO) allowed for the formation of *Z*-products with good regioselectivity (Scheme 1.28, b).
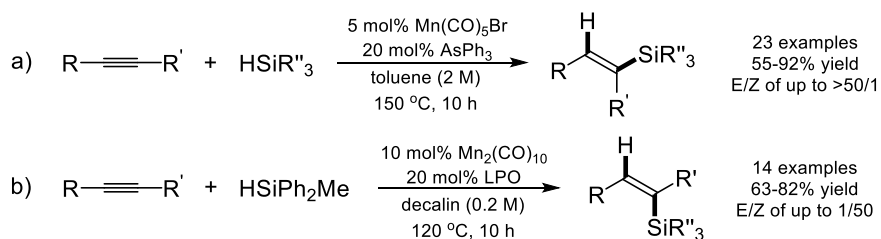
Scheme 1.28. Hydrosilylation of alkyne catalyzed by: a) Mn(CO)$_5$Br and AsPh$_3$, b) Mn$_2$(CO)$_{10}$ and LPO.

A series of experiments to isolate the key catalytic components were conducted to study the mechanism of hydrosilylation catalyzed by MnBr(CO)$_5$. Substitution of CO with AsPh$_3$ is believed to occur, followed by silane activation and HBr loss to yield intermediate **54** (Scheme 1.29). Next, **54** undergoes alkyne substitution then insertion into the Mn─Si bond to afford the (*β*-silyl)alkenyl complex **56**. In the presence of silane, Si─H coordination and σ-bond metathesis release the *E*-configured product to regenerate **54** (path A). Alternatively, **57** can undergo σ-bond metathesis to release the product and directly coordinate an alkyne to generate **55** (path B).
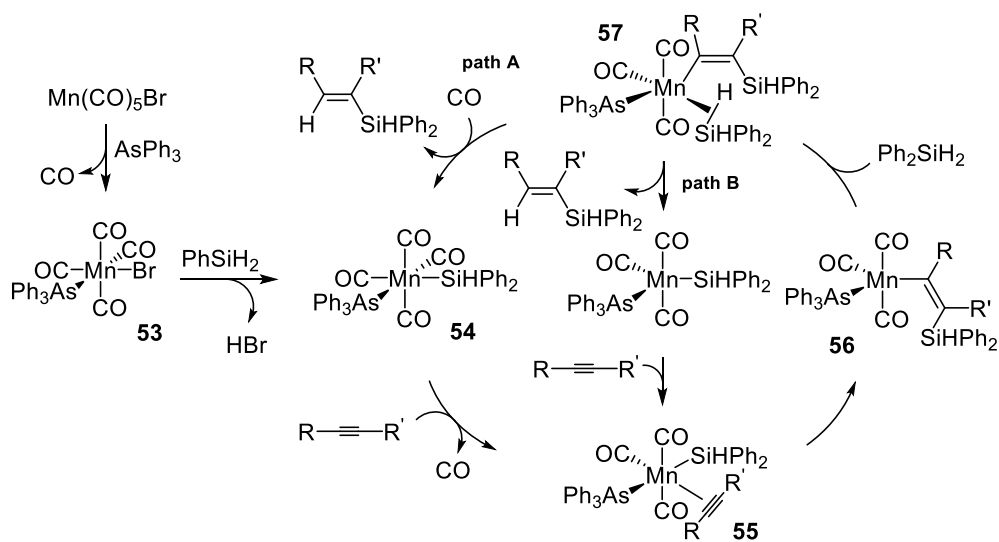
Scheme 1.29. Proposed mechanism for *E*-selective hydrosilylation catalyzed by Mn(CO)$_5$Br and AsPh$_3$.

37
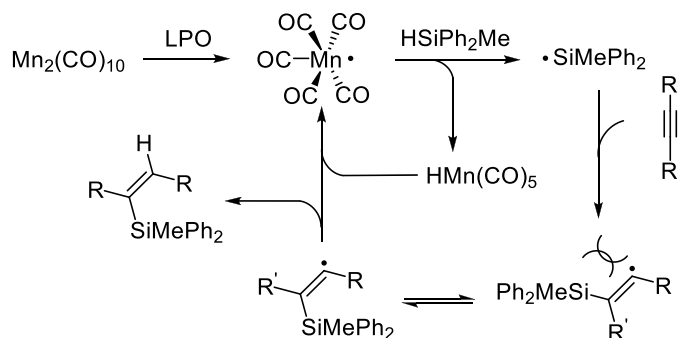
Scheme 1.30. Proposed mechanism for *Z*-selective hydrosilylation catalyzed by $Mn_2(CO)_{10}$ and LPO.

Experimental work suggested that *Z*-selective alkyne hydrosilylation catalyzed by $Mn_2(CO)_{10}$ does not follow an organometallic mechanism, but rather a radical mechanism (Scheme 1.30). The catalytic process starts with the generation of $(CO)_5Mn\bullet$ from $Mn_2(CO)_{10}$ *via* homolysis under UV irradiation, which then reacts with silane to produce a silyl radical and $HMn(CO)_5$. The reaction of silyl radical and alkyne affords *E*- and *Z*-configured alkenyl radicals. Next, H-atom transfer to these alkenyl radicals from $HMn(CO)_5$ yields the vinyl silane product and regenerates $(CO)_5Mn\bullet$. Notice that *Z*-selectivity is preferable to *E*-selectivity due to the steric hindrance of the diphenylmethylsilyl group.

1.3.2. Hydroboration

Organoboronate compounds are important reagents in synthetic chemistry due to their stability, ease of handling, impressive functional group compatibility, and ability to be applied in a variety of cross-coupling transformations. However, the development of manganese catalysts for hydroboration has lagged behind when compared to recent progress using other Earth-abundant transition metals.

Hydroboration of C=O bonds

In 2016, Zhang and Zheng reported the synthesis of a well-defined Mn(II) complex bearing an NNN chelating ligand that effectively mediates the hydroboration of aldehydes and ketones.[55] The active catalyst, (tpy)Mn(CH$_2$SiMe$_3$)$_2$ (**58**), was synthesized by treating the dichloride precursor with 2.0 equivalents of LiCH$_2$SiMe$_3$ in Et$_2$O at room temperature (Scheme 1.31, a). Mn-catalyzed carbonyl hydroboration was evaluated under mild conditions using pinacolborane (HBPin) for a scope of 15 aldehyde and ketone substrates. Boryl products were hydrolyzed and purified by SiO$_2$ column chromatography to afford the corresponding primary and secondary alcohols in good to excellent yields (Scheme 1.31, b). Interestingly, several competition reactions were conducted and **58** was found to exhibit chemoselectivity for C=O bond over C=C bond hydroboration.
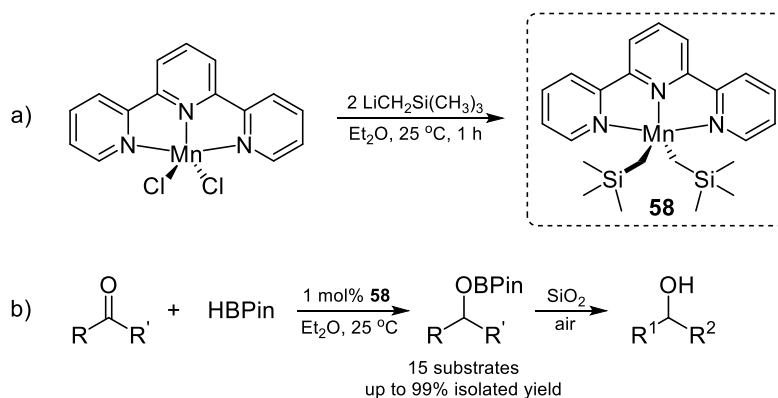
Scheme 1.31. a) Synthesis of **58**. b) Ketone hydrosilylation mediated by **58**.

In 2017, Gade's group developed the first Mn catalyst for enantioselective ketone hydroboration, (^{Ph,H}boxmi)MnCH$_2$SiMe$_3$ (**59**, Scheme 1.32, a), which features a chiral bis(oxazolinyl-methylidene)isoindoline pincer ligand (boxmi).[56] This complex was prepared by either direct reaction of boxmi ligand with Mn(CH$_2$SiMe$_3$)$_2$ or by alkylation of the manganese chloride variant with LiCH$_2$SiMe$_3$. The ligand substitution pattern, the borane reductant, solvents and 25 ketones were evaluated for hydroboration with HBPin under ambient conditions in the presence of 2.5 mol% **59** (Scheme 1.32, b). Excellent conversion and enantioselectivity was observed for all substrates (up to >99 % *ee*) and the chiral alcohol products were obtained in high yields *via* hydrolysis. Ketone substitution had minimal influence on the enantiodiscrimination. In addition, C—C multiple bond hydroboration was not observed for vinyl and alkynyl ketones, which also revealed that direct aryl group attachment to the carbonyl functionality was not essential for the selectivity. Importantly, TOFs of up to 80 min^{-1} were achieved by reducing the catalyst loading to 0.1 mol%.

40
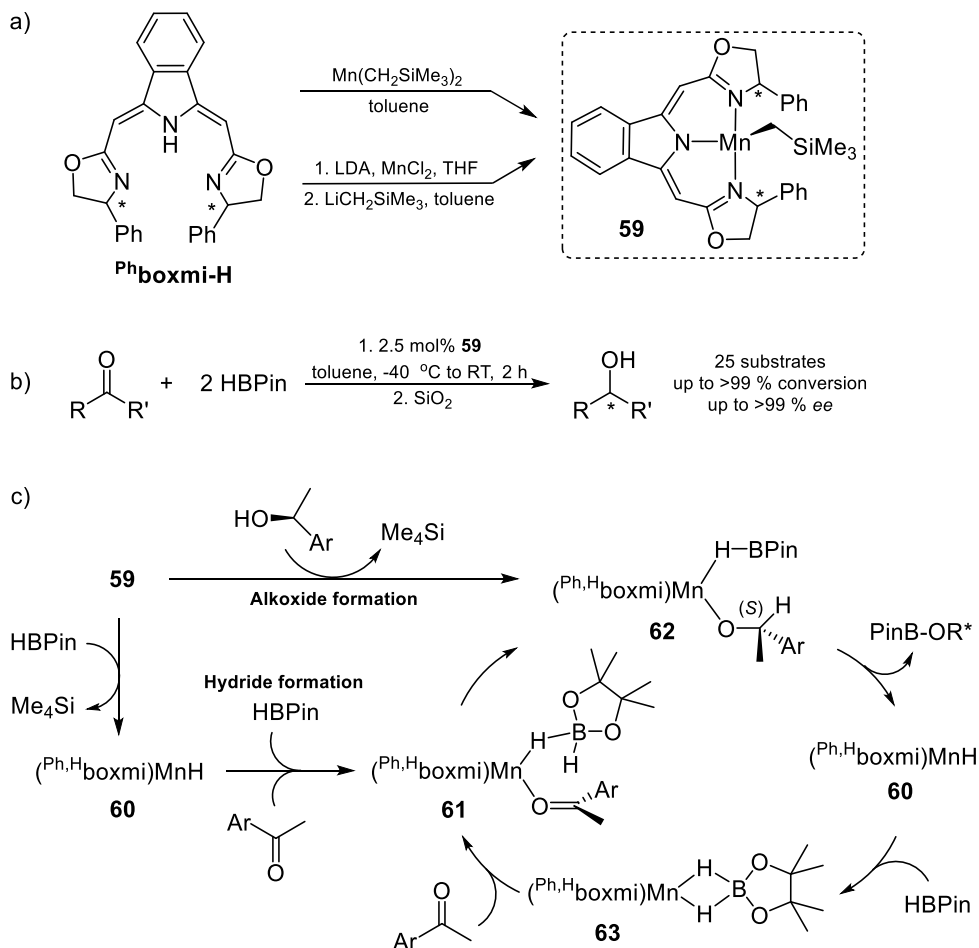
Scheme 1.32. a) Synthesis of catalyst **59**. b) Asymmetric ketone hydroboration mediated by **59**. c) Proposed mechanism for **59**-catalyzed hydroboration of ketones.

Experiments using a radical trap confirmed that this transformation does not occur *via* a radical process. The reaction of DBPin with 4-fluoroacetophenone yielded a deuterium labelled alcohol after silica work-up, which indicated borane as the hydrogen/deuterium source. Further experiments using pre-generated manganese hydride (^{Ph,H}boxmi)MnH (**60**) also suggested that hydrogen transfer takes place from the borane instead of the metal hydride. The proposed mechanism begins with the coordination of HBPin and ketone to **60** to form intermediate **61**, which is set up to stereoselectively transfer hydrogen from the borane to the carbonyl (Scheme 1.32, c). Then, σ-bond

41

metathesis releases the chiral boronic ester to regenerate **60**, which coordinates HBPin to form a borane-manganese adduct with bridging hydrides (**63**), restarting the catalytic cycle. A follow-up DFT study featuring stoichiometric and kinetic experiments suggested that **59** could enter the catalytic cycle as **60** following σ-bond metathesis with HBPin (Scheme 1.32, c, left). In addition, **59** could undergo alcoholysis with ROH to form the catalytically active Mn(II) alkoxide **62** (Scheme 1.32, c, top). The dominant pathway involves σ-bond metathesis between HBPin and the Mn alkoxide; while the previously mentioned pathway was found to be minor.[57]
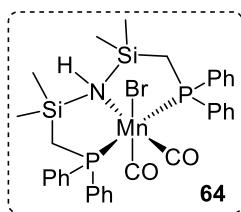
Figure 1.8. Structure of **64**.

In 2018, Leitner utilized the manganese pincer complex, $((Ph_2PCH_2SiMe_2)_2NH)Mn(CO)_2Br$ (**64**, Figure 1.8), for the hydroboration of carboxylates, carbonates, and carbon dioxide.[58] The reduction of these functionalities is important for sustainable chemical and pharmaceutical synthesis and the preparation of alternative non-fossil feedstocks derived from biomass or carbon dioxide. A wide range of 17 carboxylic acids was reduced with HBPin using 0.2 mol% of **64** in the presence of 0.5 mol% KO^{t}Bu (Scheme 1.33, a). Good to excellent conversion was observed for most substrates including aliphatic acids, benzoic acids, the biomass-derived platform chemical succinic acid, and fatty acids. Notably, unsaturated substrates were selectively hydroborated in good yield without C=C bond reduction.

The selective reduction of organic carbonates has been a challenge since the compounds are kinetically stable toward hydrogenation and are often used as solvents for reductive reactions.[59] Additionally, the reduction of carbonates derived from CO and CO_2 can provide industrially important methanol derivatives. Therefore, cyclic and linear carbonates were assessed for hydroboration at elevated temperature with 3 eq. of HBPin using 0.1 mol% of **64** and 0.3 mol% of NaO^{t}Bu under neat conditions (Scheme 1.33, b). This catalyst was found to be highly effective for the reduction of aromatic and cyclic carbonates featuring 5-membered or 6-membered rings as well as heterocyclic carbonates with up to 98% yield observed. Interestingly, the 1,2-carbonate of glycerol, which is a byproduct of industrial vegetable oil production, was also hydroborated to the corresponding boryl ether in 88% yield. However, the hydroboration of linear carboxylates was slightly less effective. Catalyst **64** (0.036 mol%) was able to reduce CO_2 (1 atm) with 3 eq. of HBPin in the presence of NaO^{t}Bu at 100 °C to yield MeOBPin (96% by ^{1}H NMR). Turnover numbers of up to 883 were observed (Scheme 1.33, c).
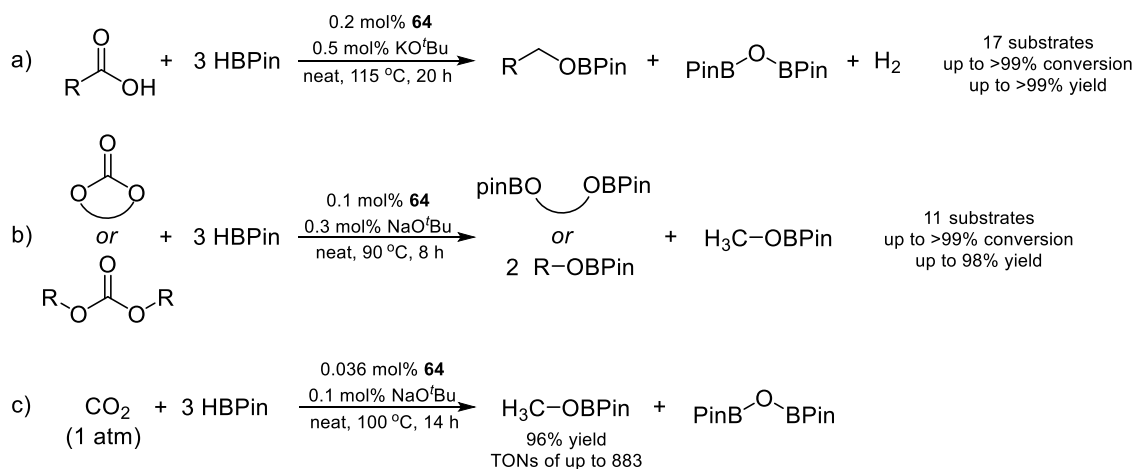
Scheme 1.33. Hydroboration of a) carboxylic acids, b) carbonates, and c) CO_2 catalyzed by **64**.

43

In 2019, Maji's group studied a series of hydrazine-based (**65**-**67**) and triazine-based catalysts (**68**-**69**) for the deoxygenative hydroboration of carboxylic acids (Scheme 1.34, a). Each catalyst was found to effectively catalyze carboxylate hydroboration under ambient conditions at low catalyst loadings (0.001-0.1 mol%).[60] In particular, 0.1 mol% of **65**-**68** were able to fully hydroborate benzoic acid to the corresponding boronate ester with TONs of up to 990. Catalyst **66** showed excellent reactivity for this transformation with a maximum TON of more than 99,000 at 25 °C (TOFs of up to 34 min^{-1}), which renders it the best homogeneous catalyst known for this process. The catalytic activity of **68** was evaluated at 0.1 mol% loading (50 µL in a stock solution in toluene) with HBPin at 25 °C for a wide range of 42 substrates including aromatic and aliphatic acids, fatty acids, and even some bioactive carboxylic acids (Scheme 1.34, b). Hydrolysis with SiO_2/methanol at 60 °C gave the corresponding alcohols in up to 96% yield.

The aromatic carboxylic acids screened were fully reduced (>99%), including derivatives that possess electron-donating or -withdrawing groups, or heteroaromatic functionalities such as furan and thiophene. In the case of aliphatic substrates, conversions up to >99% were achieved, although byproducts from C=C hydroboration were detected for cinnamic acid (22%). Cyclopropane rings were unmodified under such conditions, while hindered (pivalic acid), unhindered (acetic acid), and C_1 acids were reduced quantitatively. Long chain fatty acids reacted smoothly with HBPin to afford the corresponding alcohols in excellent yield, while drug molecules and bile acid were also successfully converted under these conditions. Notably, **68** showed great chemoselectivity for the hydroboration of carboxylic acids in the presence of reducible functional groups.

Halogenated aromatic and aliphatic substrates were tolerated, and nitro, nitrile, and ester groups were retained.

The proposed mechanism is shown in Scheme 1.34, c, which involves the addition of HBPin to precatalyst **68** to afford hydride complex **70**. Next, the insertion of RC(O)OBPin (derived from the noncatalytic reaction of carboxylic acid with HBPin) forms alkoxy intermediate **71**. This compound undergoes σ-bond metathesis with HBPin to regenerate **70** and intermediate **72**. Once formed, **72** could release O(BPin)$_2$ to liberate aldehyde, which can be inserted to yield **73**. Finally, σ-bond metathesis between **73** and HBPin affords the final product and **70**.

In Copéret's study of silica-supported Mn catalysis, Mn{N(SiMe$_3$)$_2$}$_2$·THF@SiO$_{2-400}$ was also reported to be an active catalyst for carbonyl hydroboration.[37] A scope of 8 functionalized aldehydes and ketones underwent hydroboration under mild conditions (0.5 mol% cat., 25 °C, 6 h) to achieve the desired products in up to 99% yield. Notably, this organic-ligand-free system exhibited great recyclability with no loss in activity observed after 3 catalytic cycles. Most recently, the Mn coordination polymer developed by Zhang and Zheng was found to effectively mediate the hydroboration of carbonyl compounds with TON of up to 990 following KO^{t}Bu activation.[38] Using 0.1 mol% of Mn and 1 mol% of KO^{t}Bu, a wide range of 16 functionalized ketones and 11 aldehydes were successfully transformed to the corresponding boronate esters under ambient conditions (up to 99% GC yields). The products were purified by column chromatography in up to 95% isolated yield.
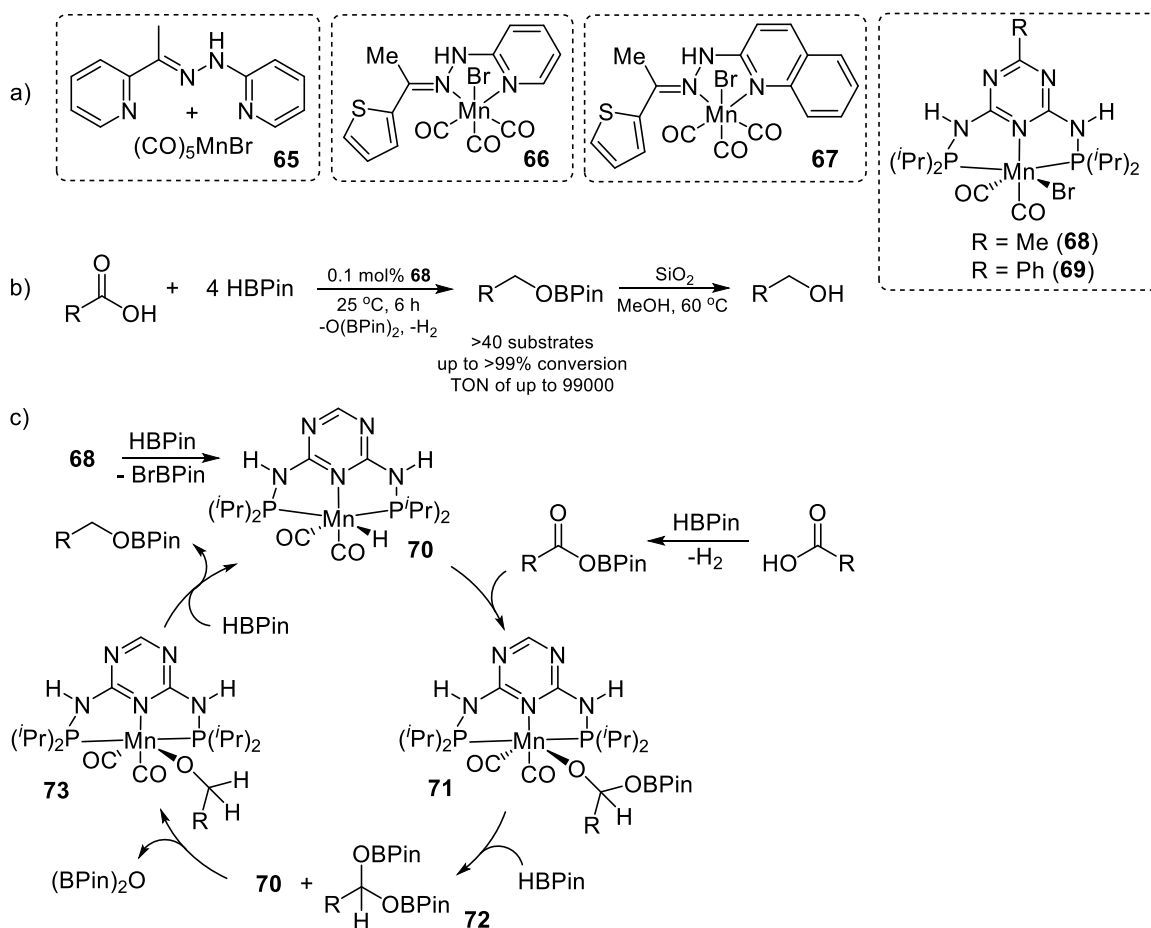
Scheme 1.34. a) Structure of catalysts **65**-**69**. b) Hydroboration of carboxylic acids catalyzed by **68**. c) Proposed mechanism for carboxylic acid hydrosilylation catalyzed by **68**.

Hydroboration of Alkenes

Zhang and Zheng's earlier study on (tpy)Mn(CH$_2$SiMe$_3$)$_2$ (**58**) mediated carbonyl hydroboration also revealed that this compound mediates the ambient temperature hydroboration of alkenes using 1.1 equivalents of HBPin (Scheme 1.35).[55] Notably, styrenes underwent hydroboration to yield the Markovnikov products with up to 98% regioselectivity, while aliphatic alkenes tended to yield the *anti*-Markovnikov products. Electron-donating or -withdrawing substituents in either the *meta*- or *para*-positions of styrene did not affect the transformation, whereas *o*-chlorostyrene required more forcing

conditions to reach 75% isolated yield (50 °C, 24 hours). Importantly, **58**-catalyzed hydroboration was not selective for substrates containing nitro, cyano and alkenyl groups, which yielded a mixture of products.
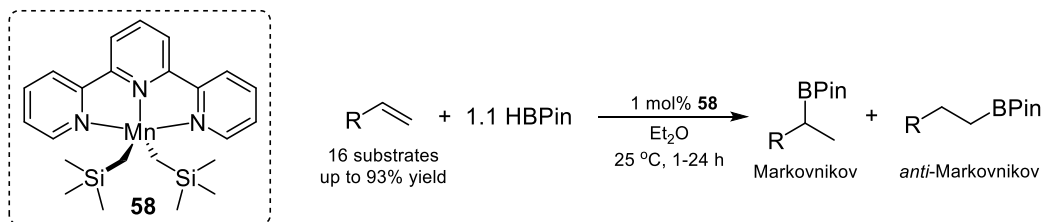
Scheme 1.35. Alkene hydroboration mediated by **58**.

In Thomas's 2018 investigation, it was found that the combination of (^{iPr_2Ph}PDI)MnBr$_2$ (**46**) and NaO^{t}Bu in a 1:3 molar ratio not only enabled alkene hydrosilylation, but also effectively mediated alkene hydroboration under mild conditions.[49] A scope of 10 alkenes and styrenes were evaluated in the presence of 3 equivalents of HBPin (Scheme 1.36). Aliphatic alkenes such as 1-octene, 4-phenylbutene, and 3-triethoxypropene were hydroborated with good regioselectivity for the *anti*-Markovnikov product (>99:1 L/B). Styrenes containing different electronic and steric substitution patterns underwent hydroboration to provide alkylboranes in moderate to excellent yield, and again with excellent regioselectivity (L/B of up to >99:1).
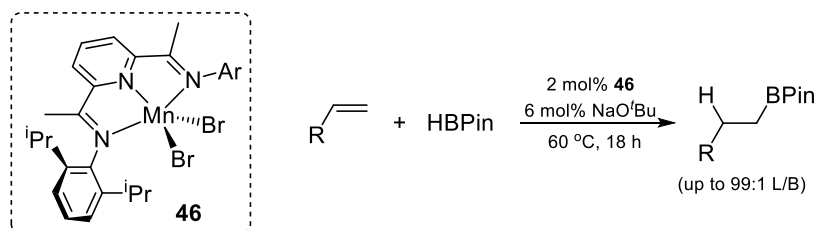
Scheme 1.36. Alkene hydroboration catalyzed by **46**.

In 2018, the Turculet, Stradiotto, Ess, Sydora, and Bischof groups reported the characterization and catalytic activity of structurally analogous first row transition metal complexes featuring an *N*-phosphinoamidinate ligand [(PN)M; M = Mn, Fe, Co, and Ni].[61] As a part of the investigation, DFT calculations were performed to evaluate the electronic structure of $[(\kappa^2\text{-P,N})Mn(N(SiMe_3)_2)]$ (**37**). The doublet, quartet, and sextet open-shell spin states were found to be accessible, which is consistent with its paramagnetic character. To compare the catalytic activity of **37** to other members of the series, the isomerization-hydroboration of 1-octene, *cis*-4-octene and *trans*-4-octene was evaluated (Scheme 1.37). Negligible conversion was observed after 1 hour at 23 °C, while poor conversion (<50%) and selectivity were observed under more forcing conditions (65 °C, 18 h). The product mixture determined by NMR spectroscopy is shown in Table 1.2 and DFT calculations revealed that the relative activity of the (PN)M catalysts is related to their spin-state energy gaps. Particularly, for the reaction of **37** with *trans*-4-octene, there is no viable spin crossover mechanism and the migratory insertion was found to be slow, resulting in a poor catalytic outcome.
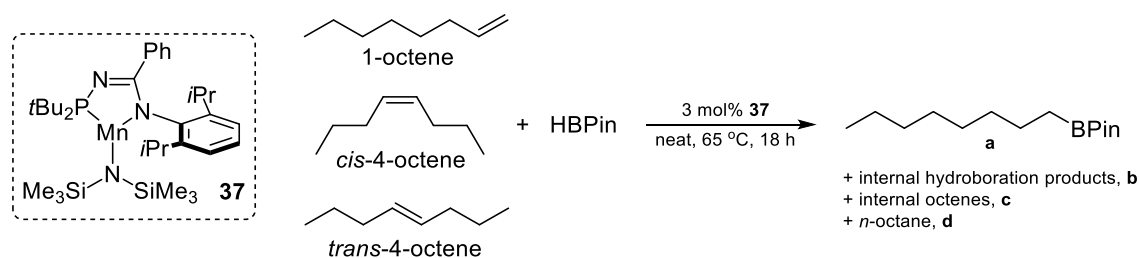
Scheme 1.37. Alkene hydroboration catalyzed by **37**.

Table 1.2. Partial isomerization-hydroboration of alkenes catalyzed by **37.**

Substrate	Residual Substrate	a	b	c	d
1-octene	55%	25%	<5%	15%	5%
cis-4-octene	>95%	<5%	<5%	<5%	<5%
trans-4-octene	>95%	<5%	<5%	<5%	<5%

Hydroboration of Alkynes

In 2020, Rueping and co-workers reported the hydroboration of propargylic alcohols and amines, as well as symmetric internal alkynes, to yield the corresponding alkenes using NaBHEt$_3$-activated Mn(II) precursors ($^{2,6-iPr_2Ph}$PDI)MnCl$_2$ and ($^{2,6-Et_2Ph}$PDI)MnCl$_2$.[62] In particular, 14 TBDMS-protected hydroxyalkynes were screened for hydroboration using the former pre-catalyst under ambient conditions, which provided the corresponding vinyl borane in excellent yield (up to 99% NMR yield and 95% isolated yield after column chromatography) (Scheme 1.38, a). Activated ($^{2,6-iPr_2Ph}$PDI)MnCl$_2$ also mediated the hydroboration of varied Bn-protected propargylic amines to yield the corresponding alkenes (up to 95% NMR yield and 85% isolated yield after column chromatography) (Scheme 1.38, b). Interestingly, ($^{2,6-Et_2Ph}$PDI)MnCl$_2$ was found to show higher activity for the selective reduction of symmetric alkynes with HBPin in the presence of NaBHEt$_3$. A scope of 9 alkynes was screened for hydroboration reaction to yield *syn*-addition products in good isolated yield (Scheme 1.38, c).
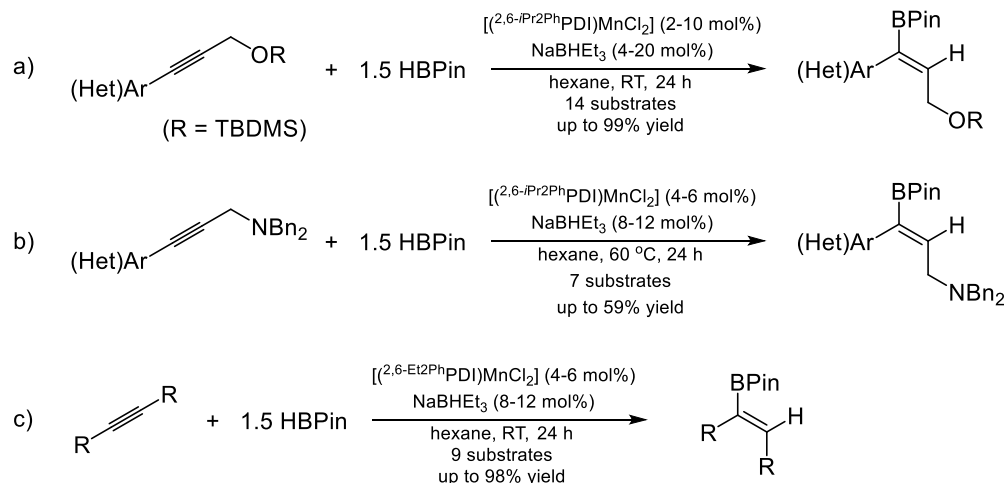
Scheme 1.38. a) Propargylic alcohol hydroboration catalyzed by $(^{2,6-iPr_2Ph}$PDI)MnCl$_2$/NaBHEt$_3$. b) Propargylic amine hydroboration catalyzed by $(^{2,6-iPr_2Ph}$PDI)MnCl$_2$/NaBHEt$_3$. c) Symmetric alkyne hydroboration catalyzed by $(^{2,6-Et_2Ph}$PDI)MnCl$_2$/NaBHEt$_3$.

1.4. Summary

This chapter highlighted the major advances in manganese-based hydrofunctionalization catalysis that have been reported in recent years. The pace of this development has accelerated dramatically. Prior to 2010, only a handful of studies had utilized manganese compounds to catalyze hydrosilylation, and remarkably, the first report of manganese-catalyzed hydroboration was published in 2016. Over the last five years, many highly active manganese catalysts for these transformations have been described and detailed mechanistic insight has been gathered. These hydrofunctionalization efforts have greatly contributed to the recent expansion of manganese catalysis.

1.5. References

(1)   Trovitch, R. J. *Synlett* **2014**, *25* (12), 1638–1642.

(2)   Garbe, M.; Junge, K.; Beller, M. *Eur. J. Org. Chem.* **2017**, *2017* (30), 4344–4362.

(3)   Trovitch, R. J. *Acc. Chem. Res.* **2017**, *50* (11), 2842–2852.

(4)   Yang, X.; Wang, C. *Chem. Asian J.* **2018**, *13* (17), 2307–2315.

(5)   Speier, J. L.; Webster, J. A.; Barnes, G. H. *J. Am. Chem. Soc.* **1957**, *79* (4), 974-979.

(6)   Karstedt, B. D. U.S. Patent Application No. 3775452A. November 27, 1973.

(7)   Ojima, I.; Nihonyanagi, M.; Nagai, Y. *J. Chem. Soc., Chem. Commun.* **1972**, *16*, 938a.

(8)   Brown, H. C. *Tetrahedron* **1961**, *12* (3), 117–138.

(9)   Kono, H.; Ito, K.; Nagai, Y. *Chem. Lett.* **1975**, *4* (10), 1095–1096.

(10) Männig, D.; Nöth, H. *Angew. Chem. Int. Ed.* **1985**, *24* (10), 878–879.

(11) Yates, R. L. *J. Catal.* **1982**, *78* (1), 111–115.

(12) Hanna, P. K.; Gregg, B. T.; Cutler, A. R. *Organometallics* **1991**, *10* (1), 31-33.

(13) DiBiase Cavanaugh, M.; Gregg, B. T.; Chiulli, R. J.; Cutler, A. R. *J. Organomet. Chem.* **1997**, *547* (1), 173–182.

(14) Mao, Z.; Gregg, B. T.; Cutler, A. R. *Organometallics* **1998**, *17* (10), 1993–2002.

(15) DiBiase Cavanaugh, M.; Gregg, B. T.; Cutler, A. R. *Organometallics* **1996**, *15* (12), 2764–2769.

(16) Mao, Z.; Gregg, B. T.; Cutler, A. R. *J. Am. Chem. Soc.* **1995**, *117* (40), 10139–10140.

(17) Son, S. U.; Paik, S.-J.; Lee, I. S.; Lee, Y.-A.; Chung, Y. K.; Seok, W. K.; Lee, H. N. *Organometallics* **1999**, *18* (20), 4114–4118.

(18) Son, S. U.; Paik, S.-J.; Chung, Y. K. *J. Mol. Catal. A: Chem.* **2000**, *151* (1), 87–90.

(19) Chidara, V. K.; Du, G. *Organometallics* **2013**, *32* (18), 5034–5037.

(20) Vijjamarri, S.; Chidara, V. K.; Du, G. *ACS Omega* **2017**, *2* (2), 582–591.

(21) Vijjamarri, S.; Streed, S.; Serum, E. M.; Sibi, M. P.; Du, G. *ACS Sustainable Chem. Eng.* **2018**, *6* (2), 2491–2497.

(22) Zheng, J.; Chevance, S.; Darcel, C.; Sortais, J.-B. *Chem. Commun.* **2013**, *49* (85), 10010–10012.

(23) Zheng, J.; Elangovan, S.; Valyaev, D. A.; Brousses, R.; César, V.; Sortais, J.-B.; Darcel, C.; Lugan, N.; Lavigne, G. *Adv. Synth. Catal.* **2014**, *356* (5), 1093–1097.

(24) Valyaev, D. A.; Wei, D.; Elangovan, S.; Cavailles, M.; Dorcet, V.; Sortais, J.-B.; Darcel, C.; Lugan, N. *Organometallics* **2016**, *35* (24), 4090–4098.

(25) Ojima, I.; Nihonyanagi, M.; Kogure, T.; Kumagai, M.; Horiuchi, S.; Nakatsugawa, K.; Nagai, Y. *J. Organomet. Chem.* **1975**, *94* (3), 449–461.

(26) Pinto, M.; Friães, S.; Franco, F.; Lloret-Fillol, J.; Royo, B. *ChemCatChem* **2018**, *10* (13), 2734–2740.

(27) Sousa, S. C. A.; Realista, S.; Royo, B. *Adv. Synth. Catal.* **2020**, *362* (12), 2437–2443.

(28)   Behera, R. R.; Ghosh, R.; Panda, S.; Khamari, S.; Bagh, B. *Org. Lett.* **2020**, *22* (9), 3642−3648.

(29) Mukhopadhyay, T. K.; Flores, M.; Groy, T. L.; Trovitch, R. J. *J. Am. Chem. Soc.* **2014**, *136* (3), 882–885.

(30) Ghosh, C.; Mukhopadhyay, T. K.; Flores, M.; Groy, T. L.; Trovitch, R. J. *Inorg. Chem.* **2015**, *54* (21), 10398–10406.

(31) Mukhopadhyay, T. K.; Ghosh, C.; Flores, M.; Groy, T. L.; Trovitch, R. J. *Organometallics* **2017**, *36* (18), 3477–3483.

(32) Mukhopadhyay, T. K.; Rock, C. L.; Hong, M.; Ashley, D. C.; Groy, T. L.; Baik, M.-H.; Trovitch, R. J. *J. Am. Chem. Soc.* **2017**, *139* (13), 4901–4915.

(33) Ma, X.; Zuo, Z.; Liu, G.; Huang, Z. *ACS Omega* **2017**, *2* (8), 4688–4692.

(34) Wenz, J.; Vasilenko, V.; Kochan, A.; Wadepohl, H.; Gade, L. H. *Eur. J. Inorg. Chem.* **2017**, *2017* (47), 5545–5556.

(35)   Martínez-Ferraté, O.; Werlé, C.; Franciò, G.; Leitner, W. *ChemCatChem* **2018**, *10* (20), 4514– 4518.

(36)   Martínez-Ferraté, O.; Chatterjee, B.; Werlé, C.; Leitner, W. *Catal. Sci. Technol.* **2019**, *9* (22), 6370–6378.

(37)   Ghaffari, B.; Mendes-Burak, J.; Chan, K.W.; Copéret, C. *Chem. Eur. J.* **2019**, *25* (61), 13869–13873.

(38)   Zhang, G.; Zeng, H.; Li, S.; Johnson, J.; Mo, Z.; Neary, M. C.; Zheng, S. *Dalton Trans.*, **2020**, *49* (8), 2610-2615.

(39) Igarashi, M.; Fuchikami, T. *Tetrahedron Lett.* **2001**, *42* (10), 1945–1947.

(40) Arias-Ugarte, R.; Sharma, H. K.; Morris, A. L. C.; Pannell, K. H. *J. Am. Chem. Soc.* **2012**, *134* (2), 848–851.

(41) Kelly, C. M.; McDonald, R.; Sydora, O. L.; Stradiotto, M.; Turculet, L. *Angew. Chem. Int. Ed.* **2017**, *56* (50), 15901–15904.

(42) Das, H. S.; Das, S.; Dey, K.; Singh, B.; Haridasan, R. K.; Das, A.; Ahmed, J.; Mandal, S. K. *Chem. Commun.* **2019**, *55* (79), 11868-11871.

(43) Bertini, F.; Glatz, M.; Stöger, B.; Peruzzini, M.; Veiros, L. F.; Kirchner, K.; Gonsalvi, L. *ACS Catal.* **2019**, *9* (1), 632–639.

(44) Pratt, S. L.; Faltynek, R. A. *J. Organomet. Chem.* **1983**, *258* (1), C5–C8.

(45) Hilal, H. S.; Abu-Eid, M.; Al-Subu, M.; Khalaf, S. *J. Mol. Catal.* **1987**, *39* (1), 1–11.

(46) Hilal, H. S.; Suleiman, M. A.; Jondi, W. J.; Khalaf, S.; Masoud, M. M. *J. Mol. Catal. A: Chem.* **1999**, *144* (1), 47–59.

(47) Jondi, W.; Zyoud, A.; Mansour, W.; Hussein, A. Q.; Hilal, H. S. *React. Chem. Eng.* **2016**, *1* (2), 194–203.

(48) Docherty, J. H.; Peng, J.; Dominey, A. P.; Thomas, S. P. *Nat. Chem.* **2017**, *9* (6), 595–600.

(49) Carney, J. R.; Dillon, B. R.; Campbell, L.; Thomas, S. P. *Angew. Chem. Int. Ed.* **2018**, *57* (33), 10620–10624.

(50) Price, J. S.; Emslie, D. J. H.; Britten, J. F. *Angew. Chem. Int. Ed.* **2017**, *56* (22), 6223–6227.

(51) Mukhopadhyay, T. K.; Flores, M.; Groy, T. L.; Trovitch, R. J. *Chem. Sci.* **2018**, *9* (39), 7673–7680.

(52) Chalk, A. J.; Harrod, J. F. *J. Am. Chem. Soc.* **1965**, *87* (1), 16–21.

(53) Yang, X.; Wang, C. *Chin. J. Chem.* **2018**, *36* (11), 1047–1051.

(54) Yang, X.; Wang, C. *Angew. Chem. Int. Ed.* **2018**, *57* (4), 923–928.

(55) Zhang, G.; Zeng, H.; Wu, J.; Yin, Z.; Zheng, S.; Fettinger, J. C. *Angew. Chem. Int. Ed.* **2016**, *55* (46), 14369–14372.

(56) Vasilenko, V.; Blasius, C. K.; Wadepohl, H.; Gade, L. H. *Angew. Chem. Int. Ed.* **2017**, *56* (29), 8393-8397.

(57) Vasilenko, V.; Blasius, C. K.; Gade, L. H. *J. Am. Chem. Soc.* **2018**, *140* (29), 9244–9254.

(58) Erken, C.; Kaithal, A.; Sen, S.; Weyhermüller, T.; Hölscher, M.; Werlé, C.; Leitner, W. *Nat. Commun.* **2018**, *9* (1), 4521–4529.

(59) Schäffner, B.; Schäffner, F.; Verevkin, S. P.; Börner, A. *Chem. Rev.* **2010**, *110* (8), 4554–4581.

(60) Barman, M. K.; Das, K.; Maji, B. *J. Org. Chem.* **2019**, *84* (3), 1570–1579.

(61) Macaulay, C. M.; Gustafson, S. J.; Fuller III, J. T.; Kwon, D.-H.; Ogawa, T.; Ferguson, M. J.; McDonald, R.; Lumsden, M. D.; Bischof, S. M.; Sydora, O. L.; Ess, D. H.; Stradiotto, M.; Turculet, L. *ACS Catal.* **2018**, *8* (11), 9907–9925.

(62) Brzozowska, A.; Zubar, V.; Ganardi, R. C.; Rueping, M. *Org. Lett.* **2020**, *22* (10), 3765−3769.

CHAPTER 2

THE ELECTRONIC STRUCTURE OF A β-DIKETIMINATE MANGANESE

HYDRIDE DIMER

2.1. Abstract

The electronic structure of a dimeric manganese hydride catalyst supported by β-diketiminate ligands, $[(^{2,6-iPr_2Ph}BDI)Mn(\mu\text{-}H)]_2$, was investigated with density functional theory. A triple bond between two manganese centers was anticipated from simple electron-counting rules; however, calculations revealed a M–M bond order of 0.2 between the metal centers. In accordance with experimentally determined Heisenberg exchange coupling constants of -15 ± 0.1 cm^{-1} (superconducting quantum interference device) and -10.2 ± 0.7 cm^{-1} (electron paramagnetic resonance spectroscopy), the calculated J_o value of -10.9 cm^{-1} confirmed that the ground state involves antiferromagnetic coupling between high spin Mn(II)-d^5 centers. The effect of steric bulk on the bond order was interrogated via a model study with the least sterically demanding version of the β-diketiminate ligand and was found to be negligible. Mixing between metal- and ligand-based orbitals was found to be responsible for the absence of a metal–metal multiple bond. The bridging hydrides give rise to a relatively close positioning of the metal centers, while bridging atoms possessing 2p-orbitals result in longer Mn-Mn distances and more stable dimers.

2.2. Introduction

Low-coordinate transition metal complexes have been extensively studied due to the reactivity enabled by their coordinatively and electronically unsaturated structures.[1] It has been widely acknowledged that bulky ligands can stabilize low-coordinate and electron-deficient complexes by preventing aggregation.[2] One ubiquitous class of bulky ligands that support electron-deficient metal centers is based on the β-diketiminate ligand, commonly abbreviated as BDI or nacnac. Practical advantages such as facile synthesis and easy modification[3] enable systematic studies on β-diketiminate ligands.[4,5] For instance, Mindiola reported catalytic carboamination with a titanium complex supported by a β-diketiminate ligand.[6] Holland described a Fe(II) fluoride β-diketiminate complex that catalyzes the hydrodefluorination of fluorocarbons.[7] Despite extensive investigations on transition metal complexes supported by β-diketiminate ligands, (BDI)Mn complexes have only recently been found to exhibit catalytic activity.
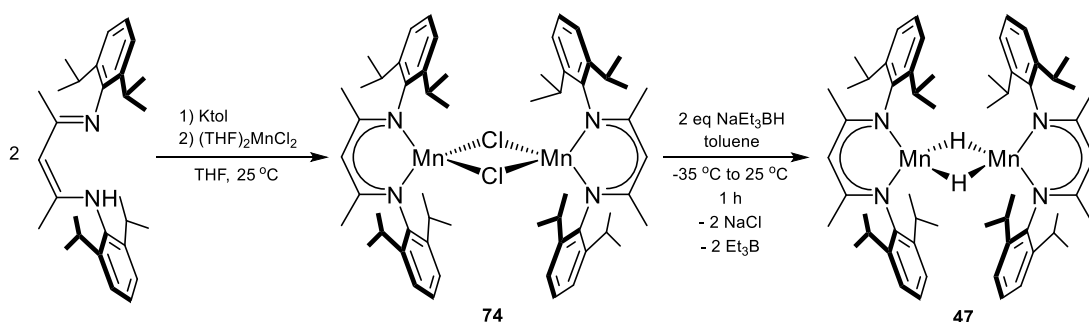
Scheme 2.1. Synthesis of **47**.[8]

Although [($^{2,6\text{-}i\text{Pr}_2\text{Ph}}$BDI)Mn(μ-H)]$_2$ was previously synthesized and characterized by a former member of the Trovitch group, Tufan Mukhopadhyay,[8] the electronic structure of this compound had not been explored. Hence, my first project began with the

preparation of 2,6-diisopropylphenyl-β-diketiminate ($^{2,6-iPr_2Ph}$BDI or NacNac) through the condensation of acetylacetone with 2 equiv. of 2,6-diisopropylaniline. Then a manganese chloride precursor was prepared via metalation of *in situ* generated [K][$^{2,6-iPr_2Ph}$BDI] with (THF)$_2$MnCl$_2$, yielding a bridging chloride complex identified as [($^{2,6-iPr_2Ph}$BDI)Mn(μ-Cl)]$_2$ (Scheme 2.1, middle, **74**). Treating the chloride dimer with 2 equiv. of NaEt$_3$BH dropwise and then warming the THF solution from -35 °C to 25 °C afforded the hydride dimer identified as **47** (Scheme 2.1).

Intuitively, one may argue that complex **47**, which has 13 electrons per metal center formally, should feature metal–metal bonding to compensate for its low electron count. The existence of a metal–metal triple bond would provide three additional electrons, allowing each Mn center to reach a 16-electron configuration. Dimeric β-diketiminate manganese complexes have been reported previously;[9–11] however, a detailed analysis of their electronic structures was not carried out. The presence of two bridging hydrides poses a challenge from an electronic structure perspective and deserves special attention. In this contribution, the electronic structure of **47** and related complexes featuring bridging p-block elements are explored using a combination of computational and experimental techniques. Given that the coordinatively and electronically unsaturated nature of monomeric (BDI)Mn moieties render them capable of catalyzing hydrofunctionalization reactions,[8,12] the main goal of this research was to interrogate why this compound exhibits catalytic activity.

2.3. Results and Discussions

Electron counting was taken into account for **47**, noting that the absence of a metal-metal bond in the complex would result in 13 electrons around each Mn center. Due to the electron deficiency of the metal centers, Mn-Mn bonding was assumed to be present. In a recent patent, we proposed an alternative structure for **47** with a Mn≡Mn triple bond, which allows both metal centers to reach a 16-electron configuration.[13] A Mn-Mn distance of 2.8138(7) Å was revealed in the crystal structure of **47** (Figure 2.1),[8] which is shorter than the Mn-Mn single bond distance of 2.90 Å for $[Mn_2(CO)_{10}]$.[14] This hypothesis was also based on the EPR spectrum of **47** (taken at 106 K), which features a binuclear compound with two Mn(II) ($S_i = 5/2$) centers that are antiferromagnetically coupled. Three spin states S = 1, 2 and 3 were observed with an isotropic g-value (g_{iso} = 2.05), which is as expected for high-spin Mn(II) and indicates the presence of resonance structures (Figure 2.2).[8]
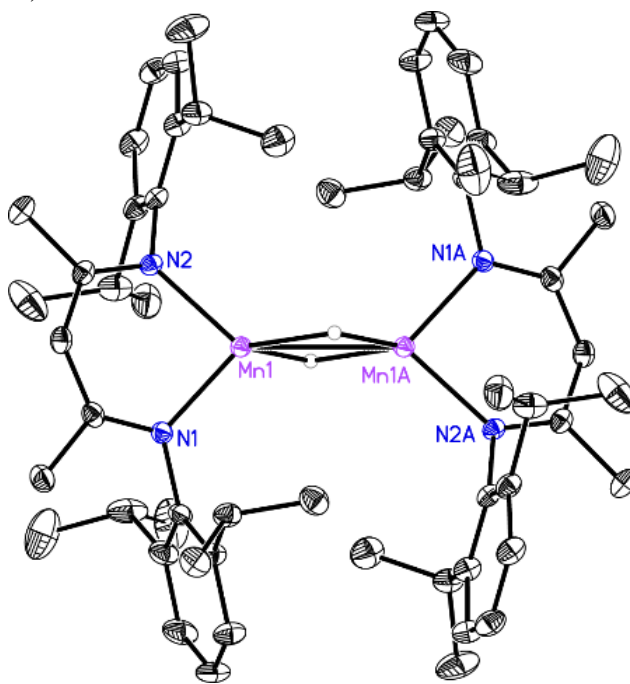
Figure 2.1. Solid-state structure of **47**.[8]
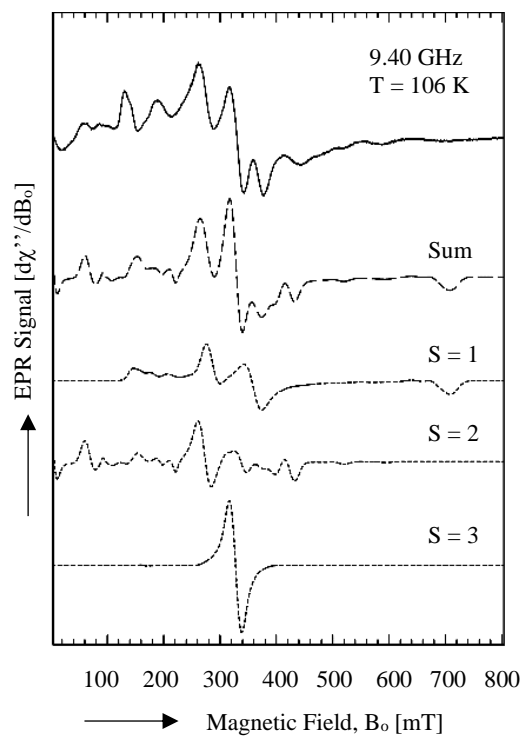
Figure 2.2. X-band EPR spectrum of **47**.[8]

Interestingly, DFT calculations performed by Baik and coworkers suggest a contrasting result, indicating that there are no actual bonds between the two metals in **47**. To clarify this investigation, conceptual MO diagrams of **47** were constructed and focused on the interaction of two Mn centers, without and with the contribution of hydrides (Figure 2.3, a and b, respectively). In both diagrams, the in-phase combinations of d_{xy}, d_{xz} and $d_{x^2-y^2}$ orbitals of the two Mn centers account for their triple bond, while non-bonding, bonding and antibonding MOs of d_{z^2} and d_{yz} are predicted to be almost degenerate, resulting in 4 unpaired electrons, which matches the solution magnetic susceptibility of 5.2 μ_B reported in our earlier paper.[8] When hydrides are taken into account (Figure 2.3b), the d_{xy} metal orbitals are considered to interact with the out-of-phase hydride s orbital combination, which causes d_{xy} to form σ^b and σ^* combinations. This interaction forces the initial Mn≡Mn triple bond electrons (Figure 2.3a) to

59

redistribute into the metal-hydride σ^b, which reduces the bond order from 3 to a range between 2 and 3. In addition, the Mn–Mn distance of 2.8138(7) Å in **47** is significantly longer than expected for a triple bond. Compounds featuring Mn≡Mn have been found to exhibit Mn–Mn distances of approximately 2.2 Å,[15,16] which suggests that the bond order for **47** is considerably lower than 3.

Via calculations, we found that **47** possess an antiferromagnetic, broken-symmetry ground state, and thermally accessible ferromagnetic excited states (the difference of electronic energy between S = 5 and the ground state was just 0.9 kcal/mol). Therefore, two extreme states including ferromagnetic (S = 5, **47-F**) and antiferromagnetic coupling (broken-symmetry $S = 0$, **47-AF**) between the metal centers were modelled for further evaluation. The pseudo-tetrahedral geometry around the Mn centers and two eclipsed β-diketiminate ligand fragments were reproduced. Table 2.1 shows the optimized geometries of **47-F** and **47-AF**, which are consistent with the crystal structure (**47-CS**). For both **47-F** and **47-AF**, the computed Mn–Mn distances are 2.871 Å, which is comparable to that of **47-CS** (2.814 Å). Noticeably, the Mayer bond orders for **47-F** and **47-AF** are 0.21 and 0.27, respectively, which indicate the absence of a multiple bond between the Mn centers. In addition, several interactions between metal-based orbitals and ligand orbitals were observed by analyzing MO-diagrams of **47-F** and **47-AF**, including the σ-interaction of d_{xy} with the out-of-phase hydride orbitals and BDI based orbitals, and of d_{z^2} with the in-phase hydride orbitals as well as between d_{xz} with ligand-based orbitals. The ligand-based orbitals were found to be antibonding with respect to the metal-based orbitals while the corresponding bonding combinations are much lower in energy and not depicted, which reveal that the interactions between BDI

ligands and metal centers are ultimately responsible for the low Mayer bond orders calculated for **47-F** and **47-AF**.
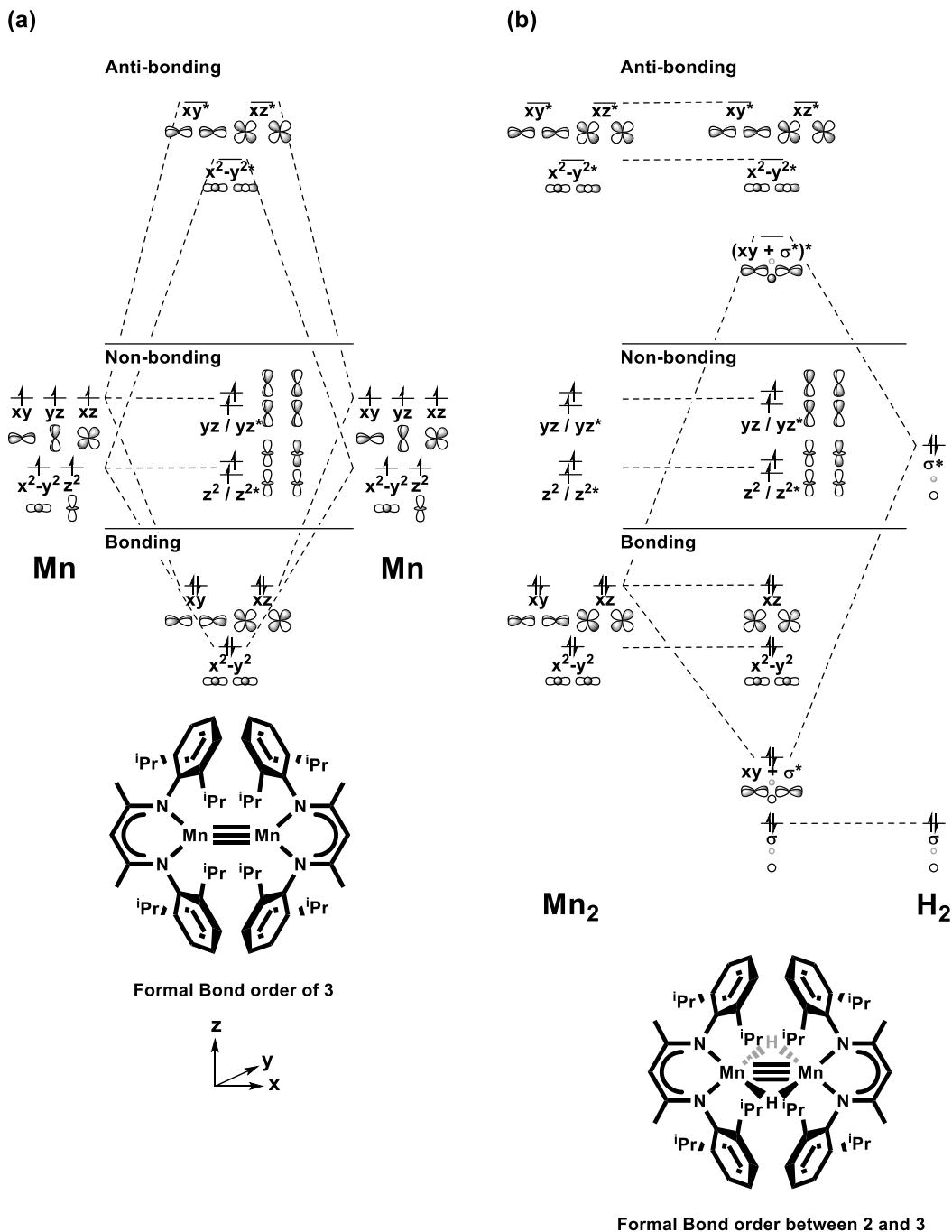
Figure 2.3. Conceptual MO diagram of **47** for a) Mn-Mn orbital interactions, and b) Mn-Mn orbital interactions including the contribution of hydrides.

Table 2.1. Optimized structural parameters of the dimanganese complexes **47-F**, **47-AF** and **47-CS.**
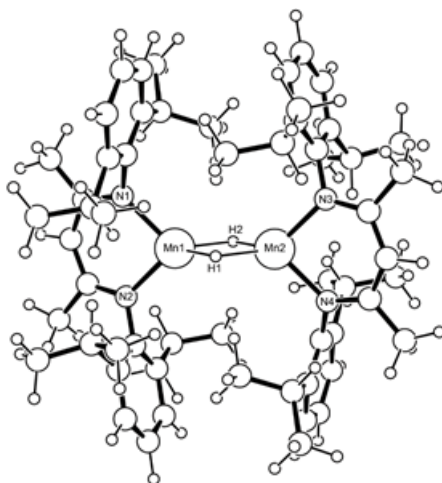
	47-F	47-AF	47-CS
	calc.	calc.	exp.
Spin-Coupling	F	AF	-
Mn1–H1 (Å)	1.897	1.834	1.791
Mn1–H2 (Å)	1.919	1.923	1.938
Mn1–N1 (Å)	2.099	2.103	2.086
Mn1–N2 (Å)	2.116	2.110	2.098
∠H1–Mn1–N2 (º)	116.9	120.5	121.1
∠N2–Mn1–N1 (º)	90.1	90.5	91.5
∠N1–Mn1–H2 (º)	121.9	119.8	118.3
∠H2–Mn1–H1 (º)	82.2	80.5	82.1
τ_4Mn1	0.86	0.85	0.85
Mn1–Mn2 (Å)	2.871	2.871	2.814
∠Mn1–H1–Mn2 (º)	97.5	99.6	97.9
Spin-Densities[a] Mn1	4.91	4.75	-
Spin-Densities[a] Mn2	4.91	- 4.75	-
Mayer Bond Order for Mn–Mn	0.21	0.27	-
Relative E_{SCF}[b] (kcal mol^{-1})	0.90	0	-

[a]Mulliken spin-density.

[b]The relative energies (kcal mol^{-1}) are referenced to the AF-coupled state.

2.3.1 *Determination of J_o*

To obtain further electronic structure information, J_o-value was determined via several methods. Computationally, a J_o-value of -10.9 cm^{-1} was calculated by Noodleman's broken-symmetry orbital method. This value is an order of magnitude lower than that of -110 cm^{-1} determined for $[(^{2,6-iPr_2Ph}BDI)Mn]_2$ by Roesky and co-workers, which features a dimer with a Mn-Mn single bond (2.7206 Å) and staggered BDI ligands.[17] The calculated J_o-value for **47** is also lower than the value of -47.5 cm^{-1} reported by Jones's group for a similar complex that features a single Mn-Mn bond arising from σ-interactions, $(L*Mn)_2$ (L* = -N(AR*)SiMe$_3$)).[18] An explanation for such weak coupling is strong superexchange interactions between the Mn centers mediated by the bridging hydrides, which possess a small ionic size and high symmetry *s*-orbital.
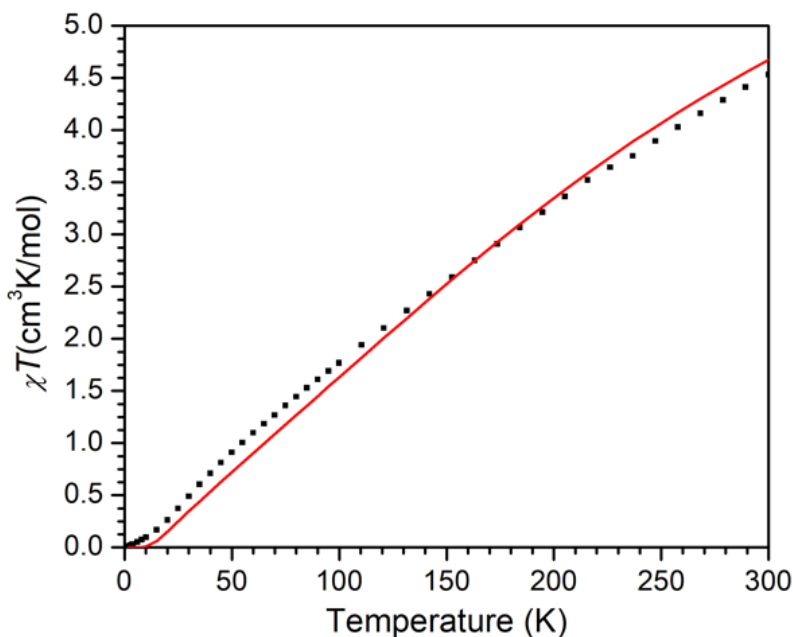
Figure 2.4. Temperature-dependent χT vs. *T* data for **47** collected under an applied field of 0.1 T. The red line is the fit where *g* is fixed at 2.05.

Experimentally, a SQUID experiment was performed by Anderson and colleagues. The data were collected at 0.1 T, between 1.8-300 K using the DAVE

program,[19] in which the Mn centers were considered as identical, isotropic, and spin-only in tetrahedral geometry with a spin of 5/2 (Figure 2.4). At room temperature, the solid-state χT value of **47** was found to be 4.5 cm^{3}K/mol (6 μ_B), which indicates a multiply bonded complex with antiferromagnetically coupled Mn centers and a lower overall spin state, or some intermediate case. Upon cooling, the χT value decreases, which is also an indication of antiferromagnetic coupling. The same trend was observed when a 1.0 T field was applied and a considerable increase of χT value was noticed when a sample of **1** was oxidized. Results reveal the best fit gives a *g*-value of 1.82 ± 0.25 and an antiferromagnetic coupling J_o-value of -15 cm^{-1} (± 0.1 cm^{-1}). Although the *g*-value determined from SQUID was slightly different from the initial EPR data (*g* = 2.05) and the reported *g*-values for normal Mn(II) (*g* ≈ 2.0), when the fit was restricted to *g* = 2.05 we obtain a J_o-value of 20 cm^{-1} (± 0.1 cm^{-1}), which is reasonable compared to literature values.[20]
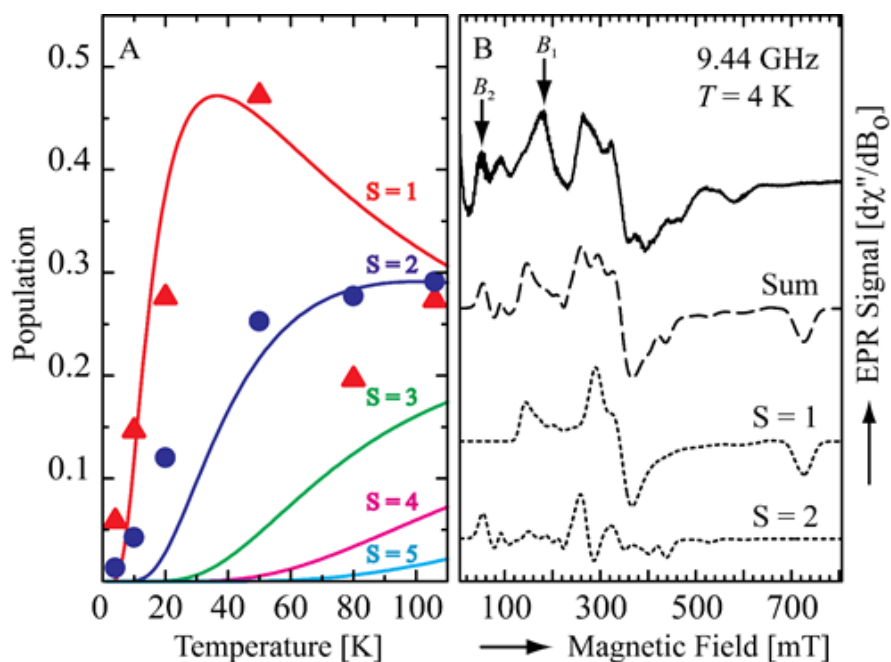
Figure 2.5. Spin state population of **47** at low temperatures determined by EPR.

To further support this finding, EPR experiments at varied temperature (4-106 K) were conducted (Figure 2.5). In particular, the temperature variation of the EPR intensity was determined by simultaneously simulating the EPR spectra of **47** at 6 different temperatures (Figure 2.5a), in which the EPR signals at 180 mT (B_1) and 60 mT (B_2) belong to the S = 1 and S = 2 spin manifolds, respectively. Figure 2.5b demonstrates the simulation of the spectrum at 4 K considering a superposition of two spin manifolds (S = 1 and S = 2). A J_o-value of -9.5 cm^{-1} was obtained when all the data points for five spin manifolds in Figure 2.5a were included in the fit, while a value of -10.8 cm^{-1} was determined if the data point corresponding to the EPR signal at B_1 (80 K) was not considered. Hence, the temperature dependent average J_o-value of -10.2 ± 0.7 cm^{-1} was obtained by X-band EPR spectroscopy. Overall, the experimental values determined by both SQUID and EPR are consistent with a J_o for weak antiferromagnetic coupling between the two metal centers in **47**.

2.3.2 *Influence of Steric Bulk and Extension to Ligands with p-Orbitals.*

The steric effect of bulky BDI ligands may sterically prohibit the proximal positioning of two Mn centers, which reduces the anticipated bond order between them. To validate this hypothesis, the most sterically simplified version of BDI was modeled, in which all the substituents are replaced with hydrogen atoms (**75**). Interestingly, it was revealed that substituents on the BDI framework do not influence the metal–metal bond order, with the corresponding Mayer bond order for the ferromagnetic (**75-F**) and antiferromagnetic (**75-AF**) compounds found to be 0.21 and 0.24, respectively. Since superexchange through the bridging hydrides was determined to have an impact on the bond order, and because the spherical 1s orbitals allow the in-phase combination of metal

d-orbitals, we decided to extend the study to bridging ligands with *p*-orbitals which have a node that precludes bonding between the Mn centers.

Table 2.2. Comparison of structural parameters of the optimized geometries of model compounds **75**, **76**, and **77**.
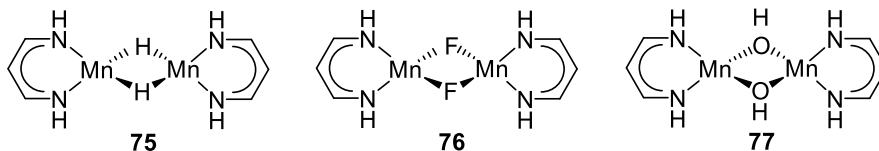
75   **76**   **77**

	75	76	77
Spin-Coupling	AF	AF	AF
Mn1–H1(O1, F1) (Å)	1.847	2.019	2.043
Mn1–H2(O2, F2) (Å)	1.856	2.019	2.043
Mn1–N1 (Å)	2.067	2.076	2.101
Mn1–N2 (Å)	2.067	2.077	2.102
∠H1(O1, F1)–Mn1–N2 (º)	121.6	121.8	130.0
∠N2–Mn1–N1 (º)	91.5	92.4	90.6
∠N1–Mn1–H2(O2, F2) (º)	121.1	121.7	122.6
∠H2(O2, F2)–Mn1–H1(O1, F1) (º)	82.3	80.8	81.3
τ_4Mn1	0.83	0.82	0.76
Mn1–Mn2 (Å)	2.789	3.074	3.100
∠Mn1–H1(O1, F1)–Mn2 (º)	97.7	99.2	98.7
Spin-Densities[a] Mn1	4.73	4.81	4.80
Spin-Densities[a] Mn2	- 4.73	- 4.81	- 4.80
Mayer Bond Order for Mn–Mn	0.24	0.02	0.03

[a]Mulliken spin-density

The difference in orbital interactions between the bridging ligands can contribute to the interaction between two Mn centers, therefore, compounds with bridging fluoride (**76**) and hydroxide ligands (**77**) were modelled. Table 2.2 demonstrates the calculations for these model compounds, in which the most noticeable feature is the elongated Mn–Mn distance from 2.789 Å (**75-AF**) to 3.074 Å and 3.100 Å for **76** and **77**, respectively. Increasing bond length leads to a significant decrease in the Mayer bond order from 0.24 (**75-AF**) to 0.02 (**76**) and 0.03 (**77**). Further study of the MO diagrams of **75**, **76** and **77**

revealed several interactions between metal d-orbitals and bridging ligand p-orbitals. In particular, d_{xy} orbitals which used to be responsible for Mn–Mn bonding are now mixed with p_x and p_y orbitals accounting for monoanionic and lone pair interactions. In addition, the symmetry in compounds **76** and **77** does not allow for bonding interaction between the two metal centers, which reduces Mn – Mn bond strength and increases the distance between them.

Calculations on these interactions also explain the stability of the dimeric compounds compared to their monomeric forms. The large electron densities located on the bridging anion contribute to an immense repulsion in the core composed of the Mn centers and bridging ligands, which outweighs the electrostatic interactions and makes the hydride compound the least stable among all the evaluated dimers. Despite the longer distances, p-orbital interaction in **76** and **77** is greater than that of the s-orbitals in **75**, hence the penalties in both non-orbital interactions and orbital interactions of **75** lead to the rise of electronic destabilization. Considering both the advantage in enthalpy and disadvantage in entropy involved in the dimerization process, the monomer-dimer Gibbs energy differences in **75**, **76**, and **77** at room temperature in benzene are 4.1, 16.5 and 24.6 kcal/mol, respectively. The energy difference for the fluoride and hydroxide congeners of **47**, [($^{2,6\text{-}i\text{Pr}_2\text{Ph}}$BDI)Mn($\mu$-F)]$_2$ (**78**) and [($^{2,6\text{-}i\text{Pr}_2\text{Ph}}$BDI)Mn($\mu$-OH)]$_2$ (**79**) are lower than their corresponding monomers by 22.6 and 28.8 kcal/mol, which is far more challenging to attain than the case of **47** (1.5 kcal/mol).
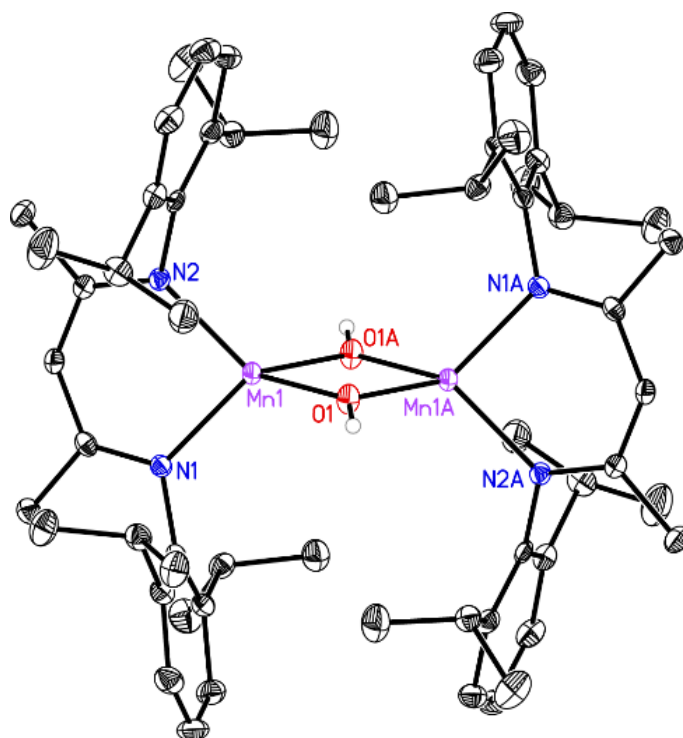
Figure 2.6. Solid-state structure of **79** at 30% probability ellipsoids.

To support the calculations conducted on model compounds, attempts were made to synthesize the fluoride- (**78**) and hydroxide-bridged dimer **79**. Unfortunately, compound **78** was not obtained from several methods. However, the slow addition of two equivalents of H_2O in cold THF solution to **47** resulted in the liberation of H_2 gas and a light-yellow product identified as $[(^{2,6\text{-}i\text{Pr}_2\text{Ph}}\text{BDI})\text{Mn}(\mu\text{-OH})]_2$ (**79**). Compound **79** was found to be paramagnetic with broadened ^{1}H NMR resonances over a range of 60 ppm. The magnetic susceptibility of **79** was analyzed by the Gouy method and determined to be 7.4 μ_B at 291 K. The deuterated version, $[(^{2,6\text{-}i\text{Pr}_2\text{Ph}}\text{BDI})\text{Mn}(\mu\text{-OD})]_2$ (**79**-d_2) was also isolated when when D_2O was employed in the synthesis. Notably, the hydroxide OH stretch of **79** at 3,695 cm^{-1} in the infrared spectrum is shifted to 2,726 cm^{-1} for the OD stretch of **79**-d_2. Recrystallization in THF afforded single crystals of **79** suitable for X-ray diffraction (Figure 2.6). The solid-state structure features a dimer with an inversion

center, eclipsed BDI ligands and an elongated Mn-Mn distance of 3.1426(9) Å, which is consistent with the computational bond distance of 3.189 Å. Interestingly, the hydrogen atoms of the hydroxide groups were in the difference map and their location was the same in two independent crystals.
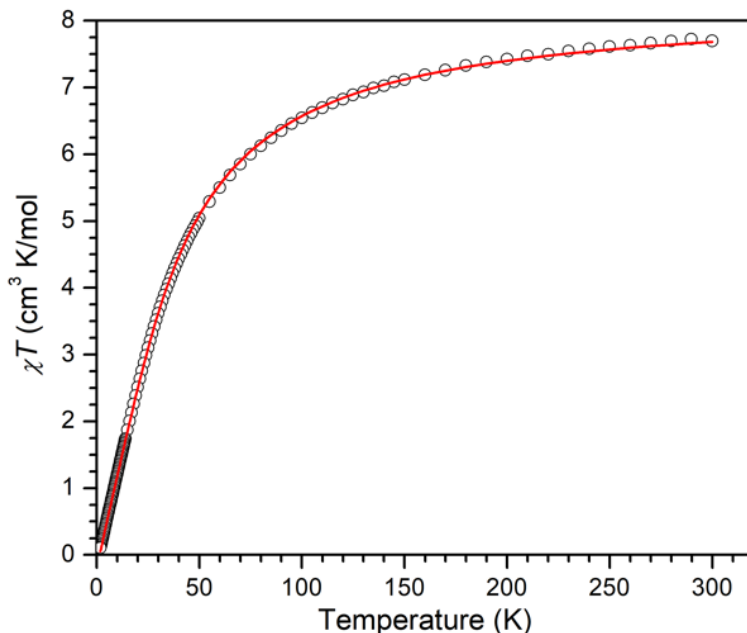
Figure 2.7. Temperature-dependent χT vs. T data for **79** collected under an applied field of 0.1 T. The red line is the fit where g is fixed at 2.05.

The electronic properties of **79** were also analyzed by SQUID magnetometry between 1.8-300 K (Figure 2.7). A χT value of 7.70 cm^{3}K/mol was determined at 298 K, which is lower than the spin-only value for two high-spin, uncoupled Mn(II) centers (χT_{SO} = 8.75 cm^{3}K/mol). The corresponding effective magnetic moment was found to be 7.8 μ_B at room temperature, which is consistent with that determined by Gouy method at 291 K (7.4 μ_B). The best fit was obtained when the g-value is 1.94 and J_o = -5 cm^{-1}, while fitting the data to g = 2.05 results in J_o-value of -4.3 cm^{-1}, which is in good agreement with the experimental data for weak antiferromagnetic coupling.

2.4. Conclusion

In conclusion, there are no bonds between the two Mn centers in **47**, hence, this complex remains a 13-electron compound. The interactions between metal- and ligand-based orbitals are the main factor inhibiting the formation of Mn-Mn bonds. Bridging ligands also impact the weak isotropic exchange coupling between the metal centers due to the interaction of p-orbitals and metal d-orbitals elongating the metal-metal distance. These findings explain why **47**, which features bridging hydrides, is more catalytically effective than compounds with other bridging ligands due to the low activation energy needed to access the more active monomeric form, ($^{2,6-iPr_2Ph}$BDI)MnH.

2.5. Experimental Procedure

Computational detail

All calculations were performed using density functional theory (DFT) as implemented in the Jaguar 9.1 suite of ab initio quantum chemistry programs. The B3LYP functional with Grimme's D3 dispersion correction (B3LYP-D3) was employed as the standard, together with the 6-31G** basis set for geometry optimizations. The Los Alamos LACVP basis was used to represent manganese. In order to obtain more reliable energies, single point calculations were performed on the optimized geometries using Dunning's correlation-consistent triple-ζ cc-pVTZ(-f) basis set for main group elements and LACV3P for manganese. The zero-point energy (ZPE), entropic and solvation contributions to the Gibbs energy are obtained from the same level of theory as the geometry optimizations (B3LYP-D3/6-31G**/LACVP). Energy decomposition was computed with the B3LYP-D3 functional using the Amsterdam Density Functional (ADF 2019) package. The

optimized geometries were confirmed to be the local minima on the potential energy surfaces by showing the absence of an imaginary frequency. The solvation calculations utilized a self-consistent reaction field (SCRF) approach on the gas phase geometry to model the solvation shell of dielectric constants $\varepsilon = 2.284$ for benzene and $\varepsilon = 2.397$ for toluene. As is the case for all continuum models, the solvation energies are subject to empirical parametrization of the atomic radii that are used to generate the solute surface. We employed the standard set of optimized radii in Jaguar for H (1.150 Å), C(1.900 Å), N(1.600 Å), O(1.600 Å), F(1.682 Å) and Mn(1.480 Å).

The energy components have been computed with the following protocol. The free energy in solution phase $G_{(sol)}$ has been calculated as follows:

$$G_{(sol)} = G_{(gas)} + G_{(solv)} \quad (1)$$

$$G_{(gas)} = H_{(gas)} - TS_{(gas)} \quad (2)$$

$$H_{(gas)} = E_{(SCF)} + ZPE \quad (3)$$

$$\Delta E_{(SCF)} = \Sigma E_{(SCF)} \text{ for products} - \Sigma E_{(SCF)} \text{ for reactants} \quad (4)$$

$$\Delta G_{(sol)} = \Sigma G_{(sol)} \text{ for products} - \Sigma G_{(sol)} \text{ for reactants} \quad (5)$$

$G_{(gas)}$ is the gas phase free energy; $G_{(solv)}$ is the free energy of solvation; $H_{(gas)}$ is the gas phase enthalpy; T is the temperature (298.15 K); $S_{(gas)}$ is the gas phase entropy; $E_{(SCF)}$ is the electronic energy derived from the SCF method and ZPE is the zero-point energy.

In principle, multi-reference methods such as CASSCF are required to rigorously describe an antiferromagnetically coupled spin state of the dimer, which

71

is impracticable for systems of this size because of computational demands. In practice, Noodleman's broken-symmetry (BS) approach, which makes use of the Heisenberg spin operator formalism to obtain a reasonable electronic structure description of transition metal dimers, provides a working protocol for single reference methods such as DFT employing the unrestricted spin formalism. We carefully followed the protocol described elsewhere to obtain the BS orbitals and used the unrestricted spin formalism in all calculations. Essentially, the valence bond descriptions of the molecules were used as initial guesses to generate a molecular wavefunction in terms of localized orbitals that undergo the SCF procedure.

Experimental detail

All reactions were performed inside an MBraun glovebox under an atmosphere of purified nitrogen. Toluene, tetrahydrofuran, diethyl ether, and pentane were purchased from Sigma-Aldrich, purified using a Pure Process Technology solvent system, and stored in the glovebox over activated 4 Å molecular sieves and potassium before use. Celite was obtained from Oakwood Chemicals. $[(^{2,6-i\text{Pr}_2\text{Ph}}\text{BDI})\text{Mn}(\mu\text{-H})]_2$ (**47**)[8] was synthesized according to the literature procedure. Elemental analysis was performed at Robertson Microlit Laboratories Inc. (Ledgewood, NJ). Ambient temperature solid-state magnetic susceptibility was recorded using a Johnson Matthey magnetic susceptibility balance calibrated with HgCo(SCN)_4 and $\text{K}_3\text{Fe(CN)}_6$. Infrared spectra were collected on a Bruker VERTEX 70 spectrophotometer with an MCT detector.

SQUID Magnetometry

Bulk magnetometry measurements were carried out on a Quantum Design MPMS 3 equipped with a superconducting quantum interference device (SQUID)

detector. Corrections were made for the diamagnetic contributions from the polycarbonate capsules and eicosane wax used to secure the sample by measuring temperature vs. moment in triplicate for each to determine a moment per gram correction. Diamagnetic corrections for the complex were made using Pascal's constants.

Fitting of the χT vs. T data to the Hamiltonian ($\hat{H} = g_1\mu_B\mathbf{S}_1.\mathbf{B}_o + g_2\mu_B\mathbf{S}_2.\mathbf{B}_o - 2J_oh\mathbf{S}_1.\mathbf{S}_2$) was carried out using both MagProp analysis software within the DAVE suite. Note that MagProp uses a convention of $-J_oh\mathbf{S}_1.\mathbf{S}_2$ for the exchange term, however it was normalized to the $-2J_oh\mathbf{S}_1.\mathbf{S}_2$ convention. The g values were constrained to be isotropic ($g_x = g_y = g_z$), and equivalent ($g_1 = g_2$).

EPR Spectroscopy

Instrumentation. Studies were performed at the EPR Facility of Arizona State University. Continuous wave (CW) EPR spectra were recorded between 4 K and 106 K using a Bruker ELEXSYS E580 CW X-band spectrometer (Bruker, Rheinstetten, Germany) equipped with a Model ESR900 liquid helium cryostat (Oxford Instruments, Oxfordshire, UK). The magnetic field modulation frequency was 100 kHz with a field modulation amplitude of 1 mT peak-to-peak. The microwave power was 1 mW, the microwave frequency was 9.44 GHz, and the sweep time was 168 seconds.

Spin Hamiltonian. The EPR spectra of a coupled dimer system can be described with the spin Hamiltonian:

$$H = -2J_o\, h\mathbf{S}_1.\mathbf{S}_2 + h\mathbf{S}_1.\boldsymbol{J}.\mathbf{S}_2 + H_1 + H_2 \quad (6)$$

where J_o is the isotropic exchange coupling constant between the two Mn(II) ions of the dimer, $\boldsymbol{J}$ is the tensor describing the dipole-dipole interaction between the two Mn(II) spin centers, both in frequency units, h is Planck's constant, and H_i (i = 1, 2) are the spin Hamiltonians corresponding to each individual Mn(II) ion. The spin Hamiltonian of each Mn(II) spin center contains the electron Zeeman interaction with the applied magnetic field $\mathbf{B_o}$, the zero-field interaction, and the hyperfine coupling interaction with the nucleus of ^{55}Mn:

$$H_i = \mu_B \mathbf{S_i} \boldsymbol{g_i} \mathbf{B_o} + h \mathbf{S_i} \boldsymbol{d_i} \mathbf{S_i} + h \mathbf{S_i} \boldsymbol{a_i} \mathbf{I_i} \quad (7)$$

where $\mathbf{S_i}$ and $\mathbf{I_i}$ are the electron and nuclear spin operators, respectively, $\boldsymbol{d_i}$, and $\boldsymbol{a_i}$ are the zero-field splitting and hyperfine coupling tensors, respectively, all in frequency units, $\boldsymbol{g_i}$ is the electronic g-tensor, and μ_B is the electron magneton. For Mn(II) dimers, the electron and nuclear spins of each Mn(II) ion are $S_i = 5/2$ and $I_i = 5/2$, respectively. Mn(II) ions have a singlet orbital ground state (^{6}A), with the first excited orbital state (^{4}T) more than 10,000 cm^{-1} above the ground state. Consequently, the zero-field energies of Mn(II) ions are generally small, $|D_i| < 0.1$ cm^{-1}. For dimeric manganese complexes, the bridging atoms typically give a Mn–Mn exchange interaction that is significantly larger than 0.1 cm^{-1}. In this strong exchange regimen, the isotropic exchange coupling energy is much larger than the electronic Zeeman energy ($|J_o| \gg g_i \mu_B B_o / h$) and the zero-field splitting ($|J_o| \gg |D_i|$). The dimer system may then be regarded as a ladder of isolated spin manifolds. These spin manifolds have total spin quantum numbers of $S = 0, 1, 2, 3, 4,$ and 5, each with a degeneracy of (2S+1). The energy separation between the spin manifolds is much larger than the microwave energy ($h\upsilon$) at the X-band (9.40 GHz) frequency and no

transitions are observable between spin manifolds. The individual spin manifolds can be considered independently, and their corresponding spectra can be simulated using a spin Hamiltonian for each individual spin manifold given by:

$$H_S = \mu_B \mathbf{S}.\boldsymbol{G}_S.\mathbf{B_o} + h\mathbf{S}.\boldsymbol{D}_S.\mathbf{S} + h\mathbf{S}.\boldsymbol{A}_1.\mathbf{I}_1 + h\mathbf{S}.\boldsymbol{A}_2.\mathbf{I}_2 \ (8)$$

where $\boldsymbol{G}_S$, $\boldsymbol{D}_S$ and $\boldsymbol{A}_i$ (i = 1, 2) are the electronic Zeeman, zero-field splitting, and hyperfine coupling tensors, respectively, of the spin manifolds of the coupled system, and $\mathbf{S}$ is the spin operator of the coupled spin manifolds. The parameters of the coupled spin system can be expressed as linear combinations of the parameters of the individual spin centers:

$$\boldsymbol{G}_S = c_1\boldsymbol{g}_1 + c_2\boldsymbol{g}_2 \ (9)$$

$$\boldsymbol{D}_S = d_1\boldsymbol{d}_1 + d_2\boldsymbol{d}_2 + d_{12}\boldsymbol{J} \ (10)$$

$$\boldsymbol{A}_i = c_i\boldsymbol{a}_i \ (11)$$

where the coefficients c_1, c_2, d_1, d_2, and d_{12} are specific to the particular spin manifold and have been tabulated elsewhere. For Mn(II) ions, the contributions from spin–orbit coupling to the $\boldsymbol{g}_i$ tensor and hyperfine coupling tensor are small, thus we will assume that both tensors $\boldsymbol{g}_i$ and $\boldsymbol{A}_i$ are isotropic. In the complex studied here, the two manganese centers of the dimer have identical ligation. The coordination geometry of one manganese ion is related to the other by a mirror plane, thus, we assume $g_1 = g_2 = g_{iso}$, $a_1 = a_2 = a$, and $\boldsymbol{d}_1 = \boldsymbol{d}_2$. In this study, hyperfine couplings due to Mn(II) were not explicitly included in the spin Hamiltonian (Eq. 9) since they were not well resolved in most of the experimental spectra. Furthermore, the

individual spin manifolds do not contribute equally to the resulting spectrum at a particular temperature, T, because of their different Boltzmann populations. For antiferromagnetic isotropic exchange coupling (i.e. $J_o < 0$), the coefficient describing the Boltzmann population of an individual spin manifold S at thermal equilibrium and zero field is given by:

$$n_S(J_o,T) = (2S+1)\exp[hS(S+1)J_o/kT]/Z \ (12)$$

where k is Boltzmann's constant and Z is the partition function defined by:

$$Z = 1 + 3\exp(2hJ_o/kT) + 5\exp(6hJ_o/kT) + 7\exp(12hJ_o/kT) + 9\exp(20hJ_o/kT) + 11\exp(30hJ_o/kT) \ (13)$$

Equation 13 shows that at very low temperature ($kT << |J_o|$) only the $S = 0$ spin manifold is populated, and consequently no EPR signal is observed. Upon increasing the temperature, the other spin manifolds gradually become populated and contribute to the EPR spectra. At high temperature ($kT >> |J_o|$), a superposition of signals, originating from all spin manifolds, is observed.

Fitting of EPR spectra. To quantitatively compare experimental and simulated spectra, we divided the spectra into N intervals (i.e., we treated the spectrum as an N-dimensional vector **R**). Each component R_j has the amplitude of the EPR signal at a magnetic field B_j, with j varying from 1 to N. The amplitudes of the experimental and simulated spectra were normalized so that the span between the maximum and minimum values of R_j is 1. We compared the calculated amplitudes R_j^{calc} of the signal with the observed values R_j defining a root-mean-square deviation by:

$$\sigma(p_1, p_2,\ldots, p_n) = [\Sigma \ (R_j^{calc}(p_1, p_2, \ldots, p_n) - R_j^{exp})^2/N]^{1/2} \ (14)$$

where the sums are over the N values of j, and p's are the fitting parameters that produced the calculated spectrum. For our simulations, N was set equal to 2048. The EPR spectra were simulated using EasySpin (v 5.2.25), a computational package developed by Stoll and Schweiger and based on Matlab (The MathWorks, Natick, MA, USA). EasySpin calculates EPR resonance fields using the energies of the states of the spin system obtained by direct diagonalization of the spin Hamiltonian (see Eq. 9). The EPR fitting procedure used a Monte Carlo type iteration to minimize the root-mean-square deviation, σ (see Eq. 14) between measured and simulated spectra. We searched for the optimum values of the following parameters: the isotropic g-value (g_{iso}), the zero-field splitting parameters (D and E), the principal components of the $\boldsymbol{J}$ tensor ($J_{x'}$, $J_{y'}$ and $J_{z'}$) and the isotropic peak-to-peak linewidth (ΔB).

Preparation of [($^{2,6-iPr2Ph}$BDI)Mn(μ-OH)]$_2$ (79): A 20 mL vial was charged with **47** (117.1 mg, 0.1237 mmol) dissolved in 10 mL THF and cooled to 238 K. A solution of H_2O (4.5 μL, 0.247 mmol) in 5 mL THF was cooled at 238 K. After 30 minutes, the solution of H_2O was added dropwise to the solution of **47** while stirring. A colour change from yellowish-orange to light yellow was noticed along with the liberation of H_2 gas. Then, the mixture was filtered through celite, and the solvent was removed under vacuum to obtain a yellow solid. The solid was washed thoroughly with Et_2O and recrystallized from THF upon cooling to 238 K, affording yellow crystals of **79** (37.8 mg, 0.038 mmol). The Et_2O wash solution was also cooled to 238 K, affording an additional quantity of **79** (13.4 mg, 0.0136 mmol). The total yield was 42%. The

deuterated variant, $[(^{2,6-iPr_2Ph}BDI)Mn(\mu\text{-OD})]_2$ (**79**-d_2), was prepared in a similar fashion using D_2O.

Elemental analysis for $C_{58}H_{84}O_2N_4Mn_2$: Calcd. C, 71.14; H, 8.65; N, 5.72. Found: C, 70.35; H, 8.76; N, 5.94.

Magnetic susceptibility (Gouy method, 291 K): $\mu_{eff} = 7.4\,\mu B$ (considering a dimeric structure).

Infrared (KBr): $\upsilon_{OH} = 3,695\ cm^{-1}$, $\upsilon_{OD} = 2,726\ cm^{-1}$.

2.6. References

(1) Power, P. P. *Chem. Rev.* **2012**, *112* (6), 3482–3507.

(2) Power, P. P. *J. Org. Chem.* **2004**, *689* (24), 3904–3919.

(3) Holland, P. L. *Acc. Chem. Res.* **2008**, *41* (8), 905–914.

(4) Chen, C.; Bellows, S. M.; Holland, P. L. *Dalton Trans.* **2015**, *44* (38), 16654–16670.

(5) Webster, R. L. *Dalton Trans.* **2017**, *46* (14), 4483–4498.

(6) Basuli, F.; Aneetha, H.; Huffman, J. C.; Mindiola, D. J. *J. Am. Chem. Soc.* **2005**, *127* (51), 17992–17993.

(7) Vela, J.; Smith, J. M.; Yu, Y.; Ketterer, N. A.; Flaschenriem, C. J.; Lachicotte, R. J.; Holland, P. L. *J. Am. Chem. Soc.* **2005**, *127* (21), 7857–7870.

(8) Mukhopadhyay, T. K.; Flores, M.; Groy, T. L.; Trovitch, R. J. *Chem. Sci.* **2018**, *9* (39), 7673–7680.

(9) Chai J.; Zhu, H.; Fan, H.; Roesky H. W.; Magull, J. *Organometallics*, **2004**, *23*, 1177.

(10) Chai, J.; Zhu, H.; Stückl, A. C.; Roesky, H. W.; Magull, J.; Bencini, A.; Caneschi, A.; Gatteschi, D. *J. Am. Chem. Soc.*, **2005**, *127*, 9201.

(11) Yao, S.; Xiong, Y.; Driess, M. *Chem. Eur. J.*, **2012**, *18*, 11356.

(12) Nguyen, T. T.; Kim, J.-H.; Kim, S.; Oh, C.; Flores, M.; Groy, T. L.; Baik, M.-H.; Trovitch, R. J. *Chem. Commun.* **2020**, *56*, 3959.

(13) Trovitch, R. J.; Nguyen, T. T.; Mukhopadhyay, T. K.; Glazier, B. M. U.S. Patent 11,273,432, **2022**.

(14) Bianchi, R.; Gervasio, G.; Marabello, D. *Inorg. Chem.* **2000**, *39*, 11, 2360–2366.

(15) Bernal, I.; Korp, J. D.; Herrmann, W. A.; Serrano, R. *Chem. Ber.* **1984**, *117* (2), 434–444.

(16) Ashley, A. E.; Cooper, R. T.; Wildgoose, G. G.; Green, J. C.; O'Hare, D. *J. Am. Chem. Soc.* **2008**, *130* (46), 15662–15677.

(17) Chai, J.; Zhu, H.; Most, K.; Roesky, H. W.; Vidovic, D.; Schmidt, H.-G.; Noltemeyer, M. *Eur. J. Inorg. Chem.* **2003**, *2003* (24), 4332–4337.

(18) Hicks, J.; Hoyer, C. E.; Moubaraki, B.; Li Manni, G.; Carter, E.; Murphy, D. M.; Murray, K. S.; Gagliardi, L.; Jones, C. *J. Am. Chem. Soc.* **2014**, *136* (14), 5283–5286.

(19) Azuah, R. T.; Kneller, L. R.; Qiu, Y.; Tregenna-Piggott, P. L. W.; Brown, C. M.; Copley, J. R. D.; Dimeo, R. M. *J. Res. Natl. Inst. Stand. Technol.* **2009**, *114* (6), 341–358.

(20) Bossek, U.; Nühlen, D.; Bill, E.; Glaser, T.; Krebs, C.; Weyhermüller, T.; Wieghardt, K.; Lengen, M.; Trautwein, A. X. *Inorg. Chem.* **1997**, *36* (13), 2834–2843.

CHAPTER 3

SYNTHESIS OF AMINOSILANE CHEMICAL VAPOR DEPOSITION

PRECURSORS AND POLYCARBOSILAZANES THROUGH MANGANESE

CATALYZED Si–N DEHYDROCOUPLING

3.1. Abstract

Compounds that feature Si–N bonds are of widespread importance to the electronics and coatings industries. Aminosilanes and polysilazanes are currently prepared by adding amines to halosilanes, an inefficient methodology that generates stoichiometric quantities of ammonium salt waste. Herein, we describe the syntheses of aminosilane chemical vapor deposition precursors, polycarbosilazanes, and perhydropolysilazane through the ambient temperature dehydrocoupling of amines to silane (SiH_4). Specifically, the β-diketiminate manganese hydride dimer $[(^{2,6-iPr_2Ph}BDI)Mn(\mu\text{-}H)]_2$ has been used to catalyze the formation of commercial aminosilane monomers from secondary and primary amines, highly cross-linked polycarbosilazane powders from diamines and triamines, and perhydropolysilazane from ammonia. The mechanism of dehydrocoupling was explored and the addition of isopropylamine to $[(^{2,6-iPr_2Ph}BDI)Mn(\mu\text{-}H)]_2$ resulted in σ-bond metathesis to eliminate H_2 and generate $[(^{2,6-iPr_2Ph}BDI)Mn(\mu\text{-}NHiPr)]_2$. In the presence of SiH_4, H–Si addition across newly formed Mn–N bonds regenerates the precatalyst, offering a straightforward catalytic cycle for halogen-free Si–N bond formation.

3.2. Introduction

Silicon nitride and silicon carbonitride coatings are widely used in industry because they offer a unique combination of chemical stability and superior mechanical properties.[1,2] These films exhibit outstanding electrical resistivity (10^{12}-10^{17} $\Omega \cdot$cm) and high dielectric strength (10^6-10^7 V/cm), rendering them ideal for protecting microelectronics, photonic devices, and solar cells.[3] Silicon nitride and silicon carbonitride thin films can be prepared using atomic layer deposition (ALD), chemical vapor deposition (CVD), and plasma-enhanced chemical vapor deposition (PECVD). Silicon nitride films obtained by ALD, CVD, and PECVD are essential for the production of integrated circuitry, microprocessors, and memory devices.[4–7]

The most common silicon sources for CVD and ALD include perhydridosilanes, hydridohalosilanes, halosilanes, and aminosilanes. High quality silicon nitride films can be obtained directly from SiH_4 and NH_3 above 300 °C,[3] or at lower temperatures (100–110 °C) by microwave PECVD.[8] Despite their corrosive nature, hydridohalosilanes and halosilanes including SiH_2Cl_2,[9] SiH_2I_2,[10] Si_2Cl_6[11] are often employed under forcing conditions (Figure 3.1, a). Aminosilanes, which can be handled as liquids near ambient conditions, are versatile precursors that can afford either silicon nitride or silicon carbonitride films.[12,13] Unfortunately, aminosilanes are themselves prepared by reacting corrosive iodosilanes[14] or chlorosilanes[15] with the respective amine (Figure 3.1, b). Alternatively, silicon nitride films can be synthesized by pyrolyzing perhydropolysilazane (PHPS, Figure 3.1, c). Once applied to a surface, this polymer can be cross-linked at 200–500 °C to form an amorphous ceramic layer that crystallizes at higher temperatures (700–1260 °C).[16] When hydrolysis is allowed to occur during PHPS curing, silicon oxynitride

81

and silicon dioxide layers are generated,[17,18] which are particularly useful gate dielectrics for thin film transistors.[19] Industrially, PHPS solutions are prepared by reacting chlorosilanes with excess NH_3 in polar solvents such as Et_2O, THF, or DCM.[20,21] Although this approach is straightforward, it is inherently atom-inefficient since one equivalent of NH_4Cl waste is generated for each Si–N bond that is formed, leading to additional purification measures that compromise sustainability and add to process cost.
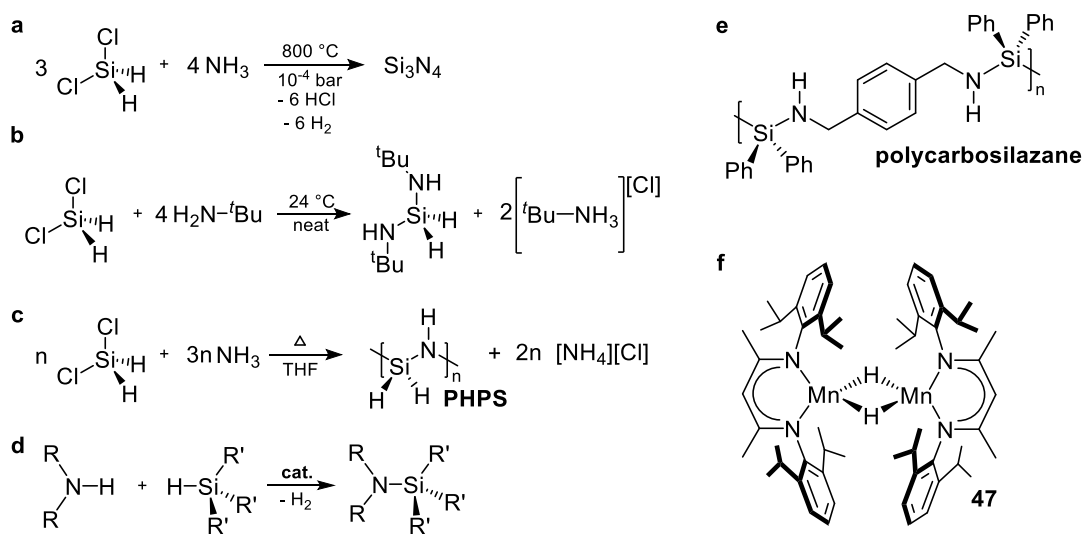
Figure. 3.1. Methods of preparing Si–N bonds, a representative polycarbosilazane, and the catalyst used in this contribution. a) Preparation of silicon nitride from SiH_2Cl_2 and NH_3. B) Atom-inefficient synthesis of aminosilane CVD precursor $H_2Si(NHtBu)_2$. c) Use of SiH_2Cl_2 to prepare PHPS. d) Generation of Si–N bonds via dehydrocoupling. e) Polycarbosilazane prepared by Carpentier and Sarazin. f) Previously described Mn catalyst **47**.

The dehydrogenative coupling of amines and silanes has long been considered a promising approach to Si–N bond formation that avoids halosilanes (Figure 3.1, d).[22,23] Over the last decade, catalysts featuring elements that span the periodic table including alkaline-earth metals,[24–27] lanthanides,[28] Zn,[29] Pt,[30] and Al[31] have been reported to mediate this transformation. While these studies have used organosilanes to prepare aminosilane monomers, researchers have also demonstrated the preparation of oligocarbosilazanes or

polycarbosilazanes using substrates that feature more than one amine functionality. In 2016, Carpentier and Sarazin found that $Ba[CH(SiMe_3)_2]_2(THF)_3$ is an effective catalyst for the dehydrogenative coupling of diphenylsilane and *p*-xylylenediamine to prepare polycarbosilazanes (Figure 3.1, e).[32] This catalyst was shown to generate oligocarbosilazanes in subsequent work.[33] In 2019, the Manners and Hill groups expanded this reactivity to the preparation of ferrocene-containing polycarbosilazanes that yielded magnetic ceramic materials upon pyrolysis.[34] Recently, Webster and co-workers prepared an oligocarbosilazane from 1,4-benzenedimethanamine and phenylsilane using the β-diketiminate iron catalyst, $(^{2,6-iPr_2Ph}BDI)Fe(CH_2TMS)$.[35] The oligomers and polymers described in these studies are promising surrogates for industrial organic polysilazanes, which afford thermally-robust and corrosion-resistant coatings on metal surfaces.[36]

In 2018, we reported the synthesis, hydrosilylation activity, and silicone curing ability of the β-diketiminate manganese hydride dimer, $[(^{2,6-iPr_2Ph}BDI)Mn(\mu-H)]_2$ (**47**, Figure 3.1, f).[37] An electronic structure investigation revealed that **47** easily dissociates into monomers to enable catalysis.[38] In this study, we demonstrate that **47** is active for the dehydrogenative coupling of amines to the widely utilized industrial gas, SiH_4. In the patent literature, the halogen-free preparation of aminosilane CVD precursors is known to proceed upon heating amines with SiH_4 to 125 °C in the presence of Ru/C;[39] however, this remains the only mention of commercial aminosilane CVD precursor synthesis by way of catalytic Si–N dehydrocoupling. With SiH_4 chosen as the silane source, this contribution details the atom-efficient and halogen-free preparation of aminosilane CVD precursors, polycarbosilazanes, and PHPS at ambient temperature. Taken together, the experiments

described herein are believed to be the only reported examples of Mn-catalyzed Si–N dehydrocoupling.

3.3. Results and Discussions

3.3.1. Preparation of CVD Precursors.

The preparation of industrially-relevant aminosilanes via dehydrocoupling requires the use of SiH_4 and this starting material can afford a variety of products depending on the number of Si–H bonds that react. Therefore, to minimize complexity, our initial trials focused on the dehydrocoupling of secondary amines that cannot undergo oligomerization or polymerization (Table 3.1). Using a calibrated gas bulb and high-vacuum line, dimethylamine gas (**1a**) was added to a J. Young tube containing 2 mol% of **47** (4 mol% of Mn) in a toluene-d_8 solution featuring 0.2 M tetramethylsilane as an internal standard. To this frozen solution, 1 atm of SiH_4 was added and the reaction was allowed to warm to ambient temperature. After 24 h, greater than 99% conversion of **1a** to a mixture of silylamine products was observed by ^{1}H NMR spectroscopy. Integration against the standard revealed a 73% NMR yield of diaminosilane product $H_2Si(NMe_2)_2$ (**A**, ^{29}Si NMR = -21.54 ppm) and triaminosilane product $HSi(NMe_2)_3$ (**B**, ^{29}Si NMR = -25.09 ppm) in a 1:2.5 ratio. At this point, the experiment was safely decommissioned by freezing the solution in liquid N_2, removing H_2 gas from the headspace, and then recollecting or slowly quenching the residual SiH_4. ***Caution: Silane is a pyrophoric gas that must be handled with care by a skilled experimentalist; for detailed experimental procedures and additional safety disclosures, please consult the Experimental Procedures.***

Table 3.1. Synthesis of CVD precursors via **47**-catalyzed dehydrocoupling of amines and SiH$_4$.
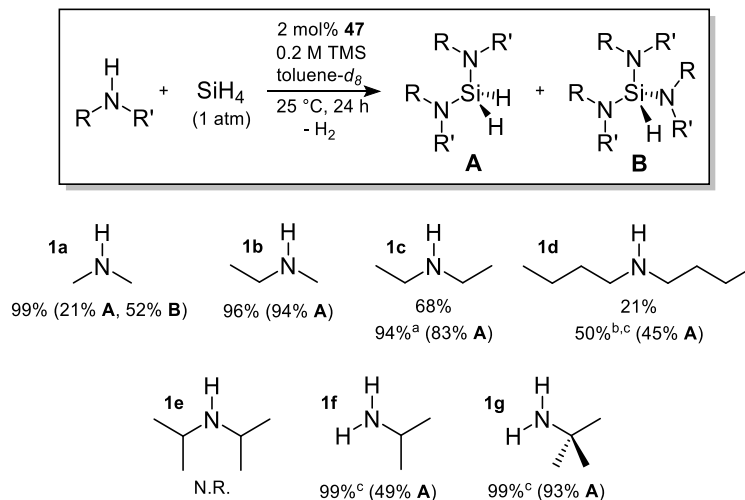
Percent conversion determined by ^{1}H NMR spectroscopy (integration of residual amine vs. silylamine product). NMR yields determined by integration of product against 0.2 M tetramethylsilane standard (shown in parentheses). ^{a}Trial conducted for 48 h. ^{b}Trial conducted for 4 days. ^{c}Trial conducted in a 100 mL bomb instead of J. Young tube.

Using a similar procedure, the steric hinderance of the amine was systematically varied. The **47**-mediated dehydrocoupling of methylethylamine (**1b**) to SiH$_4$ afforded H$_2$Si(NMeEt)$_2$ as the sole product in excellent yield. The dehydrocoupling of diethylamine (**1c**) reached 68% conversion after 24 h; however, allowing the reaction to proceed for 48 h allowed for 94% conversion and the selective formation of H$_2$Si(NEt$_2$)$_2$. Further lengthening of the alkyl chains to butyl (**1d**) considerably slowed dehydrocoupling, resulting in only 50% conversion to H$_2$Si(NBu$_2$)$_2$ after 4 days, even when the reaction was performed in a 100 mL thick-walled glass bomb under a large excess of SiH$_4$. No reaction was observed at 25 °C in the case of diisopropylamine (**1e**), further demonstrating that steric bulk about the amine inhibits catalysis. After reaching the steric limit of secondary amine dehydrocoupling, we sought to prepare CVD precursors from isopropylamine (**1f**) and *tert*-butylamine (**1g**). When these trials were performed in a J. Young tube, toluene-

insoluble polymers were generated, which prevented solution NMR analysis of the product mixture. By repeating these reactions under a large excess of SiH_4, polymerization was suppressed, affording $H_2Si(NHiPr)_2$ in modest yield and $H_2Si(NHtBu)_2$ in high yield. Importantly, $HSi(NMe_2)_3$, $H_2Si(NEt_2)_2$, and $H_2Si(NHtBu)_2$ are commercial CVD precursors for silicon nitride films that are currently prepared from halosilanes.[40,41]

3.3.2. Preparation of SiH$_4$-Derived Polycarbosilazanes.

Since polymers were observed when dehydrocoupling primary amines under low SiH_4 pressure, we purposely sought to prepare and characterize polycarbosilazane polymers from substrates that feature more than one amine functionality (Table 3.2). In a 100 mL thick-walled glass bomb, 1 atm of SiH_4 was added to a benzene solution of ethylenediamine and 2 mol% of **47**. After 2 h at 25 °C, precipitate was observed, and the transformation was allowed to proceed for an additional 22 h to ensure reaction completion. Upon washing with THF to remove residual catalyst, a tan solid identified as polycarbosilazane **2a** was obtained in 60% yield. Product **2a** is highly cross-linked and insoluble in organic solvents, properties that prevent solution-state ^{1}H NMR end-group analysis and estimation of number average molecular weight by ^{1}H DOSY NMR spectroscopy.[33] Subjecting a 1 mg sample of **2a** to THF for 1 week did not allow for observable dissolution; however, analysis of the resulting solution by MALDI-TOF mass spectrometry revealed Gaussian distributions at 469, 695, and 932 g/mol. These peaks are consistent with residual 4-, 6-, and 8-unit oligomers of **2a** that were washed off of the bulk product, which is considered to be an infinite network solid. Solid-state infrared and multinuclear cross-polarization magic angle spinning (CP-MAS) NMR spectroscopy also proved to be informative. The IR spectrum of **2a** was found to feature a strong Si–H stretch

at 2131 cm^{-1} and a weak Si–N stretch at 818 cm^{-1}.[42] The ^{15}N CP-MAS NMR spectrum of this product was found to feature a single resonance at 21.64 ppm, while the ^{29}Si NMR spectrum was found to exhibit a minor peak at -36.58 ppm and a major peak at -26.72 ppm for *Si*N$_3$H and *Si*N$_2$H$_2$, respectively.

Table 3.2. Synthesis of polycarbosilazanes from SiH$_4$ using **47**.
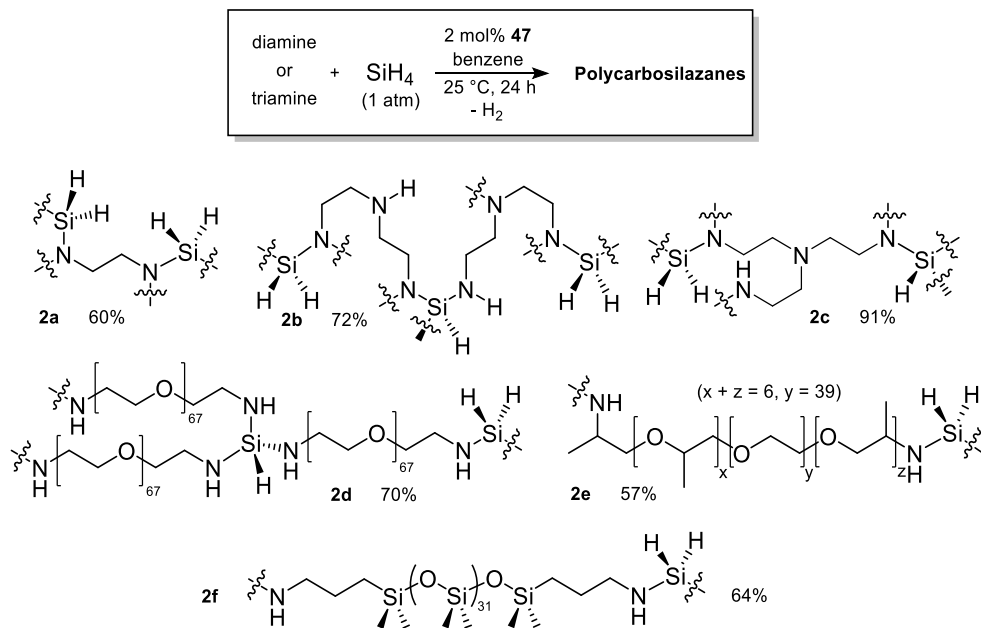
Isolated yields reported relative to diamine or triamine substrate.

Repeating this procedure with diethylenetriamine and tris(2-aminoethyl)amine afforded polycarbosilazanes **2b** and **2c**, respectively. As observed for **2a**, MALDI-TOF mass spectrometry revealed residual low molecular weight oligomers (446, 670, and 900 g/mol) that were washed off of insoluble **2b**. For illustrative purposes, data collected for **2c** is highlighted in Figure 3.2. The infrared spectrum of **2c** (Figure 3.2, a) was found to feature N–H (3293 cm^{-1}), sp^3 C–H (2936-2802 cm^{-1}), Si–H (2110 cm^{-1}), C–N (1103-1048 cm^{-1}), and Si–N (845 cm^{-1}) stretching vibrations (Figure 3.2, b).[42] The ^{15}N CP-MAS NMR spectrum of this product (Figure 3.2, c) revealed a broad, multi-component signal centered

87

at 23.65 ppm due to the presence of silylamine, disilylamine, and tertiary amine environments. Moreover, the ^{29}Si CP-MAS NMR spectrum of **2c** (Figure 3.2, d) revealed a dominant signal at -33.75 ppm that corresponds to SiN$_3$H environments and a downfield shoulder that suggests the presence of SiN$_2$H$_2$ environments. The stability of **2a**-**2c** towards ambient conditions was also analyzed by infrared spectroscopy. After 1 h of exposure to air featuring 13% humidity, a significant decrease in Si–H and Si–N infrared vibration absorbance was noted for all three compounds (Table 3.3), indicating that these products are easily hydrolyzed.
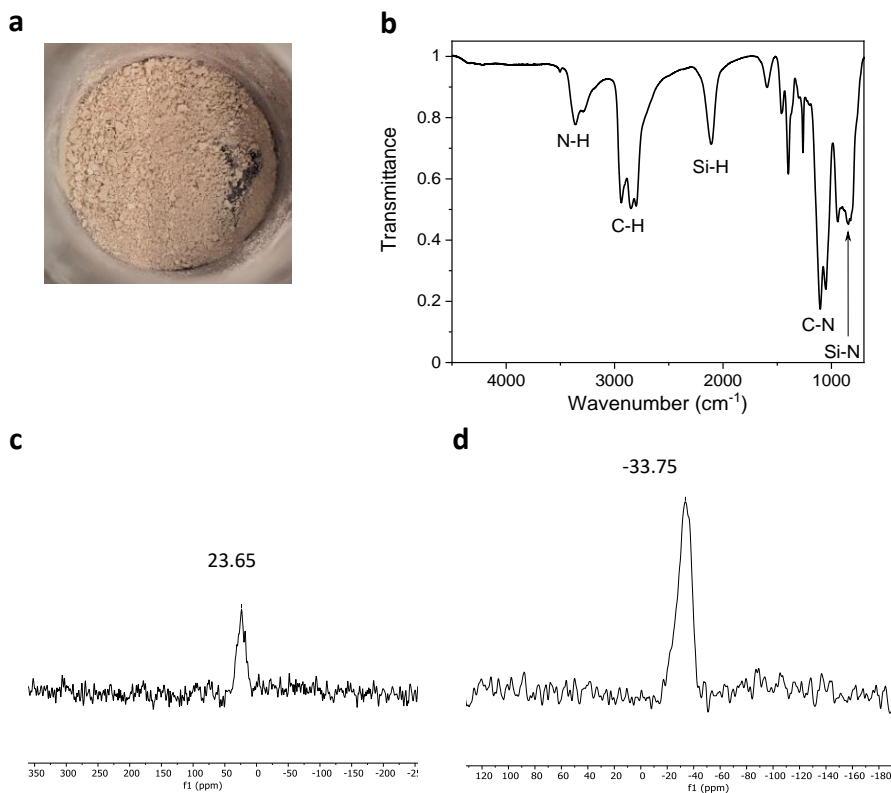
Figure 3.2. Characterization of polycarbosilazane **2c**. a) Image of solid product. b) Solid-state infrared spectrum in KBr. c) ^{15}N CP-MAS NMR spectrum. d) ^{29}Si CP-MAS NMR spectrum.

Table 3.3. Percentage decrease in Si–H and Si–N infrared vibration integration after 1 h of exposure to air at 13% humidity.

Polymer	Si–H	Si–N
2a	-49%	-26%
2b	-69%	-34%
2c	-87%	-68%
PHPS	-65%	-85%

The scope of **47**-mediated dehydrocoupling was then extended to amine-terminated polymers. The use of diaminopoly(ethyleneglycol) (M_w = 3000 g/mol) afforded **2d** as a tan solid in 70% yield and elemental analysis suggested the presence of $SiH_2(NHR)_2$ and $SiH(NHR)_3$ moieties. Jeffamine ED-2003, which features methyl substitution at the α- and ω-positions of the polymer chain, was found to yield a waxy white solid possessing $SiH_2(NHR)_2$ linkage (**2e**). Likewise, the dehydrocoupling of bis(3-aminopropyl) terminated poly(dimethylsiloxane) successfully underwent dehydrocoupling with SiH_4 to yield an off-white diaminosilane-bridged polycarbosilazane powder (**2f**). Elemental analysis was particularly helpful for characterizing and assigning the structures of **2d**-**2f**; however, the low N and Si concentration within these products prevented the collection of informative multinuclear CP-MAS NMR data. Accordingly, the infrared spectra collected for **2d**-**2f** were found to feature very weak N–H and Si–H stretching vibrations. Products of this type represent attractive alternatives to commercial organic polysilazane anti-corrosion and anti-graffiti coatings prepared through the aminolysis of functionalized chlorosilanes.[43]

3.3.3. Direct Preparation of PHPS.

The ability of **47** to generate insoluble polycarbosilazanes when dehydrocoupling primary amines suggested that it might be possible to prepare PHPS in a halogen-free manner from SiH_4 and NH_3. To a 100 mL thick-walled reaction vessel containing a

89

benzene solution of **47**, 1 atm of NH_3 was added and condensed, followed by 1 atm of SiH_4 (Figure 3.3, a). After 1 h at ambient temperature, precipitate began to form and the stepwise removal of H_2, unreacted SiH_4, and finally residual NH_3 after 24 h allowed for isolation of a light-yellow solid identified as PHPS (Figure 3.3, b). The FT-IR spectrum of this product (Figure 3.3, c) confirmed the presence of N–H (3358 cm^{-1}), Si–H (2118 cm^{-1}), Si–N (966 cm^{-1}) stretching vibrations, consistent with data that has previously been reported for PHPS.[44,45] As noted by Bauer and co-workers,[45] hydrolysis of this compound resulted in a significant decrease in Si–H and Si–N vibration absorbance over the course of 1 h at 13% humidity (Table 3.3). The CP-MAS ^{15}N NMR spectrum of our product was found to feature well-resolved resonances at 27.26 and 42.82 ppm in an approximate 1:1 ratio (Figure 3.3, d). The peak at 27.26 ppm is due to the presence of NSi$_2$H environments, while the resonance at 42.82 ppm can be attributed to tertiary NSi$_3$ moieties. Although the ^{15}N NMR shifts of silylamine compounds are sensitive to differences in silane substitution, our assignments are consistent with the trend reported for (Me$_3$Si)$_2$NH (25.6 ppm) and (Me$_3$Si)$_3$N (35.6 ppm).[46] Gratifyingly, the CP-MAS ^{29}Si NMR spectrum of our PHPS was found to exhibit a predominant resonance at -37.90 ppm along with a pair of spinning sidebands at 5 kHz spacing (Figure 3.3, e). Prior evaluations of PHPS by ^{29}Si NMR spectroscopy have assigned this peak to a mixture of SiN$_2$H$_2$ and SiN$_3$H environments,[16] which is consistent with our ^{15}N NMR data and the structure shown in Figure 3.3a. The small resonance observed at -47.12 ppm has previously been assigned to quaternary silicon sites (SiN$_4$).[16,47] Overall, the multinuclear NMR spectra shown in Figure 3.3 suggest that the **47**-mediated dehydrocoupling of SiH_4 and NH_3 affords exceptionally pure PHPS.

Adding SiH$_4$ to NH$_3$ in the absence of catalyst did not result in PHPS formation after 48 h at 25 °C.
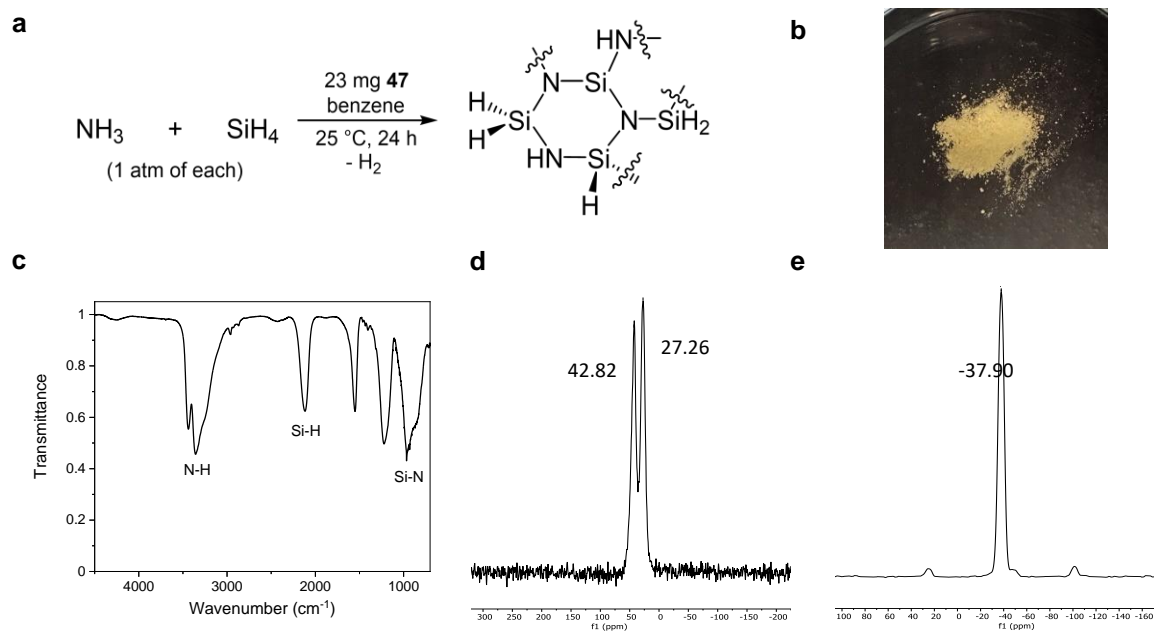
Figure 3.3. Characterization of PHPS prepared using **47**. a) Synthetic conditions. b) Image of product. c) Solid-state infrared spectrum in KBr. d) ^{15}N CP-MAS NMR spectrum. e) ^{29}Si CP-MAS NMR spectrum.

3.3.4. Mechanistic Insight.

Upon demonstrating that **47** generates Si–N bonds via dehydrocoupling, the mechanism of catalysis was explored. Initially, a J. Young tube containing a benzene-*d$_6$* solution of **47** was subjected to 1 atm of SiH$_4$. Unmodified **47** was observed by ^{1}H NMR spectroscopy over the course of 24 h, indicating that this compound does not react with SiH$_4$ under the conditions of catalysis. Similarly, no reaction was observed when 2 equivalents of diisopropylamine (**1e**) were added to **47**. While preparing CVD precursors from the substrates in Table 3.1, we observed that the addition of unencumbered secondary amines to **47** resulted in instantaneous H$_2$ evolution. Adding 2 equivalents of methylethylamine (**1b**), diethylamine (**1c**), or dibutylamine (**1d**) to **47** revealed partial

91

conversion to new paramagnetic species after 24 h by ^{1}H NMR spectroscopy (**1b**, 80%; **1c**, 50%; **1d**, 10%). Finally, when 2 equivalents of isopropylamine (**1f**) were added to **47**, complete conversion to the amido dimer [($^{2,6\text{-}i\text{Pr}_2\text{Ph}}$BDI)Mn(μ-NH$i$Pr)]$_2$ (**80**, Figure 3.4, a) was observed after 24 h. This complex was found to exhibit paramagnetically broadened ^{1}H NMR resonances over a 35-ppm range and its magnetic susceptibility of 6.3 μ$_B$ (25 °C) is consistent with the presence of high-spin Mn(II) and the value of 6.5 μ$_B$ (25 °C) reported for imino(amido) dimer, [($^{2,6\text{-}i\text{Pr}_2\text{Ph}}$BDI)Mn(μ-NCHPh)]$_2$.[48] The solid-state structure of **80** (Figure 3.4b) revealed a pseudo-tetrahedral coordination environment about each metal center and a Mn–Mn distance of 3.0487(6) Å, indicative of a weak Mn-Mn bonding interaction.[38] One hydrogen atom on each bridging amido ligand was located in the difference map, confirming that these ligands are monoanionic and that the Mn centers of **80** are divalent.

DFT calculations show a barrier of 1.5 kcal/mol for the dissociation of **47** into two equivalents of ($^{2,6\text{-}i\text{Pr}_2\text{Ph}}$BDI)MnH (Figure 3.4c, left).[48] These monomers are readily available in solution at 25 °C, and when sterically unencumbered amines are present, Mn–H and N–H σ-bond metathesis occurs to eliminate H$_2$ and generate the corresponding amido intermediate (Figure 3.4c, center). In the absence of SiH$_4$, these intermediates dimerize (Figure 3.4c, right), which has allowed for the isolation of **80** in the case of isopropylamine. When an excess of SiH$_4$ was added to a benzene-d_6 solution of isolated **80**, complete conversion to **47** was observed within 4 h at 25 °C. This result suggests that amido dimers including **80** are intermediates that can dissociate and undergo σ-bond metathesis with SiH$_4$ to regenerate **47** while forming the desired Si–N bond. Primary aminosilanes (i.e., H$_3$SiNRR') were not observed in this study and are believed to react

preferentially with Mn amido intermediates to yield diaminosilane or triaminosilane products (Figure 3.4c, bottom).
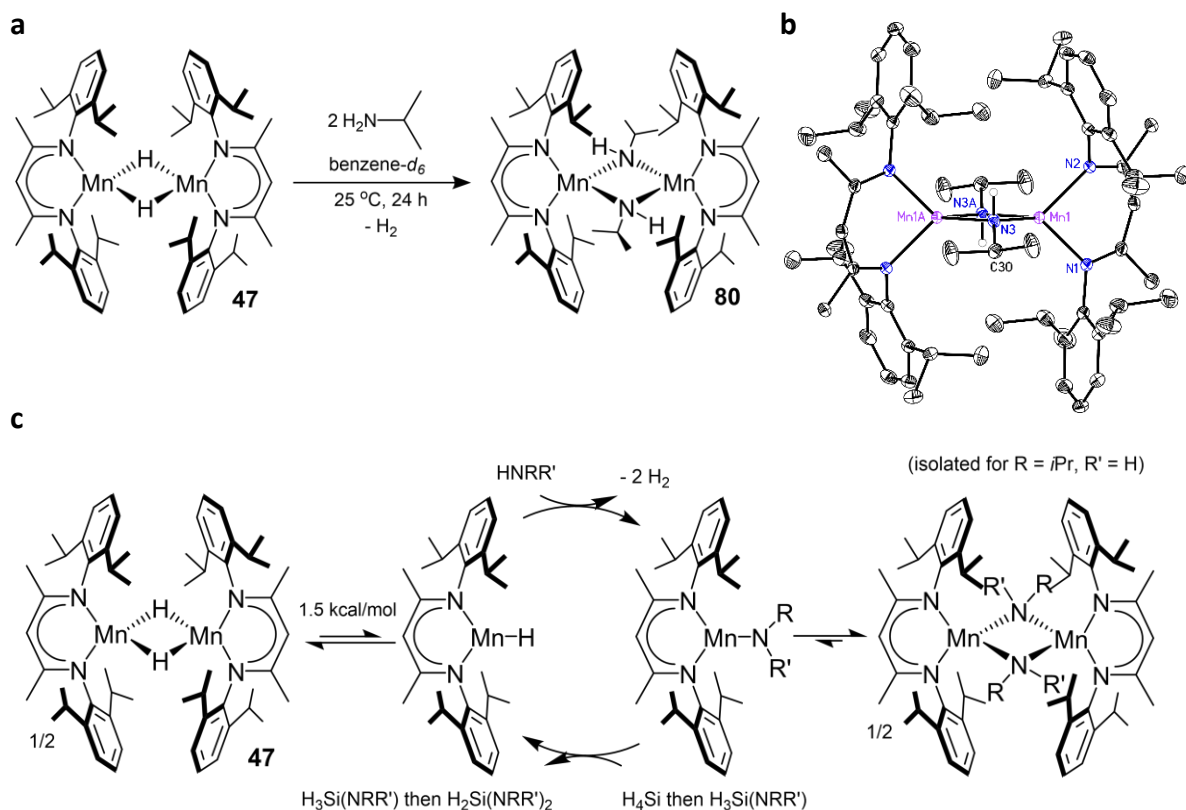
Figure 3.4. Amine activation and the mechanism of dehydrocoupling. a) Addition of isopropylamine to **47** to yield **80**. b) Solid-state structure of **80.** c) Proposed mechanism of Si–N formation involving N-H and Si-H σ-bond metathesis.

Additional experiments were performed to probe the sensitivity of Mn–N and Si–N bond formation to the presence of H_2, which represent the key steps of **47**-mediated dehydrocoupling (Figure 3.4c, center). First, a benzene-d_6 solution of isolated **80** was subjected to 4 atm of H_2. No conversion to **47** and isopropylamine was observed over the course of 24 h at ambient temperature, suggesting that H_2 present in the headspace is unlikely to inhibit dehydrocoupling. Second, attempts to hydrogenate the Si–N bonds of $H_2Si(NEt_2)_2$ using 2 mol% of **47** under 4 atm of H_2 did not allow for the observation or

SiH$_4$, diethylamine, or new aminosilanes over the course of 24 h at 25 °C. Therefore, once formed, it is believed that Si–N bonds are not reactivated by **47** under the conditions of catalysis.

3.3.5. Discussions

The use of SiH$_4$ as a dehydrocoupling partner differentiates this study from prior efforts to catalyze Si–N bond formation. Although this reagent is not commonly found in academic settings, thousands of tons of SiH$_4$ are used each year to make polysilicon, rendering it an abundant and inexpensive synthetic precursor. It is also the only silicon source that can be used to prepare commercially relevant CVD precursors via dehydrocoupling. Our exploration of **47**-mediated aminosilane synthesis suggests that the steric properties of the catalyst dictate both catalytic activity and product distribution. Although **47** enables the selective formation of secondary silanes such as H$_2$Si(NEt$_2$)$_2$ and H$_2$Si(NH*t*Bu)$_2$, the diisopropylphenyl substituents of the chelate prevent **47** from generating tertiary or quaternary silanes when bulky secondary amines are used. Minimizing steric protection could allow for the design of catalysts that favor these products when they are desired.

To prepare PHPS via dehydrocoupling, SiH$_4$ is again the only silane source that can be used. The coupling of SiH$_4$ and NH$_3$ in the presence of **47** was found to result in highly cross-linked PHPS powders that are insoluble in organic solvents. Solid PHPS can be used as a thermosetting resin or can be left to react with ammonia to yield solutions that leave behind silicon nitride or silicon oxynitride thin films. While films generated from PHPS are particularly useful for protecting electronic devices, organic polysilazanes are currently used to coat trains and automobiles. The polycarbosilazanes prepared from SiH$_4$ in this

study could become sustainably sourced alternatives to organic polysilazanes, which are currently prepared from chlorosilanes.

3.4. Conclusion

The manganese-catalyzed dehydrocoupling of amines to SiH_4 has allowed for the halogen-free synthesis of commercial aminosilane chemical vapor deposition precursors. These transformations were achieved using 1 atm of SiH_4 at ambient temperature. Extending the substrate scope to diamines and triamines allowed for the preparation of highly cross-linked polycarbosilanes, while the use of ammonia afforded solid perhydropolysilazane. When isopropylamine was independently added to [($^{2,6-iPr_2Ph}$BDI)Mn(μ-H)]$_2$, the corresponding amido dimer [($^{2,6-iPr_2Ph}$BDI)Mn(μ-NHiPr)]$_2$ was isolated and characterized. This product was found to react with SiH_4 to regenerate the catalyst, indicating that Mn–N and H–Si σ-bond metathesis is responsible for Si–N formation. It is hoped that the atom-efficient aminosilane, polycarbosilazane, and perhydropolysilazane syntheses detailed in this contribution inspire the search for specialized catalysts and the industrial adoption of dehydrogenative Si–N bond formation.

3.5. Experimental Procedures

General Considerations: All reactions were performed inside an MBraun glovebox under an atmosphere of purified nitrogen or on a high-vacuum manifold. Toluene, tetrahydrofuran, diethyl ether, and pentane were purchased from Sigma-Aldrich, purified using a Pure Process Technology solvent system, and stored in the glovebox over activated 4 Å molecular sieves and potassium prior to use. Benzene-d_6 was purchased from Oakwood Chemicals and dried over 4 Å molecular sieves and potassium prior to use. Toluene-d_8 and benzene were purchased from Sigma-Aldrich and dried over 4 Å molecular

sieves and potassium prior to use. Tetramethylsilane was purchased from Sigma-Aldrich and dried over 4 Å molecular sieves. Celite was obtained from Oakwood Chemicals. Silane was obtained from Voltaix. Dimethylamine, ethylmethylamine, dibutylamine, diisopropylamine, isopropylamine, *tert*-butylamine, ethylenediamine, diethylenetriamine, and tris(triaminoethyl)amine were purchased from Oakwood Chemicals. Diethylamine, bis(3-aminopropyl) terminated poly(dimethylsiloxane) ($M_n \approx 2,500$), poly(propylene glycol)-block-poly(ethylene glycol)-block-poly(propylene glycol) bis(2-aminopropyl ether), diaminopoly(ethylene glycol), and ammonia were purchased from Sigma Aldrich. All liquid substrates were dried over 4 Å molecular sieves prior to catalyst screening.

Elemental analyses were performed at Midwest Microlab (Indianapolis, IN). Infrared spectra were collected on a Bruker VERTEX 70 spectrophotometer with an MCT detector. Solution nuclear magnetic resonance (NMR) spectra were recorded at room temperature on a Varian 400 MHz or a Bruker 400 MHz NMR spectrometer. All ^{1}H NMR and ^{13}C NMR chemical shifts (ppm) are reported relative to $Si(Me)_4$ using ^{1}H (residual) and ^{13}C chemical shifts of the solvent as secondary standards. ^{29}Si NMR chemical shifts (ppm) are reported relative to $Si(Me)_4$ using the absolute ^{1}H NMR frequency of an internal $Si(Me)_4$ standard. Solid-state NMR spectra were recorded at room temperature on a wide-bore 400 MHz solid-state AVANCE NMR instrument (Bruker). Air-sensitive samples were packed into 4 mm zirconia magic-angle spinning (MAS) rotors in an inert atmosphere glovebox and spun at 5 kHz. CP-MAS experiments were performed such that the measurements could rely on the increased sensitivity and shorter relaxation time provided by the protons. A relaxation delay of approximately 3 s was used between acquisitions and measurement time ranged from 12 to 24 h, depending on the concentration of ^{29}Si and ^{15}N

in each material. For ^{15}N CP-MAS measurements, the ^{1}H $\pi/2$ pulse was 4.1 μsec, 1.5 msec contact time and SPINAL64 decoupling. All ^{15}N CP-MAS NMR chemical shifts (ppm) are reported relative to a saturated NH_4^+ solution at 0 ppm (unified scale) using α-glycine (33.4 ppm) as an external standard. For ^{29}Si CP-MAS experiments the ^{1}H $\pi/2$ pulse was 6.0 μsec, 3.0 msec contact time and SPINAL64 decoupling. All ^{29}Si NMR chemical shifts are referenced relative to $Si(Me)_4$ using tetrakis(trimethylsilyl)silane (-8.9 ppm) as an external standard.

X-ray Crystallography: Low-temperature X-ray diffraction data for **2** were collected on a Rigaku XtaLAB Synergy diffractometer coupled to a Rigaku Hypix detector with Cu Kα radiation (λ = 1.54184 Å), from a PhotonJet micro-focus X-ray source at 100 K. The diffraction images were processed and scaled using the CrysAlisPro software. The structures were solved through intrinsic phasing using SHELXT and refined against F^2 on all data by full-matrix least squares with SHELXL following established refinement strategies. These data were refined as a 2-component twin with a BASF factor of 0.2144(7). All non-hydrogen atoms were refined anisotropically. All hydrogen atoms bound to carbon were included in the model at geometrically calculated positions and refined using a riding model. Hydrogen atoms bound to nitrogen were located in the difference Fourier synthesis and subsequently refined semi-freely with the help of distance restraints. The isotropic displacement parameters of all hydrogen atoms were fixed to 1.2 times the Ueq value of the atoms they are linked to (1.5 times for methyl groups).

MALDI-TOF Mass Spectrometry: Samples were analyzed on a Bruker microFlex LRF instrument (Billerica, MA, USA) with a 337 nm laser in positive mode scanning from 200

to 200,000 m/z. The ion source 1 voltage was 19.50 kV, ion source 2 voltage was 18.15 kV, the lens voltage was 7.00 kV, and ion suppression was off.

General Procedure for Preparing CVD Compounds using a Liquid Amine: Under N_2 atmosphere, a J. Young tube was charged with 0.010 g (0.010 mmol) of **47** in 0.4 mL of 0.2 M TMS in toluene-d_8, followed by 0.50 mmol of amine. The tube was sealed under N_2 and attached to the vacuum line. The solution was frozen in liquid N_2, gas was removed from the head space under vacuum, and 1 atm of SiH_4 was introduced. ***DANGER: SiH₄ will react violently with air and must be added under vacuum.*** The tube was closed, disconnected from the vacuum line, and placed in a steel container to warm to room temperature in the back of an empty fume hood with the sash closed. The reaction was allowed to occur at ambient temperature for 24 h. Multinuclear NMR data was collected after 24 h, conversion was determined by examining the consumption of starting amine ^{1}H NMR resonances, and NMR yields were determined by integrating the products against the internal TMS standard. To safely end the experiment, the tube was attached to the vacuum line, the solution was frozen in liquid N_2, and H_2 was removed under vacuum. Residual SiH_4 was recollected in a lecture bottle (preferred) or allowed to slowly evaporate through repeated warming and cooling of the solution in liquid N_2 under dynamic vacuum. Allowing H_2 and SiH_4 mixtures to disperse in a large volume of N_2 that can be purged in a controlled manner (i.e., by opening the tube in a glovebox) proved to be a safe alternative to slow removal under vacuum.

General Procedure for Preparing Polycarbosilazanes: Under N_2 atmosphere, a 100 mL thick-walled glass bomb was charged with 0.020 g (0.021 mmol) of **47** in 3 mL benzene, followed by 1.05 mmol of amine. The evolution of hydrogen gas was observed instantly.

The bomb was sealed under N_2 and attached to the vacuum line. The solution was frozen in liquid N_2, gas was removed from the head space under vacuum, and 1 atm of SiH_4 was introduced. *DANGER: SiH_4 will react violently with air and must be added under vacuum.* The bomb was closed, disconnected from the vacuum line, and placed in a steel container to warm to room temperature in the back of an empty fume hood with the sash closed. Polycarbosilazane precipitate was observed after 2 h and the reactions were allowed to occur at ambient temperature for 24 h. The bomb was then attached to the vacuum line, the solution was frozen in liquid N_2, and H_2 was removed under vacuum. Following H_2 removal, residual SiH_4 was recollected in a lecture bottle (preferred) or allowed to slowly evaporate through repeated warming and cooling of the solution in liquid N_2 under dynamic vacuum. The bomb was brought into the glove box, the product was washed with THF (2 x 5 mL), and pentane (2 x 5 mL) then dried *in vacuo* to isolate the corresponding polycarbosilazane.

Preparation of $H_2Si(NMe_2)_2$ and $HSi(NMe_2)_3$ from silane and dimethylamine (1a) using 2 mol% 47: Under N_2 atmosphere, a J. Young tube was charged with 0.014 g (0.015 mmol) of **47** in 0.4 mL of 0.2 M TMS in toluene-d_8 and sealed. The tube was then attached to the vacuum line, the solution was frozen in liquid N_2, and gas was removed from the head space under vacuum. Next, 27.1 mL of dimethylamine gas at 507 mmHg (0.74 mmol) and 1 atm of SiH_4 were introduced. *DANGER: SiH_4 will react violently with air and must be added under vacuum.* The tube was closed, disconnected from the vacuum line, and placed in a steel container to warm to room temperature in the back of an empty fume hood with the sash closed. Upon warming, the solution darkened to orange-yellow in color. Multinuclear NMR data was collected after 24 h. To safely end the experiment, the tube

was attached to the vacuum line and the solution was frozen in liquid N_2. The vacuum gauge read a pressure of approximately 2500 mTorr of H_2 upon opening the tube. Following H_2 removal, residual SiH_4 was allowed to slowly evaporate through repeated warming and cooling of the solution in liquid N_2 under dynamic vacuum. ***DANGER: Allowing a significant quantity of H_2 and SiH_4 to pass through the vacuum pump into a ventilation system at the same time can result in detonation.*** More than 99% conversion was observed after 24 h by examining the consumption of starting amine ^{1}H NMR resonances. By integrating the product Si-H peaks against the internal TMS standard, an overall NMR yield of 73% was determined for $H_2Si(NMe_2)_2$ (21% yield) and $HSi(NMe_2)_3$ (52% yield).

^{1}H NMR (400 MHz, toluene-d_8): 4.60 (s, 2H, J_{SiH} = 109 Hz, H_2Si[N(CH$_3$)$_2$]$_2$), 4.40 (s, 1H, J_{SiH} = 115 Hz, HSi[N(CH$_3$)$_2$]$_3$), 2.46 (s, H_2Si[N(CH_3)$_2$]$_2$ and HSi[N(CH_3)$_2$]$_3$ overlapped). ^{13}C NMR (100 MHz, toluene-d_8): 38.00 (H_2Si[N(CH_3)$_2$]$_2$), 36.87 (HSi[N(CH_3)$_2$]$_3$). ^{29}Si NMR (79 MHz, toluene-d_8): -21.54 (H_2Si[N(CH$_3$)$_2$]$_2$), -25.09 (HSi[N(CH$_3$)$_2$]$_3$).
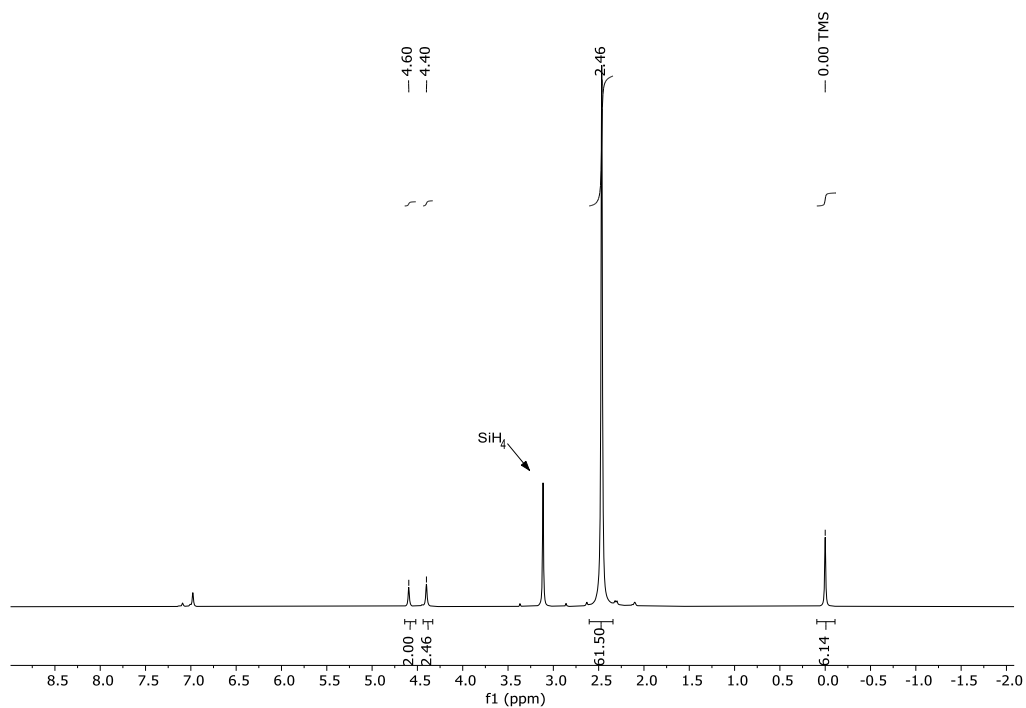
Figure 3.5. Representative ^{1}H NMR spectrum of $H_2Si(NMe_2)_2$ and $HSi(NMe_2)_3$ prepared from silane and dimethylamine in toluene-d_8.
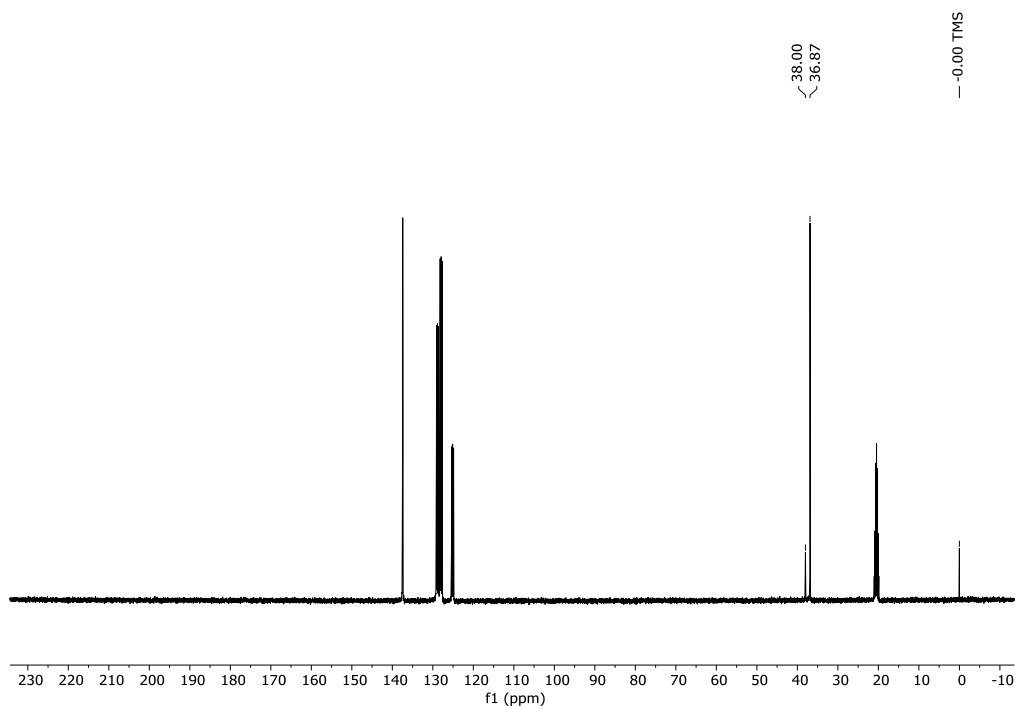
Figure 3.6. Representative ^{13}C NMR spectrum of $H_2Si(NMe_2)_2$ and $HSi(NMe_2)_3$ prepared from silane and dimethylamine in toluene-d_8.

101
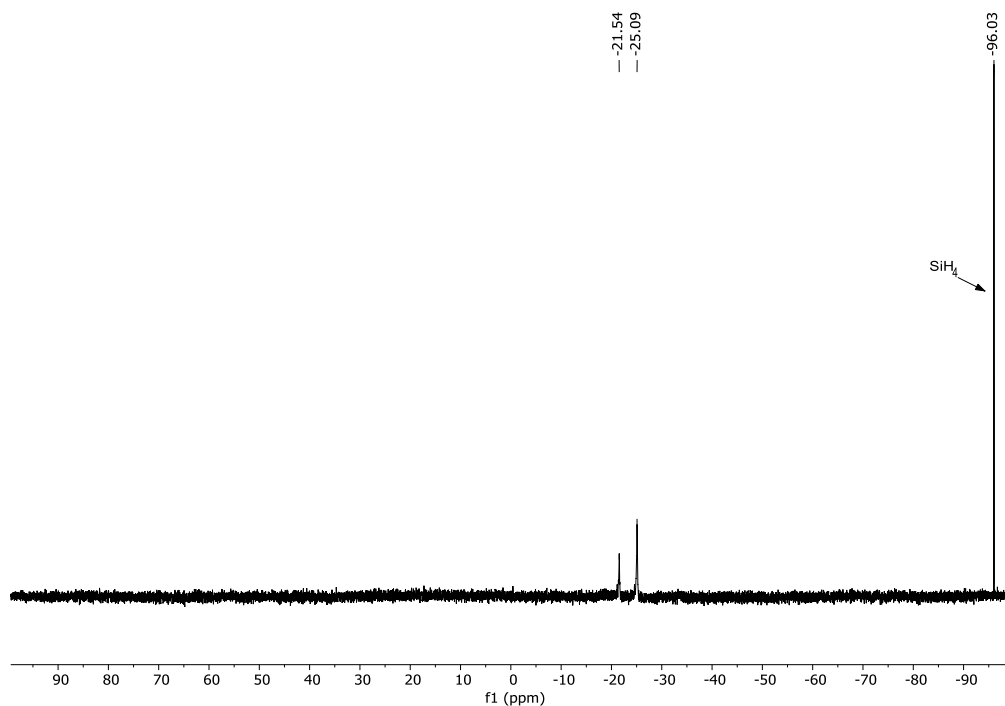
Figure 3.7. Representative ^{29}Si NMR spectrum of $H_2Si(NMe_2)_2$ and $HSi(NMe_2)_3$ prepared from silane and dimethylamine in toluene-d_8.

Preparation of $H_2Si(NMeEt)_2$ from silane and N-ethylmethylamine (1b) using 2 mol% 47: Under N_2 atmosphere, a J. Young tube was charged with 0.009 g (0.009 mmol) of **47** in 0.4 mL of 0.2 M TMS in toluene-d_8, followed by 39 µL (0.45 mmol) of N-ethylmethylamine. The formation of H_2 was observed. Then, the tube was sealed under N_2 and attached to the vacuum line. The solution was frozen in liquid N_2, gas was removed from the head space under vacuum, and 1 atm of SiH_4 was introduced. *DANGER: SiH$_4$ will react violently with air and must be added under vacuum.* The tube was closed, disconnected from the vacuum line, and placed in a steel container to warm to room temperature in the back of an empty fume hood with the sash closed. The reaction was allowed to occur at ambient temperature for 24 h. The tube was then brought into the glovebox, the solution was placed in a liquid nitrogen-cooled cold well for 30 min, and the

tube was opened to release H_2 and residual SiH_4. ***NOTE: Allowing H_2 and SiH_4 to disperse in a large volume of N_2 that can be purged in a controlled manner proved to be a safe alternative to controlled removal under vacuum.*** More than 96% conversion was observed after 24 h by examining the consumption of starting amine ^{1}H NMR resonances. By integrating the Si-H peaks of the products against an internal TMS standard, 94% NMR yield was determined for $H_2Si(NMeEt)_2$.

^{1}H NMR (400 MHz, toluene-d_8): 4.65 (s, 2H, J_{SiH} = 108 Hz, H_2Si), 2.81 (s, 4H, NCH_2CH_3), 2.48 (broad s, 6H, NCH_2CH_3), 0.99 (s, 6H, NCH_3). ^{13}C NMR (100 MHz, toluene-d_8): 44.62 (NCH_2CH_3), 33.95 (NCH_3), 14.46 (NCH_2CH_3). ^{29}Si NMR (79 MHz, toluene-d_8): -24.07 (H_2Si).

Preparation of $H_2Si(NEt_2)_2$ from silane and diethylamine (1c) using 2 mol% 47: Under N_2 atmosphere, a J. Young tube was charged with 0.009 g (0.009 mmol) of **47** in 0.4 mL of 0.2 M TMS in toluene-d_8, followed by 48 µL (0.46 mmol) of diethylamine. The formation of H_2 was observed. Then, the tube was sealed under N_2 and attached to the vacuum line. The solution was frozen in liquid N_2, gas was removed from the head space under vacuum, and 1 atm of SiH_4 was introduced. ***DANGER: SiH_4 will react violently with air and must be added under vacuum.*** The tube was closed, disconnected from the vacuum line, and placed in a steel container to warm to room temperature in the back of an empty fume hood with the sash closed. The reaction was allowed to occur at ambient temperature for 48 h. Multinuclear NMR data was collected after 24 h and 48 h. The tube was then brought into the glovebox, the solution was placed in a liquid nitrogen-cooled cold well for 30 min, and the tube was opened to release H_2 and residual SiH_4. ***NOTE: Allowing H_2 and SiH_4 to disperse in a large volume of N_2 that can be purged in a***

controlled manner proved to be a safe alternative to controlled removal under vacuum.
At 24 h, 68% conversion was observed, while 94% conversion was observed after 48 h by following the consumption of starting amine ^{1}H NMR resonances. By integrating the product Si-H peaks against the internal TMS standard, an 83% NMR yield of $H_2Si(NEt_2)_2$ was obtained.

^{1}H NMR (400 MHz, toluene-d_8): 4.69 (s, 2H, J_{SiH} = 108 Hz, H_2Si), 2.86 (q, 8H, J = 6 Hz, NCH_2CH_3), 1.00 (broad m, 12H, NCH$_2$CH_3). ^{13}C NMR (100 MHz, toluene-d_8): 40.92 (NCH$_2$CH$_3$), 15.72 (NCH$_2$$CH_3$). ^{29}Si NMR (79 MHz, toluene-d_8): -26.03 (H_2Si).

Preparation of $H_2Si(NBu_2)_2$ from silane and dibutylamine (1d) using 2 mol% 47:
Under N_2 atmosphere, a 100 mL thick-walled glass bomb was charged with 0.010 g (0.011 mmol) of **47** in 0.4 mL of 0.2 M TMS in toluene-d_8, followed by 90 µL (0.54 mmol) of dibutylamine. The formation of H_2 was observed. Then, the bomb was sealed under N_2 and attached to the vacuum line. The solution was frozen in liquid N_2, gas was removed from the head space under vacuum, and 1 atm of SiH_4 was introduced. *DANGER: SiH_4 will react violently with air and must be added under vacuum.* The bomb was closed, disconnected from the vacuum line, and placed in a steel container to warm to room temperature in the back of an empty fume hood with the sash closed. The reaction was allowed to occur at ambient temperature for 4 days. At that time, the solution was placed in a liquid nitrogen-cooled cold well for 30 min, and the bomb was slowly opened to release H_2 and residual SiH_4. *NOTE: Allowing H_2 and SiH_4 to disperse in a large volume of N_2 that can be purged in a controlled manner proved to be a safe alternative to controlled removal under vacuum.* After 4 days, 50% conversion was observed by examining the

consumption of starting amine ^{1}H NMR resonances. By integrating the product Si-H peaks against the internal TMS standard, a 45% NMR yield was obtained for $H_2Si(NBu_2)_2$.

^{1}H NMR (400 MHz, toluene-d_8): 4.75 (s, 2H, J_{SiH} = 108 Hz, H_2Si), 2.85 (t, 8H, NCH_2CH$_2$CH$_2$CH$_3$), 1.45 (m, 8H, NCH$_2$CH_2CH$_2$CH$_3$), 1.29 (m, 8H, NCH$_2$CH$_2$CH_2CH$_3$), the methyl resonance of $H_2Si(NBu_2)_2$ overlaps with the starting material methyl resonance. ^{13}C NMR (100 MHz, toluene-d_8): 47.19 (NCH$_2$CH$_2$CH$_2$CH$_3$), 32.49 (NCH$_2$$CH_2CH_2CH_3$), 20.67 (NCH$_2CH_2$$CH_2CH_3$), 14.16 (NCH$_2CH_2CH_2$$CH_3$). [29]Si NMR (79 MHz, toluene-d_8): -24.85 (H$_2$$Si$).

Attempt to dehydrocouple diisopropylamine (1e) and silane using 2 mol% 47: Under N_2 atmosphere, a J. Young tube was charged with 0.016 g (0.017 mmol) of **47** in 0.4 mL of TMS 0.2 M in toluene-d_8, followed by 120 µL (0.85 mmol) of diisopropylamine. Then, the tube was sealed under N_2 and attached to the vacuum line. The solution was frozen in liquid N_2, gas was removed from the head space under vacuum, and 1 atm of SiH_4 was introduced. *DANGER: SiH₄ will react violently with air and must be added under vacuum.* The tube was closed, disconnected from the vacuum line, and placed in a steel container to warm to room temperature in the back of an empty fume hood with the sash closed. The reaction was allowed to occur at ambient temperature for 24 h. The tube was then brought into the glovebox, the solution was placed in a liquid nitrogen-cooled cold well for 30 min, and the tube was opened to release H_2 and residual SiH_4. *NOTE: Allowing H₂ and SiH₄ to disperse in a large volume of N₂ that can be purged in a controlled manner proved to be a safe alternative to controlled removal under vacuum.* No conversion was observed after 24 h by examining the consumption of starting amine ^{1}H NMR resonances.

Preparation of H₂Si(NH*i*Pr)₂ from silane and isopropylamine (1f) using 2 mol% 47:

Under N_2 atmosphere, a 100 mL thick-walled glass bomb was charged with 0.008 mg (0.009 mmol) of **47** in 0.4 mL of 0.2 M TMS in toluene-d_8, followed by 35 µL (0.43 mmol) of isopropylamine. The formation of H_2 was observed. The bomb was sealed under N_2 and attached to the vacuum line. The solution was frozen in liquid N_2, gas was removed from the head space under vacuum, and 1 atm of SiH_4 was introduced. ***DANGER: SiH₄ will react violently with air and must be added under vacuum.*** The bomb was closed, disconnected from the vacuum line, and placed in a steel container to warm to room temperature in the back of an empty fume hood with the sash closed. The reaction was allowed to occur at ambient temperature for 24 h. The bomb was then attached to the vacuum line and the solution was frozen in liquid N_2. The vacuum gauge read a pressure of approximately 700 mTorr of H_2 upon opening the bomb. Following H_2 removal, residual SiH_4 was allowed to slowly evaporate through repeated warming and cooling of the solution in liquid N_2 under dynamic vacuum. ***DANGER: Allowing a significant quantity of H₂ and SiH₄ to pass through the vacuum pump into a ventilation system at the same time can result in detonation.*** Greater than 99% conversion was observed after 24 h by examining the consumption of starting amine ^{1}H NMR resonances. By integrating the product Si-H peaks against the internal TMS standard, approximately 49% NMR yield was determined for H₂Si(NH*i*Pr)₂.

^{1}H NMR (400 MHz, toluene-d_8): 4.78 (s, 2H, J_{SiH} = 103 Hz, H_2Si), 3.19 (broad m, 2H, NHC*H*(CH₃)₂), 1.06 (d, J = 6.2 Hz, 12H, NHCH(C*H*₃)₂). ^{13}C NMR (100 MHz, toluene-d_8): 42.77 (NH*C*H(CH₃)₂), 27.95 (NHCH(*C*H₃)₂). ^{29}Si NMR (29 MHz, toluene-d_8): -58.99 (H₂*Si*).

Preparation of H₂Si(NH*t*Bu)₂ from silane and *tert*-butylamine (1g) using 2 mol% 47:

Under N_2 atmosphere, a 100 mL thick-walled glass bomb was charged with 0.014 g (0.014 mmol) of **47** in 0.4 mL of 0.2 M TMS in toluene-d_8, followed by 75.5 µL (0.72 mmol) of *tert*-butylamine. The formation of H_2 was observed. The bomb was sealed under N_2 and attached to the vacuum line. The solution was frozen in liquid N_2, gas was removed from the head space under vacuum, and 1 atm of SiH_4 was introduced. ***DANGER: SiH₄ will react violently with air and must be added under vacuum.*** The bomb was closed, disconnected from the vacuum line, and placed in a steel container to warm to room temperature in the back of an empty fume hood with the sash closed. The reaction was allowed to occur at ambient temperature for 24 h. The bomb was then attached to the vacuum line and the solution was frozen in liquid N_2. The vacuum gauge read a pressure of more than 1 atm of H_2 upon opening the bomb. Following H_2 removal, residual SiH_4 was allowed to slowly evaporate through repeated warming and cooling of the solution in liquid N_2 under dynamic vacuum. ***DANGER: Allowing a significant quantity of H₂ and SiH₄ to pass through the vacuum pump into a ventilation system at the same time can result in detonation.*** Approximately 99% conversion was observed after 24 h by examining the consumption of starting amine ^{1}H NMR resonances. By integrating the product Si-H peaks against the internal TMS standard, 93% NMR yield of H₂Si(NH*t*Bu)₂ was obtained.

^{1}H NMR (400 MHz, toluene-d_8): 4.69 (s, 2H, J_{SiH} = 109 Hz, H_2Si), 1.14 (s, 18H, NHC(CH_3)₃), 0.77 (s, 2H, NHC(CH₃)₃). ^{13}C NMR (100 MHz, toluene-d_8): 49.30 (NHC(CH₃)₃), 33.29 (NHC(CH₃)₃). ^{29}Si NMR (79 MHz, toluene-d_8): -45.45 (H₂Si).

Preparation of polycarbosilazane 2a from silane and ethylenediamine using 2 mol%

47: Under N_2 atmosphere, a 100 mL thick-walled glass bomb was charged with 0.041 g

(0.043 mmol) of **47** in 3 mL benzene followed by 144 µL (2.17 mmol) of ethylenediamine.

The evolution of hydrogen gas was observed instantly. The bomb was sealed under N_2 and

attached to the vacuum line. The solution was frozen in liquid N_2, gas was removed from

the head space under vacuum, and 1 atm of SiH_4 was introduced. ***DANGER: SiH_4 will***

react violently with air and must be added under vacuum. The bomb was closed,

disconnected from the vacuum line, and placed in a steel container to warm to room

temperature in the back of an empty fume hood with the sash closed. The formation of a

light-yellow solid was observed after 2 h and the reaction was allowed to occur at ambient

temperature for 24 h. The bomb was then attached to the vacuum line and the solution was

frozen in liquid N_2. The vacuum gauge read a pressure of several atm of H_2 upon opening

the bomb. Following H_2 removal, residual SiH_4 was allowed to slowly evaporate through

repeated warming and cooling of the solution in liquid N_2 under dynamic vacuum.

DANGER: Allowing a significant quantity of H_2 and SiH_4 to pass through the vacuum

pump into a ventilation system at the same time can result in detonation. The bomb was

brought into the glove box, the product was washed with THF (2 x 5 mL) and pentane (2

x 5 mL) then thoroughly dried *in vacuo* to isolate 0.152 g (60%) of a tan solid identified as

polycarbosilazane **2a**.

Elemental analysis for $(C_2H_8N_2Si_2)_n$: Calcd. C, 20.66; H, 6.94; N, 24.09. Found: C, 21.13;

H, 6.55; N, 17.53. Low N content due to Si_3N_4 formation upon combustion.

CP-MAS ^{15}N NMR (41 MHz): -21.64 (br m, Si*N*HEt and Si$_2$*N*Et). CP-MAS ^{29}Si NMR (79

MHz): -26.72 (*Si*N$_2$H$_2$), -36.58 (*Si*N$_3$H).

IR (KBr, cm^{-1}): 3369 (broad, N–H), 2912-2847 (strong, C–H), 2131 (strong, Si–H), 1394 (medium, CH$_2$), 1121-1024 (strong, C–N), 942 (weak, C–C), 818 (weak, Si–N).

MALDI-TOF [M+H]$^+$: 469.6 (n = 4), 695.130 (n = 6), 932.6 (n = 8), majority of product did not dissolve in THF.

Preparation of polycarbosilazane 2b from silane and diethylenetriamine using 2 mol% 47: Under N$_2$ atmosphere, a 100 mL thick-walled glass bomb was charged with 0.018 g (0.019 mmol) of **47** in 3 mL benzene, followed by 103 µL (0.956 mmol) of diethylenetriamine. The evolution of hydrogen gas was observed instantly. The bomb was sealed under N$_2$ and attached to the vacuum line. The solution was frozen in liquid N$_2$, gas was removed from the head space under vacuum, and 1 atm of SiH$_4$ was introduced. *DANGER: SiH$_4$ will react violently with air and must be added under vacuum.* The bomb was closed, disconnected from the vacuum line, and placed in a steel container to warm to room temperature in the back of an empty fume hood with the sash closed. The formation of a light brown solid was observed after 2 h and the reaction was allowed to occur at ambient temperature for 24 h. The bomb was then attached to the vacuum line and the solution was frozen in liquid N$_2$. The vacuum gauge read a pressure of approximately 1 atm of H$_2$ upon opening the bomb. Following H$_2$ removal, residual SiH$_4$ was allowed to slowly evaporate through repeated warming and cooling of the solution in liquid N$_2$ under dynamic vacuum. *DANGER: Allowing a significant quantity of H$_2$ and SiH$_4$ to pass through the vacuum pump into a ventilation system at the same time can result in detonation.* The bomb was brought into the glove box, the product was washed with THF (2 x 5 mL), and pentane (2 x 5 mL) then dried *in vacuo* to isolate 0.119 g (72%) of a light-brown solid identified as polycarbosilazane **2b**.

Elemental analysis for $(C_8H_{24}N_6Si_3)_n$: Calcd. C, 33.30; H, 8.38; N, 29.12. Found: C, 33.49; H, 8.34; N, 20.45. Low N content due to Si_3N_4 formation upon combustion.

IR (KBr, cm^{-1}): 3504 (weak, NH_2), 3368 (broad, N–H), 2868 (strong, C–H), 2119 (strong, Si–H), 1103-1021 (strong, C–N), 955 (weak, C–C), 839 cm^{-1} (weak, Si–N).

MALDI-TOF $[M+H]^+$: 446.3 (5 Si + 3 diethylenetriamine), 669.9 (6 Si + 5 diethylenetriamine), 900.4 (7 Si + 7 diethylenetriamine), majority of product did not dissolve in THF.

Preparation of polycarbosilazane 2c from silane and tris(2-aminoethyl)amine using 2 mol% 47: Under inert atmosphere, a 100 mL thick-walled glass bomb was charged with 0.016 mg (0.016 mmol) of **47** in 3 mL benzene, followed by 123 µL (0.819 mmol) of tris(2-aminoethyl)amine. The release of hydrogen gas was observed instantly. The bomb was sealed under N_2 and attached to the vacuum line. The solution was frozen in liquid N_2, gas was removed from the head space under vacuum, and 1 atm of SiH_4 was introduced. *DANGER: SiH_4 will react violently with air and must be added under vacuum.* The bomb was closed, disconnected from the vacuum line, and placed in a steel container to warm to room temperature in the back of an empty fume hood with the sash closed. The formation of an off-white solid was observed after 2 h and the reaction was allowed to occur at ambient temperature for 24 h. The bomb was then attached to the vacuum line and the solution was frozen in liquid N_2. The vacuum gauge read a pressure of several atm of H_2 upon opening the bomb. Following H_2 removal, residual SiH_4 was allowed to slowly evaporate through repeated warming and cooling of the solution in liquid N_2 under dynamic vacuum. *DANGER: Allowing a significant quantity of H_2 and SiH_4 to pass through the vacuum pump into a ventilation system at the same time can result in detonation.* The

bomb was brought into the glove box, the product was then washed with THF (2 x 5 mL), and pentane (2 x 5 mL) then dried *in vacuo* to isolate 0.153 g (91%) of a beige solid identified as polycarbosilazane **2c**.

Elemental analysis for $(C_6H_{20}N_4Si_2)_n$: Calcd. C, 38.85; H, 9.31; N, 25.89. Found: C, 37.45; H, 9.30; N, 26.16. Carbon content sufficient to prevent Si_3N_4 formation upon combustion.

CP-MAS ^{15}N NMR (41 MHz): -23.65 (br m, *N*Et₃, Si*N*HEt, and Si₂*N*Et). CP-MAS ^{29}Si NMR (79 MHz): -33.75 (br m, *Si*N₃H with *Si*N₂H₂ shoulder).

IR (KBr, cm⁻¹): 3360 (weak, NH₂), 3293 (broad, N–H), 2936-2802 (strong, C–H), 2110 (strong, Si–H), 1592 (weak, NH₂), 1461-1397 (weak, CH₂), 1103-1048 (medium, C–N), 941.5 (weak, C–C), 845 (weak, Si–N).

Preparation of polycarbosilazane 2d from silane and diaminopoly(ethylene glycol) using 2 mol% 47: Under N_2 atmosphere, a 100 mL thick-walled glass bomb was charged with 0.0008 g (0.0008 mmol) of **47** in 3 mL benzene. Then 0.120 g (0.04 mmol) of diaminopoly(ethylene glycol) (M_w = 3000 g/mol) in 5 mL benzene was added to the mixture. The release of hydrogen gas was observed instantly. The bomb was sealed under N_2 and attached to the vacuum line. The solution was frozen in liquid N_2, gas was removed from the head space under vacuum, and 1 atm of SiH_4 was introduced. *DANGER: SiH₄ will react violently with air and must be added under vacuum.* The bomb was closed, disconnected from the vacuum line, and placed in a steel container to warm to room temperature in the back of an empty fume hood with the sash closed. The formation of an orange-brown gel was observed after 2 h and the reaction was allowed to occur at ambient temperature for 24 h. The bomb was then attached to the vacuum line and the solution was frozen in liquid N_2. The vacuum gauge read a pressure of approximately 1 atm of H_2 upon

opening the bomb. Following H_2 removal, residual SiH_4 was allowed to slowly evaporate through repeated warming and cooling of the solution in liquid N_2 under dynamic vacuum. ***DANGER: Allowing a significant quantity of H_2 and SiH_4 to pass through the vacuum pump into a ventilation system at the same time can result in detonation.*** The bomb was brought into the glove box, the product was washed with THF (2 x 5 mL) and pentane (2 x 5 mL) then thoroughly dried *in vacuo* to isolate 0.085 g (70%) of a tan solid identified as polycarbosilazane **2d**.

Elemental analysis for $(C_{406}H_{820}N_6O_{200}Si_2)_n$: Calcd. C, 53.92; H, 9.14; N, 0.93. Found: C, 53.86; H, 9.13; N, 1.10. Carbon content sufficient to prevent Si_3N_4 formation upon combustion.

IR (KBr, cm^{-1}): 3357 (broad, N–H), 2887 (strong, C–H), 2163 (weak, Si–H), 1467-1343 (weak, CH_2), 1110 (strong, C–O), 1150-1061 (sharp, C–N), 963-842 (weak, C–C).

Preparation of polycarbosilazane 2e from silane and Jeffamine ED-2003 [poly(propylene glycol)-block-poly(ethylene glycol)-block-poly(propylene glycol) bis(2-aminopropyl ether)] using 2 mol% 47: Under N_2 atmosphere, a thick-walled glass bomb was charged with 0.013 g (0.014 mmol) of **47** in 3 mL benzene. Then 1.285 g (0.676 mmol) of poly(propylene glycol)-block-poly(ethylene glycol)-block-poly(propylene glycol) bis(2-aminopropyl ether) in 3 mL benzene was added to the mixture. The release of hydrogen gas was observed instantly. The bomb was sealed under N_2 and attached to the vacuum line. The solution was frozen in liquid N_2, gas was removed from the head space under vacuum, and 1 atm of SiH_4 was introduced. ***DANGER: SiH_4 will react violently with air and must be added under vacuum.*** The bomb was closed, disconnected from the vacuum line, and placed in a steel container to warm to room temperature in the

back of an empty fume hood with the sash closed. The solution changed from yellow to colorless after 1 h and the reaction was allowed to proceed at ambient temperature for 24 h. The bomb was then attached to the vacuum line and the solution was frozen in liquid N_2. The vacuum gauge read a pressure of approximately 1 atm of H_2 upon opening the bomb. Following H_2 removal, residual SiH_4 was allowed to slowly evaporate through repeated warming and cooling of the solution in liquid N_2 under dynamic vacuum. ***DANGER: Allowing a significant quantity of H_2 and SiH_4 to pass through the vacuum pump into a ventilation system at the same time can result in detonation.*** The bomb was brought into the glove box, the product was washed with THF (2 x 5 mL) and pentane (2 x 5 mL) and thoroughly dried *in vacuo* to isolate 0.961 g of a waxy solid (57%) identified as polycarbosilazane **2e**.

Elemental analysis for $(C_{117}H_{238}N_2O_{51}Si)_n$: Calcd. C, 55.82; H, 9.53; N, 1.11. Found: C, 56.52; H, 9.75; N, 1.34. Carbon content sufficient to prevent Si_3N_4 formation upon combustion.

IR (KBr, cm^{-1}): 3375 (broad, N–H), 2884 (strong, C–H), 2165 (weak, Si–H), 1471-1281 (weak, CH$_2$), 1115 (strong, C–O), 965-847 (weak, C–C).

Preparation of polycarbosilazane 2f from silane and bis(3-aminopropyl) terminated poly(dimethylsiloxane) using 2 mol% 47: Under N_2 atmosphere, a 100 mL thick-walled glass bomb was charged with 0.013 g (0.013 mmol) of **47** in 3 mL benzene, followed by the addition of 0.17 mL (0.66 mmol) of bis(3-aminopropyl) terminated poly(dimethylsiloxane). The release of hydrogen gas was observed instantly. The bomb was sealed under N_2 and attached to the vacuum line. The solution was frozen in liquid N_2, gas was removed from the head space under vacuum, and 1 atm of SiH_4 was introduced.

DANGER: SiH₄ will react violently with air and must be added under vacuum. The bomb was closed, disconnected from the vacuum line, and placed in a steel container to warm to room temperature in the back of an empty fume hood with the sash closed. The formation of a dark solid was observed after 1 h and the reaction was allowed to occur at ambient temperature for 24 h. The bomb was then attached to the vacuum line and the solution was frozen in liquid N_2. The vacuum gauge read a pressure of several atm of H_2 upon opening the bomb. Following H_2 removal, residual SiH_4 was allowed to slowly evaporate through repeated warming and cooling of the solution in liquid N_2 under dynamic vacuum. ***DANGER: Allowing a significant quantity of H_2 and SiH_4 to pass through the vacuum pump into a ventilation system at the same time can result in detonation.*** The bomb was brought into the glove box, the product was washed with THF (2 x 5 mL), and pentane (2 x 5 mL) then dried *in vacuo* to isolate 0.105 g (64%) of an off-white solid identified as polycarbosilazane **2f**.

Elemental analysis for $(C_{70}H_{208}N_2O_{31}Si_{33})_n$: Calcd. C, 33.61; H, 8.38; N, 1.12. Found: C, 34.32; H, 8.55; N, 1.55. Carbon content sufficient to prevent Si_3N_4 formation upon combustion.

IR (KBr, cm^{-1}): 2964 (strong, C–H), 1261 (sharp, C–Si), 1098-1022 (strong, Si–O), 801 (sharp, C–C).

Preparation of perhydropolysilazane (PHPS) from silane and ammonia using 2 mol% 47: Under N_2 atmosphere, a 100 mL thick-walled glass bomb was charged with 0.023 g (0.024 mmol) of **47** in 3 mL benzene. The bomb was sealed under N_2 and attached to the vacuum line. The solution was frozen in ice water and gas was removed from the head space under vacuum. Subsequently, 1 atm of NH_3 was added and condensed using liquid

nitrogen, and then 1 atm of SiH_4 was introduced. ***DANGER: SiH_4 will react violently with air and must be added under vacuum.*** The bomb was closed, disconnected from the vacuum line, and placed in a steel container to warm to room temperature in the back of an empty fume hood with the sash closed. The formation of a light-yellow solid was observed after 1 h and a freeze-pump-thaw cycle was performed under vacuum to release approximately 2500 mTorr of H_2 gas. The reaction was allowed to occur at ambient temperature for an additional 23 h. The bomb was then attached to the vacuum line and the solution was frozen in liquid N_2. The vacuum gauge read a pressure of several atm of H_2 upon opening the bomb. Following H_2 removal, residual NH_3 and SiH_4 was allowed to slowly evaporate through repeated warming and cooling of the solution in liquid N_2 under dynamic vacuum. ***DANGER: Allowing a significant quantity of H_2, NH_3, and SiH_4 to pass through the vacuum pump into a ventilation system at the same time can result in detonation.*** The bomb was brought into the glove box, the product was washed with THF (2 x 5 mL) and pentane (2 x 5 mL) then thoroughly dried *in vacuo* to isolate 0.225 g of a light-yellow powder identified as PHPS.

Elemental analysis for $(H_6N_2Si_3)_n$: Calcd. H, 5.11; N, 23.67. Found: H, 5.00; N, 15.60. Low N content due to Si_3N_4 formation upon combustion.

CP-MAS ^{15}N NMR (41 MHz): -27.26 (HN(SiH$_2$)$_2$), -42.82 (N(SiH$_2$)$_3$). CP-MAS ^{29}Si NMR (79 MHz): -37.90 (SiN$_2$H$_2$ and SiN$_3$H), -47.12 (SiN$_4$).

IR (KBr, cm^{-1}): 3438 (broad, NH$_2$), 3358 (broad, N–H), 2118 (strong, Si–H), 1551 (strong, NH$_2$), 1220 (medium, N–H), 967 (broad, Si–N).

MALDI-TOF [M+H]$^+$: 235.5 (n = 2), 469.6 (n = 4), 695.1 (n = 6), 932.5 (n = 8), majority of product did not dissolve in THF.

Control experiments showing a lack of reactivity between SiH₄ and NH₃ in the absence of catalyst: A J. Young tube was charged with 2 mL of 0.2 M TMS in benzene-d_6, sealed under N_2, and then attached to the vacuum line. The solution was frozen in ice water and gas was removed from the head space under vacuum. At that point, 1 atm of NH_3 was introduced and then condensed using liquid nitrogen, followed by the addition of 1 atm SiH_4. ***DANGER: SiH₄ will react violently with air and must be added under vacuum.*** The tube was closed, disconnected from the vacuum line, and placed in a steel container to warm to room temperature in the back of an empty fume hood with the sash closed. The reaction was allowed to occur at ambient temperature for 28 h and no color change or precipitate were observed. No reaction was observed by ^{1}H NMR spectroscopy.

In a second experiment, a 100 mL thick-walled glass bomb was charged with 5 mL benzene-d_6, sealed under N_2, and attached to the vacuum line. The solution was frozen in ice water and gas was removed from the head space under vacuum. Subsequently, 1 atm of NH_3 was introduced and condensed using liquid nitrogen, and then 1 atm of SiH_4 was added. ***DANGER: SiH₄ will react violently with air and must be added under vacuum.*** The reaction was allowed to occur at ambient temperature for 48 h, over which time no color change or precipitate were observed. The bomb was then attached to the vacuum line and the solution was frozen in liquid N_2. No H_2 was released upon admitting vacuum. At that point, residual SiH_4 and then NH_3 were allowed to slowly evaporate through repeated warming and cooling of the solution with liquid N_2 under dynamic vacuum. ***DANGER: Allowing a significant quantity of SiH₄ to pass through the vacuum pump into a ventilation system can result in detonation.*** No soluble products were observed by ^{1}H NMR spectroscopy.

Preparation of [($^{2,6\text{-}iPr_2Ph}$BDI)Mn(μ-NHiPr)]$_2$ (80): Under N$_2$ atmosphere, a 20 mL scintillation vial was charged with 0.022 g (0.023 mmol) of **47** in 10 mL of toluene. Next 3.8 μL of isopropylamine was added. The solution changed from yellow to orangish-yellow and the liberation of H$_2$ gas was observed. The mixture was allowed to stir at room temperature for 2 h. The solution was then filtered through Celite, and the volatiles were removed under vacuum. The product was washed with 5 mL of diethyl ether and dried under vacuum to yield 0.019 g (0.018 mmol, 79%) of a yellow solid identified as [($^{2,6\text{-}iPr_2Ph}$BDI)Mn(μ-NHiPr)]$_2$ (**80**). Single crystals suitable for X-ray diffraction were grown from a concentrated toluene solution at –35 °C.

Anal. for C$_{64}$H$_{98}$Mn$_2$N$_6$: Calcd. C, 72.42; H, 9.31; N, 7.92. Found: C, 72.42; H, 9.23; N, 6.75. Low nitrogen content due to reaction with oxygen or moisture prior to analysis.

Magnetic susceptibility (Evans method, 25 °C): μ_{eff} = 6.3 μ_B.

^{1}H NMR (400 MHz, benzene-d_6, 25 °C): 42.39 (peak width at half-height = 1370 Hz), 18.23 (1331 Hz), 3.58 (88 Hz), 1.43 (181 Hz), -19.46 (565 Hz).
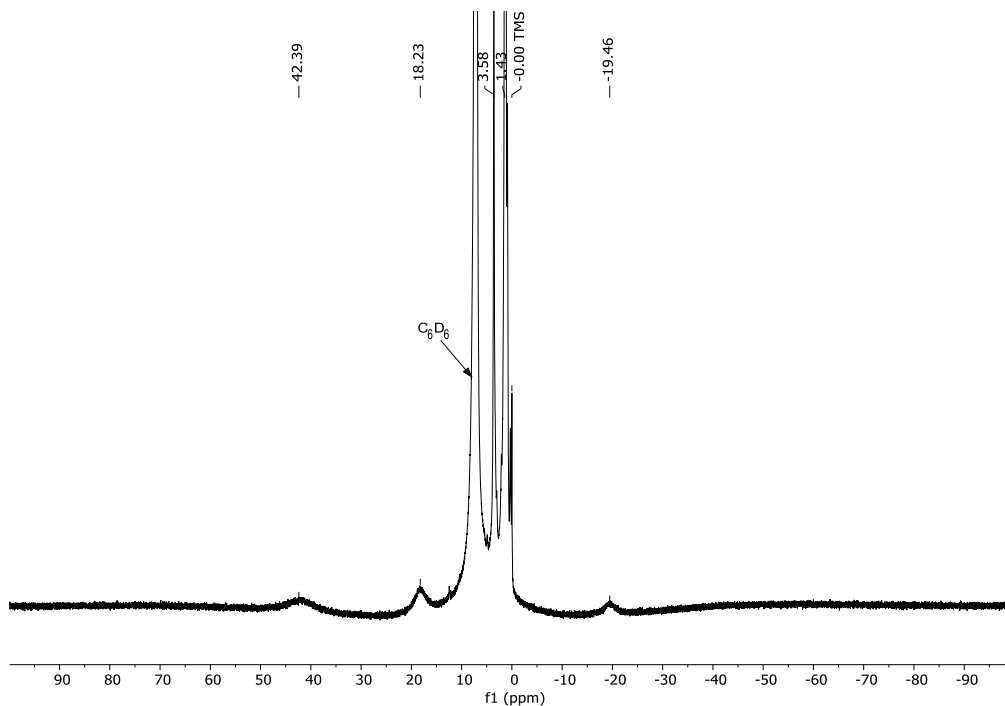
Figure 3.8. ^{1}H NMR spectrum of $[(^{2,6-i\mathrm{Pr}_2\mathrm{Ph}}\mathrm{BDI})\mathrm{Mn}(\mu\text{-}\mathrm{NH}^i\mathrm{Pr})]_2$ in benzene-d_6 at 25 °C.

3.6. References

(1)   Philipp, H. R. *J. Electrochem. Soc.* **1973**, *120* (2), 295.

(2)   De Brito Mota, F.; Justo, J. F.; Fazzio, A. *Phys. Rev. B* **1998**, *58* (13), 8323–8328.

(3)   Kaloyeros, A. E.; Pan, Y.; Goff, J.; Arkles, B. *ECS J. Solid-State Sci. Technol.* **2020**, *9* (6), 063006.

(4)   Khomenkova, L.; Normand, P.; Gourbilleau, F.; Slaoui, A.; Bonafos, C. *Thin Solid Films* **2016**, *617*, 143–149.

(5)   Kaga, Y.; Imamura, H.; Watanabe, J. U.S. Patent No. 7,915,533 (2011).

(6)   Kuo, Y. *Vacuum* **1998**, *51* (4), 741–745.

(7)   El amrani, A.; Menous, I.; Mahiou, L.; Tadjine, R.; Touati, A.; Lefgoum, A. *Renewable Energy* **2008**, *33* (10), 2289–2293.

(8) van Assche, F. J. H.; Unnikrishnan, S.; Michels, J. J.; van Mol, A. M. B.; van de Weijer, P.; van de Sanden, M. C. M.; Creatore, M. *Thin Solid Films* **2014**, *558*, 54–61.

(9) Roenigk, K. F.; Jensen, K. F. *J. Electrochem. Soc.* **1987**, *134* (7), 1777.

(10) Niskanen, A. J.; Chen, S.; Pore, V.; Fukazawa, A.; Fukuda, H.; Haukka, S. P. U.S. Patent No. 9,564,309 (2017).

(11) Yusup, L. L.; Park, J.-M.; Noh, Y.-H.; Kim, S.-J.; Lee, W.-J.; Park, S.; Kwon, Y.-K. *RSC Adv.* **2016**, *6* (72), 68515–68524.

(12) Laxman, R. K.; Roberts, D. A.; Hochberg, A. K.; Hockenhull, H. G.; Kaminsky, F. D. U.S. Patent No. 5,874,368 (1999).

(13) Kim, K.-H. *J. Korean Phys. Soc.* **2015**, *67* (12), 2115–2119.

(14) Aylett, B. J.; Emsley, J. *J. Chem. Soc. A* **1967**, No. 0, 652–655.

(15) Anderson, D. G.; Rankin, D. W. H. *Dalton Trans.* **1989**, *0* (5), 779–783.

(16) Schwab, S. T.; Graef, R. C.; Blanchard, C. R.; Dec, S. F.; Maciel, G. G. *Ceram. Int.* **1998**, *24* (6), 411–414.

(17) Wang, K.; Zheng, X.; Ohuchi, F. S.; Bordia, R. K. *J. Am. Ceram. Soc.* **2012**, *95* (12), 3722–3725.

(18) Zhang, Z.; Shao, Z.; Luo, Y.; An, P.; Zhang, M.; Xu, C. *Polym. Int.* **2015**, *64* (8), 971–978.

(19) Kang, Y. H.; Min, B. K.; Kim, S. K.; Bae, G.; Song, W.; Lee, C.; Cho, S. Y.; An, K.-S. *ACS Appl. Mater. Interfaces* **2020**, *12* (13), 15396–15405.

(20) Seyferth, D.; Wiseman, G. H.; Prud'homme, C. *J. Am. Ceram. Soc.* **1983**, *66* (1), C-13-C–14.

(21) Schwab, S. T. U.S. Patent No. 5,294,425 (1994).

(22) Liu, H. Q.; Harrod, J. F. *Organometallics* **1992**, *11* (2), 822–827.

(23) Reuter, M. B.; Hageman, K.; Waterman, R. *Chem. Eur. J.* **2021**, *27* (10), 3251–3261.

(24) Dunne, J. F.; Neal, S. R.; Engelkemier, J.; Ellern, A.; Sadow, A. D. *J. Am. Chem. Soc.* **2011**, *133* (42), 16782–16785.

(25)   Hill, M. S.; Liptrot, D. J.; MacDougall, D. J.; Mahon, M. F.; Robinson, T. P. *Chem. Sci.* **2013**, *4* (11), 4212–4222.

(26)   Bellini, C.; Dorcet, V.; Carpentier, J.-F.; Tobisch, S.; Sarazin, Y. *Chem. Eur. J.* **2016**, *22* (13), 4564–4583.

(27)   Li, N.; Guan, B.-T. *Eur. J. Inorg. Chem.* **2019**, *2019* (16), 2231–2235.

(28)   Pindwal, A.; Ellern, A.; Sadow, A. D. *Organometallics* **2016**, *35* (11), 1674–1683.

(29)   Yonekura, K.; Iketani, Y.; Sekine, M.; Tani, T.; Matsui, F.; Kamakura, D.; Tsuchimoto, T. *Organometallics* **2017**, *36* (17), 3234–3249.

(30)   Ríos, P.; Roselló-Merino, M.; Rivada-Wheelaghan, O.; Borge, J.; López-Serrano, J.; Conejero, S. *Chem. Commun.* **2018**, *54* (6), 619–622.

(31)   Allen, L. K.; García-Rodríguez, R.; Wright, D. S. *Dalton Trans.* **2015**, *44* (27), 12112–12118.

(32)   Bellini, C.; Orione, C.; Carpentier, J.-F.; Sarazin, Y. *Angew. Chem. Int. Ed.* **2016**, *55* (11), 3744–3748.

(33)   Bellini, C.; Roisnel, T.; Carpentier, J.-F.; Tobisch, S.; Sarazin, Y. *Chem. Eur. J.* **2016**, *22* (44), 15733–15743.

(34)   Morris, L. J.; Whittell, G. R.; Eloi, J.-C.; Mahon, M. F.; Marken, F.; Manners, I.; Hill, M. S. *Organometallics* **2019**, *38* (19), 3629–3648.

(35)   Gasperini, D.; King, A. K.; Coles, N. T.; Mahon, M. F.; Webster, R. L. *ACS Catal.* **2020**, *10* (11), 6102–6112.

(36)   Barroso, G.; Döring, M.; Horcher, A.; Kienzle, A.; Motz, G. *Adv. Mater. Interfaces* **2020**, *7* (10), 1901952.

(37)   Mukhopadhyay, T. K.; Flores, M.; Groy, T. L.; Trovitch, R. J. *Chem. Sci.* **2018**, *9* (39), 7673–7680.

(38)   Oh, C.; Siewe, J.; Nguyen, T. T.; Kawamura, A.; Flores, M.; Groy, T. L.; Anderson, J. S.; Trovitch, R. J.; Baik, M.-H. *Dalton Trans.* **2020**, *49* (41), 14463–14474.

(39)   Sanchez, A.; Itov, G.; Zhang, P.; Stephens, M. D.; Khandelwal, M. U.S. Patent Application No. 2018/0230171 (2018).

(40)   Levy, R. A.; Lin, X.; Grow, J. M.; Boeglin, H. J.; Shalvoy, R. *J. Mater. Res.* **1996**, *11* (6), 1483–1488.

(41) Gumpher, J.; Bather, W.; Mehta, N.; Wedel, D. *J. Electrochem. Soc.* **2004**, *151* (5), G353.

(42) Smith, A. L. *Spectrochimica Acta* **1960**, *16* (1), 87–105.

(43) Abel, A. E.; Kruger, T. A.; Mouk, R. W.; Knasiak, G. J. U.S. Patent No. 6,329,487 (2001).

(44) Iwamoto, Y.; Kikuta, K.; Hirano, S. *J. Mater. Res.* **1999**, *14* (11), 4294–4301.

(45) Bauer, F.; Decker, U.; Dierdorf, A.; Ernst, H.; Heller, R.; Liebe, H.; Mehnert, R. *Prog. Org. Coat.* **2005**, *53* (3), 183–190.

(46) Witanowski, M.; Stefaniak, I.; Webb, G. A. In *Annual Reports on NMR Spectroscopy*; Webb, G. A., Ed.; Academic Press, 1978; Vol. 7, pp 117–244.

(47) Lewis, R. H.; Maciel, G. E. *J. Mater. Sci.* **1995**, *30* (19), 5020–5030.

(48) Nguyen, T. T.; Kim, J.-H.; Kim, S.; Oh, C.; Flores, M.; Groy, T. L.; Baik, M.-H.; Trovitch, R. J. *Chem. Commun.* **2020**, *56*, 3959.

CHAPTER 4

THE SYNTHESIS OF ORGANIC POLYSILAZANES AND

POLYCARBOSILAZANES THROUGH MANGANESE CATALYZED Si–N

DEHYDROCOUPLING

4.1. Abstract

Organic polysilazanes are widely used in industry as a protective coating for automobiles and electronic devices. Industrial preparation of these materials involves the use of substituted halosilanes and ammonia, a methodology that generates a significant amount of ammonium salt which compromises sustainability. Herein, we demonstrate the first synthesis of organic polysilazanes through the Mn-catalyzed ambient temperature dehydrocoupling of ammonia to organic silanes. In addition, this study was extended to prepare a broad scope of polycarbosilazanes from organic silanes and diamines that show promise for coating applications. Specifically, the dehydrocoupling of ethylenediamine and phenyl silane in the presence of the β-diketiminate manganese hydride dimer $[(^{2,6-iPr_2Ph}BDI)Mn(\mu-H)]_2$ was found to achieve a maximum turnover frequency of 300 s^{-1}, the highest number ever reported for this transformation. The mechanism of dehydrocoupling was explored with the isolation of an amido dimer, $[(^{2,6-iPr_2Ph}BDI)Mn(\mu-NH_2)]_2$, which undergoes σ-bond metathesis with H–Si to regenerate the precatalyst while affording the desired Si–N bond.

4.2. Introduction

Compounds that possess Si–N bonds are of great significance since they can be used to deposit coatings that exhibit high chemical and thermal stability. A wide range of ceramic materials including Si_3N_4, SiON, SiCN, SiCNO, or SiC can be synthesized depending on the composition of the polymer precursors and the curing conditions, and they offer excellent protective coatings for microelectronics, photonic devices and solar cells.[1–4] Organic polysilazanes, in which the hydrogens of the halosilane precursors are replaced with organic functional groups, allow for the fine-tuning of performance properties for coating applications (Figure 4.1, a). In addition, the hydrolytic instability of Si–N linkages has been exploited for surface functionalization. For example, a hydrophilic surface can be changed to a hydrophobic one after treating with hexamethyldisilazane without the need for any catalyst.[5] Organic polysilazanes can undergo radical or hydrosilylation cross-linking followed by pyrolysis to afford ceramic precursors, or can react with alcohol to form RTV silicone networks.[6–8] Furthermore, these are cured by moisture at or slightly higher than room temperature to yield amorphous SiO_x rich dense coatings. This makes them ideal for applications where thermal curing is not suitable, such as the application of anti-fouling, anti-graffiti, and non-stick coatings for weather protection.[9–11] Polycarbosilazanes are another type of Si–N polymer which contains Si–N–C moieties (Figure 4.1, b). This material can be prepared by using functionalized halosilanes and amine precursors which contain more than one amino group; however, the product portfolio of commercially available polycarbosilazanes is still under-developed. Although the properties and applications of polycarbosilazanes have been less explored

than commonly used organic polysilazanes, coatings derived from polycarbosilazanes can offer crack resistance and thermal insulation properties.[12,13]
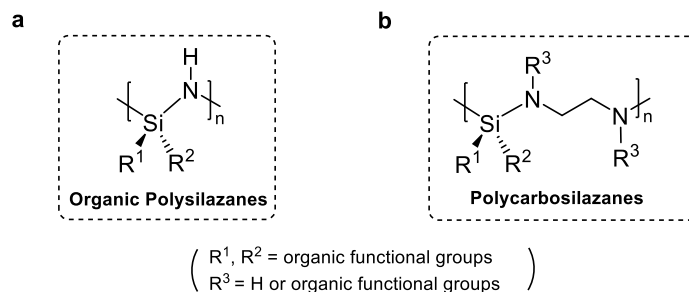
Figure 4.1. a) Structure of organic polysilazanes. b) An example of polycarbosilazanes.

Researchers have demonstrated the synthesis of polycarbosilazanes through Si-N dehydrogenative coupling as an alternative way to avoid the use of corrosive precursors. In 2016, Carpentier and Sarazin group reported the use of $Ba[CH(SiMe_3)_2]_2(THF)_3$ to catalytically dehydrocouple diphenylsilane and *p*-xylylenediamine to yield cyclic or linear polycarbosilazanes and further explored the sequential cross-dehydrocoupling of amines and hydrosilanes to afford oligocarbosilazanes (Figure 4.2, a).[14,15] Later on, the Manners and Hill team explored the reactivity of alkaline-earth metal catalysts to prepare ferrocene-containing polycarbosilazanes which were pyrolyzed to afford magnetic ceramic materials (Figure 4.2, b).[16] In 2020, Wester and co-workers reported the synthesis of an oligocarbosilazane from 1,4-benzenedimethanamine and phenylsilane using an Fe(II) catalyst (Figure 4.2, c).[17] Recently, we demonstrated the preparation of aminosilane CVD precursors and polycarbosilazanes from amines and SiH_4 using the β-diketiminate manganese dimer, $[(^{2,6-iPr_2Ph}BDI)Mn(\mu-H)]_2$ (**47**, Figure 4.2f).[18] Our report also demonstrated the preparation of perhydropolysilazane from NH_3 and SiH_4 (Figure 4.2, d).
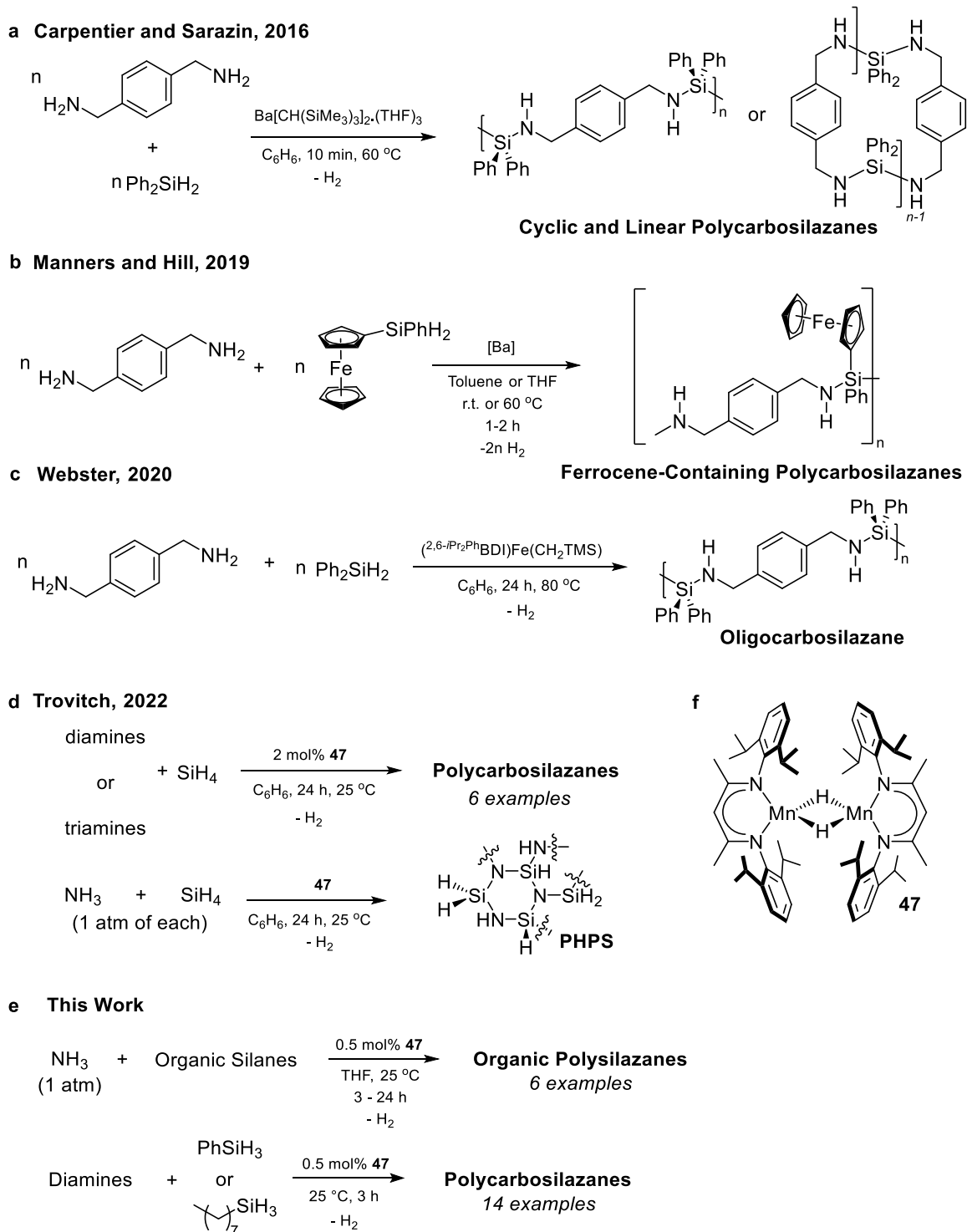
Figure 4.2. a)-d) Previous reports on metal-catalyzed dehydrocoupling to synthesize polycarbosilazanes and oligocarbosilazanes. e) Contribution of this work. f) The previously described Mn catalyst (**47**).

After these findings, we sought to develop a way to synthesize and characterize organic polysilazanes and polycarbosilazanes using organic silanes and amines through Mn-catalyzed dehydrocoupling. Herein, we demonstrate the preparation of organic polysilazanes from NH_3 and organic silanes for the first time (Figure 4.2, e). The report also describes the preparation and characterization of 14 polycarbosilazanes from the dehydrocoupling of diamines to phenylsilane and octylsilane under mild conditions. The coating applications of these polycarbosilazanes were evaluated and compared with organic polysilazanes, which indicates both materials can be used for coating purposes.

4.3. Results and Discussions

4.3.1. Preparation of Organic Polysilazanes

Knowing that **47** is active for the dehydrocoupling of SiH_4 and amines, this project began with the preparation of organic polysilazanes. In particular, a thick-walled glass bomb was charged with phenylsilane and 1 mol% of **47** (0.5 mol% of Mn), no reaction was observed. The bomb was then sealed under N_2 and attached to the vacuum line, where the solution was frozen in liquid nitrogen and gas was removed from the head space under vacuum, followed by the introduction of 1 atm of NH_3. The reaction was allowed to warm to room temperature for 1 h, then H_2 gas was removed through a free-pump-thaw cycle to avoid the build-up of H_2 pressure. The reaction was allowed to occur at ambient temperature for an additional 2 h, when H_2 and residual NH_3 was removed by warming the solution under dynamic vacuum. A clear oil identified as **3a**, was obtained in 60% yield after work-up under inert atmosphere. The IR spectrum of **3a** features N–H stretching vibrations from 3462 to 3387 cm^{-1}, a strong Si–H vibration at 2150 cm^{-1} and a vibration at 906 cm^{-1} for Si–N stretching. The ^{29}Si NMR spectrum of this compound shows several

resonances at -23.35, -23.92, -30.81 and -31.28 ppm. The peaks at -23.35 and -23.92 ppm are assigned to PhHSiN$_2$ units in the middle of the chain, while the latter resonances are believed to belong to PhH$_2$$Si$N moieties at the end of the chain. MALDI-TOF mass spectroscopy data for **3a** reveals oligomers of up to n = 11 (m/z = 1351.6). Repeating the same protocol with octylamine and diphenylsilane afforded product **3b** (64% yield) and **3c** (72% yield), as dark oils. FT-IR spectra of these products confirms the presence of residual N–H and Si–H functionalities and the formation of Si–N bonds. This data is consistent with the observation in our previous report, in which steric hindrance was found to inhibit the catalysis and prevent the formation of quaternary aminosilanes.[18] Because of this, extra time was required for the dehydrocoupling of bis(ethylamino)silane, 1,1,3,3-tetramethyldisiloxane and 1,1,3,3-tetramethyldisilazane with NH$_3$. For example, product **3e** was obtained from the dehydrocoupling of 1,1,3,3-tetramethyldisiloxane and NH$_3$ after 24 h as a dark oil in 78% yield. This product is notable because it represents a key intermediate of organic polysilazanes curing in air. The FT-IR spectrum of this product shows a weak vibration of unreacted Si–H at 2120 cm^{-1} and a strong Si–O–Si stretch at 1014 cm^{-1}. This data is consistent with the resonances observed in the ^{29}Si NMR spectrum of **3e**, which features a peak at -13.15 ppm [(CH$_3$)$_2$NSi-OSi-] while the peak at -21.81 ppm is assigned to residual [(CH$_3$)$_2$NSi-OSiH(CH$_3$)$_2$] linkages at the end of the chain.

Table 4.1. The preparation of organic polysilazanes from **47**-catalyzed dehydrocoupling of NH_3 and organic silanes.

3a 99% **3b** 99% **3c** 99%

3d[a] 99% **3e**[a] 99%
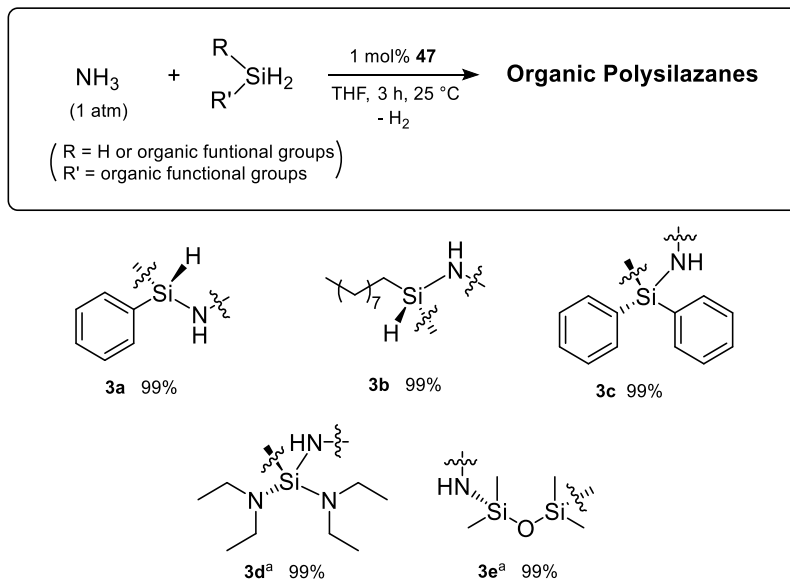
Percent conversion determined by ^{1}H NMR spectroscopy. [a] Trial conducted at ambient temperature for 24 h. Percent yield was given.

4.3.2 Preparation of Polycarbosilazanes from Phenylsilane

After preparing highly crossed link polycarbosilazanes from SiH_4, we sought to prepare and study these types of compounds through the dehydrocoupling of diamines and $PhSiH_3$, which is a more approachable silane that is often found in academic laboratories. A scope of 7 diamines were screened for dehydrocoupling with $PhSiH_3$ using 0.5 mol% of **47** (1 mol% of Mn), which is demonstrated in Table 4.2. In particular, $PhSiH_3$ and ethylenediamine was added to a 20 mL scintillation vial containing a mixture of **47** and 0.35 µL of mesitylene as the internal standard. The vial was kept uncapped to avoid the buildup of H_2, which might limit the polymerization reaction. After 3 h under inert atmosphere, the reaction mixture turned into a viscous gel, which was then washed with benzene-d_6 and the liquor was collected for NMR characterization. Greater than 99% conversion was observed for all trials by examining the consumption of starting amine [1]H

NMR resonances. Isolated product **4a** was obtained by following the same procedure without the use of mesitylene. After the transformation, the catalyst was deactivated by quickly exposing the reaction to air while the work-up was carried out under inert-atmosphere. The insoluble products were washed with dry pentane and ether to remove short chain length species and any residues of the catalyst, and a 72% yield of polycarbosilazane was obtained. The IR spectrum of **4a** was found to feature a broad N-H stretch at 3372 cm^{-1}, a strong Si–H stretch at 2119 cm^{-1} and a weak Si–N stretch at 830 cm^{-1}.[19] The ^{29}Si NMR spectrum was found to exhibit several peaks at -20.72, -21.37 and -21.71 ppm, which were assigned to HPh*Si*(NR)$_2$ moieties in the middle of the polymer chain; while the peaks at -25.30 and -25.85 ppm belong to different H$_2$Ph*Si*NR environments on the end of the polymer chain. From last chapter and other literature review, the instability of the polymer toward halogenated and hydrophilic solvents (such as chloroform, methanol, water) and the insolubility of the polymer in normal organic solvents can be a limiting factor for studying the molecular weight of the polymer.[18,20] Although product **4a** is not soluble in THF, analysis of the resulting solution by MALDI-TOF mass spectrometry revealed Gaussian distributions from 329 to 3079 g/mol. These peaks are consistent with residual 3- up to 17-unit oligomers of **4a** that were washed off of the bulk product.

Table 4.2. Synthesis of polycarbosilazanes via **47**-catalyzed dehydrogenative coupling of diamines and phenylsilane.
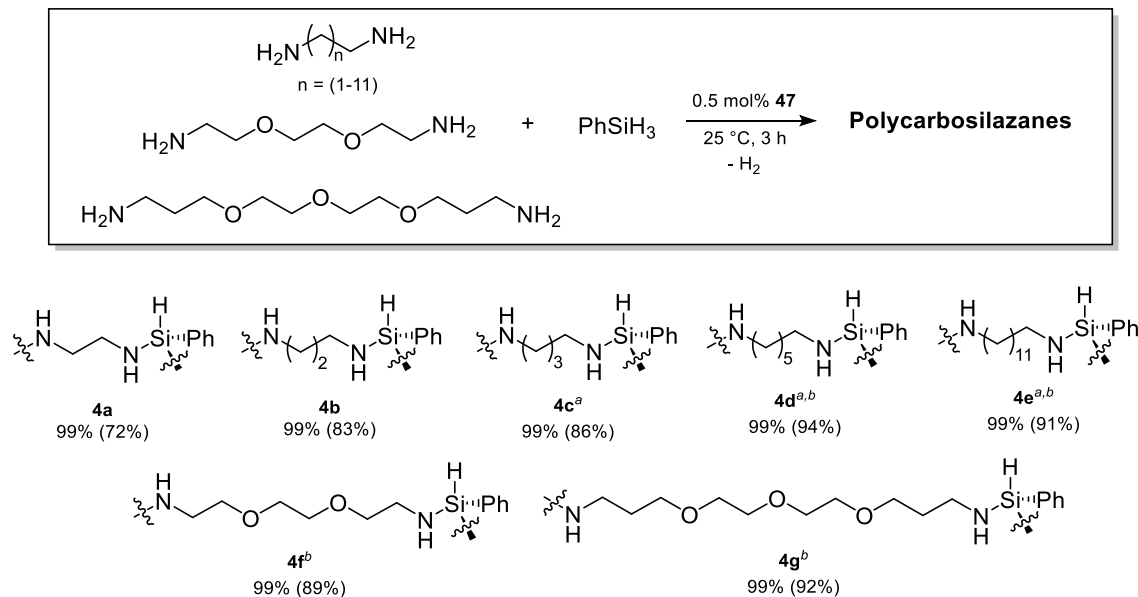
Percent conversion determined by ^{1}H NMR spectroscopy (integration of residual amine against mesitylene standard). Isolated yields (shown in parentheses). ^{a} Trial conducted in 2 mL of benzene-d_6. ^{b} Trial conducted for 3 h at 60 °C.

The chain length of diamines was systematically varied from C$_2$ to C$_{12}$ (**4a-4e**) and diamines containing ether functional groups were also evaluated for the polymerization (**4f**, **4g**). Using the same procedure with 1,3-diaminopropane and 1,4-diaminobutane afforded an 83% yield of polycarbosilazane **4b** and 86% of **4c**, respectively. ^{1}H NMR revealed that product **4c** contained an *H*PhSi(NR)$_2$ environment (5.21 ppm), which corresponds to the peak at -23.5 ppm in the ^{29}Si NMR spectrum. The end-chain H$_2$Ph*Si*NR moieties were observed from -26.59 to -27.28 ppm. As observed for **4a**, only oligomers from n=1 to n=8 were observed via MALDI – TOF spectroscopy (from 189 to 1507 g/mol). The infrared spectrum of **4c** was found to feature N–H (3388-3290 cm^{-1}), sp^3 C–H (3057-2851 cm^{-1}), Si–H (2101 cm^{-1}), and Si–N (810 cm^{-1}) stretching vibrations. It is noted that heating the reaction to 60 °C is required for the complete dehydrocoupling of solid

substrates (**4d**, **4e**) and ether-functionalized amines (**4f**, **4g**). In particular, the use of 1,6-diaminohexane afforded **4d** as a yellow solid in 94% yield, while the dehydrocoupling of 1,12-diaminododecane yielded 91% of **4e**. ^{29}Si NMR of product **4d** shows a major peak at -26.55 ppm, which indicates the presence of Ph*Si*H(NHR)$_2$ linkages. Although the majority of **4e** did not dissolve in THF, the liquid washed-off from the bulk product afforded a maximum M_n = 3396 g/mol (n=11). Likewise, the transformation of 2,2'-(ethylenedioxy)bis(ethylamine) and 4,7,10-trioxa-1,13-tridecanediamine yielded dark brown solids (89% yield for **4f** and 92% for **4g**, respectively). MALDI-TOF spectra of the oligomers that are soluble in THF reveal the highest average M_n = 3110 g/mol (n=12) for **4f** and 3036 g/mol (n=9) for **4g**.

4.3.3. Preparation of Polycarbosilazanes from Octylsilane.

Octyl silane was evaluated in this study as it a commercially available liquid alkyl silanes that can allow for the preparation of polycarbosilazanes that mimic the products used in industry, which are prepared from chloromethyl silane. Following a similar procedure, all the dehydrocoupling transformations with octylsilane reached 99% conversion after 3 h (Table 4.3). The dehydrocoupling of octylsilane and ethylenediamine at ambient temperature yielded 81% of a dark brown solid after 3 h (**5a**). The FT-IR spectrum of **5a** shows a broad stretching vibration at 3404 cm^{-1} for N–H, a strong resonance from 2924 to 2845 cm^{-1} (C–H), and a vibration of Si–H bond at 2115 cm^{-1}. The maximum average molecular weight of the oligomer that can detected by MALDI-MS is up to 2251 g/mol (n=11). The dehydrocoupling of 1,3-diaminopropane and 1,4-diaminobutane yielded an oily product **5b** (73% yield) and solid **5c** (83% yield), respectively. Data from NMR spectrometry of **5c** revealed H(C$_8$H$_{17}$)Si(NR)$_2$ linkages, which are assigned to the

peaks at 4.79 ppm (^{1}H NMR) and -14.75 ppm (^{29}Si NMR). Likewise, the mass spectrum of **5c** shows distributions of low-weight oligomers at 445 (n=2), 694 (n=3), 932 (n=4), 1170 (n=6) and 1694 (n=7). Heating the reaction to 60 °C is required to dehydrocouple 1,6-aminosilane and 1,12-diaminododecane and octylsilane, affording 77% of isolated solid product **5d** and 90% of **5e**, respectively. As predicted, diaminosilane is the major linkage in both of the cases and ^{29}Si NMR spectroscopy shows peaks at -18.34 ppm (for the middle-chain environment) and -23.99 ppm (for the beginning or the end of the polymer chain) for **5d**, with peaks at -18.34 and -23.99 ppm for **5e**. Although the majority of **5d** is insoluble in THF, MALDI-TOF data from the THF-washed liquid from **2e** reveals the highest molecular weight of 2826 g/mol (n=8). Lastly, 94% of dark solid **5f** and 88% of **5g** were obtained from the polymerization of 2,2'-(ethylenedioxy)bis(ethylamine) and 4,7,10-trioxa-1,13-tridecanediamine with octylsilane at 60 °C in 3 h. The presence of amino and hydrosilane functional groups within the polymer were confirmed by FT-IR spectroscopy, in particular, the spectrum of **5f** in KBr demonstrated a broad stretch at 3390 cm^{-1} for N–H, a strong peak at 2104 cm^{-1} for Si–H vibration, and a weak peak at 835 cm^{-1} which belongs to the Si–N vibration.

Table 4.3. Synthesis of polycarbosilazanes via **47**-catalyzed dehydrogenative coupling of diamines and octylsilane.
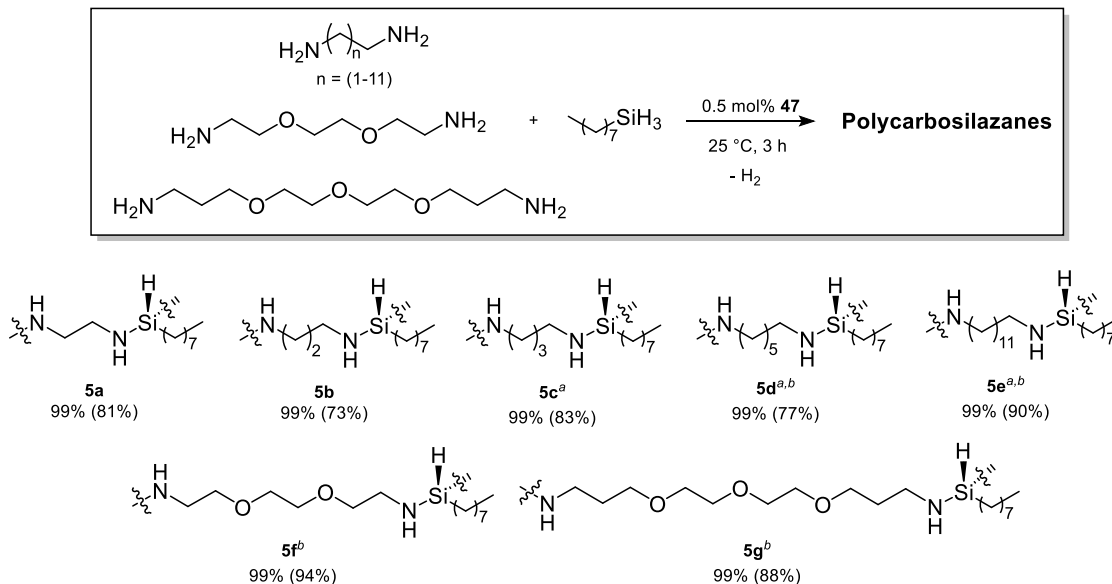
Percent conversion determined by ^{1}H NMR spectroscopy (integration of residual amine against mesitylene standard). Isolated yields (shown in parentheses). [a] Trial conducted in 2 mL of benzene-d_6. [b] Trial conducted for 3 h at 60 °C.

4.3.4. Turnover Frequency Experiment.

To examine the maximum reactivity of the catalyst, a neat dehydrocoupling experiment between ethylenediamine and phenylsilane was conducted using 0.01 mol% of **47** in the presence of mesitylene as the internal standard. Aliquots of the reaction were collected over the course of 3 h, the catalyst was deactivated by I_2 and the percent conversion was determined by ^{1}H NMR spectroscopy by integrating the starting amine versus the internal standard. For demonstration, images of the experiment over time are shown in Figure 4.3. Surprisingly, 30% of ethylenediamine was converted after only 10 seconds of catalysis, which equates to a TOF of 300 s^{-1}. Then 99% conversion was noted after 30 minutes, which equates to TON of 9,900 based on substrates, 19,800 based on N–H bond dehydrocoupling (Table 4.4). This is the highest data reported for this

133

transformation, which is three times higher observations using [Pt(I^{t}Bu')(I^{t}Bu)][BAr$^F_4$], which claimed to have the maximum TOF of 92 s^{-1} for the dehydrocoupling of diethylamine and phenylsilane.[21] Interestingly, it took 1 minute to see vigorous H$_2$ gas evolution, followed by the changes in color of the solution. This is due to the nature of the neat reaction that involves only a small amount of the solid catalyst. Another reason can be the initiation of [($^{2,6-iPr_2Ph}$BDI)Mn(μ-H)]$_2$ to form the corresponding monomers, and the reaction of the hydride monomer and the amine taking place. One can argue that the final product is black due to the presence of Mn nanoparticles. However, we believe that it is the color of the polycarbosilazane product since only 5 mg of the catalyst (containing 0.5 mg of Mn) was used in this reaction, which is unlikely to make a major contribution to the color of the reaction considering the volume of substrate employed.

Table 4.4. Percent conversion for the dehydrogenative coupling of ethylenediamine and phenylsilane using 0.01 mol% **47** determined by ^{1}H NMR over 3 h.

Time	% Conversion
10 s	30
30 s	52
1 min	78.5
5 min	89
10 min	91
30 min	99
60 min	99
120 min	99

| 5 s | 1 min | 2 min | 2 min 30 s |

| 3 min | 5 min | 1 h | 3 h |
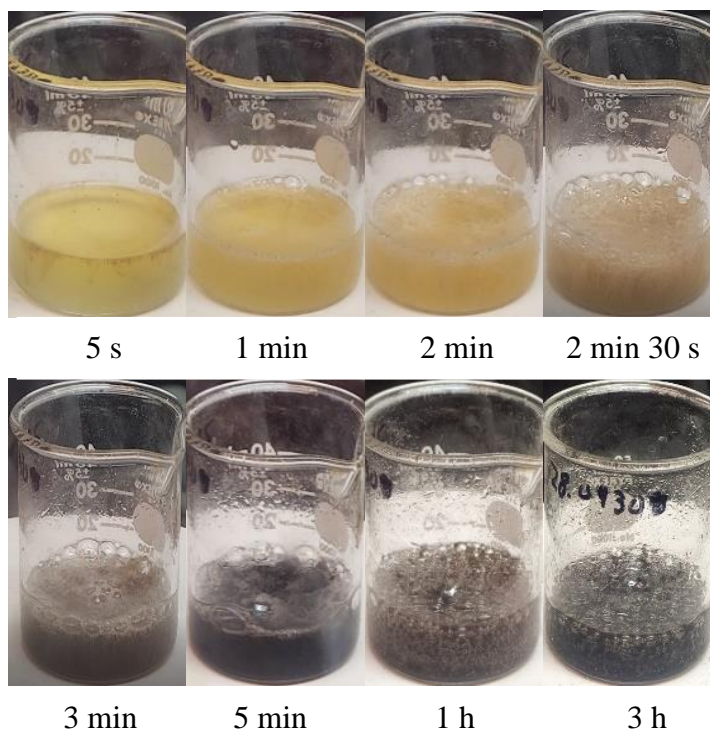
Figure 4.3. Images of the dehydrogenative coupling of ethylenediamine and phenylsilane using 0.01 mol% of **47** collected over the course of 3 h at ambient temperature.

4.3.5. Degradation Study

As observed in Chapter 3, polycarbosilazanes prepared from SiH_4 possess unstable Si–H and Si–N bonds that can be hydrolyzed by moisture at ambient temperature.[18] The stability of product **4a** was similarly evaluated by FT-IR spectroscopy under air featuring 23% humidity (Figure 4.4). A significant decrease in Si–H and Si–N infrared vibration absorbance was noticed over the course of 24 h, followed by the appearance of an Si–O vibration. Visually, **4a** was observed to reacted with moisture in the air instantly after being removed from the glovebox and turned to a hard white solid after 24 h of exposure (Figure 4.5). Droplets of ethylenediamine condensation from the degradation were observed around the polymer and it was confirmed by NMR that this polycarbosilazane reacted with water to regenerate amine and yield a siloxane network.
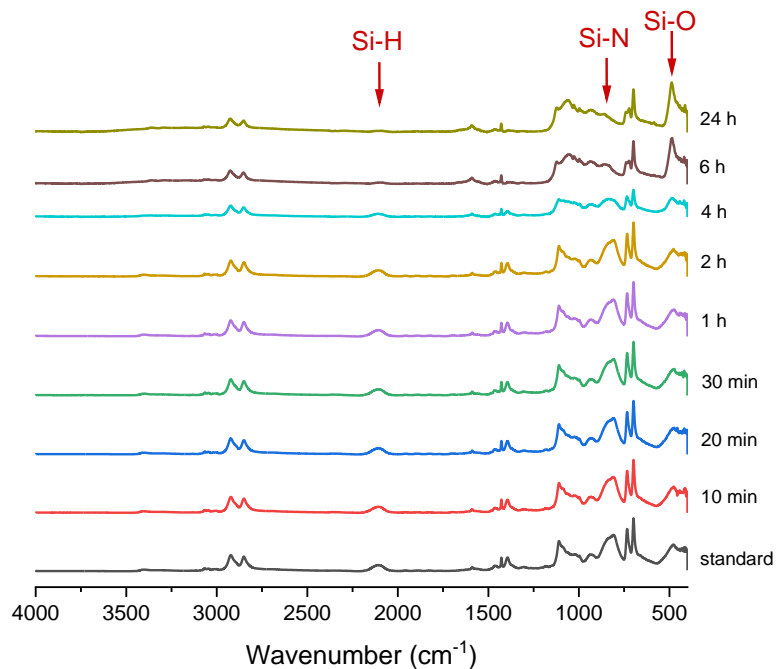
Figure 4.4. FT-IR spectra of polycarbosilazane **4a** collected before (black) and after exposure to air (23% humidity).
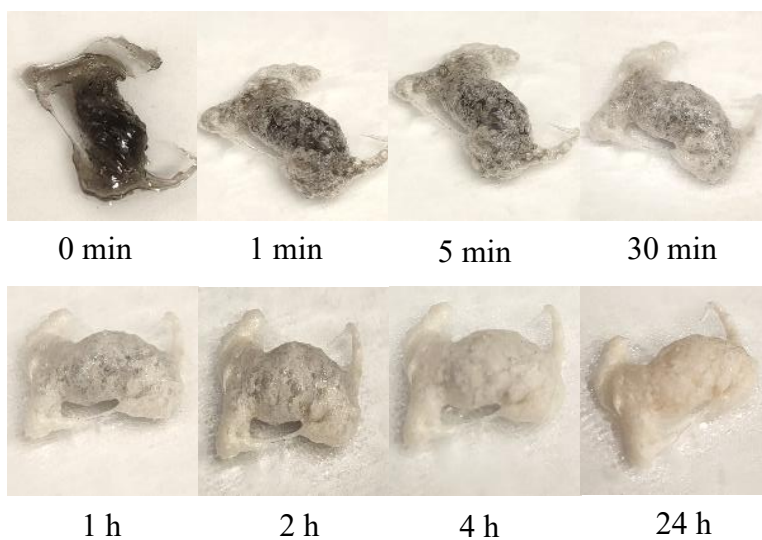
Figure 4.5. Images of polycarbosilazane **4a** collected before and after 24 h exposure to air (23% humidity).

4.3.6. Coating Applications

      To evaluate the coating ability of our organic polysilazanes and polycarbosilazanes, catalysis was conducted in THF to obtain soluble polycarbosilazanes and the products were further diluted in THF to prepare 20% solutions. A piece of copper tape was dip-coated in a solution of **3a** in THF under inert atmosphere. A similar procedure was conducted to obtain **4a**-coated and **5a**-coated copper tape. The morphology and composition of the coated tapes were evaluated by SEM (Figure 4.6) and EDX (Figure 4.7). In particular, SEM images of **3a**-coated copper tape under N_2 at room temperature demonstrate that organic polysilazane **3a** formed a clear, uniform (thick) coating on the surface. Although small cracks were observed at 25000 x magnification, the overall coating was found to be fairly smooth. Interestingly, polycarbosilazanes **4a** and **5a** were found to also form a stable coating on copper under N_2 at room temperature (Figure 4.6). Both 100 x magnification and the 25000 x images show thick and uniform coatings. EDX data of the coating surfaces shows little-to-no Mn (< 0.1 at%) for all the cases (Figure 4.7). Organic polysilazane **3a** was found to have less Si content in the coating with high Si-accumulated areas observed (Figure 4.7, top). The Si/Cu molar ratio was found to be 0.021 in flat areas, 0.035 near the edge and 0.91 in high-accumulation areas. Likewise, polycarbosilazane **4a** was well coated on copper with molar ratio of Si/Cu = 0.14 in flat areas and 0.42 in the high Si-accumulation areas, respectively. EDX data of **5a**-coated copper demonstrates Si/Cu = 0.061 in flat areas and 0.88 in high-accumulation areas.
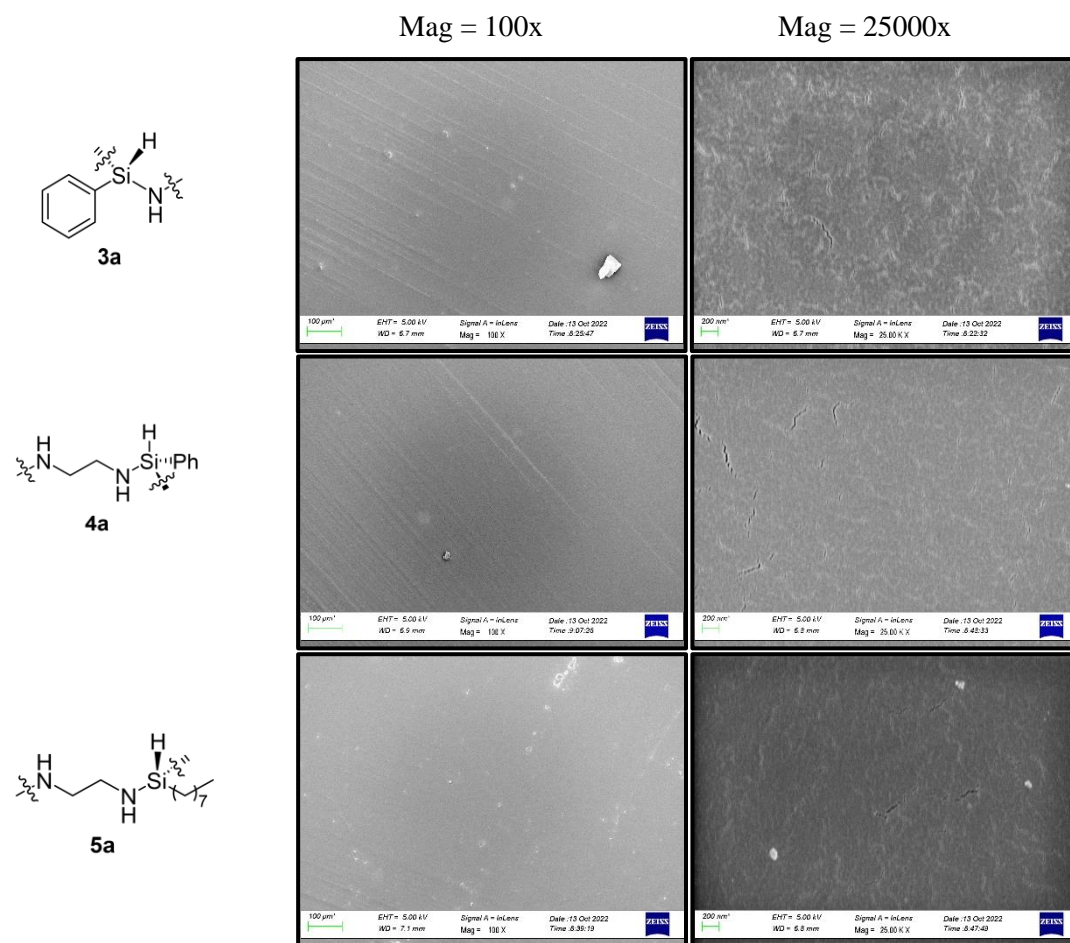
Figure 4.6. SEM images of copper tape coated with **3a**, **4a**, **5a** under N_2.
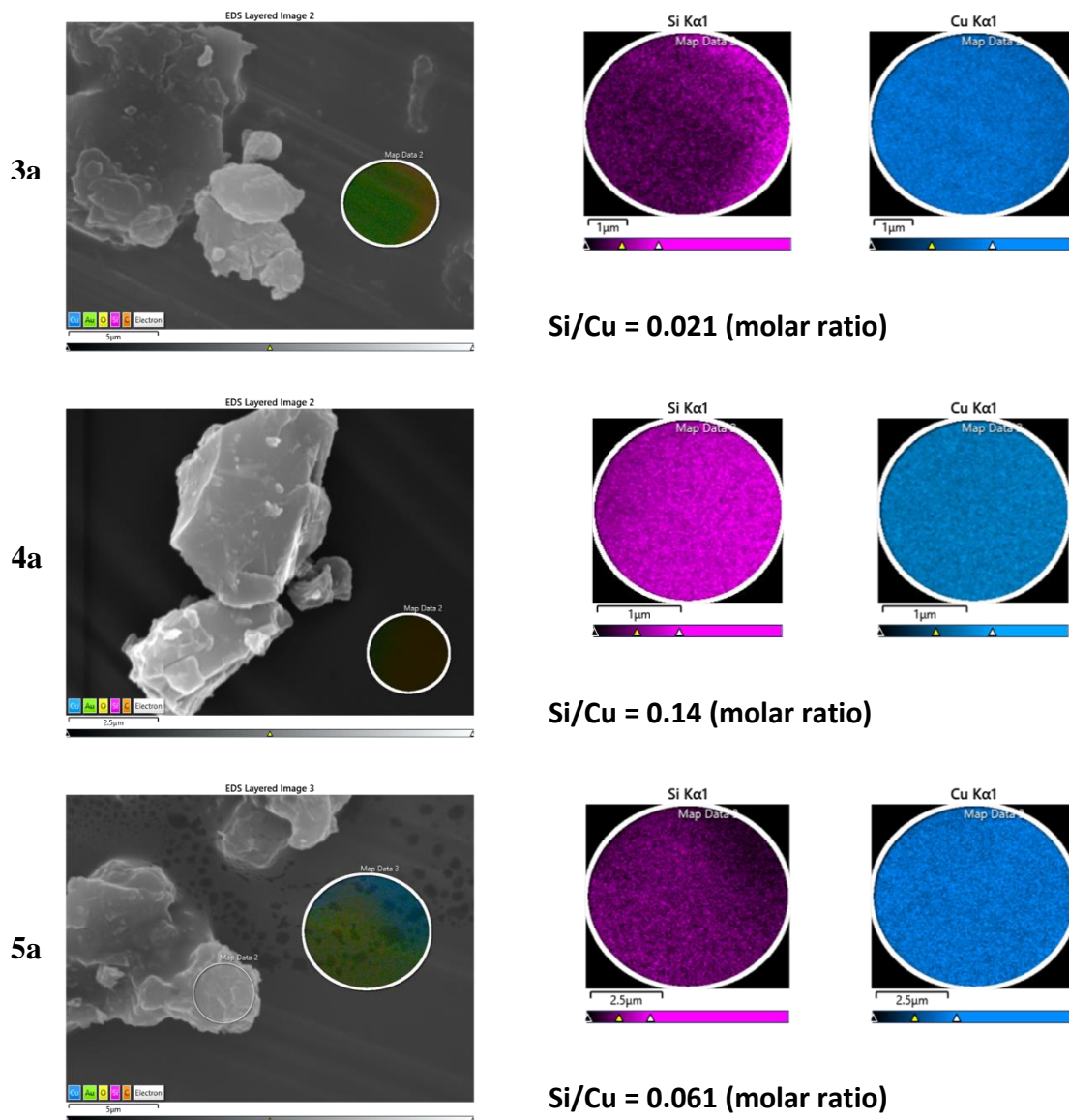
Figure 4.7. EDX data of copper tape coated with **3a**, **4a**, **5a** under N_2.

Since product **4a** was found to form the best coating on copper, further bulk hydrolysis of this material was evaluated by examining the morphology of the **4a**-coated copper tape after curing in air at room temperature. As discussed above, **4a** was coated on copper to form a glass-like coating with little-to-no cracks observed (Figure 4.8, top). After 1 day of air exposure, the coating was found to be transparent with a few small cracks

139

observed (Figure 4.8, middle). However, the morphology of the coating was fairly smooth considering the hydrolysis after 24 h. Larger cracks were observed after 3-day air exposure (Figure 4.8, bottom). The SEM image at 25000 x magnification of **4a**-coated copper after 3 days curing in air demonstrates a rough surface due to the forming of a Si–O amorphous network. EDX data of **4a-**coated copper tape after 1 day exposing to air reveals Si/Cu = 1 (molar ratio) overall but many areas feature high-Si accumulation up to Si/Cu= 8.7 due to the hydrolysis which eliminates amine fragments.
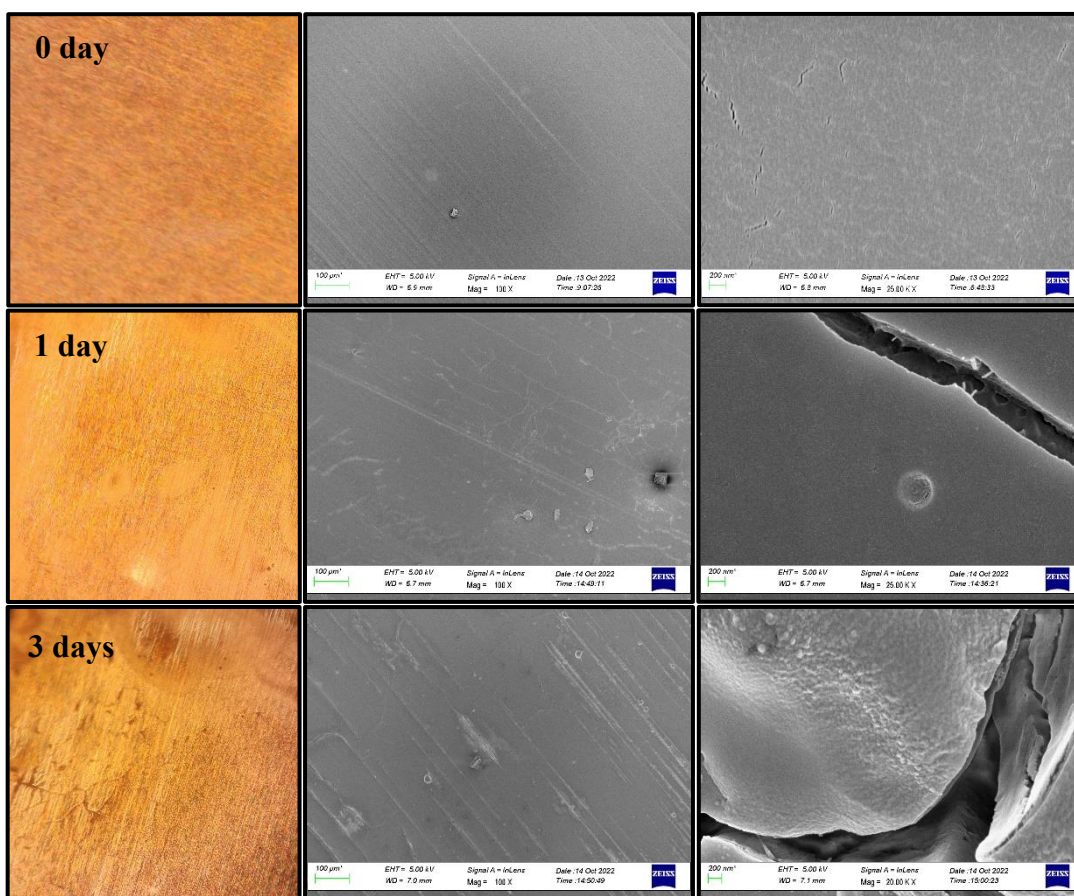
Figure 4.8. SEM images of **4a**-coated copper tape after 1-day and 3-day of air exposure at room temperature.

4.3.7. Swelling Study

Interestingly, products **4c**-**4g** and **5c**-**5g** were found to swell and adsorb organic solvents. The swelling is due to the ability of these polymers to form networks which branch from a central silicon atom. This property was evaluated for **4c** as a representative example (Table 4.5). In particular, a dry sample of **4c** was preweighed and added to a vial which was filled with dry solvent (toluene, THF, diethylether or pentane) until the sample was fully submerged. After 1 day and 3 days at room temperature, **4c** was removed from the solvent, dried on a Kimwipe, and reweighed. Data from Table 4.5 demonstrates a 4x increase in mass when **4c** was submerged in toluene or diethylether for 3 days at room temperature, while there was only a 2.3x increase in mass for pentane absorbance in the same amount of time. This product shows an even better swelling effect when left in THF, with a 6.3x increase in mass observed after 3 days.

Table 4.5. Swelling study of **4c** in organic solvents at ambient temperature.

Entry	Solvents	Dry mass (m_0) [mg]	Wet mass after 1 day (m_1)	Wet mass after 3 days (m_3)	m_1/m_0	m_3/m_0
1	Toluene	25	90.6	99.1	3.62	3.96
2	THF	23.6	104.5	146.4	4.5	6.31
3	Diethylether	13.5	52.4	54	3.88	4
4	Pentane	38.5	84.1	88.5	2.18	2.30

4.3.7. Thermal Properties

The thermal stability of the polycarbosilazane products was evaluated by Thermogravimetric Analysis and Differential Scanning Calorimetry (TGA-DSC), where the samples were heated up to 1000 °C under N_2 and in air. Overall, it was found that the polycarbosilazane products are stable under both conditions at modest temperatures. In

particular, TGA data shows that product **4a** loses 5% of weight at 173 °C under N_2 and 183 °C in air, while the same temperatures were found to be higher for **4c** ($T_{-5\%,N2}$ = 273 °C, $T_{-5\%,O2}$ = 272 °C). Interestingly, we observed decreases in the stability of the products when octylsilane was employed. As compared to **4c**, **5c** loses 5% of weight at 116.5 °C and at 179.5 °C in air. This difference might be due to π-interactions of the phenyl ring that contribute to the thermal stability of the derived products. However, this trend was found to be reversed when using functionalized amines. In particular, **4f**, which was obtained from phenylsilane and 2,2'-(ethylenedioxy)bis(ethylamine), possess $T_{-5\%,N2}$ at 156.7 °C and $T_{-5\%,O2}$ at 125.8 °C. In contrast, these values were 237 under N_2 and 206 in air for compound **2f**, respectively. Overall, the polycarbosilazanes were found to lose between 52% to 82% of their weight at the end of the heating treatment to afford silicon nitride or siliconcarbonitride ceramic materials.

4.3.8. Mechanistic Insight

Experiments described in Chapter 3 showed that **47** does not react with SiH_4,[18] which is consistent with observations in this study (Figure 4.9). Hydrogen evolution was only noticed when amines were introduced to **47**. In particular, adding 1 atm of NH_3 to **47** resulted in the formation of an amido dimer $[(^{2,6-iPr_2Ph}BDI)Mn(\mu\text{-}NH_2)]_2$ (**81**) (Figure 4.8, a). The solid-state structure of **81** revealed a pseudo-tetrahedral coordination environment around each metal center and a Mn–Mn distance of 3.042(1) Å, which is slightly shorter than the Mn–Mn bond length of 3.0487(6) found in **80**.[18] This distance is consistent with a weak Mn-Mn bonding interaction. The hydrogen atoms on each bridging NH_2 ligand were located in the difference map, confirming that these ligands are monoanionic and that the Mn centers of **81** are divalent.
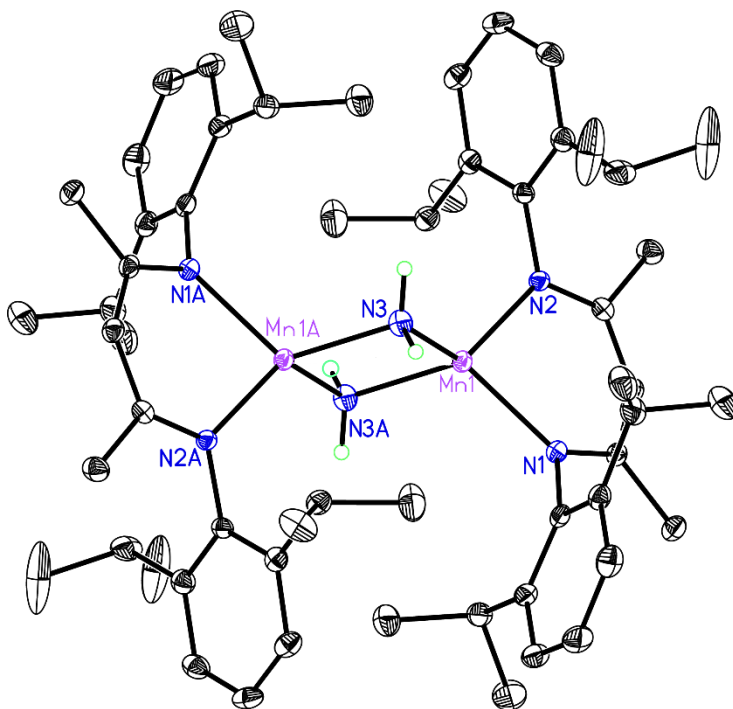
Figure 4.9. Solid-state structure of **81**.
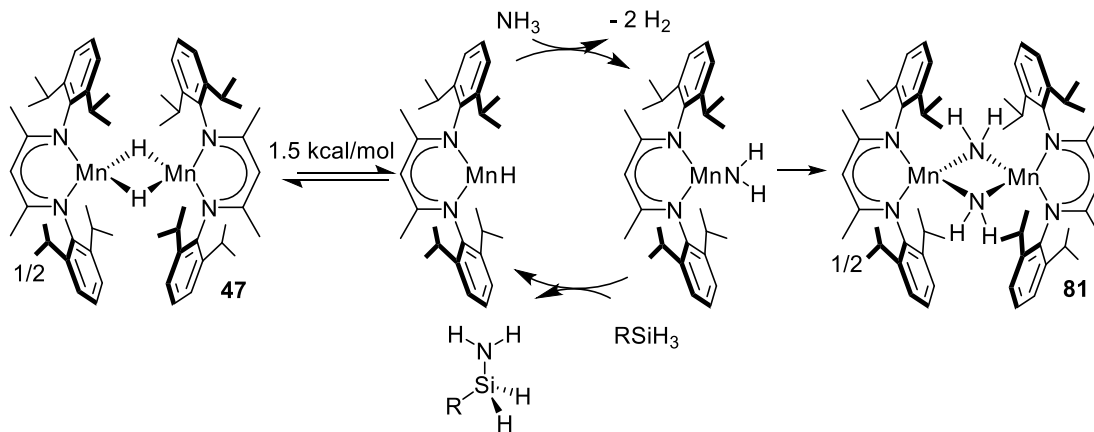
Figure 4.10. Proposed mechanism of **47**-catalyzed dehydrocoupling of NH_3 and silanes.

Based on our previous findings, the monomer of **47** is readily available at 25 °C with a dissociation barrier of 1.5 kcal/mol (Figure 4.9).[22] Therefore, when ammonia is present, Mn–H and N–H σ-bond metathesis occurs to eliminate H_2 and generate the corresponding amido intermediate. In the absence of silane, these intermediates dimerize, which has allowed for the isolation and the characterization of **81**. When silane is

143

introduced, this intermediate can dissociate and undergo σ-bond metathesis with an Si-H bond in the silane substrate to regenerate **47** and afford Si–N bond formation.

4.4. Conclusion

To summarize, this study demonstrates the first halogen-free preparation of organic polysilazanes through Mn-catalyzed dehydrocoupling of NH_3 and organic silanes at ambient temperature. The report greatly contributes to the development of polycarbosilazanes through the efficient synthesis of 14 polycarbosilazanes using organic silanes and a broad scope of diamines which feature varied alkyl chain lengths and functionality under mild conditions using a low catalyst loading. A turnover frequency experiment revealed a TOF of 300 s^{-1}, which renders **47** the best catalyst known for this transformation. Substrate utilization characteristics of the product were evaluated through NMR spectroscopy, FT-IR and MALDI-TOF mass spectroscopy. The polycarbosilazane products were easily hydrolyzed in air featuring 23% humidity to afford an amorphous Si–O network and the amine precursor. The morphology of the polycarbosilazane-coating material was then studied by SEM and EDX, which demonstrates the ability to evenly coat substrates under N_2 and form a stable, uniform coating after 1000 °C heating treatment under argon. Interestingly, the polycarbosilazanes derived from phenylsilane and *n*-octylsilane with diamines were found to swell in organic solvents, which might be useful for absorption applications. A mechanism of the Mn-catalyzed dehydrocoupling of amines and silanes is proposed, which involves the reaction between **47** and NH_3 to afford **81**. This intermediate was found to undergo σ-bond metathesis with Si–H bonds to regenerate the active precatalyst and release the silylamine product.

144

4.5. Experimental Procedures

General considerations: All reactions were performed inside an MBraun glovebox under an atmosphere of purified nitrogen or on a high-vacuum manifold. Toluene, tetrahydrofuran, diethyl ether, and pentane were purchased from Sigma-Aldrich, purified using a Pure Process Technology solvent system, and stored in the glovebox over activated 4 Å molecular sieves and potassium in prior use. Benzene-d_6 was purchased from Oakwood Chemicals and dried over 4 Å molecular sieves and potassium prior to use. Toluene-d_8 and benzene were purchased from Sigma-Aldrich and dried over 4 Å molecular sieves and potassium prior to use. Mesitylene was purchased from Sigma-Aldrich and dried over 4 Å molecular sieves. Celite was obtained from Oakwood Chemicals. Phenylsilane and diphenylsilane were obtained from Oakwood. Octylsilane, tetramethyldisilazane, tetramethyldisiloxane were obtained from Gelest. Ammonia was purchased from Sigma-Aldrich. Ethylenediamine, 1,3-diaminopropane, 1,4-diaminobutane, 1,6-diaminohexane, 1,12-diaminododecane, 2,2'-(ethylenedioxy)bis(ethylamine) and 4,7,10-trioxa-1,13-tridecanediamine were purchased from Oakwood Chemicals. All liquid substrates were dried over 4 Å molecular sieves prior to catalyst screening.

Solution nuclear magnetic resonance (NMR) spectra were recorded at room temperature on a Varian 400 MHz or a Bruker 500 MHz NMR spectrometer. All ^{1}H NMR and ^{13}C NMR chemical shifts (ppm) are reported relative to Si(Me)$_4$ using [1]H (residual) and ^{13}C chemical shifts of the solvent as secondary standards. ^{29}Si NMR chemical shifts (ppm) are reported relative to Si(Me)$_4$ using the absolute ^{1}H NMR frequency of an internal Si(Me)$_4$ standard.

MALDI-TOF Mass Spectrometry: Samples were analyzed on a Bruker microFlex LRF instrument (Billerica, MA, USA) with a 337 nm laser in positive mode scanning from 200 to 200,000 *m/z*. The ion source 1 voltage was 19.50 kV, ion source 2 voltage was 18.15 kV, the lens voltage was 7.00 kV, and ion suppression was off.

Thermogravimetric Analysis and Differential Scanning Calorimetry (TGA-DSC): TGA-DSC were performed using a METTLER Toledo TGA/DSC1 STAR system. All samples were heated from 30 °C to 1000 °C at a rate of 10 °C per minute under nitrogen or air atmosphere.

Powder X-ray Diffraction (PXRD): PXRD patterns of all samples after TGA were collected on a Bruker D2 Phaser powder X-ray diffractometer with a Cu Kα radiation wavelength of 1.5406 Å at a scan speed of 1 second/step and a step size of 0.02°.

Scanning Electron Microscopy and Energy-Dispersive X-ray Analysis (SEM-EDX): Scanning electron microscopy (SEM) images of selected samples were collected on a FIB Zeiss Auriga microscope operating at 5.0 kV acceleration voltage. Energy-dispersive X-ray data was collected on the same microscope at 20 kV acceleration voltage.

Preparation of organic polysilazane 3a from ammonia and phenylsilane using 0.5 mol% 47.

Under N_2 atmosphere, a 100 mL thick-walled glass bomb was charged with 0.010 g (0.011 mmol) of **47** in 3 mL THF. Next, 268 μL (2.17 mmol) of phenylsilane was added and no obvious color change was noted. The bomb was sealed under N_2 and attached to the vacuum line. The solution was frozen in liquid nitrogen and gas was removed from the head space under vacuum. Subsequently, 1 atm of NH_3 was added and condensed using liquid nitrogen. The bomb was closed, disconnected from the vacuum line, and placed in a

146

steel container to warm to room temperature in the back of an empty fume hood with the sash closed. After 1 h, a freeze-pump-thaw cycle was performed under vacuum to release approximately 2500 mTorr of H_2 gas. The reaction was allowed to occur at ambient temperature for an additional 2 h. The bomb was then attached to the vacuum line and the solution was frozen in liquid N_2. The vacuum gauge read a pressure of 2500 mTorr of H_2 upon opening the bomb. Following H_2 removal, residual NH_3 was allowed to slowly evaporate through warming the solution under dynamic vacuum. The bomb was brought into the glove box, the solution was filtered through Celite, and the solvent was removed *in vacuo* to isolate 0.326 g of a clear oil identified as **3a** (60% yield).

^{29}Si NMR (99 MHz, C_6D_6): -23.35 (HPh*Si*N), -23.92 (HPh*Si*N), -30.81 (H_2Ph*Si*N), -31.28 (H_2Ph*Si*N).

IR (KBr, cm^{-1}): 3462-3387 (broad, N–H), 3068-3006 (strong, C–H), 2150 (strong, Si–H), 906 (weak, Si–N).

MALDI-TOF [M+H]$^+$: 235.5 (n = 2), 469.6 (n = 4), 695.1 (n = 6), 932.5 (n = 8), majority of product did not dissolve in THF.

Figure 4.11. Representative ^{29}Si NMR spectrum of **3a** in benzene-d_6.
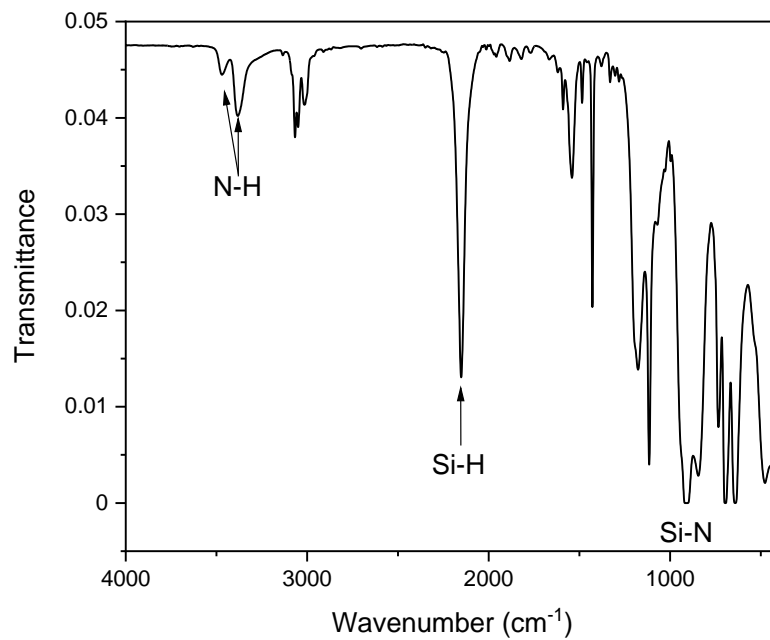
Figure 4.12. Representative FT-IR spectrum of **3a**.
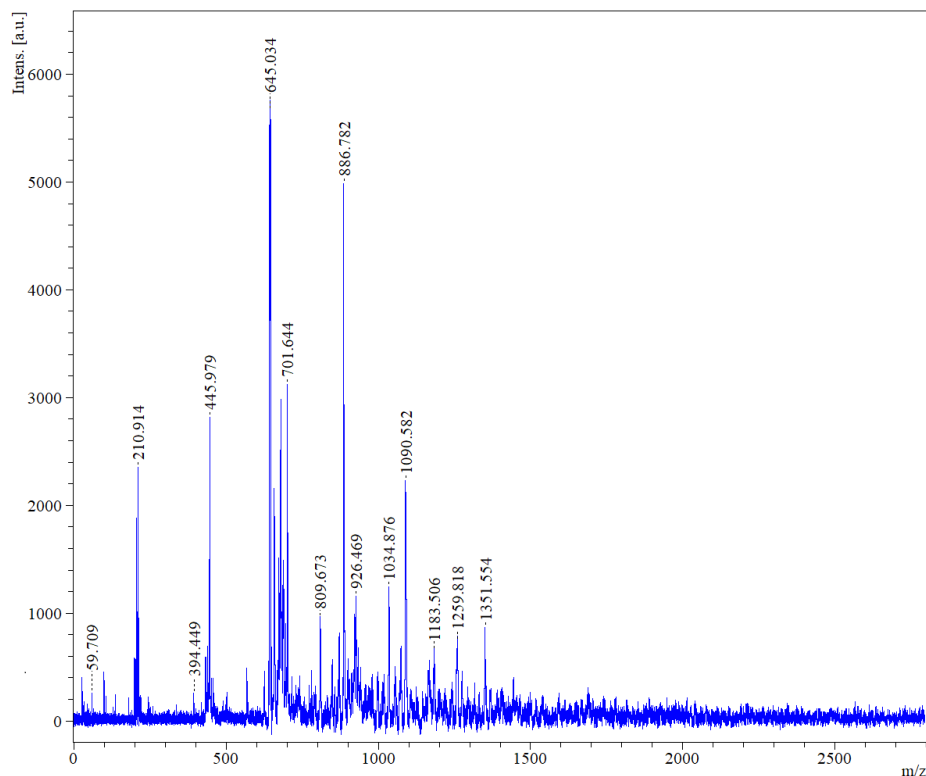
Figure 4.13. Representative MALDI-TOF mass spectrum of **3a**.

Preparation of organic polysilazane 3b from ammonia and octyl silane using 0.5 mol% 47.

Under N_2 atmosphere, a 100 mL thick-walled glass bomb was charged with 0.011 g (0.012 mmol) of **47** in 3 mL THF. Next, 450 µL (2.324 mmol) of octylsilane was added and no obvious color change was noted. The bomb was sealed under N_2 and attached to the vacuum line. The solution was frozen in liquid nitrogen and gas was removed from the head space under vacuum. Subsequently, 1 atm of NH_3 was added and condensed using liquid nitrogen. The bomb was closed, disconnected from the vacuum line, and placed in a steel container to warm to room temperature in the back of an empty fume hood with the sash closed. After 1 h, a freeze-pump-thaw cycle was performed under vacuum to release approximately 2500 mTorr of H_2 gas. The reaction was allowed to occur at ambient

149

temperature for an additional 2 h. The bomb was then attached to the vacuum line and the solution was frozen in liquid N_2. The vacuum gauge read a pressure of 2500 mTorr of H_2 upon opening the bomb. Following H_2 removal, residual NH_3 was allowed to slowly evaporate through warming the solution under dynamic vacuum. The bomb was brought into the glove box, the solution was filtered through Celite, and the solvent was removed *in vacuo* to isolate 0.24 g of a dark oil identified as **3b** (64% yield).

^{29}Si NMR (99 MHz, C_6D_6): -15.57 (H*Si*N), -15.85 (H*Si*N), -16.13 (H*Si*N), -21.19 (H_2*Si*N).

IR (KBr, cm^{-1}): 3468-3391 (broad, N–H), 2107 (strong, Si–H), 918 (weak, Si–N).

Preparation of organic polysilazane 3c from ammonia and diphenylsilane using 0.5 mol% 47.

Under N_2 atmosphere, a 100 mL thick-walled glass bomb was charged with 0.008 g (0.009 mmol) of **47** in 3 mL THF. Next, 338 µL (1.7 mmol) of diphenylsilane was added and no obvious color change was noted. The bomb was sealed under N_2 and attached to the vacuum line. The solution was frozen in liquid nitrogen and gas was removed from the head space under vacuum. Subsequently, 1 atm of NH_3 was added and condensed using liquid nitrogen**.** The bomb was closed, disconnected from the vacuum line, and placed in a steel container to warm to room temperature in the back of an empty fume hood with the sash closed. After 1 h a freeze-pump-thaw cycle was performed under vacuum to release approximately 2500 mTorr of H_2 gas. The reaction was allowed to occur at ambient temperature for an additional 2 h. The bomb was then attached to the vacuum line and the solution was frozen in liquid N_2. The vacuum gauge read a pressure of 2500 mTorr of H_2 upon opening the bomb. Following H_2 removal, residual NH_3 was allowed to slowly evaporate through warming the solution under dynamic vacuum. The bomb was brought

into the glove box, the solution was filtered through Celite, and the solvent was removed *in vacuo* to isolate 0.246 g of a dark oil identified as **3c** (92% yield).

^{29}Si NMR (99 MHz, C_6D_6): -20.20 (Ph_2SiN_2), -20.81 (Ph_2SiN_2), -22.09 (HPh_2SiN), -22.51 (HPh_2SiN).

IR (KBr, cm^{-1}): 3478-3394 (broad, N–H), 2133 (strong, Si–H), 926 (weak, Si–N).

Preparation of organic polysilazane 3d from ammonia and bis(diethylamino)silane using 0.5 mol% 47.

Under N_2 atmosphere, a 100 mL thick-walled glass bomb was charged with 0.015 g (0.016 mmol) of **47** in 3 mL THF. Next, 355 µL (1.61 mmol) of bis(diethylamino)silane was added and no obvious color change was noted. The bomb was sealed under N_2 and attached to the vacuum line. The solution was frozen in liquid nitrogen and gas was removed from the head space under vacuum. Subsequently, 1 atm of NH_3 was added and condensed using liquid nitrogen. The bomb was closed, disconnected from the vacuum line, and placed in a steel container to warm to room temperature in the back of an empty fume hood with the sash closed. After 1 h a freeze-pump-thaw cycle was performed under vacuum to release approximately 300 mTorr of H_2 gas. The reaction was allowed to occur at ambient temperature for an additional 23 h. The bomb was then attached to the vacuum line and the solution was frozen in liquid N_2. The vacuum gauge read a pressure of 500 mTorr of H_2 upon opening the bomb. Following H_2 removal, residual NH_3 was allowed to slowly evaporate through warming the solution under dynamic vacuum. The bomb was brought into the glove box, the solution was filtered through Celite, and the solvent was removed *in vacuo* to isolate 0.169 g of a dark oil identified as **3d** (55% yield).

IR (KBr, cm^{-1}): 3486-3371 (broad, N–H), 2126 (strong, Si–H), 918 (weak, Si–N).

Preparation of organic polysilazane 3e from ammonia and 1,1,3,3-tetramethyldisiloxane using 0.5 mol% 47.

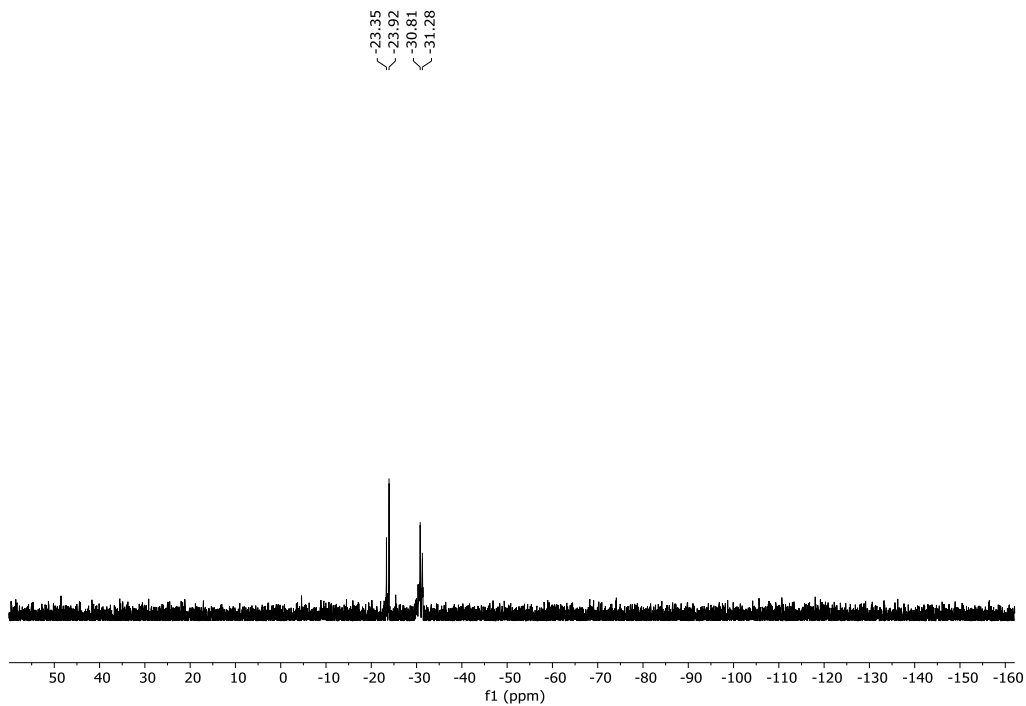Under N_2 atmosphere, a 100 mL thick-walled glass bomb was charged with 0.017 g (0.018 mmol) of **47** in 3 mL THF. Next, 320 µL (1.8 mmol) of 1,1,3,3-tetramethyldisiloxane was added and no obvious color change was noted. The bomb was sealed under N_2 and attached to the vacuum line. The solution was frozen in liquid nitrogen and gas was removed from the head space under vacuum. Subsequently, 1 atm of NH_3 was added and condensed using liquid nitrogen. The bomb was closed, disconnected from the vacuum line, and placed in a steel container to warm to room temperature in the back of an empty fume hood with the sash closed. After 1 h a freeze-pump-thaw cycle was performed under vacuum to release approximately 300 mTorr of H_2 gas. The reaction was allowed to occur at ambient temperature for an additional 23 h. The bomb was then attached to the vacuum line and the solution was frozen in liquid N_2. The vacuum gauge read a pressure of 300 mTorr of H_2 upon opening the bomb. Following H_2 removal, residual NH_3 was allowed to slowly evaporate through warming the solution under dynamic vacuum. The bomb was brought into the glove box, the solution was filtered through Celite, and the solvent was removed *in vacuo* to isolate 0.212 g of a dark oil identified as **3e** (78% yield).

^{29}Si NMR (99 MHz, C_6D_6): -13.15 [$(CH_3)_2 Si ONSiO(CH_3)_2H$], -21.81 [$(CH_3)_2SiONSiO(CH_3)_2H$].

Preparation of polycarbosilazane 4a from phenylsilane and ethylenediamine using 0.5 mol% 47.

Procedure for solution NMR characterization: In a N_2 filled glovebox, a 20 mL vial was pre-weighed before adding 0.002 g (0.002 mmol) of **47** in 1 mL of benzene-d_6. Afterwards, 55 µL (0.444 mmol) of phenylsilane was added and no obvious color change was noted.

Next, 30 µL (0.444 mmol) of ethylenediamine was added. Instantly, the evolution of hydrogen gas was observed and the solution turned orange in color. The vial was kept uncapped under N_2 atmosphere for 3 h at ambient temperature to yield a dark brown solution. Then the catalyst was deactivated by exposing to air and quickly degassed under vacuum for 30 s. The solution was transferred to a J. Young tube to obtain solution NMR characterization. More than 99% conversion was observed after 3 h by examining the consumption of starting amine ^{1}H NMR resonances.

Procedure for isolated yield and solid-state characterization: In a N_2 filled glovebox, a 20 mL vial was pre-weighed before adding 0.021 g (0.022 mmol) of **47**, followed by 550 µL (4.48 mmol) of phenylsilane, no obvious color change was noted. Next, 300 µL (4.48 mmol) of ethylenediamine was added. The formation of H_2 was observed and the solution turned orange in color. The reaction was kept uncapped at room temperature for 3 h to obtain a dark greenish-brown solid. Next, the vial was brought outside the glovebox, when the catalyst was deactivated by exposing to air. The reaction was then brought back into the glovebox and quickly degassed under vacuum for 30 s. The product was washed with pentane and ether and dried under vacuum to obtain 0.533 g a solid product identified as **4a** (72% yield).

IR (KBr, cm^{-1}): 3372 (broad, N–H), 3066-2848 (strong, C–H), 2119 (strong, Si–H), 830 (weak, Si–N).

MALDI-TOF [M+H]$^+$: 329.1 (n=2), 696 (n=4), 934.5 (n=5 + 1 phenylsilane), 1165.8 (n=7), 1455 (n=8), 1694 (n=10 +1 ethylenediamine), 1976.7 (n=12), 2257 (n=13 + 1 phenylsilane), 2541.4 (n=15 + 1 ethylenediamine), 2825.8 (n=17 + 1 ethylenediamine), 3079.2 (n=18 + 1 phenylsilane).

TGA (N_2): T_5 = 173 °C, total %wt. loss at 1000 °C = 52%. TGA (O_2): T_5 = 183 °C, total %wt. loss at 1000 °C = 66.4%.

Preparation of polycarbosilazane 4b from phenylsilane and 1,3-diaminopropane using 0.5 mol% 47.

Procedure for solution NMR characterization: In a N_2 filled glovebox, a 20 mL vial was pre-weighed before adding 0.003 g (0.003 mmol) of catalyst **47** in 1 mL of benzene-d_6. Afterwards, 65 µL (0.53 mmol) of phenylsilane was added and no obvious color change was noted. Next, 44 µL (0.53 mmol) of 1,3-diaminopropane was added. Instantly, the evolution of hydrogen gas was observed and the solution turned orange in color. The vial was kept uncapped under N_2 atmosphere for 3 h at ambient temperature to yield a dark brown solution. Then the catalyst was deactivated by exposing to air and quickly degassed under vacuum for 30 s. The solution was transferred to a J. Young tube to obtain solution NMR characterization. More than 99% conversion was observed after 24 h by examining the consumption of starting amine ^{1}H NMR resonances.

Procedure for isolated yield and solid-state characterization: In a N_2 filled glovebox, a 20 mL vial was pre-weighed before adding 0.021 g (0.023 mmol) of **1**, followed by 550 µL (4.5 mmol) of phenylsilane, no obvious color change was noted. Next, 400 µL (4.5 mmol) of 1,3-diaminopropane was added. The formation of H_2 was observed and the solution turned orange in color. The reaction was kept uncapped at room temperature for 3 h to obtain a dark brown oil. Next, the vial was brought outside the glovebox, when the catalyst was deactivated by exposing to air. The reaction was then brought back into the glovebox and quickly degassed under vacuum for 30 s. The product was washed with pentane and

ether and dried under vacuum to obtain 0.666 g of an oily product identified as **4b** (83% yield).

IR (KBr, cm^{-1}): 3402 (broad, N–H), 3062-2839 (strong, C–H), 2103 (strong, Si–H), 795-849 (weak, Si–N).

Preparation of polycarbosilazane 4c from phenylsilane and 1,4-diaminobutane using 0.5 mol% 47.

Procedure for solution NMR characterization: In a N_2 filled glovebox, a 20 mL vial was pre-weighed before adding 0.002 g (0.002 mmol) of catalyst **47**. Afterwards, 39 µL (0.317 mmol) of phenylsilane was added and no obvious color change was noted. Next, 32 µL (0.317 mmol) of 1,4-diaminobutane in 1 mL of benzene-d_6 was added. Instantly, the evolution of hydrogen gas was observed and the solution turned orange in color. The vial was kept uncapped under N_2 atmosphere for 3 h at ambient temperature to yield a dark brown solution. Then the catalyst was deactivated by exposing to air and quickly degassed under vacuum for 30 s. The solution was transferred to a J. Young tube to obtain solution NMR characterization. More than 99% conversion was observed after 24 h by examining the consumption of starting amine ^{1}H NMR resonances.

^{1}H NMR (500 MHz, C_6D_6) δ 7.74 (d, 2H, phenyl), 7.26 (m, J = 12.6 Hz, 3H, phenyl), 5.21 (s, 1H, Ph*H*SiN), 2.85 (s, 4H, HNC*H*$_2$), 1.36 (s, 4H, HNCH$_2$C*H*$_2$).

^{13}C NMR (126 MHz, C_6D_6) 134.94 (phenyl), 134.58 (phenyl), 130.34 (phenyl), 130.27 (phenyl), 43.33 (HNC*H*$_2$), 42.24 (HNC*H*$_2$), 35.75 (HNCH$_2$C*H*$_2$), 32.57 (HNCH$_2$C*H*$_2$).

^{29}Si NMR (99 MHz, C_6D_6): -23.50 (HPh*Si*N), -26.56 (H$_2$Ph*Si*N), -26.59 (H$_2$Ph*Si*N), -27.17 (H$_2$Ph*Si*N), -27.20 (H$_2$Ph*Si*N), -27.28 (H$_2$Ph*Si*N).
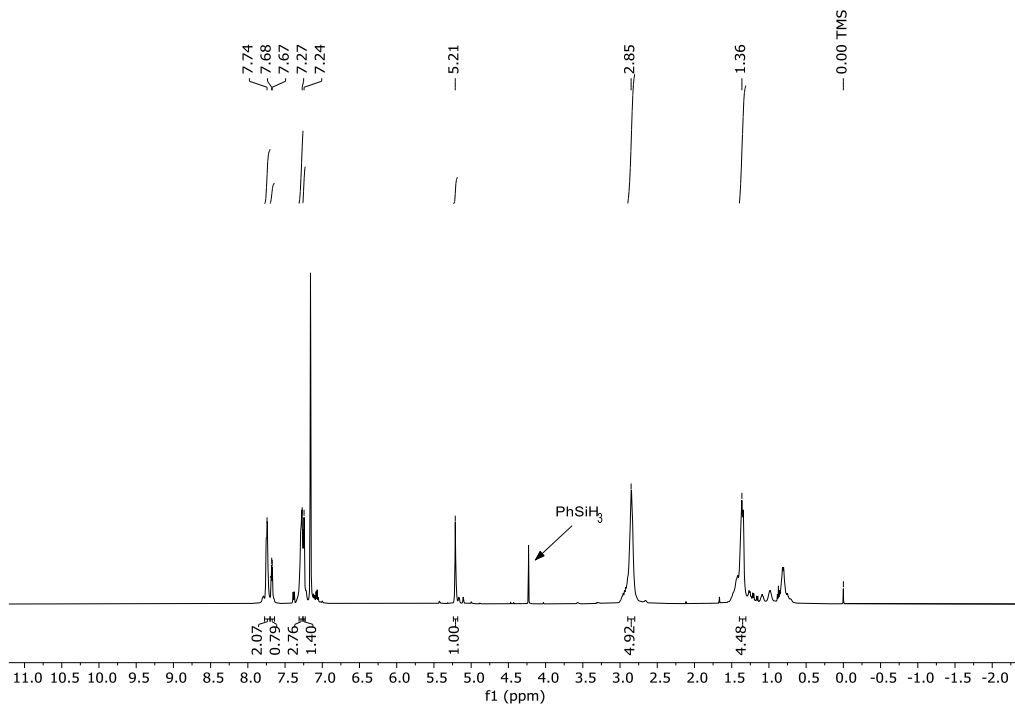
Figure 4.14. Representative ^{1}H NMR spectrum of **4c** in benzene-d_6.

Figure 4.15. Representative ^{13}C NMR spectrum of **4c** in benzene-d_6.

156
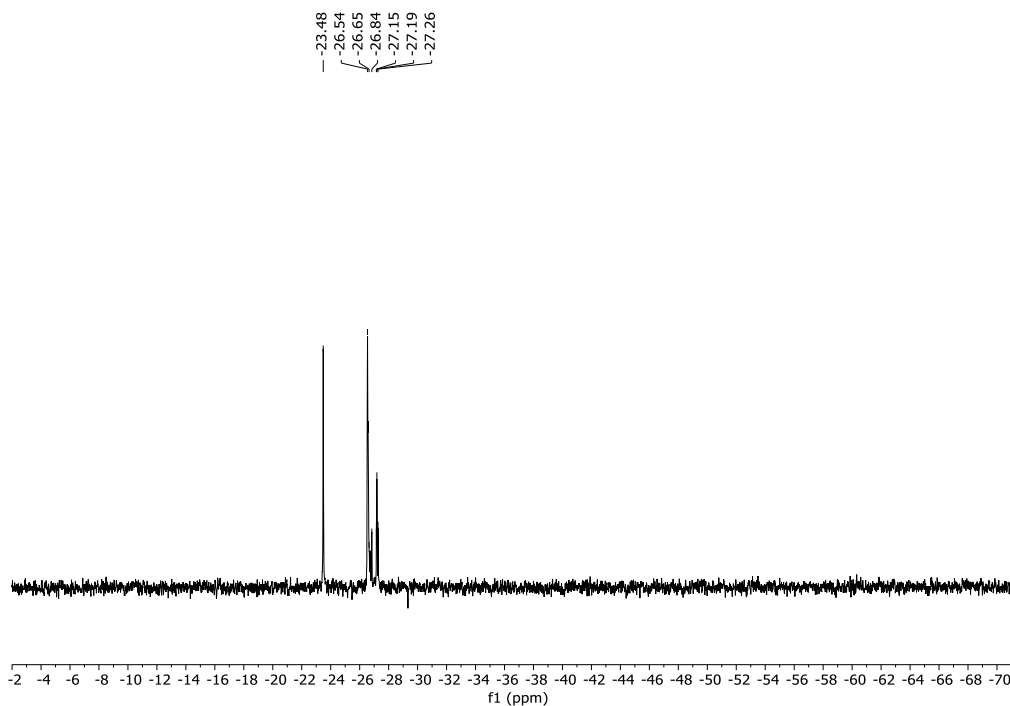
Figure 4.16. Representative ^{29}Si NMR spectrum of **4c** in benzene-d_6.

Procedure for isolated yield and solid-state characterization: In a N$_2$ filled glovebox, a 20 mL vial was pre-weighed before adding 0.021 g (0.023 mmol) of **47**, followed by 560 μL (4.6 mmol) of phenylsilane, no obvious color change was noted. Next, 0.422 g (4.6 mmol) of 1,4-diaminobutane in 1 mL toluene was added. The formation of H$_2$ was observed and the solution turned orange in color. The reaction was kept uncapped at room temperature for 3 h to obtain a dark brown solid. Next, the vial was brought outside the glovebox, when the catalyst was deactivated by exposing to air. The reaction was then brought back into the glovebox and quickly degassed under vacuum for 30 s. The product was washed with pentane and ether and dried under vacuum to obtain 0.774 g of a solid product identified as **4c** (86% yield).

IR (KBr, cm^{-1}): 3388-3290 (broad, N–H), 3057-2851 (strong, C–H), 2101 (strong, Si–H), 810 (weak, Si–N).

157

MALDI-TOF [M+H]$^+$: 189.2 (n = 1), 393.8 (n = 2), 941.5 (n = 5), 1149.5 (n=6), 1381.9 (n=7), 1507.4 (n=8), majority of product did not dissolve in THF.

TGA (N$_2$): T$_5$ = 273 °C, total %wt. loss at 1000 °C = 60.94%. TGA (O$_2$): T$_5$ = 272 °C, total %wt. loss at 1000 °C = 69.65%.
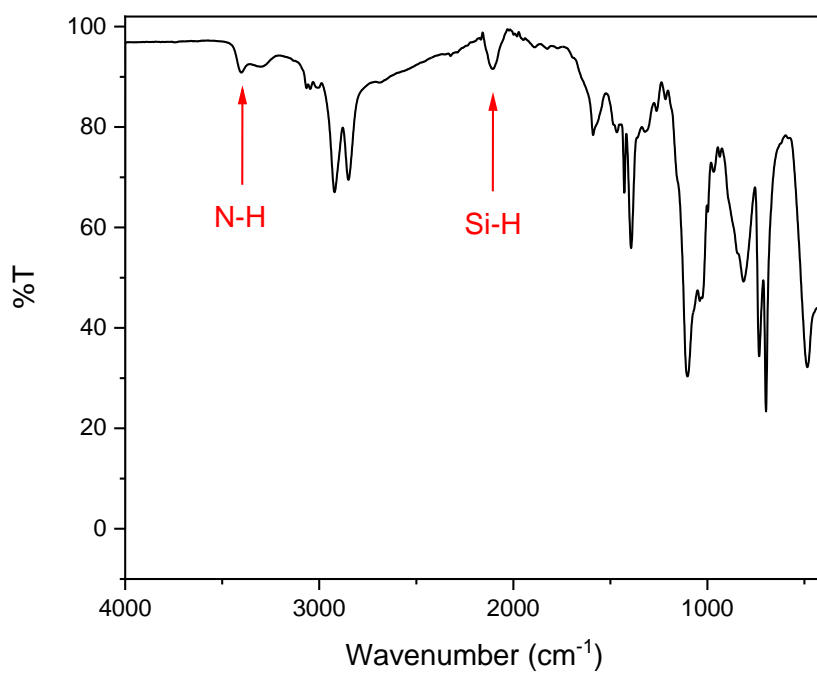
Figure 4.17. Representative FT-IR spectrum of **4c** in KBr.
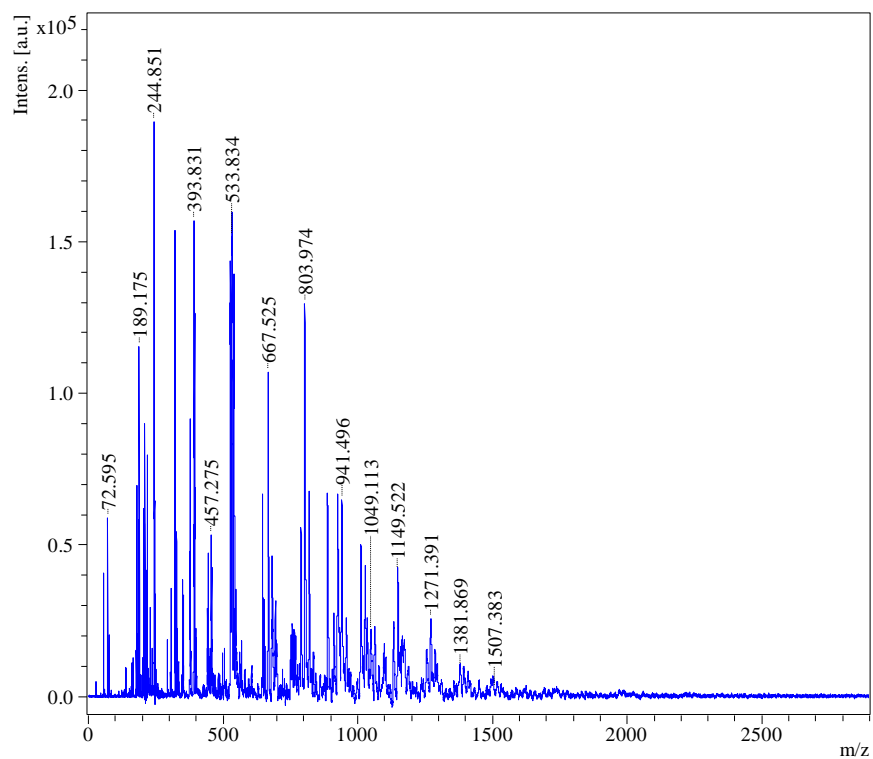
Figure 4.18. Representative MALDI-TOF spectrum of **4c** in THF.
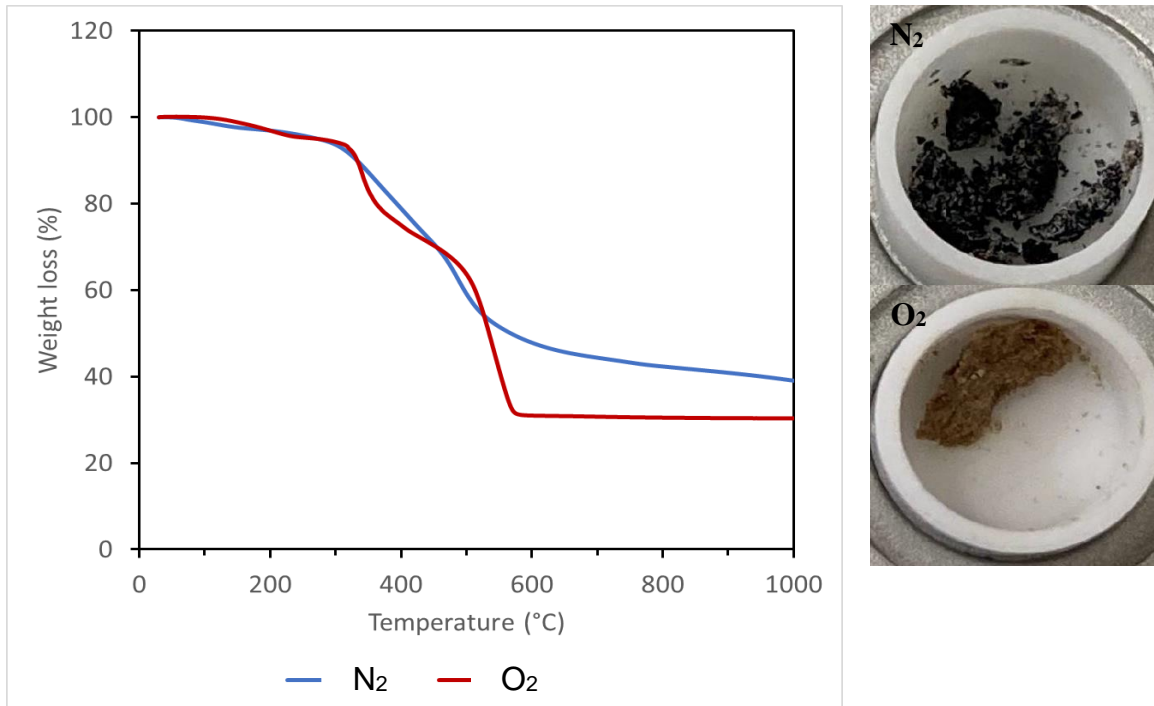
Figure 4.19. Representative TGA spectrum of **4c** and image of product after TGA under N_2 and O_2.
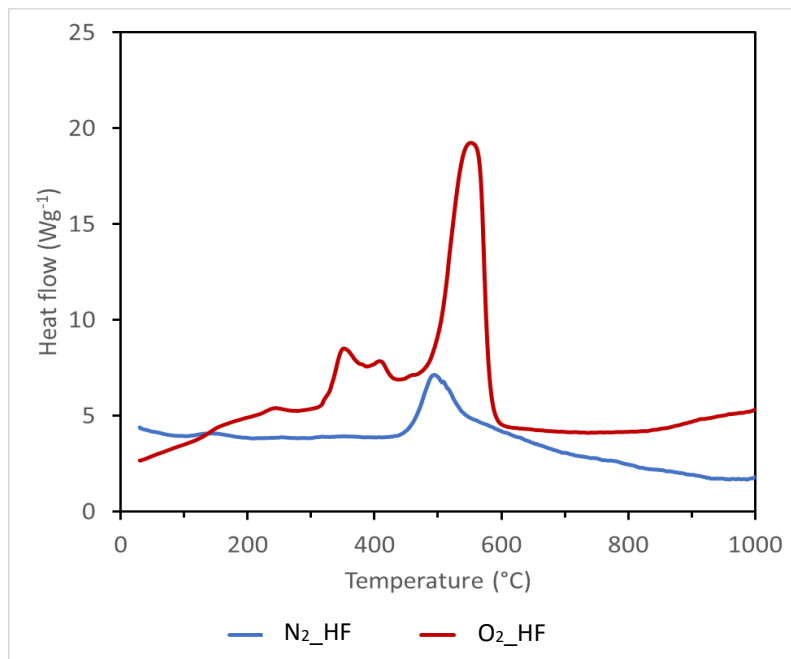
Figure 4.20. Representative DSC spectrum of **4c** under N_2 and O_2.
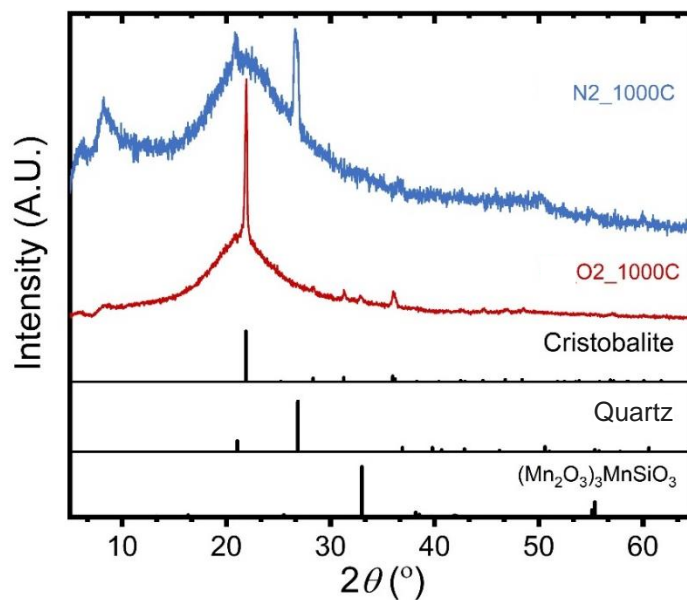
Figure 4.21. Representative XRD patterns of polycarbosilazane **4c** after TGA under N_2 and O_2.

Preparation of polycarbosilazane 4d from phenylsilane and 1,6-diaminohexane using 0.5 mol% 47.

Procedure for solution NMR characterization: In a N_2 filled glovebox, a 20 mL vial was pre-weighed before adding 0.002 g (0.002 mmol) of **47**. Afterwards, 44 μL (0.36 mmol) of phenylsilane was added and no obvious color change was noted. Next, 0.041 g (0.36 mmol) of 1,6-diaminohexane in 1 mL of benzene-d_6 was added. Instantly, the evolution of hydrogen gas was observed and the solution turned orange in color. The vial was heated at 60 °C for 3 h to yield a dark brown solution. Then the catalyst was deactivated by exposing to air and quickly degassed under vacuum for 30 s. The solution was transferred to a J. Young tube to obtain solution NMR characterization. More than 99% conversion was observed after 24 h by examining the consumption of starting amine ^{1}H NMR resonances. ^{1}H NMR (500 MHz, C_6D_6): δ 7.75 (d, *J* = 7.4 Hz, 1H, phenyl), 7.28 (d, *J* = 7.2 Hz, 2H, phenyl), 5.22 (s, 1H, *H*PhSiN$_2$), 5.11 (s, *H*PhSiN$_2$ end of chain), 2.86 (d, *J* = 7.4 Hz, 2H, SiHNC*H$_2$*CH$_2$CH$_2$), 1.37 (s, 2H, SiHNCH$_2$C*H$_2$*CH$_2$), 1.23 (s, 2H, SiHNCH$_2$C*H$_2$*CH$_2$), 0.84 (s, 1H, Si*H*N).

^{13}C NMR (126 MHz, C_6D_6): 137.82 (phenyl), 134.23 (phenyl), 129.60 (phenyl), 127.83 (phenyl), 41.62 (SiHN*C*H$_2$CH$_2$CH$_2$), 34.70 (SiHNCH$_2$*C*H$_2$CH$_2$), 26.79 (SiHNCH$_2$CH$_2$*C*H$_2$).

^{29}Si NMR (99 MHz, C_6D_6) -26.55 (H$_2$Ph*Si*N), -27.32 (H$_2$Ph*Si*N), -29.82 (H$_2$Ph*Si*N).

Procedure for isolated yield and solid-state characterization: In a N_2 filled glovebox, a 20 mL vial was pre-weighed before adding 0.01 g (0.01 mmol) of **47**, followed by 260 μL (2.1 mmol) of phenylsilane, no obvious color change was noted. Next, 0.243 g (2.1 mmol) of 1,6-diaminohexane in 1 mL toluene was added. The formation of H_2 was observed and the

solution turned orange in color. The reaction was heated at 60 °C for 3 h to obtain an orangish-brown solid. Next, the vial was brought outside the glovebox, when the catalyst was deactivated by exposing to air. The reaction was then brought back into the glovebox and quickly degassed under vacuum for 30 s. The product was washed with pentane and ether and dried under vacuum to obtain 0.432 g of a solid product identified as **4d** (94% yield).

IR (KBr, cm-1): 3401 (broad, N–H), 3065-2845 (strong, C–H), 2164-2094 (strong, Si–H), 850 (weak, Si–N).

Preparation of polycarbosilazane 4e from phenylsilane and 1,12-diaminododecane using 0.5 mol% 47.

Procedure for solution NMR characterization: In a N_2 filled glovebox, a 20 mL vial was pre-weighed before adding 0.001 g (0.001 mmol) of catalyst **47**. Afterwards, 18 μL (0.148 mmol) of phenylsilane was added and no obvious color change was noted. Next, 0.029 g (0.148 mmol) of 1,12-diaminohexane in 1 mL of benzene-d_6 was added. Instantly, the evolution of hydrogen gas was observed and the solution turned orange in color. The vial was heated at 60 °C for 3 h to yield a brown solution. Then the catalyst was deactivated by exposing to air and quickly degassed under vacuum for 30 s. The solution was transferred to a J. Young tube to obtain solution NMR characterization. More than 99% conversion was observed after 24 h by examining the consumption of starting amine ^{1}H NMR resonances.

Procedure for isolated yield and solid-state characterization: In a N_2 filled glovebox, a 20 mL vial was pre-weighed before adding 0.011 g (0.011 mmol) of **47**, followed by 300 μL (2.345 mmol) of phenylsilane, no obvious color change was noted. Next, 0.47 g (2.345

mmol) of 1,12-diaminododecane in 1 mL toluene was added. The formation of H_2 was observed the solution turned orange in color. The reaction was heated at 60 °C for 3 h to obtain an orangish-brown solid. Next, the vial was brought outside the glovebox, when the catalyst was deactivated by exposing to air. The reaction was then brought back into the glovebox and quickly degassed under vacuum for 30 s. The product was washed with pentane and ether and dried under vacuum to obtain 0.659 g of a solid product identified as **4e** (91% yield).

IR (KBr, cm^{-1}): 3395 (broad, N–H), 2914-2840 (strong, C–H), 2109 (strong, Si–H), 835 (weak, Si–N).

MALDI-TOF [M+H]$^+$: 1165.1 (n=3 + 1 amine), 1454.1 (n=4 + 1 amine), 1693.2 (n=5 + 1 amine), 1976 (n=6 + 1 amine), 2258.3 (n=7 + 1 phenylsilane), 2540.5 (n=8 + 1 phenylsilane), 2822.9 (n=9 + 1 phenylsilane), 3080 (n=10), 3396.6 (n=11), majority of product did not dissolve in THF.

Preparation of polycarbosilazane 4f from phenylsilane and 2,2'-(ethylenedioxy)bis(ethylamine) using 0.5 mol% 47.

Procedure for solution NMR characterization: In a N_2 filled glovebox, a 20 mL vial was pre-weighed before adding 0.004 g (0.004 mmol) of catalyst **47** in 2 mL of benzene-*d_6*. Afterwards, 93 µL (0.76 mmol) of phenylsilane was added and no obvious color change was noted. Next, 111 µL (0.76 mmol) of 2,2'-(ethylenedioxy)bis(ethylamine) was added. Instantly, the evolution of hydrogen gas was observed and the solution turned orange in color. The vial was heated at 60 °C for 3 h to yield a brown solution. Then the catalyst was deactivated by exposing to air and quickly degassed under vacuum for 30 s. The solution was transferred to a J. Young tube to obtain solution NMR characterization. More than

99% conversion was observed after 24 h by examining the consumption of starting amine ^{1}H NMR resonances.

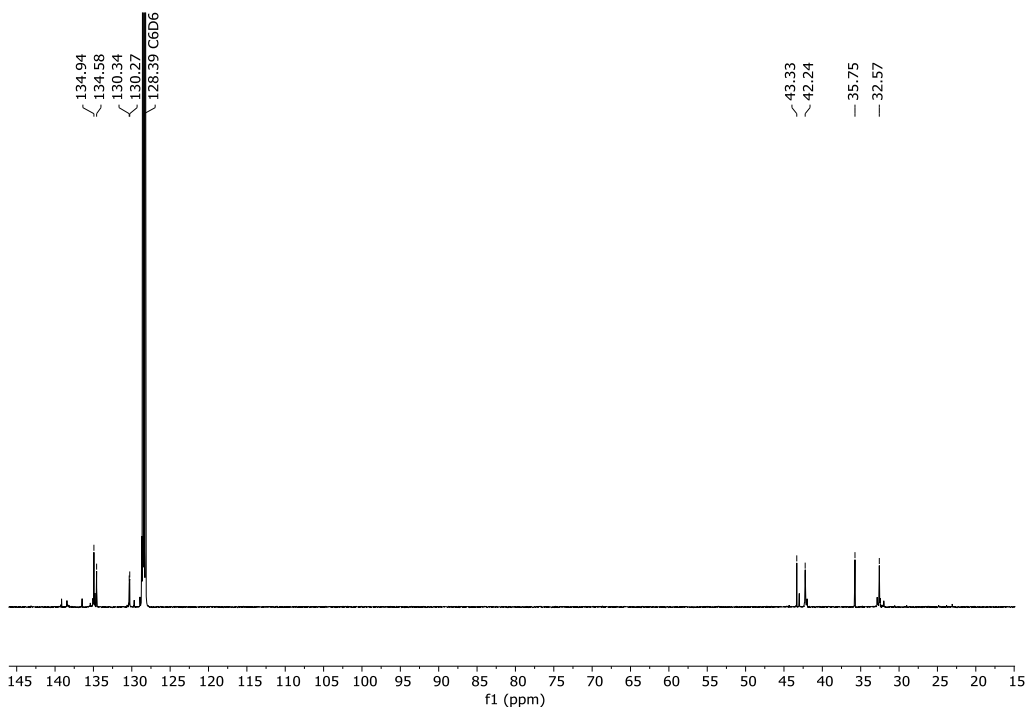*Procedure for isolated yield and solid-state characterization:* In a N_2 filled glovebox, a 20 mL vial was pre-weighed before adding 0.012 g (0.013 mmol) of **47**, followed by 320 µL (2.62 mmol) of phenylsilane, no obvious color change was noted. Next, 400 µL (2.62 mmol) of 2,2'-(ethylenedioxy)bis(ethylamine) was added. The formation of H_2 was observed and the solution turned orange in color. The reaction was heated at 60 °C for 3 h to obtain a dark brown solid. Next, the vial was brought outside the glovebox, when the catalyst was deactivated by exposing to air. The reaction was then brought back into the glovebox and quickly degassed under vacuum for 30 s. The product was washed with pentane and ether and dried under vacuum to obtain 0.705 g of a solid product identified as **4f** (89% yield).

IR (KBr, cm^{-1}): 3374 (broad, N–H), 2934-2854 (strong, C–H), 2094 (strong, Si–H), 830 (weak, Si–N).

MALDI-TOF [M+H]$^+$: 1172.1 (n=4 +1 amine), 1454.4 (n=5 + 2 phenylsilane), 1693.6 (n=6 + 1 amine), 1977.1 (n=7 + 2 phenylsilane), 2218.6 (n=8 + 2 phenylsilane), 2513.0 (n=10), 2792.1 (n=10 + 2 amine), 3110.1 (n=12 + 1 phenylsilane), majority of product did not dissolve in THF.

TGA (N_2): T_5 = 156.7 °C, total %wt. loss at 1000 °C = 78.13%. TGA (O_2): T_5 = 125.8 °C, total %wt. loss at 1000 °C = 80.31%.

Preparation of polycarbosilazane 4g from phenylsilane and 4,7,10-trioxa-1,13-tridecanediamine using 0.5 mol% 47.

Procedure for solution NMR characterization: In a N_2 filled glovebox, a 20 mL vial was pre-weighed before adding 0.003 g (0.003 mmol) of catalyst **47** in 2 mL of benzene-d_6. Afterwards, 81 µL (0.66 mmol) of phenylsilane was added and no obvious color change was noted. Next, 139 µL (0.66 mmol) of 4,7,10-trioxa-1,13-tridecanediamine was added. Instantly, the evolution of hydrogen gas was observed and the solution turned orange in color. The vial was heated at 60 °C for 3 h to yield a brown solution. Then the catalyst was deactivated by exposing to air and quickly degassed under vacuum for 30 s. The solution was transferred to a J. Young tube to obtain solution NMR characterization. More than 99% conversion was observed after 24 h by examining the consumption of starting amine ^{1}H NMR resonances.

Procedure for isolated yield and solid-state characterization: In a N_2 filled glovebox, a 20 mL vial was pre-weighed before adding 0.011 g (0.011 mmol) of **47**, followed by 300 µL (2.219 mmol) of phenylsilane, no obvious color change was noted. Next, 500 µL (2.219 mmol) of 4,7,10-trioxa-1,13-tridecanediamine was added. The formation of H_2 was observed and the solution turned orange in color. The reaction was heated at 60 °C for 3 h to obtain a dark brown solid. Next, the vial was brought outside the glovebox, when the catalyst was deactivated by exposing to air. The reaction was then brought back into the glovebox and quickly degassed under vacuum for 30 s. The product was washed with pentane and ether and dried under vacuum to obtain 0.662 mg a solid product identified as **4g** (92% yield).

IR (KBr, cm^{-1}): 3374 (broad, N–H), 2914-2845 (strong, C–H), 2350 (strong, Si–H), 810 (weak, Si–N).

MALDI-TOF [M+H]$^+$: 933.9 (n=3), 1172.4 (n=3 + 2 phenylsilane), 1454.3 (n = 4 + 2 phenylsilane), 1779.3 (n=5 + 1 phenylsilane), 1977.1 (n=6), 2258.7 (n=7), 2540.3 (n=8), 2777.8 (n=8 + 1 amine), 3036.3 (n=9 + 1 phenylsilane), majority of product did not dissolve in THF.

Preparation of polycarbosilazane 5a from octylsilane and ethylenediamine using 0.5 mol% 47.

Procedure for solution NMR characterization: In a N_2 filled glovebox, a 20 mL vial was pre-weighed before adding 0.005 g (0.005 mmol) of **47** in 1 mL of benzene-d_6. Afterwards, 188 µL (0.97 mmol) of octylsilane was added and no obvious color change was noted. Next, 65 µL (0.97 mmol) of ethylenediamine was added. Instantly, the evolution of hydrogen gas was observed and the solution turned orange in color. The vial was kept uncapped under N_2 atmosphere for 3 h at ambient temperature to yield a dark brown solution. Then the catalyst was deactivated by exposing to air and quickly degassed under vacuum for 30 s. The solution was transferred to a J. Young tube to obtain solution NMR characterization. More than 99% conversion was observed after 24 h by examining the consumption of starting amine ^{1}H NMR resonances.

Procedure for isolated yield and solid-state characterization: In a N_2 filled glovebox, a 20 mL vial was pre-weighed before adding 0.023 g (0.024 mmol) of **47**, followed by 900 µL (4.818 mmol) of octylsilane, no obvious color change was noted. Next, 320 µL (4.818 mmol) of ethylenediamine was added. The formation of H_2 was observed and the solution turned orange in color. The reaction was kept uncapped at room temperature for 3 h to

obtain a brown solid. Next, the vial was brought outside the glovebox, when the catalyst was deactivated by exposing to air. The reaction was then brought back into the glovebox and quickly degassed under vacuum for 30 s. The product was washed with pentane and ether and dried under vacuum to obtain 0.783 g of a solid product identified as **5a** (81% yield).

IR (KBr, cm^{-1}): 3404 (broad, N–H), 2924-2845 (strong, C–H), 2115 (strong, Si–H), 805 (weak, Si–N).

MALDI-TOF [M+H]$^{+}$: 932.9 (n=4 + 1 octylsilane), 1169.5 (n=5 + 1 octylsilane), 1451.9 (n=7 + 1 ethylenediamine), 1690.5 (n=9), 1974.9 (n=9 + 2 ethylenediamine), 2251.3 (n=11 + 1 ethylenediamine), majority of product did not dissolve in THF.

Preparation of polycarbosilazane 5b from octylsilane and 1,3-diaminopropane using 0.5 mol% 47.

Procedure for solution NMR characterization: In a N_2 filled glovebox, a 20 mL vial was pre-weighed before adding 0.005 g (0.005 mmol) of **47** in 1 mL of benzene-d_6. Afterwards, 192 µL (0.993 mmol) of octylsilane was added and no obvious color change was noted. Next, 83 µL (0.993 mmol) of 1,3-diaminopropane was added. Instantly, the evolution of hydrogen gas was observed and the solution turned orange in color. The vial was kept uncapped under N_2 atmosphere for 3 h at ambient temperature to yield a dark brown solution. Then the catalyst was deactivated by exposing to air and quickly degassed under vacuum for 30 s. The solution was transferred to a J. Young tube to obtain solution NMR characterization. More than 99% conversion was observed after 24 h by examining the consumption of starting amine ^{1}H NMR resonances.

Procedure for isolated yield and solid-state characterization: In a N_2 filled glovebox, a 20 mL vial was pre-weighed before adding 0.007 g (0.007 mmol) of **47**, followed by 274 μL (1.415 mmol) of octylsilane, no obvious color change was noted. Next, 119 μL (1.415 mmol) of 1,3-diaminopropane was added. The formation of H_2 was observed and the solution turned orange in color. The reaction was kept uncapped at room temperature for 3 h to obtain a dark brown polymer coating. Next, the vial was brought outside the glovebox, when the catalyst was deactivated by exposing to air. The reaction was then brought back into the glovebox and quickly degassed under vacuum for 30 s. The product was washed with pentane and ether and dried under vacuum to obtain 0.303 g of an oily product (73% yield).

IR (KBr, cm^{-1}): 3413 (broad, N–H), 2914-2848 (strong, C–H), 2100 (strong, Si–H), 792 (weak, Si–N).

Preparation of polycarbosilazane 5c from octylsilane and 1,4-diaminobutane using 0.5 mol% 47.

Procedure for solution NMR characterization: In a N_2 filled glovebox, a 20 mL vial was pre-weighed before adding 0.002 g (0.002 mmol) of **47** in 1 mL of benzene-d_6. Afterwards, 66 μL (0.338 mmol) of octylsilane was added and no obvious color change was noted. Next, 0.03 g (0.338 mmol) of 1,4-diaminobutane in 1 mL benzene-d_6 was added. Instantly, the evolution of hydrogen gas was observed and the solution turned orange in color. The vial was kept uncapped under N_2 atmosphere for 3 h at ambient temperature to yield a dark brown solution. Then the catalyst was deactivated by exposing to air and quickly degassed under vacuum for 30 s. The solution was transferred to a J. Young tube to obtain solution

NMR characterization. More than 99% conversion was observed after 24 h by examining the consumption of starting amine ^{1}H NMR resonances.

^{1}H NMR (500 MHz, C$_6$D$_6$): 4.79 (s, 1H, [CH$_3$CH$_2$(CH$_2$)$_6$]HSi(NR)$_2$), 4.66 (s, [CH$_3$CH$_2$(CH$_2$)$_6$]HSi(NR)$_2$ end of chain), 2.89 (m, 4H, HSi[NHCH_2(CH$_2$)$_3$CH_2NH]$_2$), 2.83 (m, 4H, HSi[NHCH2(CH$_2$)$_3$CH_2NH]$_2$), 1.54 (m, 6H, HSi[NHCH$_2$(CH_2)$_3$CH$_2$NH]$_2$), 1.46 (m, 12H, HSi[NHCH$_2$(CH_2)$_3$CH$_2$NH]$_2$), 1.32 (d, J = 17.3 Hz, 28H, CH$_2$ of diaminobutane and octylsilane overlapped), 0.90 (t, 3H, [CH_3CH$_2$(CH$_2$)$_6$]HSiN$_2$) 0.68 (m, 2H, [CH$_3$CH_2(CH$_2$)$_6$]HSiN$_2$).

^{29}Si NMR (99 MHz, C$_6$D$_6$): -14.75 ([CH$_3$(CH$_2$)$_7$]HSi(NR)$_2$), -18.21, -18.27, -18.47 (different environments of [CH$_3$(CH$_2$)$_7$]H$_2$$Si$N).

Procedure for isolated yield and solid-state characterization: In a N$_2$ filled glovebox, a 20 mL vial was pre-weighed before adding 0.005 g (0.005 mmol) of **47**, followed by 188 µL (0.972 mmol) of octylsilane, no obvious color change was noted. Next, 0.09 g (0.972 mmol) of 1,4-diaminobutane in 1 mL of toluene was added. The formation of H$_2$ was observed the solution turned orange in color. The reaction was kept uncapped at room temperature for 3 h to obtain a dark brown solid. Next, the vial was brought outside the glovebox, when the catalyst was deactivated by exposing to air. The reaction was then brought back into the glovebox and quickly degassed under vacuum for 30 s. The product was washed with pentane and ether and dried under vacuum to obtain 0.184 g of a solid product identified as **5c** (83% yield).

IR (KBr, cm^{-1}): 3414 (broad, N–H), 2919-2854 (strong, C–H), 2090 (strong, Si–H), 800 (weak, Si–N).

MALDI-TOF $[M+H]^+$: 445.4 (n=2), 694.9 (n=3), 932.9 (n=4), 1169.7 (n=6 + 1 amine), 1693.7 (n=7 + 1 amine), majority of product did not dissolve in THF.

TGA (N_2): T_5 = 116.5 °C, total %wt. loss at 1000 °C = 76.79%. TGA (O_2): T_5 = 179.5 °C, total %wt. loss at 1000 °C = 75.58%.

Preparation of polycarbosilazane 5d from octylsilane and 1,6-diaminohexane using 0.5 mol% 47.

Procedure for solution NMR characterization: In a N_2 filled glovebox, a 20 mL vial was pre-weighed before adding 0.006 g (0.006 mmol) of **47** in 1 mL of benzene-d_6. Afterwards, 233 μL (1.2 mmol) of octylsilane was added and no obvious color change was noted. Next, 0.14 g (1.2 mmol) of 1,6-diaminohexane in 1 mL benzene-d_6 was added. Instantly, the evolution of hydrogen gas was observed and the solution turned orange in color. The vial was heated at 60 °C for 3 h to yield a yellow solution. Then the catalyst was deactivated by exposing to air and the solution was quickly degassed under vacuum for 30 s. The solution was transferred to a J. Young tube to obtain solution NMR characterization. More than 99% conversion was observed after 24 h by examining the consumption of starting amine ^{1}H NMR resonances.

^{1}H NMR (500 MHz, C_6D_6): 4.72 (s, 1H, [$CH_3CH_2(CH_2)_6$]HSi(NR)$_2$), 4.61 (s, [$CH_3(CH_2)_7$]HSi(NR)$_2$) end of chain), 2.84 (t, 4H, HSiNHCH_2(CH$_2$)$_4$CH_2N), 2.53 (t, HSi[NHCH_2(CH$_2$)$_4$CH_2N]$_2$), 1.49 (s, 3H, [CH_3(CH$_2$)$_7$]HSi(NR)$_2$), 1.43 (s, 8H, H$_2$SiNHCH$_2$(CH_2)$_4$CH$_2$N and [CH$_3$(CH_2)$_7$]H$_2$SiN overlapped), 1.33 (s, 12H, [CH$_3$CH$_2$(CH_2)$_6$]HSi(NR)$_2$), 0.92 (s, [CH$_3$CH$_2$(CH_2)$_6$]HSi(NR)$_2$ end of chain), 0.63 (s, 4H, [CH$_3$CH_2(CH$_2$)$_6$]HSi(NR)$_2$).

^{29}Si NMR (99 MHz, C$_6$D$_6$): -12.96, -18.34, -23.99 (different environments of [CH$_3$(CH$_2$)$_7$]H*Si*(NR)$_2$).

Procedure for isolated yield and solid-state characterization: In a N$_2$ filled glovebox, a 20 mL vial was pre-weighed before adding 0.006 g (0.006 mmol) of **47**, followed by 249 μL (1.288 mmol) of octylsilane, no obvious color change was noted. Next, 0.15 g (1.288 mmol) of 1,6-diaminohexane in 1 mL of toluene was added. The formation of H$_2$ was observed and the solution turned orange in color. The reaction was heated at 60 °C for 3 h to obtain a yellow solid. Next, the vial was brought outside the glovebox, when the catalyst was deactivated by exposing to air. The reaction was then brought back into the glovebox and quickly degassed under vacuum for 30 s. The product was washed with pentane and ether and dried under vacuum to obtain 0.254 g of a solid product identified as **5d** (77% yield).

IR (KBr, cm^{-1}): 3404-3290 (broad, N–H), 2914-2835 (strong, C–H), 2099 (strong, Si–H), 805 (weak, Si–N).

Preparation of polycarbosilazane 5e from octylsilane and 1,12-diaminododecane using 0.5 mol% 47.

Procedure for solution NMR characterization: In a N$_2$ filled glovebox, a 20 mL vial was pre-weighed before adding 0.002 g (0.002 mmol) of **47** in 1 mL of benzene-*d$_6$*. Afterwards, 57 μL (0.296 mmol) of octylsilane was added and no obvious color change was noted. Next, 0.059 g (0.296 mmol) of 1,4-diaminobutane in 1 mL benzene-*d$_6$* was added. Instantly, the evolution of hydrogen gas was observed and the solution turned orange in color. The vial was heated at 60 °C for 3 h to yield a dark brown solution. Then the catalyst was deactivated by exposing to air and quickly degassed under vacuum for 30 s. The

solution was transferred to a J. Young tube to obtain solution NMR characterization. More than 99% conversion was observed after 24 h by examining the consumption of starting amine ^{1}H NMR resonances.

^{1}H NMR (500 MHz, C_6D_6): 4.79 (s, 1H, [CH$_3$CH$_2$(CH$_2$)$_5$CH$_2$]HSiNR$_2$), 2.89 (m, 4H, SiNHCH_2(CH$_2$)$_{10}$CH_2NH), 2.83 (m, 4H, SiNHCH$_2$(CH$_2$)$_{10}$CH_2NH), 1.54 (m, 2H, [CH$_3$CH$_2$(CH$_2$)$_5$CH_2]HSiNR$_2$), 1.46 (s, 10H, [CH$_3$CH$_2$(CH_2)$_5$CH$_2$]HSiNR$_2$), 1.32 (d, J = 17.3 Hz, 20H, SiNHCH$_2$(CH_2)$_{10}$CH$_2$NH), 0.90 (t, 3H, [CH_3CH$_2$(CH$_2$)$_5$CH$_2$]HSiNR$_2$), 0.68 (s, 2H, [CH$_3$CH_2(CH$_2$)$_5$CH$_2$]HSiNR$_2$).

^{29}Si NMR: (99 MHz, C_6D_6) -18.32, -23.99 (different environments of [CH$_3$CH$_2$(CH$_2$)$_5$CH$_2$]HSiNR$_2$).

Procedure for isolated yield and solid-state characterization: In a N$_2$ filled glovebox, a 20 mL vial was pre-weighed before adding 0.006 g (0.006 mmol) of **47**, followed by 254 μL (1.31 mmol) of octylsilane, no obvious color change was noted. Next, 0.262 g (1.31 mmol) of 1,12-diaminododecane in 1 mL of toluene was added. The formation of H$_2$ was observed and the solution turned orange in color. The reaction was heated at 60 °C for 3 h to obtain a dark brown solid. Next, the vial was brought outside the glovebox, when the catalyst was deactivated by exposing to air. The reaction was then brought back into the glovebox and quickly degassed under vacuum for 30 s. The product was washed with pentane and ether and dried under vacuum to obtain 0.406 g of a solid product identified as **5e** (90% yield).

IR (KBr, cm^{-1}): 3409-3309 (broad, N–H), 2909-2845 (strong, C–H), 2135 (strong, Si–H), 820 (weak, Si–N).

MALDI-TOF [M+H]$^+$: 681.5 (n=2), 813.1 (n=2 + 1 octylsilane), 971.9 (n=2 + 2 octylsilane), 1130.8 (n=3 + 1 octylsilane), 1449.6 (n=4 + 1 octylsilane), 1692.6 (n=5),

1975.5 (n=5 + 2 octylsilane), 2258 (n=6 + 1 octylsilane), 2538 (n=7 + 1 octylsilane), 2826.1 (n=8 + 1 octylsilane), majority of product did not dissolve in THF.

Preparation of polycarbosilazane 5f from octylsilane and 2,2'-(ethylenedioxy)bis(ethylamine) using 0.5 mol% 47.

Procedure for solution NMR characterization: In a N_2 filled glovebox, a 20 mL vial was pre-weighed before adding 0.005 g (0.006 mmol) of **47** in 1 mL of benzene-d_6. Afterwards, 217 µL (1.12 mmol) of octylsilane was added and no obvious color change was noted. Next, 163 µL (1.12 mmol) of 2,2'-(ethylenedioxy)bis(ethylamine) was added. Instantly, the evolution of hydrogen gas was observed and the solution turned orange in color. The vial was kept uncapped under N_2 atmosphere for 3 h at ambient temperature to yield a dark brown solution. Then the catalyst was deactivated by exposing to air and quickly degassed under vacuum for 30 s. The solution was transferred to a J. Young tube to obtain solution NMR characterization. More than 99% conversion was observed after 24 h by examining the consumption of starting amine ^{1}H NMR resonances.

Procedure for isolated yield and solid-state characterization: In a N_2 filled glovebox, a 20 mL vial was pre-weighed before adding 0.006 g (0.006 mmol) of **47**, followed by 245 µL (1.267 mmol) of octylsilane, no obvious color change was noted. Next, 185 µL (1.015 mmol) of 2,2'-(ethylenedioxy)bis(ethylamine) was added. The formation of H_2 was observed and the solution turned orange in color. The reaction was heated at 60 °C for 3 h to obtain a dark brown solid. Next, the vial was brought outside the glovebox, when the catalyst was deactivated by exposing to air. The reaction was then brought back into the glovebox and quickly degassed under vacuum for 30 s. The product was washed with

pentane and ether and dried under vacuum to obtain 0.344 g of a solid product identified as **5f** (94% yield).

IR (KBr, cm^{-1}): 3390 (broad, N–H), 2919-2840 (strong, C–H), 2104 (strong, Si–H), 835 (weak, Si–N).

TGA (N$_2$): T_5 = 156.7 °C, total %wt. loss at 1000 °C = 82.05%. TGA (O$_2$): T_5 = 125.8 °C, total %wt. loss at 1000 °C = 80.1%.

Preparation of polycarbosilazane 5g from octylsilane and 4,7,10-trioxa-1,13-tridecanediamine using 0.5 mol% 47.

Procedure for solution NMR characterization: In a N$_2$ filled glovebox, a 20 mL vial was pre-weighed before adding 0.005 g (0.005 mmol) of **47** in 1 mL of benzene-d_6. Afterwards, 188 µL (0.97 mmol) of octylsilane was added and no obvious color change was noted. Next, 206 µL (0.97 mmol) of 4,7,10-trioxa-1,13-tridecanediamine was added. Instantly, the evolution of hydrogen gas was observed and the solution turned orange in color. The vial was kept uncapped under N$_2$ atmosphere for 3 h at ambient temperature to yield a dark brown solution. Then the catalyst was deactivated by exposing to air and quickly degassed under vacuum for 30 s. The solution was transferred to a J. Young tube to obtain solution NMR characterization. More than 99% conversion was observed after 24 h by examining the consumption of starting amine ^{1}H NMR resonances.

Procedure for isolated yield and solid-state characterization: In a N$_2$ filled glovebox, a 20 mL vial was pre-weighed before adding 0.005 g (0.005 mmol) of **47**, followed by 209 µL (1.078 mmol) of octylsilane, no obvious color change was noted. Next, 230 µL (1.078 mmol) of 4,7,10-trioxa-1,13-tridecanediamine was added. The formation of H$_2$ was observed and the solution turned orange in color. The reaction was heated at 60 °C for 3 h

to obtain a dark brown solid. Next, the vial was brought outside the glovebox, when the catalyst was deactivated by exposing to air. The reaction was then brought back into the glovebox and quickly degassed under vacuum for 30 s. The product was washed with pentane and ether and dried under vacuum to obtain 0.342 g of a solid product identified as **5g** (88% yield).

IR (KBr, cm^{-1}): 3391 (broad, N–H), 2928-2844 (strong, C–H), 2112 (strong, Si–H), 838 (weak, Si–N).

Preparation of [($^{2,6\text{-iPr}_2\text{Ph}}$BDI)Mn(μ-NH$_2$)]$_2$ (81): Under N$_2$ atmosphere, a 100 mL thick-walled glass bomb was charged with 0.2 g (0.2 mmol) of **47** in 5 mL THF. The bomb was sealed under N$_2$ and attached to the vacuum line. The solution was frozen in liquid N$_2$, gas was removed from the head space under vacuum, and 1 atm of NH$_3$ was introduced. The bomb was closed, disconnected from the vacuum line, and placed in a steel container to warm to room temperature in the back of an empty fume hood with the sash closed. The evolution of H$_2$ gas and the formation of yellow precipitate were observed instantly. The reaction was allowed to occur at ambient temperature for 1 h. The bomb was then attached to the vacuum line and the solution was frozen in an ice-water bath, followed by H$_2$ and NH$_3$ removal. The bomb was brought into the glove box, the solid product was filtered, washed with THF and dried under vacuum to obtain a yellow powder identified as **81** (0.186 g, 90% yield).

Turnover frequency experiment: In a N$_2$ filled glovebox, to a 50 mL beaker was added 0.005 g (0.005 mmol) of **47**. Then, 7.14 mL (58.11 mmol) of phenylsilane was added, followed by 2.5 mL of mesitylene and no obvious color change was noted. Next, 3.9 mL (58.11 mmol) of ethylenediamine was added. The evolution of hydrogen gas was observed

after 10 sec, and the solution turned from yellow to orange and then dark brown in color over the course of 5 min. Aliquots of the reaction liquor were collected at several intervals and transferred to a vial containing I_2 to deactivate the catalyst. The solution was then washed with benzene-d_6 and filtered through a micro glass fiber for ^{1}H NMR characterization. The beaker was kept uncapped under N_2 atmosphere for 3 h at ambient temperature to yield a dark brown solid.

4.6. References

(1)   Khomenkova, L.; Normand, P.; Gourbilleau, F.; Slaoui, A.; Bonafos, C. *Thin Solid Films* **2016**, *617*, 143–149.

(2)   Kuo, Y. *Vacuum* **1998**, *51* (4), 741–745.

(3)   El amrani, A.; Menous, I.; Mahiou, L.; Tadjine, R.; Touati, A.; Lefgoum, A. *Renewable Energy* **2008**, *33* (10), 2289–2293.

(4)   Colombo, P.; Mera, G.; Riedel, R.; Sorarù, G. D. In *Ceramics Science and Technology*; John Wiley & Sons, Ltd, 2013; pp 245–320.

(5)   Slavov, S. V.; Sanger, A. R.; Chuang, K. T. *J. Phys. Chem. B.* **1998**, *102* (28), 5475–5482.

(6)   Coan, T.; Barroso, G. S.; Machado, R. A. F.; de Souza, F. S.; Spinelli, A.; Motz, G. *Prog. Org. Coat.* **2015**, *89*, 220–230.

(7)   Kozuka, H.; Fujita, M.; Tamoto, S. *J. Sol-Gel Sci. Technol.* **2008**, *48* (1), 148–155.

(8)   Sønderbæk-Jørgensen, R.; Meier, S.; Dam-Johansen, K.; Skov, A. L.; Daugaard, A. E. *Macromol. Mater. Eng.* **2022**, *307*, 2200157

(9)   Marceaux, S.; Bressy, C.; Perrin, F.-X.; Martin, C.; Margaillan, A. *Prog. Org. Coat.* **2014**, *77* (11), 1919–1928.

(10) Nguyen, T. D. H.; Perrin, F.-X.; Nguyen, D. L. *J. Nanotechnol.* **2013**, *4* (1), 671–677.

(11) Krannich, H.; Mehnert, R.; Reiser, J.; Weseloh, S., WO2008135262, November 13, 2008.

(12) Suzuki, K.; Okamura, T.; Okayasu, T.; Stein, T. Patent No. WO2022084022A1 (2022).

(13) Quenard, S.; Laucournet, R.; Roumanie, M.; Flassayer, C.; Moreac-Njeim, G.; Abramczuk, M. Patent No. FR3116823A1 (2022).

(14) Bellini, C.; Roisnel, T.; Carpentier, J.-F.; Tobisch, S.; Sarazin, Y. *Chem. Eur. J.* **2016**, *22* (44), 15733–15743.

(15) Bellini, C.; Orione, C.; Carpentier, J.-F.; Sarazin, Y. *Angew. Chem. Int. Ed.* **2016**, *55* (11), 3744–3748.

(16) Morris, L. J.; Whittell, G. R.; Eloi, J.-C.; Mahon, M. F.; Marken, F.; Manners, I.; Hill, M. S. *Organometallics* **2019**, *38* (19), 3629–3648.

(17) Gasperini, D.; King, A. K.; Coles, N. T.; Mahon, M. F.; Webster, R. L. *ACS Catal.* **2020**, *10* (11), 6102–6112.

(18) Nguyen, T. T.; Mukhopadhyay, T. K.; MacMillan, S. N.; Janicke, M. T.; Trovitch, R. J. *ACS Sustainable Chem. Eng.* **2022**, *10* (13), 4218–4226.

(19) Smith, A. L. *Spectrochimica Acta* **1960**, *16* (1), 87–105.

(20) Farcaş-Johnson, M. A.; Kyne, S. H.; Webster, R. L. *Chem. Eur. J.* **2022**, e202201.

(21) Ríos, P.; Roselló-Merino, M.; Rivada-Wheelaghan, O.; Borge, J.; López-Serrano, J.; Conejero, S. *Chem. Commun.* **2018**, *54* (6), 619–622.

(22) Nguyen, T. T.; Kim, J.-H.; Kim, S.; Oh, C.; Flores, M.; Groy, T. L.; Baik, M.-H.; Trovitch, R. J. *Chem. Commun.* **2020**, *56*, 3959.

CHAPTER 5

SCOPE AND MECHANISM OF NITRILE DIHYDROBORATION MEDIATED BY A

β-DIKETIMINATE MANGANESE HYDRIDE CATALYST

5.1. Abstract

The manganese hydride dimer, $[(^{2,6-iPr_2Ph}BDI)Mn(\mu-H)]_2$, was found to mediate nitrile dihydroboration, rendering it the first manganese catalyst for this transformation. Stoichiometric experiments revealed that benzonitrile insertion affords $[(^{2,6-iPr_2Ph}BDI)Mn(\mu-NCHC_6H_5)]_2$ en route to *N,N*-diborylamine formation. Density functional theory calculations reveal the precise mechanism and demonstrate that catalysis is promoted by monomeric species.

5.2. Introduction

Borylamines have emerged as promising reagents for organic synthesis. In 2004, Murakami and Suginome found aminoboranes to be effective iminium ion generators for a 3-component Mannich protocol involving the coupling of aldehydes, secondary amines, and silyl ketene acetals.[1] Nikonov showed that $PhCH_2N(BCat)_2$ reacts with benzaldehyde to yield the corresponding imine without the use of a dehydrating agent.[2] In 2019, Tobita was able to prepare *N*-arylimines and *N,N*-diarylamines from the corresponding borylimines and diborylamines using bromoarenes, KO^{t}Bu, Pd(dba)$_2$, and CyJohnPhos.[3] Moreover, the Jazzar and Bertrand groups reported the catalyst-free preparation of primary aminoboranes that chemoselectively react with aldehydes to afford aldimines.[4] Recently, we disclosed the first examples of *N*-substituted amide synthesis using *N,N*-diborylamines and carboxylic acids.[5]

Nitrile dihydroboration is an efficient and mild method to prepare *N,N*-diborylamines. Nikonov initially found that $(2,6-^iPr_2PhN)Mo(H)(Cl)(PMe_3)_3$ and $(2,6-^iPr_2PhN)MoH_2(PMe_3)_3$ mediate the dihydroboration of benzonitrile and acetonitrile with turnover frequencies (TOFs) of up to 1.7 h^{-1}.[2,6] In 2015, Szymczak reported the dihydroboration of nitriles using a proton-switchable, bifunctional Ru complex with TOFs of up to 60 h^{-1}.[7] Gunanathan also found that [Ru(*p*-cymene)Cl$_2$]$_2$ can mediate the hydroboration of nitriles and imines with maximum TOFs of 6.7 h^{-1}.[8] Hill and Ma developed Mg catalysts featuring β-diketiminate ligands for this transformation and reported TOF of up to 20 h^{-1},[9,10] while Shimada demonstrated nitrile dihydroboration using Ni(II) salts featuring bis(acetylacetonato) ligands in the presence of HBCat under ambient temperature (TOF = 11 h^{-1}).[11] Nakazawa achieved nitrile dihydroboration using a binuclear

iron-indium complex, $[Fe(CH_3CN)_6][cis\text{-}Fe(CO)_4(InCl_3)_2]$ (TOF = 0.4 h^{-1})[12] and Fout described a Co-pincer catalyst for nitrile dihydroboration at 70 °C.[13] In Tobita's recent demonstration of borylamine cross-coupling, it was found that Ru catalysts featuring a bis(silyl)xanthene ligand showed modest activity.[3] Since 2017, nitrile dihydroboration catalysis has been extended to a number of metals including Er,[14] Y,[14] Dy,[14] Gd,[14] Al,[15–17] Th,[18] Ti,[19] and Zn,[20] and has even been catalyzed by a Co-H functionalized MOF.[21]

Our group has also contributed to the development of nitrile dihydroboration catalysis. In 2017, we demonstrated that 1.0 mol% of the α-diimine cobalt hydride complex, (^{Ph_2PPr}DI)CoH, catalyzes this transformation at 60 °C.[22] Our work to develop a second generation variant that exhibits nitrile dihydroboration TOFs of up to 380 h^{-1} at 25 °C, (^{PyEt}IP^{CHMe}N^{EtPy})Co, was reported earlier this year.[5] The high activity of this catalyst was attributed to its redox non-innocent ligand, the accessibility of a triplet spin manifold, and the ability of the chelate to promote inner-sphere boryl group transfer. Given recent interest in Mn-based hydrofunctionalization catalysis, [23–26] we aimed to leverage our study of the β-diketiminate Mn alkene hydrosilylation catalyst, $[(^{2,6\text{-}iPr_2Ph}BDI)Mn(\mu\text{-}H)]_2$ (**47**),[27] to achieve Mn-catalyzed nitrile dihydroboration for the first time.

5.3. Results and Discussions

The activity of **47** for benzonitrile dihydroboration was evaluated by monitoring reactions in benzene-d_6 by ^{1}H NMR spectroscopy (Table 5.1). Pinacolborane (HBPin) was chosen as the borane source and a slight excess was used to promote complete nitrile reduction. In particular, adding 2.2 equiv. of HBPin to benzonitrile in the presence of 2.5 mol% of **47** (5 mol% of Mn) in benzene-d_6 resulted in modest conversion after 2 days (27%) at room temperature (entry 1). Heating the same mixture to 60 °C afforded 80% conversion

after 2 days (entry 2) and complete conversion was achieved at 80 °C after 12 h (entry 3). Nitrile reduction using other reagents was also evaluated (entry 4-6). Particularly, no reaction was observed between benzonitrile and 9-BBN or phenyl silane under identical conditions, while HBCat gave poor conversion after 24 h. Therefore, HBPin was chosen for **47**-catalyzed nitrile dihydroboration. To optimize the conditions, the catalyst loading was lowered to 0.5 mol% (1 mol% Mn), allowing for complete benzonitrile dihydroboration after 24 h at 80 °C (entry 7).

Table 5.1. Optimization of **47**-catalyzed benzonitrile dihydroboration conditions.
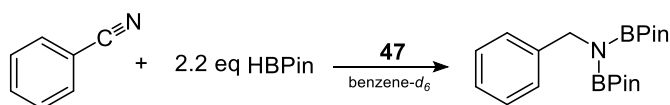
Entry	Mol %	Reductant	Temp. (°C)	Time (h)	% Conversion[a]
1	2.5	HBPin	25	48	27%
2	2.5	HBPin	60	48	80%
3	2.5	HBPin	80	12	99%
4	2.5	9-BBN	80	24	n. r.
5	2.5	PhSiH$_3$	80	24	n. r.
6	2.5	HBCat	80	24	9%
7	0.5	HBPin	80	24	99%

[a]Percent conversion determined by ^{1}H NMR spectroscopy (integration of residual benzonitrile vs. diborylamine product).

Table 5.2. Dihydroboration of nitriles using 0.5 mol% **47**.[a]
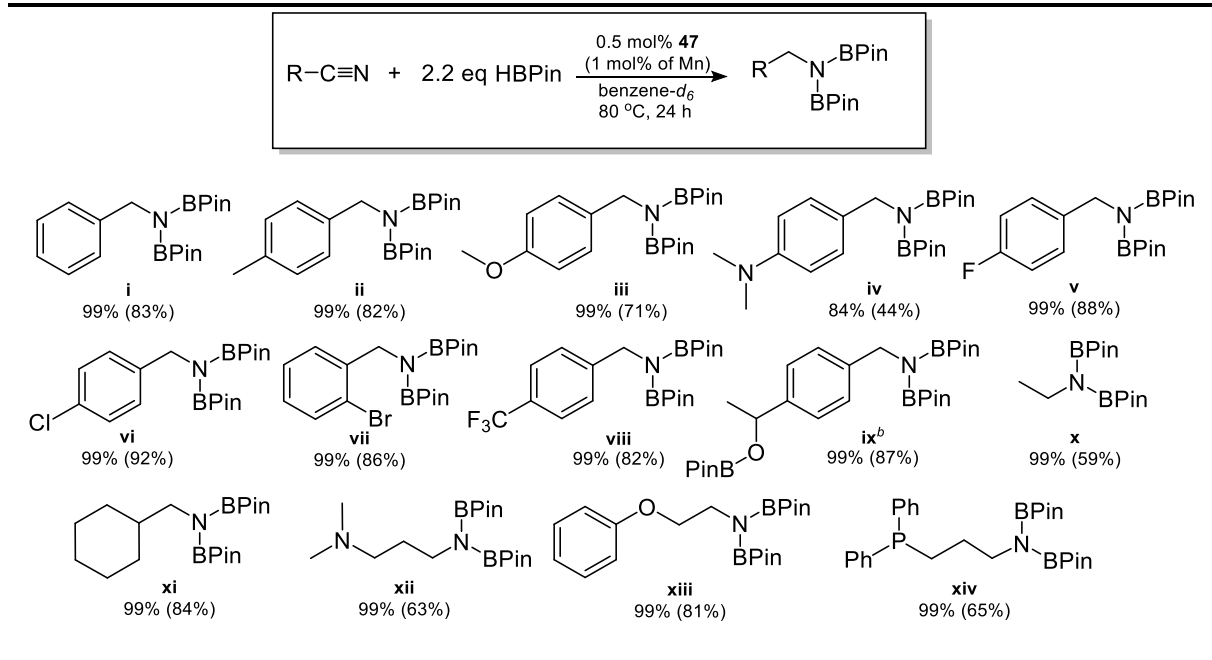
$$R-C\equiv N \;+\; 2.2 \text{ eq HBPin} \xrightarrow[\substack{\text{benzene-}d_6 \\ 80\ ^{\circ}C,\ 24\ h}]{\substack{0.5\ \text{mol\%}\ \mathbf{47} \\ (1\ \text{mol\%}\ \text{of Mn})}} R\diagup N \diagdown \substack{BPin \\ BPin}$$

i
99% (83%)

ii
99% (82%)

iii
99% (71%)

iv
84% (44%)

v
99% (88%)

vi
99% (92%)

vii
99% (86%)

viii
99% (82%)

ix[b]
99% (87%)

x
99% (59%)

xi
99% (84%)

xii
99% (63%)

xiii
99% (81%)

xiv
99% (65%)

[a]Percent conversion determined by ^{1}H NMR spectroscopy (integration of residual benzonitrile vs. diborylamine product) with isolated yield in parentheses. [b]Trial conducted with 3.3 equiv. of HBPin.

Under the same conditions, 13 additional substrates were screened for **47**-catalyzed nitrile dihydroboration (Table 5.2). Greater than 99% conversion was observed in most cases and modest isolated yields of the respective diborylamines were obtained following recrystallization. In particular, benzonitrile substitution did not hinder the rate of catalysis and substrates possessing electron-donating (entries **ii-iv**) and electron-withdrawing (entries **v-viii**) substituents were reduced. In the case of *p*-acetylbenzonitrile (**ix**), the addition of 3.3 equiv. of HBPin allowed for simultaneous reduction of both the carbonyl and nitrile functionalities. The fact that **47** exhibits activity for carbonyl hydroboration is not surprising, considering that this catalyst was found to hydrosilylate the ketone functionality of 5-hexen-2-one in the presence of PhSiH3 at ambient temperature.[27] Aliphatic nitriles including acetonitrile (**x**), cyclohexyl nitrile (**xi**), and 2-

phenoxyacetonitrile (**xiii**) were successfully converted, as were 3-(dimethylamino)propionitrile (**xii**), and 3-(diphenylphosphino)-propionitrile (**xiv**). These trials indicate that donor substituents do not inhibit the catalytic activity of **47**; an issue of concern during our efforts to prepare well-defined Co nitrile hydroboration catalysts.[5,22]

To determine the maximun TOF of **47** catalyzed nitrile dihydroboration, 0.1 mol% of this catalyst was added to a neat mixture of benzonitrile and HBPin. After 24 h at 80 °C, 94% conversion was noted by ^{1}H NMR spectroscopy (TOF = 39 h^{-1}). After only 2 h under the same conditions, 52% conversion was observed, equating to a maximum TOF of 260 h^{-1} (80 °C).

5.4. Mechanistic Insight

To determine the mechanism, additional experiments were conducted to identify intermediates relevant to catalysis. First, 2 equiv. of HBPin were added to a solution of **47** in benzene-d_6, but no reaction was observed. In contrast, adding 2 equiv. of benzonitrile to **47** in benzene-d_6 resulted in the formation of a yellowish orange product identified as [($^{2,6-iPr_2Ph}$BDI)Mn(μ-NCHPh)]$_2$ (**82**). This compound was found to be paramagnetic (μ$_{eff}$ = 6.54 μ$_B$, 25 °C) and it exhibits broadened ^{1}H NMR resonances over a range of 60 ppm.

Single crystals of **82** suitable for X-ray diffraction were obtained upon cooling a concentrated toluene solution layered with pentane to -35 °C (Figure 5.1). The solid-state structure of **82** revealed a short N3–C30 bond length of 1.267(3) Å, indicating that a C=N double bond remains following nitrile insertion. It should also be pointed out that the Mn–Mn bond length of 3.0819(6) Å in **82** is significantly longer than the 2.8138(7) Å length found for **47**.
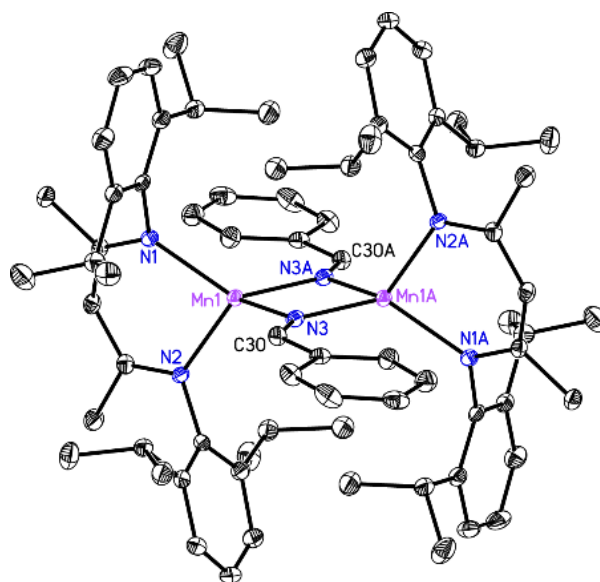
Figure 5.1. Solid-state structure of **82**. Hydrogen atoms have been omitted for clarity.

To obtain additional electronic information, an X-band (9.43 GHz) electron paramagnetic resonance (EPR) spectrum of **82** was collected in a toluene glass at 114 K. The EPR spectrum was found to exhibit a broad and anisotropic signal over 700 mT (Figure 5.2). As expected, the observed spectral features correspond to a complex in which the two Mn(II) centers are strongly antiferromagnetically coupled (*i.e.* $|J_o| \gg g_i b_e B_o/h$).[27] The EPR spectrum was simulated using a spin Hamiltonian that included the Zeeman and zero-field splitting (ZFS) interactions of the individual Mn(II) ($S_i = 5/2$) sites within the dimer and the dipole-dipole interaction between the two Mn(II) centers.
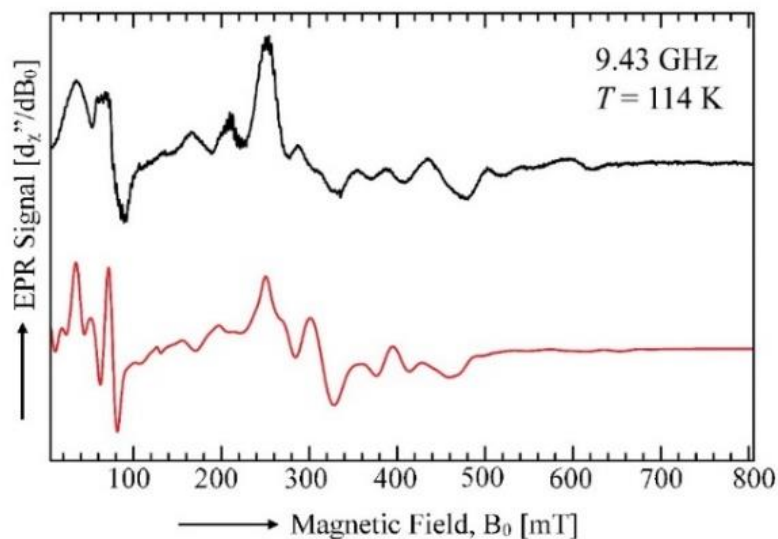
Figure 5.2. The X-band EPR spectrum of **82** at 114 K. The black line is the experimental spectrum and the red line is the simulated spectrum, which was calculated considering the EPR transitions corresponding to the S = 1, 2, 3, 4, and 5 spin states of **8. Parameters used to fit the EPR spectra of 47 and 82 in toluene glass at X-band and low temperature.**

Parameter	47 (T = 106 K)	82 (T = 114 K)
g_{iso}	2.05	2.06
D	0.0932	0.1153
$|E/D|$	0.138	0.256
$J_{x'}$ (cm^{-1})	–0.0089	–0.0061
$J_{y'}$ (cm^{-1})	–0.0036	–0.0015
$J_{z'}$ (cm^{-1})	0.0125	0.0076
ΔB (MHz)	600	600

The fitting parameters were the isotropic g-value, g_{iso}, the zero-field splitting parameters, D and E, the principal components of the dipole-dipole interaction tensor $\boldsymbol{J}$, (i.e., $J_{x'}$, $J_{y'}$, and $J_{z'}$), and the isotropic line width, ΔB.

The best fit was obtained considering the EPR transitions corresponding to the total spin manifolds S = 1, 2, 3, 4, and 5. The parameters obtained from the fit are shown in Table 5.3 and correspond to high-spin Mn(II) centres.[27] However, the rhombic distortion of the ZFS interaction (*i.e.* |*E/D*|) obtained for **82** (0.256) is significantly larger than the

185

one previously reported for **47** (0.138). This result suggests that the larger bridging ligand in **82** (*i.e.*, $NCHC_6H_5$) introduces larger electrostatic distortions to the crystal field surrounding the Mn(II) ions. Furthermore, the value of $J_{z'}$ obtained for **82** (0.0076 cm^{-1}) is considerably smaller than that obtained earlier for **47** (0.0125 cm^{-1}). $J_{z'}$ is the principal component of the dipole-dipole interaction tensor along the Mn(II)–Mn(II) axis and its value is to first order proportional to the inverse of the Mn(II)–Mn(II) distance to the third. Thus, the smaller value of $J_{z'}$ observed for **82** indicates a longer Mn(II)–Mn(II) distance, which agrees with the crystallographically determined Mn–Mn bond lengths in **80** (3.08 Å) and **47** (2.81 Å).

Importantly, **82** was found to mediate the dihydroboration of benzonitrile under the same conditions as **47**, suggesting that it is an intermediate that is relevant to catalysis. To clarify this hypothesis and construct a complete catalytic cycle, density functional calculations (DFT) were performed. Figure 5.4 summarizes the most likely mechanism for dihydroboration. We assigned an open-shell singlet state for the ground state of **47**, where five unpaired electrons in one manganese center are antiferromagnetically coupled to the electrons in the other manganese center. Given that spin crossover is easy for first-row metals, all plausible spin states were taken into account, and we found that sextet is the ground state for all of the monomeric species, exhibiting good agreement with the observed solution magnetic susceptibility data of 6.0 μ_B (25 °C) for the related monomeric intermediate, $(^{2,6\text{-}i\text{Pr}_2\text{Ph}}BDI)Mn(CH(CH_3)(4\text{-}^t\text{BuPh}))$.[27]
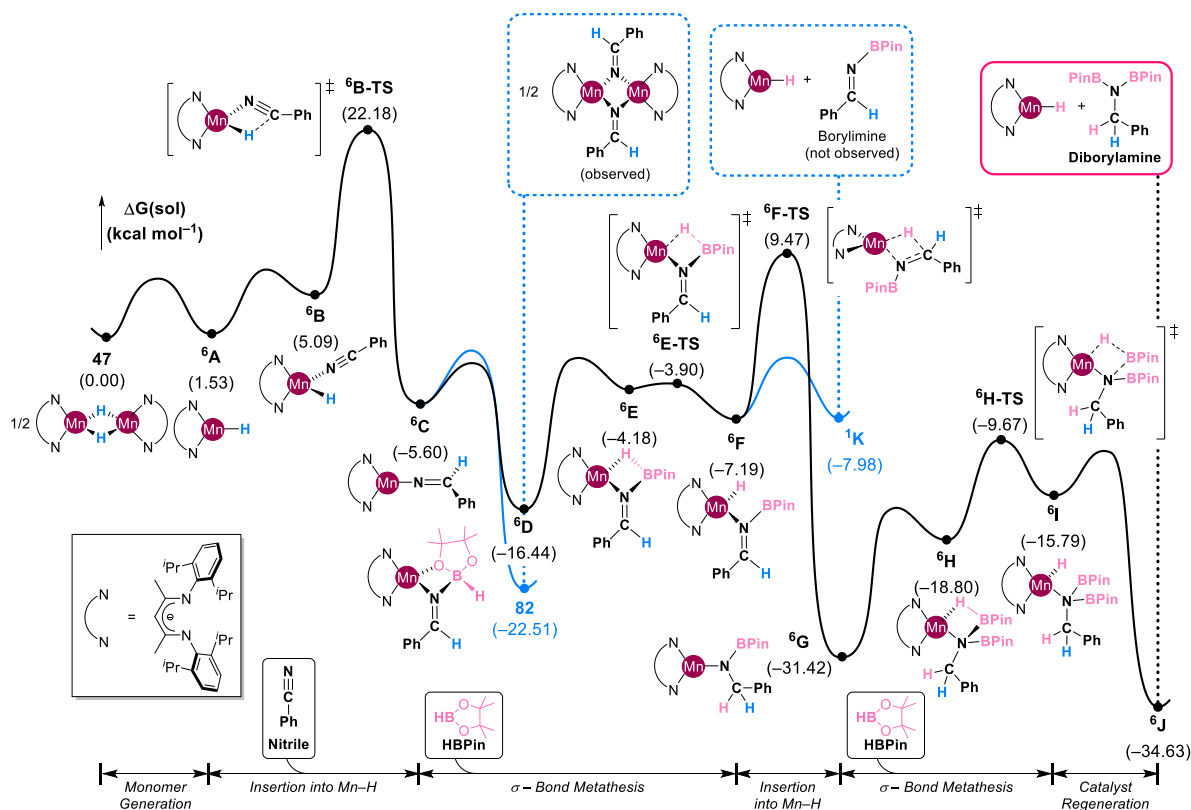
Figure 5.3. DFT-calculated energy profile of **47**-catalyzed benzonitrile dihydroboration.

The energy difference between **47** and the corresponding monomer (**⁶A**) is calculated to be 1.5 kcal mol⁻¹, indicating that the monomeric species is readily available in solution. In our calculations, we employed benzonitrile as a representative substrate and found that it can bind to the active catalyst **⁶A** to furnish intermediate **⁶B** at 5.1 kcal mol⁻¹. The nitrile group is inserted into the Mn–H moiety through **⁶B-TS** with a barrier of 17.1 kcal mol⁻¹. Having an overall barrier of 22.2 kcal mol⁻¹ during the first reduction cycle, the insertion step is exergonic and is mediated by the formation of a stable C–H bond in imino(amide) complex **⁶C**. In accordance with the fact that **82** is isolable, dimerization of **⁶C** to afford **82** features a relative energy of –22.5 kcal mol⁻¹. While the formation of **82**

might be preferred due to electron-deficient nature of ^{6}C, dissociation of **82** is accessible to regenerate catalytically relevant ^{6}C at the given reaction temperature of 80 °C.

Competing with the dimerization, consumption of HBPin drives the reaction to proceed further. Binding of HBPin to ^{6}C leads to a stable Lewis acid-base pair ^{6}D which temporarily adopts an *O*-bound conformation. The following endothermic rearrangement gives ^{6}E at –4.2 kcal mol^{-1}. Its characteristic Mn–H–B–N metallacycle pre-activates the B–H bond, allowing σ-bond metathesis to occur traversing a pseudo-transition state, ^{6}E-TS. Although the resulting Mn–H complex ^{6}F may formally release the borylimine to access ^{1}K, our computation suggests that the dissociation is reversible to regenerate ^{6}F, which will undergo the insertion to generate the stable Mn-amido complex ^{1}G located at – 31.4 kcal mol^{-1}. The overall barrier starting from **82** to the second insertion transition state, ^{6}F-TS, is 32.0 kcal mol^{-1}. It is affordable at 80 °C and consistent with the prolonged reaction time (24 h). Association of a second equivalent of HBPin generates intermediate ^{6}H involving the aforementioned metallacycle. In this case, the *H*-bound conformation is favored over the *O*-bound conformation due to steric congestion between the BPin moiety and bulky substituents on the BDI framework. Finally, σ-bond metathesis regenerates the active catalyst ^{6}A to furnish the final product, *N,N*-diborylamine. Based on the mechanism, we suspect that the Lewis acidity of 9-BBN renders it inactive for nitrile dihydroboration due to formation of a stable Lewis acid/base pair[28] with ^{6}C, which raises the barrier for σ-bond metathesis to the point where it cannot be accessed at 80 °C.

5.5. Conclusion

In summary, the dihydroboration of nitriles to yield *N,N*-diborylamines has been demonstrated for the first time using a well-defined manganese catalyst. Broad functional

188

group tolerance was demonstrated at relatively low catalyst loadings. Experimental and computational studies reveal that **47**-catalyzed nitrile dihydroboration proceeds following insertion into the Mn–H moiety, followed by σ-bond metathesis between amido monomers and incoming HBPin.

5.6. Experimental Procedures

General Considerations: All reactions were performed inside an MBraun glovebox under an atmosphere of purified nitrogen. Toluene, tetrahydrofuran, diethyl ether, and pentane were purchased from Sigma-Aldrich, purified using a Pure Process Technology solvent system, and stored in the glovebox over activated 4 Å molecular sieves and potassium before use. Benzene-d_6 was purchased from Oakwood Chemicals and dried over 4 Å molecular sieves and potassium. Celite was obtained from Oakwood Chemicals. Pinacolborane, phenylsilane, catecholborane, benzonitrile, *p*-tolunitrile, 4-methoxybenzonitrile, 4-fluorobenzonitrile, 4-chlorobenzonitrile, 2-bromobenzonitrile, 4-(trifluoromethyl)benzonitrile, 4-acetylbenzonitrile, acetonitrile, cyclohexanecarbonitrile, and 2-phenoxyacetonitrile were purchased from Oakwood Chemicals. 9-Borabicyclo[3.3.1]nonane and 3-(dimethylamino)propionitrile were purchased from Sigma Aldrich. All substrates were dried over 3 Å molecular sieves prior to catalyst screening.

Solution nuclear magnetic resonance (NMR) spectra were recorded at room temperature on a Varian 400 MHz or a Bruker 400 MHz NMR spectrometer. All ^{1}H NMR and ^{13}C NMR chemical shifts (ppm) are reported relative to Si(Me)$_4$ using ^{1}H (residual) and ^{13}C chemical shifts of the solvent as secondary standards. ^{19}F NMR chemical shifts (ppm) are reported relative to trichlorofluoromethane upon referencing an external

trifluorotoluene standard at -63.72 ppm. ^{31}P NMR chemical shifts (ppm) are reported relative to phosphoric acid upon referencing an external triphenylphosphate standard at -17.54 ppm. Elemental analyses were performed at Robertson Microlit Laboratories Inc. (Ledgewood, NJ). Solution-state magnetic susceptibility was determined via Evans method on the Varian 400 MHz NMR spectrometer.

X-ray Crystallography: A single crystal of **82** was coated with polyisobutylene oil in the glovebox and transferred to a glass fiber, which was then mounted on the goniometer head of a Bruker APEX Diffractometer equipped with Mo K_a radiation (Arizona State University). A hemisphere routine was used for data collection and determination of the lattice constants. The space group was identified, and the data was processed using the Bruker SAINT+ program and corrected for absorption using SADABS. The structures were solved using direct methods (SHELXS), completed by subsequent Fourier synthesis, and refined by full-matrix, least square procedures on $[F^2]$ (SHELXL).

EPR Spectroscopy:

Instrumentation. Studies were performed at the EPR Facility of Arizona State University. Continuous wave (CW) EPR spectra were recorded at 114 K using a Bruker ELEXSYS E580 CW X-band spectrometer (Bruker, Rheinstetten, Germany) equipped with a liquid nitrogen temperature control system (ER 4131VT). The magnetic field modulation frequency was 100 kHz with a field modulation amplitude of 0.5 mT peak-to-peak. The microwave power was 1 mW, the microwave frequency was 9.43 GHz, and the sweep time was 168 seconds.

Spin Hamiltonian. The EPR spectra of a coupled dimer system can be described with the spin Hamiltonian:

$$\text{(1)}$$

$$H = -2J_0 h \mathbf{S_1} \cdot \mathbf{S_2} + h \mathbf{S_1} \cdot \mathbf{J} \cdot \mathbf{S_2} + H_1 + H_2$$

where J_o is the isotropic exchange coupling constant between the two Mn(II) ions of the dimer, $\mathbf{J}$ is the tensor describing the dipole-dipole interaction between the two Mn(II) spin centers, both in frequency units, h is Planck's constant, and H_i ($i = 1, 2$) are the spin Hamiltonians corresponding to each individual Mn(II) ion. The spin Hamiltonian of each Mn(II) spin center contains the electron Zeeman interaction with the applied magnetic field $\mathbf{B_o}$, the zero-field interaction, and the hyperfine coupling (hfc) interaction with the nucleus of ^{55}Mn:

$$H_i = \beta_e \mathbf{S}_i \cdot \mathbf{g}_i \cdot \mathbf{B}_0 + h \mathbf{S}_i \cdot \mathbf{d}_i \cdot \mathbf{S}_i + h \mathbf{S}_i \cdot \mathbf{a}_i \cdot \mathbf{I}_i \quad (2)$$

where $\mathbf{S_i}$ and $\mathbf{I_i}$ are the electron and nuclear spin operators, respectively, $\mathbf{d_i}$ and $\mathbf{a_i}$ are the zero-field splitting and hfc tensors, respectively, all in frequency units, $\mathbf{g_i}$ is the electronic g-tensor, and β_e is the electron magneton. For Mn(II) dimers, the electron and nuclear spins of each Mn(II) ion are $S_i = 5/2$ and $I_i = 5/2$, respectively. Mn(II) ions have a singlet orbital ground state (^{6}A), with the first excited orbital state (^{4}T) more than 10,000 cm^{-1} above the ground state. Consequently, the zero-field energies of Mn(II) ions are generally small, $|D_i| < 0.1$ cm^{-1}. For dimeric manganese complexes, the bridging atoms typically give a Mn–Mn exchange interaction that is significantly larger than 0.1 cm^{-1}. In this strong exchange regimen, the isotropic exchange coupling energy is much larger than the electronic Zeeman energy ($|J_o| \gg g_i\beta_e B_o/h$) and the zero-field splitting ($|J_o| \gg |D_i|$). The dimer system may then be regarded as a ladder of isolated spin manifolds. These spin manifolds have total spin quantum numbers of $S = 0, 1, 2, 3, 4,$ and 5, each with a degeneracy of ($2S+1$). The energy separation between the spin manifolds is much larger than the microwave energy ($h\nu$) at the X-band (9.40 GHz) frequency and no transitions are observable between spin

manifolds. The individual spin manifolds can be considered independently, and their corresponding spectra can be simulated using a spin Hamiltonian for each individual spin manifold given by: (3)

$$H_S = \beta_e \mathbf{S} \cdot \mathbf{G_S} \cdot \mathbf{B_0} + h\mathbf{S} \cdot \mathbf{D_S} \cdot \mathbf{S} + h\mathbf{S} \cdot \mathbf{A_1} \cdot \mathbf{I_1} + h\mathbf{S} \cdot \mathbf{A_2} \cdot \mathbf{I_2}$$

where $\mathbf{G_S}$, $\mathbf{D_S}$, and $\mathbf{A_i}$ (i = 1, 2) are the electronic Zeeman, zero-field splitting, and hfc tensors, respectively, of the spin manifolds of the coupled system, and $\mathbf{S}$ is the spin operator of the coupled spin manifolds. The parameters of the coupled spin system can be expressed as linear combinations of the parameters of the individual spin centers:

$$\mathbf{G_S} = c_1\mathbf{g_1} + c_2\mathbf{g_2} \quad (4)$$

$$\mathbf{D_S} = d_1\mathbf{d_1} + d_2\mathbf{d_2} + d_{12}\mathbf{J} \quad (5)$$

$$\mathbf{A_i} = c_i\mathbf{a_i} \quad (6)$$

where the coefficients c_1, c_2, d_1, d_2, and d_{12} are specific to the particular spin manifold and have been tabulated elsewhere. For Mn(II) ions, the contributions from spin-orbit coupling to the $\mathbf{g_i}$ tensor and hfc tensor are small, thus we will assume that both tensors $\mathbf{g_i}$ and $\mathbf{a_i}$ are isotropic. In the complex studied here, the two manganese centers of the dimer have identical ligation. The coordination geometry of one manganese ion is related to the other by a mirror plane, thus, we assume $g_1 = g_2 = g_{iso}$, $a_1 = a_2 = a$, and $\mathbf{d_1} = \mathbf{d_2}$. In this study, hfc's due to Mn(II) were not explicitly included in the spin Hamiltonian (Eq. 3).

Fitting of EPR spectra. To quantitatively compare experimental and simulated spectra, we divided the spectra into N intervals (*i.e.*, we treated the spectrum as an N-dimensional vector $\mathbf{R}$). Each component R_j has the amplitude of the EPR signal at a magnetic field B_j, with j varying from 1 to N. The amplitudes of the experimental and simulated spectra were normalized so that the span between the maximum and minimum values of R_j is 1. We

192

compared the calculated amplitudes R_j^{calc} of the signal with the observed values R_j defining

a root-mean-square deviation σ by:

$$\sigma(p_1, p_2, \cdots, p_n) = [\sum_j (R_j^{calc}(p_1, p_2, \cdots, p_n) - R_j^{exp})^2 / N]^{1/2} \quad (7)$$

where the sums are over the N values of j, and p's are the fitting parameters that produced

the calculated spectrum. For our simulations, N was set equal to 2048. The EPR spectrum

was simulated using EasySpin (v 5.2.25), a computational package developed by Stoll and

Schweiger[9] and based on Matlab (The MathWorks, Natick, MA, USA). EasySpin

calculates EPR resonance fields using the energies of the states of the spin system obtained

by direct diagonalization of the spin Hamiltonian (see Eq. 3). The EPR fitting procedure

used a Monte Carlo type iteration to minimize the root-mean-square deviation, σ (see Eq.

7) between measured and simulated spectra. We searched for the optimum values of the

following parameters: the isotropic g-value (g_{iso}), the zero-field splitting parameters (D and

E), the principal components of the $\mathbf{J}$ tensor ($J_{x'}$, $J_{y'}$ and $J_{z'}$) and the isotropic peak-to-peak

linewidth (ΔB).

Computational Details

        All calculations were carried out using DFT as implemented in the Jaguar 9.1 suite

of ab initio quantum chemistry programs. Geometry optimizations were performed with

B3LYP functional including Grimme's D3 dispersion correction and the 6-31G** basis set

for main group atoms. Mn was represented using the Los Alamos LACVP basis. The

energies of the optimized structures were reevaluated by additional single-point

calculations on each optimized geometry using Dunning's correlation consistent triple-ζ

basis set cc-pVTZ(-f), which includes a double set of polarization functions. For Mn, we

used a modified version of LACVP, designated as LACV3P, in which the exponents were

decontracted to match the effective core potential with triple-ζ quality. For boron, 6-311G** containing the decontracted exponent with triple-ζ quality was used. For boron, 6-311G** containing the decontracted exponent with triple-ζ quality was used. Solvation energies were evaluated by a self-consistent reaction field (SCRF) approach based on accurate numerical solutions of the Poisson−Boltzmann equation. In the results reported, solvation calculations were carried out with the 6-31G**/LACVP basis at the optimized gas-phase geometry employing the dielectric constants of $\varepsilon = 2.284$ for benzene. As is the case for all continuum models, the solvation energies are subject to empirical parametrization of the atomic radii that are used to generate the solute surface. We employed the standard set of optimized radii in Jaguar for H (1.150 Å), B (2.042 Å), C (1.900 Å), N (1.600 Å), O (1.600 Å), and Mn (1.480 Å). Analytical vibrational frequencies within the harmonic approximation were computed with the 6-31G**/LACVP basis to confirm proper convergence to well-defined minima or saddle points on the potential energy surface. The energy components have been computed with the following protocol. The free energy in solution-phase, G(sol), has been calculated as follows:

$$G(\text{sol}) = G(\text{gas}) + G_{\text{solv}} \quad (8)$$

$$G(\text{gas}) = H(\text{gas}) - TS(\text{gas}) \quad (9)$$

$$H(\text{gas}) = E(\text{SCF}) + \text{ZPE} \quad (10)$$

$$\Delta E(\text{SCF}) = \sum E(\text{SCF}) \text{ for products} - \sum E(\text{SCF}) \text{ for reactants} \quad (11)$$

$$\Delta G(\text{sol}) = \sum G(\text{sol}) \text{ for products} - \sum G(\text{sol}) \text{ for reactants} \quad (12)$$

Synthesis of [($^{2,6-iPr_2Ph}$BDI)Mn(μ-NCHPh)]$_2$ (82): A 20 mL vial was charged with **47** (0.073 g, 0.077 mmol) dissolved in 10 mL toluene. Then, a solution of benzonitrile (15.88 μL, 0.154 mmol) in 5 mL of toluene was added to the vial. A color change from yellow to

orange was observed. After stirring at room temperature for 1 h, the orange solution was filtered through Celite, and the solvent was removed under vacuum to obtain a reddish-orange solid. The solid was washed with Et_2O and recrystallized in toluene layered with pentane upon cooling to –35 °C, affording orange crystals of **82** (0.063 g, 0.055 mmol, 71%).

Elemental analysis for $C_{72}H_{94}N_6Mn_2$: Calcd. C, 74.97; H, 8.21; N, 7.29. Found: C, 74.65; H, 8.02; N, 7.01.

Magnetic susceptibility (Evans method, 25 °C): μ_{eff} = 6.54 μ_B (considering a dimeric structure in solution).

^{1}H NMR (benzene-d_6, 25 °C): 26.82 (peak width at half-height = 14988 Hz), 14.92 (7011 Hz), 3.90 (2891 Hz), -12.36 (23042 Hz).
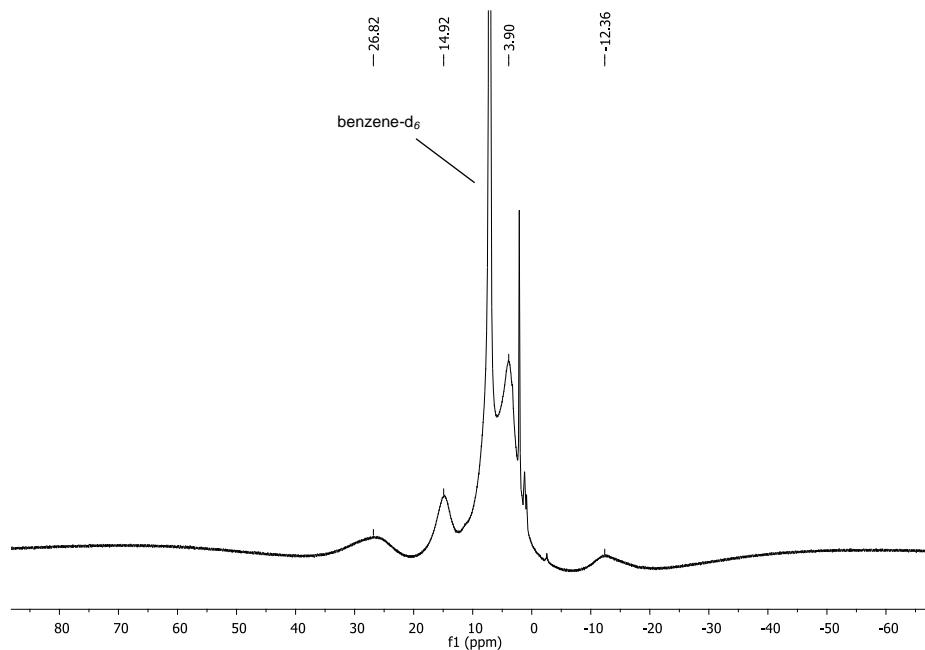
Figure 5.4. ^{1}H NMR spectrum of **82** in benzene-d_6 at 25 °C.

Hydroboration of benzonitrile catalyzed by 0.5 mol% of 47 (1 mol% based on Mn):

In the glove box, HBPin (337.25 μL, 2.32 mmol) and benzonitrile (110 μL, 1.06 mmol)

195

were added to a vial containing a benzene-d_6 solution of **47** (0.005 g, 0.005 mmol). The vial was sealed under N_2 atmosphere and stirred at 80 °C. After 24 h of heating, I_2 was added to the solution to deactivate the catalyst. Greater than 99% conversion was observed by ^{1}H NMR spectroscopy. The solvent and remaining borane were removed under vacuum, resulting in a white solid. Recrystallization from pentane at –35 °C yielded 0.316 g (83%) of *N*-benzyl-4,4,5,5-tetramethyl-*N*-(4,4,5,5-tetramethyl-1,3,2-dioxaborolan-2-yl)-1,3,2-dioxaborolan-2-amine.

^{1}H NMR (benzene-d_6, 400 MHz): 7.60 (d, J = 7.6 Hz, 2H, *phenyl*), 7.26 (pseudo t, J = 7.6 Hz, 2H, *phenyl*), 7.12 (m, 1H, *phenyl*), 4.63 (s, 2H, C*H₂*), 1.04 (s, 24H, CC*H₃*). ^{13}C NMR (benzene-d_6, 100 MHz): 144.61 – 143.76 (m, *phenyl*), 128.71 (s, *phenyl*), 128.41 (s, *phenyl*), 127.00 (s, *phenyl*), 82.94 (s, *C*CH₃), 48.32 (s, *C*H₂), 25.15 (s, *C*H₃).
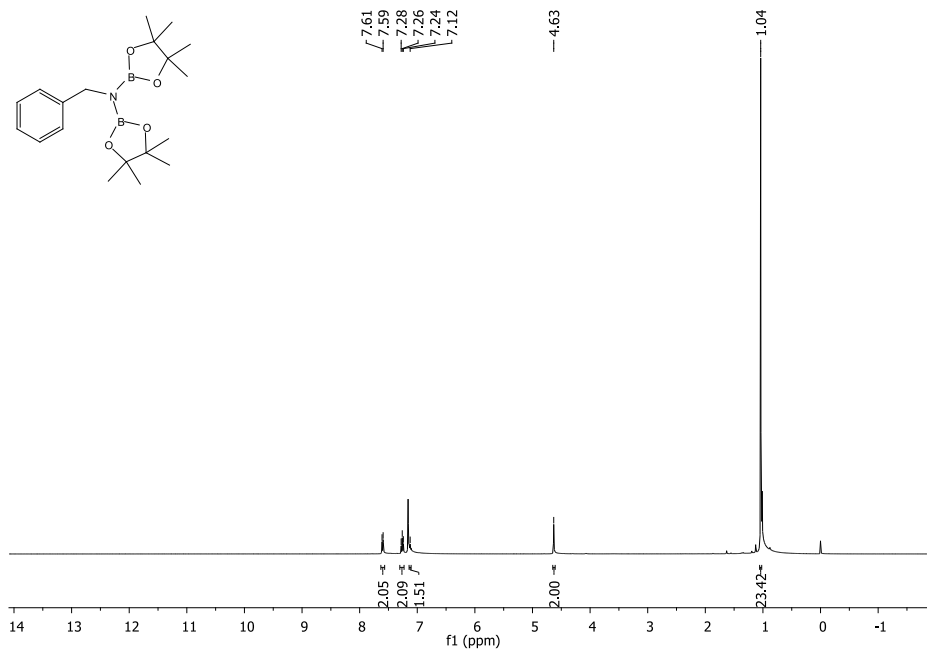
Figure 5.5. Representative ^{1}H NMR spectrum of *N*-benzyl-4,4,5,5-tetramethyl-*N*-(4,4,5,5-tetramethyl-1,3,2-dioxaborolan-2-yl)-1,3,2-dioxaborolan-2-amine in benzene-d_6.

196
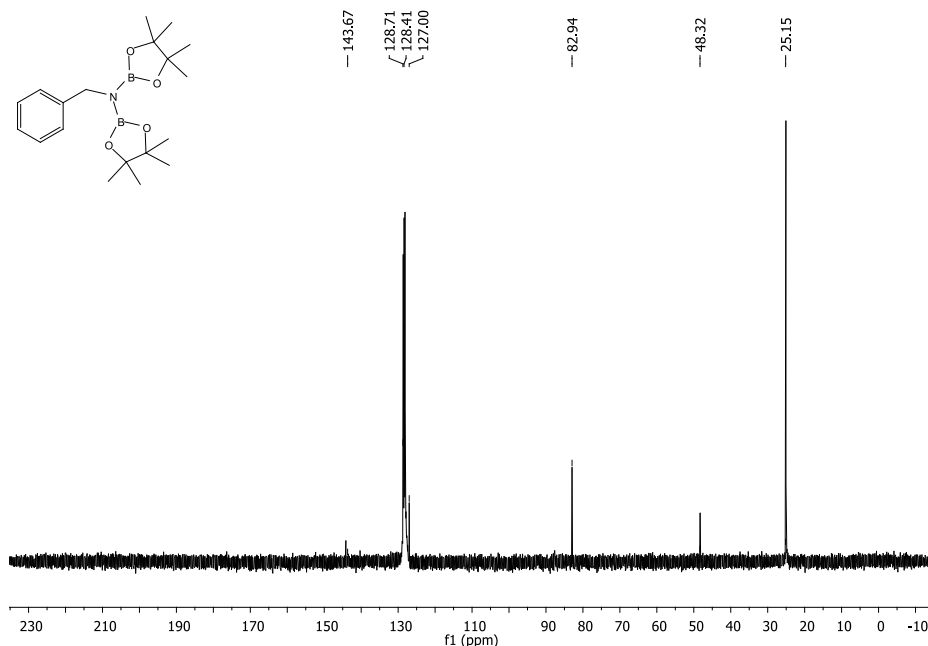
Figure 5.6. Representative ^{13}C NMR spectrum of *N*-benzyl-4,4,5,5-tetramethyl-*N*-(4,4,5,5-tetramethyl-1,3,2-dioxaborolan-2-yl)-1,3,2-dioxaborolan-2-amine in benzene-*d₆*.

Hydroboration of *p*-tolunitrile catalyzed by 0.5 mol% of 47 (1 mol% based on Mn):

In the glove box, HBPin (278 μL, 1.92 mmol) and *p*-tolunitrile (0.102 g, 0.871 mmol) were added to a vial containing a benzene-*d₆* solution of **47** (0.004 g, 0.004 mmol). The vial was sealed under N_2 atmosphere and stirred at 80 °C. After 24 h of heating, I_2 was added to the solution to deactivate the catalyst. Greater than 99% conversion was observed by ^1H NMR spectroscopy. The solvent and remaining borane were removed under vacuum, resulting in a white solid. Recrystallization from pentane at –35 °C yielded 0.267 g (82%) of 4,4,5,5-tetramethyl-*N*-(4-methylbenzyl)-*N*-(4,4,5,5-tetramethyl-1,3,2-dioxaborolan-2-yl)-1,3,2-dioxaborolan-2-amine.

^1H NMR (benzene-*d₆*, 400 MHz): 7.55 (d, *J* = 7.6 Hz, 2H, *phenyl*), 7.09 (d, *J* = 7.6 Hz, 2H, *phenyl*), 4.63 (s, 2H, C*H₂*), 2.16 (s, 3H, C*H₃*), 1.05 (s, 24H, CC*H₃*). ^{13}C NMR (benzene-*d₆*,

100 MHz): 141.26 (s, *phenyl*), 136.12 (s, *phenyl*), 129.43 (s, *phenyl*), 128.47 (s, *phenyl*), 82.91 (s, *C*CH$_3$), 47.99 (s, *C*H$_2$), 25.10 (s, C*C*H$_3$), 21.50 (s, *C*H$_3$).

Hydroboration of 4-methoxybenzonitrile catalyzed by 0.5 mol% of 47. In the glove box, HBPin (404.7 μL, 2.79 mmol) and 4-methoxybenzonitrile (0.169 g, 1.27 mmol) were added to a vial containing a benzene-*d$_6$* solution of **47** (0.006 g, 0.006 mmol). The vial was sealed under N$_2$ atmosphere and stirred at 80 ºC. After 24 h of heating, I$_2$ was added to the solution to deactivate the catalyst. Greater than 99% conversion was observed by ^{1}H NMR spectroscopy. The solvent and remaining borane were removed under vacuum, resulting in a white solid. Recrystallization from pentane at –35 °C yielded 0.351 g (71%) of *N*-(4-methoxybenzyl)-4,4,5,5-tetramethyl-*N*-(4,4,5,5-tetramethyl-1,3,2-dioxaborolan-2-yl)-1,3,2-dioxaborolan-2-amine.

^{1}H NMR (benzene-*d$_6$*, 400 MHz): 7.58 (d, *J* = 8.1 Hz, 2H, *phenyl*), 6.89 (d, *J* = 8.1 Hz, 2H, *phenyl*), 4.61 (s, 2H, C*H$_2$*), 3.35 (s, 3H, -OC*H$_3$*), 1.06 (s, 24H, CC*H$_3$*). ^{13}C NMR (benzene-*d$_6$*, 100 MHz): 159.36 (s, *phenyl*), 136.43 (s, *phenyl*), 129.83 (s, *phenyl*), 114.22 (s, *phenyl*), 82.90 (s, *C*CH$_3$), 55.10 (s, *C*H$_2$), 47.68 (s, *C*H$_3$), 25.12 (s, C*C*H$_3$).

Hydroboration of 4-(dimethylamino)benzonitrile catalyzed by 0.5 mol% of 47 (1 mol% based on Mn). In the glove box, HBPin (347 μL, 2.515 mmol) and 4-(dimethylamino)benzonitrile (0.167 g, 1.143 mmol) were added to vial containing a benzene-*d$_6$* solution of **47** (0.005 g, 0.006 mmol). The vial was sealed under N$_2$ atmosphere and stirred at 80 ºC. After 24 h of heating, I$_2$ was added to the solution to deactivate the catalyst. ^{1}H NMR spectroscopy revealed 84% conversion. The solvent and remaining borane were removed under vacuum and the resulting solid was washed with Et$_2$O. Recrystallization from pentane at -35 ºC yielded 0.203 g (44%) of *N*-(4-

(dimethylamino)benzyl)-4,4,5,5-tetramethyl-N-(4,4,5,5-tetramethyl-1,3,2-dioxaborolan-2-yl)-1,3,2-dioxaborolan-2-amine.

^{1}H NMR (benzene-d_6, 400 MHz): 7.55 (d, J = 8.6 Hz, 2H, *phenyl*), 6.67 (d, J = 8.6 Hz, 2H, *phenyl*), 4.55 (s, 2H, CH_2), 2.57 (s, 6H, NCH_3), 1.05 (s, 24H, CCH_3). ^{13}C NMR (benzene-d_6, 100 MHz): 150.22 (s, *phenyl*), 132.61 (s, *phenyl*), 129.56 (s, *phenyl*), 113.30 (s, *phenyl*), 82.75 (s, CCH$_3$), 47.65 (s, CH$_2$), 40.95 (s, NCH$_3$), 25.15 (s, CCH$_3$).

Hydroboration of 4-fluorobenzonitrile catalyzed by 0.5 mol% of 47 (1 mol% based on Mn). In the glove box, HBPin (344.2 μL, 2.372 mmol) and 4-fluorobenzonitrile (0.131 g, 1.08 mmol) were added to a vial containing a benzene-d_6 solution of **47** (0.005 g, 0.005 mmol). The vial was sealed under N$_2$ atmosphere and stirred at 80 °C. After 24 h of heating, I$_2$ was added to the solution to deactivate the catalyst. Greater than 99% conversion was observed by ^{1}H NMR spectroscopy. The solvent and remaining borane were removed under vacuum, resulting in a white solid. Recrystallization from pentane at –35 °C yielded 0.358 g (88%) of N-(4-fluorobenzyl)-4,4,5,5-tetramethyl-N-(4,4,5,5-tetramethyl-1,3,2-dioxaborolan-2-yl)-1,3,2-dioxaborolan-2-amine.

^{1}H NMR (benzene-d_6, 400 MHz): 7.45-7.41 (dd, J = 8.5, 5.7 Hz, 2H, *phenyl*), 6.92-6.88 (t, J = 8.8 Hz, 2H, *phenyl*), 4.49 (s, 2H, CH_2), 1.03 (s, 24H, CCH_3). ^{13}C NMR (benzene-d_6, 100 MHz): 130.15 (d, J = 7.8 Hz, *phenyl*), 128.87 (d, J = 11.4 Hz, *phenyl*), 115.36 (d, J = 21.0 Hz, *phenyl*), 83.00 (s, CCH$_3$), 47.50 (s, CH$_2$), 25.06 (s, CCH$_3$). ^{19}F NMR (benzene-d_6, 407.6 MHz): -118.41.

Hydroboration of 4-chlorobenzonitrile catalyzed by 0.5 mol% of 47 (1 mol% based on Mn). In the glove box, HBPin (472 μL, 3.254 mmol) and 4-chlorobenzonitrile (0.203 g, 1.48 mmol) were added to vial containing a benzene-d_6 solution of **47** (0.007 g, 0.007

mmol). The vial was sealed under N_2 atmosphere and stirred at 80 °C. After 24 h of heating, I_2 was added to the solution to deactivate the catalyst. Greater than 99% conversion was observed by ^{1}H NMR spectroscopy. The solvent and remaining borane were removed under vacuum, resulting in a white solid. Recrystallization from pentane at –35 °C yielded 0.536 g (92%) of *N*-(4-chlorobenzyl)-4,4,5,5-tetramethyl-*N*-(4,4,5,5-tetramethyl-1,3,2-dioxaborolan-2-yl)-1,3,2-dioxaborolan-2-amine.

^{1}H NMR (benzene-*d₆*, 400 MHz): 7.35 (d, *J* = 7.7 Hz, 2H, *phenyl*), 7.18 (d, *J* = 13.7 Hz, 2H, *phenyl*), 4.44 (s, 2H, C*H₂*), 1.02 (s, 24H, CC*H₃*). ^{13}C NMR (benzene-*d₆*, 100 MHz): 142.59 (s, *phenyl*), 132.80 (s, *phenyl*), 129.89 (s, *phenyl*), 128.83 (s, *phenyl*), 83.03 (s, *C*CH₃), 47.53 (s, *C*H₂), 25.05 (s, C*C*H₃).

Hydroboration of 2-bromobenzonitrile catalyzed by 0.5 mol% of 47 (1 mol% based on Mn). In the glove box, HBPin (263 μL, 1.813 mmol) and 2-bromobenzonitrile (0.15 g, 0.824 mmol) were added to a vial containing a benzene-*d₆* solution of **47** (0.004 g, 0.004 mmol). The vial was sealed under N_2 atmosphere and stirred at 80 °C. After 24 h of heating, I_2 was added to the solution to deactivate the catalyst. Greater than 99% conversion was observed by ^{1}H NMR spectroscopy. The solvent and remaining borane were removed under vacuum, resulting in a white solid. Recrystallization from pentane at –35 °C yielded 0.31 g (86%) of *N*-(2-bromobenzyl)-4,4,5,5-tetramethyl-*N*-(4,4,5,5-tetramethyl-1,3,2-dioxaborolan-2-yl)-1,3,2-dioxaborolan-2-amine.

^{1}H NMR (benzene-*d₆*, 400 MHz): 7.57 (d, *J* = 7.7 Hz, 1H, *phenyl*), 7.35 (d, *J* = 7.9 Hz, 1H, *phenyl*), 7.10 (d, *J* = 7.5 Hz, 1H, *phenyl*), 6.72 (t, *J* = 7.6 Hz, 1H, *phenyl*), 4.85 (s, 2H, C*H₂*), 1.01 (s, 24H, CC*H₃*). ^{13}C NMR (benzene-*d₆*, 100 MHz): 142.53 (s, *phenyl*), 133.14

(s, *phenyl*), 128.81 (s, *phenyl*), 128.10 (s, *phenyl*), 127.55 (s, *phenyl*), 127.34 (s, *phenyl*), 83.10 (s, *C*CH$_3$), 48.88 (s, *C*H$_2$), 24.94 (s, C*C*H$_3$).

Hydroboration of 4-(trifluoromethyl)benzonitrile catalyzed by 0.5 mol% of 47 (1 mol% based on Mn). In the glove box, HBPin (371 μL, 2.555 mmol) and 4-(trifluoromethyl)benzonitrile (0.198 g, 1.16 mmol) were added to a vial containing a benzene-*d$_6$* solution of **47** (0.006 g, 0.006 mmol). The vial was sealed under N$_2$ atmosphere and stirred at 80 °C. After 24 h of heating, I$_2$ was added to the solution to deactivate the catalyst. Greater than 99% conversion was observed by ^{1}H NMR spectroscopy. The solvent and remaining borane were removed under vacuum, resulting in a white solid. Recrystallization from pentane at –35 °C yielded 0.406 g (82%) of 4,4,5,5-tetramethyl-*N*-(4,4,5,5-tetramethyl-1,3,2-dioxaborolan-2-yl)-*N*-(4-trifluoromethyl)benzyl)-1,3,2-dioxaborolan-2-amine.

^{1}H NMR (benzene-*d$_6$*, 400 MHz): 7.41 (s, 4H, *phenyl*), 4.47 (s, 2H, C*H$_2$*), 1.01 (s, 24H, CC*H$_3$*). ^{13}C NMR (benzene-*d$_6$*, 100 MHz): 148.06 (s, *C*F$_3$), 128.51 (s, *phenyl*), 128.26 (s, *phenyl*), 125.62 (q, *J* = 3.7 Hz, *phenyl*), 83.13 (s, *C*CH$_3$), 47.81 (s, *C*H$_2$), 25.02 (s, *C*CH$_3$). ^{19}F NMR (benzene-*d$_6$*, 470.6 MHz): -63.57.

Hydroboration of 4-acetylbenzonitrile catalyzed by 0.5 mol% of 47 (1 mol% based on Mn). In the glove box, HBPin (635 μL, 4.379 mmol) and 4-acetylbenzonitrile (0.193 g, 1.327 mmol) were added to a vial containing a benzene-*d$_6$* solution of **47** (0.006 g, 0.007 mmol). The vial was sealed under N$_2$ atmosphere and stirred at 80 °C. After 24 h of heating, I$_2$ was added to the solution to deactivate the catalyst. Greater than 99% conversion was observed by ^{1}H NMR spectroscopy. The solvent and remaining borane were removed under vacuum, resulting in a white solid. Recrystallization from pentane at –35 °C yielded

0.463 g (87%) of 4,4,5,5-tetramethyl-*N*-(4,4,5,5-tetramethyl-1,3,2-dioxaborolan-2-yl)-*N*-(4-(1-((4,4,5,5-tetramethyl-1,3,2-dioxaborolan-2-yl)oxy)ethyl)benzyl)-1,3,2-dioxaborolan-2-amine.

^{1}H NMR (benzene-*d$_6$*, 400 MHz): 7.56 (d, *J* = 11.3 Hz, 2H, *phenyl*), 7.43 (d, *J* = 7.8 Hz, 2H, *phenyl*), 5.46 (q, *J* = 11.2, 5.1 Hz, 1H, C*H*), 4.59 (s, 2H, C*H$_2$*), 1.49 (d, *J* = 10.2 Hz, 3H, C*H$_3$*), 1.04 (s, 12H, CC*H$_3$*), 1.03 (s, 12H, CC*H$_3$*), 1.01 (s, 12H, CC*H$_3$*). ^{13}C NMR (benzene-*d$_6$*, 100 MHz): 143.73 (s, *phenyl*), 142.96 (s, *phenyl*), 125.87 (s, *phenyl*), 82.92 (s, *C*H), 82.79 (s, *C*CH$_3$), 73.31 (s, *C*CH$_3$), 47.99 (s, *C*H$_2$), 26.05 (s, *C*H$_3$), 25.08 (s, *C*H$_3$), one resonance not located.

Hydroboration of acetonitrile catalyzed by 0.5 mol% of 47 (1 mol% based on Mn). In the glove box, HBPin (230 μL, 1.58 mmol) and acetonitrile (37.5 μL, 0.718 mmol) were added to a vial containing a benzene-*d$_6$* solution of **47** (0.003 g, 0.004 mmol). The vial was sealed under N$_2$ atmosphere and stirred at 80 °C. After 24 h of heating, I$_2$ was added to the solution to deactivate the catalyst. Greater than 99% conversion was observed by ^{1}H NMR spectroscopy. The solvent and remaining borane were removed under vacuum, resulting in a white solid. Recrystallization from pentane at –35 °C yielded 0.126 g (59%) of *N*-ethyl-4,4,5,5-tetramethyl-*N*-(4,4,5,5-tetramethyl-1,3,2-dioxaborolan-2-yl)-1,3,2-dioxaborolan-2-amine.

^{1}H NMR (benzene-*d$_6$*, 400 MHz): 3.44 (q, *J* = 6.2 Hz, 2H, C*H$_2$*), 1.29 (t, 3H, C*H$_3$*), 1.06 (s, 24H, C*H$_3$*). ^{13}C NMR (benzene-*d$_6$*, 100 MHz): 82.53 (s, *C*H), 39.44 (s, *C*H$_2$), 25.15 (s, *C*H$_3$), 19.54 (s, *C*H$_3$).

Hydroboration of cyclohexanecarbonitrile catalyzed by 0.5 mol% of 47 (1 mol% based on Mn). In the glove box, HBPin (271 μL, 1.87 mmol) and cyclohexanecarbonitrile (101 μL, 0.85 mmol) were added to a vial containing a benzene-d_6 solution of **47** (0.004 g, 0.004 mmol). The vial was sealed under N_2 atmosphere and stirred at 80 °C. After 24 h of heating, I_2 was added to the solution to deactivate the catalyst. Greater than 99% conversion was observed by ^{1}H NMR spectroscopy. The solvent and remaining borane were removed under vacuum, resulting in a white solid. Recrystallization from pentane at –35 °C yielded 0.408 g (89%) of *N*-(cyclohexylmethyl)-4,4,5,5-tetramethyl-*N*-(4,4,5,5-tetramethyl-1,3,2-dioxaborolan-2-yl)-1,3,2-dioxaborolan-2-amine.

^{1}H NMR (benzene-d_6, 400 MHz): 3.30 (d, J = 7.0 Hz, 2H, CH_2), 2.76 (t, J = 7.1 Hz, 1H, CH), 1.89 (d, J = 12.4 Hz, 2H, CH_2), 1.72 (d, J = 12.3 Hz, 4H, CH_2), 1.65 – 1.53 (m, 4H, CH_2), 1.07 (s, 24H, CCH_3). ^{13}C NMR (benzene-d_6, 100 MHz): 82.48 (s, CCH$_3$), 50.71 (s, CH$_2$), 41.13 (s, CH), 31.47 (s, CH$_2$), 27.64 (s, CH$_2$), 26.96 (s, CH$_2$), 25.16 (s, CCH$_3$).

Hydroboration of 3-(dimethylamino)propionitrile catalyzed by 0.5 mol% of 47 (1 mol% based on Mn). In the glove box, HBPin (472 μL, 3.25 mmol) and 3-(dimethylamino)propionitrile (157 μL, 1.4 mmol) were added to a vial containing a benzene-d_6 solution of **47** (0.007 g, 0.007 mmol). The vial was sealed under N_2 atmosphere and stirred at 80 °C. After 24 h of heating, I_2 was added to the solution to deactivate the catalyst. Greater than 99% conversion was observed by ^{1}H NMR spectroscopy. The solvent and remaining borane were removed under vacuum, resulting in a white solid. Recrystallization from pentane at –35 °C yielded 0.322 g (65%) of *N1,N1*-dimethyl-*N3,N3*-bis(4,4,5,5-tetramethyl-1,3,2-dioxaborolan-2-yl)propane-1,3-diamine.

^{1}H NMR (benzene-d_6, 400 MHz): 3.35 (t, J = 7.2 Hz, 2H, CH_2), 2.23 (t, J = 7.2 Hz, 2H, CH_2), 2.08 (s, 6H, CH_3), 1.85 – 1.73 (m, 2H, CH_2), 1.02 (s, 24H, CCH_3). ^{13}C NMR (benzene-d_6, 100 MHz): 81.69 (s, CCH$_3$), 57.31 (s, CH$_2$), 45.12 (s, CH$_3$), 42.15 (s, CH$_2$), 31.62 (s, CH$_2$), 24.30 (s, CCH$_3$).

Hydroboration of 2-phenoxyacetonitrile catalyzed by 0.5 mol% of 47 (1 mol% based on Mn). In the glove box, HBPin (209 μL, 1.441 mmol) and 2-phenoxyacetonitrile (80 μL, 0.655 mmol) were added to a vial containing a benzene-d_6 solution of **47** (0.003 g, 0.003 mmol). The vial was sealed under N_2 atmosphere and stirred at 80 °C. After 24 h of heating, I_2 was added to the solution to deactivate the catalyst. Greater than 99% conversion was observed by ^{1}H NMR spectroscopy. The solvent and remaining borane were removed under vacuum, resulting in a white solid. Recrystallization from pentane at –35 °C yielded 0.206 g (81%) of 4,4,5,5-tetramethyl-N-(2-phenoxyethyl)-N-(4,4,5,5-tetramethyl-1,3,2-dioxaborolan-2-yl)-1,3,2-dioxaborolan-2-amine.

^{1}H NMR (benzene-d_6, 400 MHz): 7.17 (m, 2H, *phenyl*), 7.03 (d, J = 8.4 Hz, 2H, *phenyl*), 6.85 (t, J = 7.3 Hz, 1H, *phenyl*), 4.12 (t, J = 6.5 Hz, 2H, CH_2), 3.81 (t, J = 6.5 Hz, 2H, CH_2), 1.06 (s, 24H, CCH_3). ^{13}C NMR (benzene-d_6, 100 MHz): 160.22 (s, *phenyl*), 130.03 (s, *phenyl*), 121.00 (s, *phenyl*), 115.28 (s, *phenyl*), 82.92 (s, CCH$_3$), 69.55 (s, CH$_2$), 43.69 (s, CH$_2$), 25.08 (s, CCH$_3$).

Hydroboration of 3-(diphenylphosphino)propanenitrile catalyzed by 0.5 mol% of 47 (1 mol% based on Mn). In the glove box, HBPin (73 μL, 0.505 mmol) and 3-(diphenylphosphino)propanenitrile (0.542 g, 0.23 mmol) were added to a vial containing a benzene-d_6 solution of **47** (0.001 g, 0.001 mmol). The vial was sealed under N_2 atmosphere and stirred at 80 °C. After 24 h of heating, I_2 was added to the solution to deactivate the

catalyst. Greater than 99% conversion was observed by ^{1}H NMR spectroscopy. The solvent and remaining borane were removed under vacuum, resulting in a white solid. Recrystallization from pentane at –35 °C yielded 0.074 g (65%) of *N*-(3-(diphenylphosphino)propyl)-4,4,5,5-tetramethyl-*N*-(4,4,5,5-tetramethyl-1,3,2-dioxaborolan-2-yl)-1,3,2-dioxaborolan-2-amine.

^{1}H NMR (benzene-*d₆*, 400 MHz): 7.47 (t, *J* = 7.1 Hz, 4H, *phenyl*), 7.08 (dt, *J* = 21.5, 7.2 Hz, 7H, *phenyl*), 3.51 (t, *J* = 6.9 Hz, 2H, C*H₂*), 2.15 – 2.05 (m, 2H, C*H₂*), 1.94 – 1.84 (m, 2H, C*H₂*), 1.05 (s, 24H, CC*H₃*). ^{13}C NMR (benzene-*d₆*, 100 MHz): 139.54 (s, *phenyl*), 132.79 (d, *J* = 18.5 Hz, *phenyl*), 128.30 (s, *phenyl*), 128.22 (d, *J* = 6.5 Hz, *phenyl*), 81.65 (s, *C*CH₃), 42.37 (s, *C*H₂), 30.10 (s, *C*H₂), 25.21 (s, *C*H₂), 24.46 (s, C*C*H₃). ^{31}P NMR (benzene-*d₆*, 162 MHz): -16.04.

Determination of maximum benzonitrile dihydroboration turnover frequency using 0.1 mol% of 47 under neat conditions. In the glove box, HBPin (1653 μL, 11.39 mmol) and benzonitrile (534 μL, 5.18 mmol) were added to a vial containing 0.005 g of **47** (0.005 mmol). The vial was sealed under N₂ atmosphere and stirred at 80 °C. After 2 h of heating, the resulting solid was dissolved in benzene and I₂ was added to the solution to deactivate the catalyst. ^{1}H NMR spectroscopy revealed 52% conversion which equates to a maximum TOF of 260 h^{-1} at 80 °C. Repeating this experiment and heating to 80 °C for 24 h revealed 94% conversion (TOF = 39 h^{-1}).

5.7. References

(1) Suginome, M.; Uehlin, L.; Murakami, M. *J. Am. Chem. Soc.* **2004**, *126* (41), 13196–13197.

(2) Khalimon, A. Y.; Farha, P. M.; Nikonov, G. I. *Dalton Trans.* **2015**, *44* (43), 18945–18956.

(3) Kitano, T.; Komuro, T.; Tobita, H. *Organometallics* **2019**, *38* (7), 1417–1420.

(4) Junor, G. P.; Romero, E. A.; Chen, X.; Jazzar, R.; Bertrand, G. *Angew. Chem. Int. Ed.* **2019**, *58* (9), 2875–2878.

(5) Ghosh, C.; Kim, S.; Mena, M. R.; Kim, J.-H.; Pal, R.; Rock, C. L.; Groy, T. L.; Baik, M.-H.; Trovitch, R. J. *J. Am. Chem. Soc.* **2019**, *141* (38), 15327–15337.

(6) Khalimon, A. Y.; Farha, P.; Kuzmina, L. G.; Nikonov, G. I. *Chem. Commun.* **2011**, *48* (3), 455–457.

(7) Geri, J. B.; Szymczak, N. K. *J. Am. Chem. Soc.* **2015**, *137* (40), 12808–12814.

(8) Kaithal, A.; Chatterjee, B.; Gunanathan, C. *J. Org. Chem.* **2016**, *81* (22), 11153–11161.

(9) Weetman, C.; Anker, M. D.; Arrowsmith, M.; Hill, M. S.; Kociok-Köhn, G.; Liptrot, D. J.; Mahon, M. F. *Chem. Sci.* **2015**, *7* (1), 628–641.

(10) Li, J.; Luo, M.; Sheng, X.; Hua, H.; Yao, W.; Pullarkat, S. A.; Xu, L.; Ma, M. *Org. Chem. Front.* **2018**, *5* (24), 3538–3547.

(11) Nakamura, G.; Nakajima, Y.; Matsumoto, K.; Srinivas, V.; Shimada, S. *Catal. Sci. Technol.* **2017**, *7* (15), 3196–3199.

(12) Ito, M.; Itazaki, M.; Nakazawa, H. *Inorg. Chem.* **2017**, *56* (22), 13709–13714. .

(13) Ibrahim, A. D.; Entsminger, S. W.; Fout, A. R. *ACS Catal.* **2017**, *7* (5), 3730–3734.

(14) Huang, Z.; Wang, S.; Zhu, X.; Yuan, Q.; Wei, Y.; Zhou, S.; Mu, X. *Inorg. Chem.* **2018**, *57* (24), 15069–15078.

(15) Harinath, A.; Bhattacharjee, J.; Panda, T. K. *Adv. Synth. Catal.* **2019**, *361* (4), 850–857.

(16) Liu, W.; Ding, Y.; Jin, D.; Shen, Q.; Yan, B.; Ma, X.; Yang, Z. *Green Chem.* **2019**, *21* (14), 3812–3815.

(17) Ding, Y.; Ma, X.; Liu, Y.; Liu, W.; Yang, Z.; Roesky, H. W. *Organometallics* **2019**, *38* (15), 3092–3097.

(18) Saha, S.; Eisen, M. S. *ACS Catal.* **2019**, *9* (7), 5947–5956.

(19) Banerjee, I.; Anga, S.; Bano, K.; Panda, T. K. *J. Organomet. Chem.* **2019**, *902*, 120958.

(20) Das, S.; Bhattacharjee, J.; Panda, T. K. *New J. Chem.* **2019**, *43* (43), 16812–16818.

(21) Feng, X.; Ji, P.; Li, Z.; Drake, T.; Oliveres, P.; Chen, E. Y.; Song, Y.; Wang, C.; Lin, W. *ACS Catal.* **2019**, *9* (4), 3327–3337.

(22) Ben-Daat, H.; Rock, C. L.; Flores, M.; Groy, T. L.; Bowman, A. C.; Trovitch, R. J. *Chem. Commun.* **2017**, *53* (53), 7333–7336.

(23) Trovitch, R. J. *Synlett*, **2014**, *25*, 1638–1642.

(24) Garbe, M.; Junge, K.; Beller, M. *Eur. J. Org. Chem.*, **2017**, *2017*, 4344–4362.

(25) Trovitch, R. J. *Acc. Chem. Res.*, **2017**, *50*, 2842–2852.

(26) Yang, X.; Wang, C. *Chem. Asian J.*, **2018**, *13*, 2307–2315.

(27) Mukhopadhyay, T. K.; Flores, M.; Groy, T. L.; Trovitch, R. J. *Chem. Sci.* **2018**, *9* (39), 7673–7680.

(28) Song, H.; Ye, K.; Geng, P.; Han, X.; Liao, R.; Tung, C.-H.; Wang, W. *ACS Catal.* **2017**, *7* (11), 7709–7717.

CHAPTER 6

CONCLUSION

This dissertation focused on the development of manganese catalysts for organic transformations and the formation of inorganic polymers. Chapter 1 reviewed the previous advances in Mn-based hydrofunctionalization catalysis. In particular, the development of homogenous and heterogeneous manganese catalysts for carbonyl, formate, ester, alkene, and alkyne hydrosilylation were gathered. Furthermore, examples of Mn-catalyzed amide and carbon dioxide reduction were also discussed. A considerable amount of mechanistic information has been gathered throughout these contributions. Remarkably, it was not until 2016 that the first report of manganese-catalyzed hydroboration was published. The hydroboration of carbonyls, alkenes and alkynes was discussed in this chapter, highlighting the activity of Mn catalysts for the preparation of organoboronate compounds.

In Chapter 2, the electronic structure of $[(^{2,6-iPr_2Ph}BDI)Mn(\mu-H)]_2$ was explored. The Heisenberg exchange coupling constant, J_0, was determined by density functional theory calculations, SQUID magnetometry and EPR spectroscopy at low temperature. Single crystal X-ray diffraction data was collected for this compound and the interaction between metal- and ligand-based orbitals was found to be responsible for the absence of a metal–metal multiple bond. The effect of steric interactions between the β-diketiminate ligands was found to be negligible. In addition, the overlap obtained between the p-orbitals of bridging ligands and Mn d-orbitals impacts the Mayer bond order between the two Mn atoms, lengthening the Mn-Mn distance, and supporting the generation of stable dimers. In contrast, the dissociation energy was found to be relatively low in the case of $[(^{2,6-}$

$^{i\text{Pr}_2\text{Ph}}$BDI)Mn(μ-H)]$_2$ which allows this compound to be more active for organic transformations.

Chapter 3 demonstrates the activity of [($^{2,6\text{-iPr}_2\text{Ph}}$BDI)Mn($\mu$-H)]$_2$ for the dehydrogenative coupling of amines and SiH$_4$ to prepare aminosilane CVD precursors and polycarbosilazanes at ambient temperature. In particular, diamino silane and triamino silane monomers were successfully prepared and characterized through the dehydrogenative coupling of secondary and primary amines and SiH$_4$ at room temperature. Three of these compounds, tris(dimethyl)amino silane, bis(diethyl)amino silane and di(*t*-butyl)amino silane, are commercial precursors for CVD that are currently prepared from corrosive chlorosilanes. In addition, six solid polycarbosilazanes were synthesized and characterized in good yields under ambient conditions. The use of multi-amine precursors allowed for the modification of chain length and functionality, which guided the properties of the polymer products. Furthermore, exceptionally pure perhydropolysilazane was directly prepared from ammonia and silane at room temperature through dehydrogenative coupling. To explore the mechanism, isopropyl amine was added to [($^{2,6\text{-}i\text{Pr}_2\text{Ph}}$BDI)Mn($\mu$-H)]$_2$, which resulted in the formation of [($^{2,6\text{-}i\text{Pr}_2\text{Ph}}$BDI)Mn($\mu$-NH*i*Pr)]$_2$. This finding indicates that σ-bond metathesis is the first step of catalysis, which is followed by the addition of H–Si bonds of SiH$_4$ across the Mn–N bonds to regenerate the catalyst and release the silylamine products. This chapter represents the first study to systematically demonstrate commercial aminosilane CVD precursor synthesis by way of SiH$_4$ and amine dehydrocoupling. These are also the first reported examples of Mn-catalyzed Si–N dehydrocoupling. This efficient and halogen-free preparation of highly cross-linked

polycarbosilazanes and perhydropolysilazane at ambient temperature suggests that this could become an industrially viable method.

In Chapter 4, the Mn-catalyzed dehydrogenative coupling of diamines and organic silanes was demonstrated. Fourteen polycarbosilazanes were synthesized from phenylsilane and *n*-octylsilane in good yields. Their structures were characterized by NMR, FT-IR, and MALDI-TOF spectroscopy. The thermal properties of the products were evaluated by TGA, DSC and X-ray powder diffraction. In addition, this project also demonstrates the synthesis of organic polysilazanes from NH_3 and organic hydrosilane dehydrocoupling. Importantly, the ability of polycarbosilazanes to coat substrates in air or inert atmosphere was examined by SEM and EDX, which revealed the potential to form uniform coatings. The dehydrocoupling of ethylenediamine and phenyl silane using 0.01 mol% of $[(^{2,6-iPr_2Ph}BDI)Mn(\mu-H)]_2$ revealed a turnover number of 19,800 based on Si–N bond dehydrocoupling and a turnover frequency of 300 s^{-1}, which is the highest activity ever reported for this transformation.

In Chapter 5, the catalytic activity of $[(^{2,6-iPr_2Ph}BDI)Mn(\mu-H)]_2$ for nitrile dihydroboration was evaluated. In the presence of 0.5 mol% of the catalyst, 14 nitriles were reduced with HBPin at 80 °C to afford *N,N*-diborylamines after 24 h. A mechanism was proposed based on the isolation of $[(^{2,6-iPr_2Ph}BDI)Mn(NCHPh)]_2$ as an intermediate and was further substantiated by DFT. This chapter described the first examples of Mn-catalyzed nitrile dihydroboration.

BIBLIOGRAPHY

Chapter 1

(1) Trovitch, R. J. Comparing Well-Defined Manganese, Iron, Cobalt, and Nickel Ketone Hydrosilylation Catalysts. *Synlett* **2014**, *25* (12), 1638–1642.

(2) Garbe, M.; Junge, K.; Beller, M. Homogeneous Catalysis by Manganese-Based Pincer Complexes. *Eur. J. Org. Chem.* **2017**, *2017* (30), 4344–4362.

(3) Trovitch, R. J. The Emergence of Manganese-Based Carbonyl Hydrosilylation Catalysts. *Acc. Chem. Res.* **2017**, *50* (11), 2842–2852.

(4) Yang, X.; Wang, C. Diverse Fates of β-Silyl Radical under Manganese Catalysis: Hydrosilylation and Dehydrogenative Silylation of Alkenes. *Chem. Asian J.* **2018**, *36* (11), 1047–1051.

(5) Speier, J. L.; Webster, J. A.; Barnes, G. H. The Addition of Silicon Hydrides to Olefinic Double Bonds. Part II. The Use of Group VIII Metal Catalysts. *J. Am. Chem. Soc.* **1957**, *79* (4), 974–979.

(6) Karstedt, B. D. U.S. Patent Application No. 3775452A. November 27, 1973.

(7) Ojima, I.; Nihonyanagi, M.; Nagai, Y. Rhodium Complex Catalysed Hydrosilylation of Carbonyl Compounds. *J. Chem. Soc., Chem. Commun.* **1972**, No. 16, 938a.

(8) Brown, H. C. Hydroboration—a Powerful Synthetic Tool. *Tetrahedron* **1961**, *12* (3), 117–138.

(9) Kono, H.; Ito, K.; Nagai, Y. Oxidative Addition of 4,4,6-Trimethyl-1,3,2-Dioxaborinane and Benzo[1,3,2]Dioxaborole to Tris(Triphenylphosphine)Halogenorhodium. *Chem. Lett.* **1975**, *4* (10), 1095–1096.

(10) Männig, D.; Nöth, H. Catalytic Hydroboration with Rhodium Complexes. *Angew. Chem. Int. Ed.* **1985**, *24* (10), 878–879.

(11) Yates, R. L. Photoactivated Homogeneous Catalytic Hydrosilylation of Carbonyl Compounds. *J. Catal.* **1982**, *78* (1), 111–115.

(12) Hanna, P. K.; Gregg, B. T.; Cutler, A. R. Manganese Carbonyl Compounds as Hydrosilation Catalysts for Organoiron Acyl Complexes. *Organometallics;* **1991**, *10* (1), 31-33.

(13) DiBiase Cavanaugh, M.; Gregg, B. T.; Chiulli, R. J.; Cutler, A. R. The Reactions of Hydrosilanes with the Methoxycarbonyl Complexes Cp(L)(CO)MCO$_2$Me(M = Fe,

Ru; L = CO, PPh$_3$) and (L)(CO)XMCO$_2$Me(M=Co, Mn; L = CO, PPh$_3$; x = 3,4, with and without Catalysis. *J. Organomet. Chem.* **1997**, *547* (1), 173–182.

(14) Mao, Z.; Gregg, B. T.; Cutler, A. R. Manganese- and Rhodium-Catalyzed Phenylsilane Hydrosilation−Deoxygenation of Iron Acyl Complexes Cp(L)(CO)FeC(O)R (L = CO, PPh$_3$, P(OMe)$_3$, P(OPh)$_3$; R = CH$_3$, Ph, CHMe$_2$, CMe$_3$). *Organometallics* **1998**, *17* (10), 1993–2002.

(15) DiBiase Cavanaugh, M.; Gregg, B. T.; Cutler, A. R. Manganese Carbonyl Complexes as Catalysts for the Hydrosilation of Ketones: Comparison with RhCl(PPh$_3$)$_3$. *Organometallics* **1996**, *15* (12), 2764–2769.

(16) Mao, Z.; Gregg, B. T.; Cutler, A. R. Catalytic Hydrosilylation of Organic Esters Using Manganese Carbonyl Acetyl Complexes. *J. Am. Chem. Soc.* **1995**, *117* (40), 10139–10140.

(17) Son, S. U.; Paik, S.-J.; Lee, I. S.; Lee, Y.-A.; Chung, Y. K.; Seok, W. K.; Lee, H. N. Chemistry of [(^1H-Hydronaphthalene)Mn(CO)$_3$]: The Role of Ring-Slippage in Substitution, Catalytic Hydrosilylation, and Molecular Crystal Structure of [(η$_3$-C$_{10}$H$_9$)Mn(CO)$_3$P(OMe)$_3$]. *Organometallics* **1999**, *18* (20), 4114–4118.

(18) Son, S. U.; Paik, S.-J.; Chung, Y. K. Hydrosilylation of Ketones Catalyzed by Tricarbonyl(Naphthalene)Manganese Cation. *J. Mol. Catal. A: Chem.* **2000**, *151* (1), 87–90.

(19) Chidara, V. K.; Du, G. An Efficient Catalyst Based on Manganese Salen for Hydrosilylation of Carbonyl Compounds. *Organometallics* **2013**, *32* (18), 5034–5037.

(20) Zheng, J.; Chevance, S.; Darcel, C.; Sortais, J.-B. Selective Reduction of Carboxylic Acids to Aldehydes through Manganese Catalysed Hydrosilylation. *Chem. Commun.* **2013**, *49* (85), 10010–10012.

(21) Zheng, J.; Elangovan, S.; Valyaev, D. A.; Brousses, R.; César, V.; Sortais, J.-B.; Darcel, C.; Lugan, N.; Lavigne, G. Hydrosilylation of Aldehydes and Ketones Catalyzed by Half-Sandwich Manganese(I) N-Heterocyclic Carbene Complexes. *Adv. Synth. Catal.* **2014**, *356* (5), 1093–1097.

(22) Valyaev, D. A.; Wei, D.; Elangovan, S.; Cavailles, M.; Dorcet, V.; Sortais, J.-B.; Darcel, C.; Lugan, N. Half-Sandwich Manganese Complexes Bearing Cp Tethered N-Heterocyclic Carbene Ligands: Synthesis and Mechanistic Insights into the Catalytic Ketone Hydrosilylation. *Organometallics* **2016**, *35* (24), 4090–4098.

(23) Ojima, I.; Nihonyanagi, M.; Kogure, T.; Kumagai, M.; Horiuchi, S.; Nakatsugawa, K.; Nagai, Y. Reduction of Carbonyl Compounds via Hydrosilylation: I.

Hydrosilylation of Carbonyl Compounds Catalyzed by Tris(Triphenylphosphine)Chlororhodium. *J. Organomet. Chem.* **1975**, *94* (3), 449–461.

(24) Pinto, M.; Friães, S.; Franco, F.; Lloret-Fillol, J.; Royo, B. Manganese N-Heterocyclic Carbene Complexes for Catalytic Reduction of Ketones with Silanes. *ChemCatChem* **2018**, *10* (13), 2711–2711.

(25) Sousa, S. C. A.; Realista, S.; Royo, B. Bench-Stable Manganese NHC Complexes for the Selective Reduction of Esters to Alcohols with Silanes. *Adv. Synth. Catal.* **2020**, *362* (12), 2437–2443.

(26) Behera, R. R.; Ghosh, R.; Panda, S.; Khamari, S.; Bagh, B. Hydrosilylation of Esters Catalyzed by Bisphosphine Manganese(I) Complex: Selective Transformation of Esters to Alcohols. *Org. Lett.* **2020**, *22* (9), 3642–3648.

(27) Mukhopadhyay, T. K.; Flores, M.; Groy, T. L.; Trovitch, R. J. A Highly Active Manganese Precatalyst for the Hydrosilylation of Ketones and Esters. *J. Am. Chem. Soc.* **2014**, *136* (3), 882–885.

(28) Ghosh, C.; Mukhopadhyay, T. K.; Flores, M.; Groy, T. L.; Trovitch, R. J. A Pentacoordinate Mn(II) Precatalyst That Exhibits Notable Aldehyde and Ketone Hydrosilylation Turnover Frequencies. *Inorg. Chem.* **2015**, *54* (21), 10398–10406.

(29) Mukhopadhyay, T. K.; Ghosh, C.; Flores, M.; Groy, T. L.; Trovitch, R. J. Hydrosilylation of Aldehydes and Formates Using a Dimeric Manganese Precatalyst. *Organometallics* **2017**, *36* (18), 3477–3483.

(30) Mukhopadhyay, T. K.; Rock, C. L.; Hong, M.; Ashley, D. C.; Groy, T. L.; Baik, M.-H.; Trovitch, R. J. Mechanistic Investigation of Bis(Imino)Pyridine Manganese Catalyzed Carbonyl and Carboxylate Hydrosilylation. *J. Am. Chem. Soc.* **2017**, *139* (13), 4901–4915.

(31) Ma, X.; Zuo, Z.; Liu, G.; Huang, Z. Manganese-Catalyzed Asymmetric Hydrosilylation of Aryl Ketones. *ACS Omega* **2017**, *2* (8), 4688–4692.

(32) Wenz, J.; Vasilenko, V.; Kochan, A.; Wadepohl, H.; Gade, L. H. Coordination Chemistry of the PdmBOX Pincer Ligand: Reactivity at the Metal and the Ligand. *Eur. J. Inorg. Chem.* **2017**, *2017* (47), 5545–5556.

(33) Martínez-Ferraté, O.; Werlé, C.; Franciò, G.; Leitner, W. Aminotriazole Mn(I) Complexes as Effective Catalysts for Transfer Hydrogenation of Ketones. *ChemCatChem* **2018**, *10* (20), 4514–4518.

(34) Martínez-Ferraté, O.; Chatterjee, B.; Werlé, C.; Leitner, W. Hydrosilylation of Carbonyl and Carboxyl Groups Catalysed by Mn(I) Complexes Bearing Triazole Ligands. *Catal. Sci. Technol.* **2019**, *9* (22), 6370–6378.

(35) Ghaffari, B.; Mendes-Burak, J.; Chan, K. W.; Copéret, C. Silica-Supported MnII Sites as Efficient Catalysts for Carbonyl Hydroboration, Hydrosilylation, and Transesterification. *Chem. Eur. J.* **2019**, *25* (61), 13869–13873.

(36) Zhang, G.; Zeng, H.; Li, S.; Johnson, J.; Mo, Z.; Neary, M. C.; Zheng, S. 1-D Manganese(II)-Terpyridine Coordination Polymers as Precatalysts for Hydrofunctionalisation of Carbonyl Compounds. *Dalton Trans.* **2020**, *49* (8), 2610–2615.

(37) Igarashi, M.; Fuchikami, T. Transition-Metal Complex-Catalyzed Reduction of Amides with Hydrosilanes: A Facile Transformation of Amides to Amines. *Tetrahedron Letters* **2001**, *42* (10), 1945–1947.

(38) Arias-Ugarte, R.; Sharma, H. K.; Morris, A. L. C.; Pannell, K. H. Metal-Catalyzed Reduction of HCONR′$_2$, R′ = Me (DMF), Et (DEF), by Silanes to Produce R′$_2$NMe and Disiloxanes: A Mechanism Unraveled. *J. Am. Chem. Soc.* **2012**, *134* (2), 848–851.

(39) Kelly, C. M.; McDonald, R.; Sydora, O. L.; Stradiotto, M.; Turculet, L. A Manganese Pre-Catalyst: Mild Reduction of Amides, Ketones, Aldehydes, and Esters. *Angew. Chem. Int. Ed.* **2017**, *56* (50), 15901–15904.

(40) Das, H. S.; Das, S.; Dey, K.; Singh, B.; Haridasan, R. K.; Das, A.; Ahmed, J.; Mandal, S. K. Primary Amides to Amines or Nitriles: A Dual Role by a Single Catalyst. *Chem. Commun.* **2019**, *55* (79), 11868–11871.

(41) Bertini, F.; Glatz, M.; Stöger, B.; Peruzzini, M.; Veiros, L. F.; Kirchner, K.; Gonsalvi, L. Carbon Dioxide Reduction to Methanol Catalyzed by Mn(I) PNP Pincer Complexes under Mild Reaction Conditions. *ACS Catal.* **2019**, *9* (1), 632–639.

(42) Pratt, S. L.; Faltynek, R. A. Hydrosilation Catalysis via Silylmanganese Carbonyl Complexes: Thermal vs. Photochemical Activation. *J. Organomet. Chem.* **1983**, *258* (1), C5–C8.

(43) Hilal, H. S.; Abu-Eid, M.; Al-Subu, M.; Khalaf, S. Hydrosilylation Reactions Catalysed by Decacarbonyldimanganese(0). *J. Mol. Catal.* **1987**, *39* (1), 1–11.

(44) Hilal, H. S.; Suleiman, M. A.; Jondi, W. J.; Khalaf, S.; Masoud, M. M. Poly(Siloxane)-Supported Decacarbonyldimanganese(0) Catalyst for Terminal Olefin Hydrosilylation Reactions: The Effect of the Support on the Catalyst Selectivity, Activity and Stability. *J. Mol. Catal. A: Chem.* **1999**, *144* (1), 47–59.

(45) Jondi, W.; Zyoud, A.; Mansour, W.; Hussein, A. Q.; Hilal, H. S. Highly Active and Selective Catalysts for Olefin Hydrosilylation Reactions Using Metalloporphyrins Intercalated in Natural Clays. *React. Chem. Eng.* **2016**, *1* (2), 194–203.

(46) Docherty, J. H.; Peng, J.; Dominey, A. P.; Thomas, S. P. Activation and Discovery of Earth-Abundant Metal Catalysts Using Sodium *Tert*-Butoxide. *Nature Chem.* **2017**, *9* (6), 595–600.

(47) Carney, J. R.; Dillon, B. R.; Campbell, L.; Thomas, S. P. Manganese-Catalyzed Hydrofunctionalization of Alkenes. *Angew. Chem. Int. Ed.* **2018**, *57* (33), 10620–10624.

(48) Price, J. S.; Emslie, D. J. H.; Britten, J. F. Manganese Silylene Hydride Complexes: Synthesis and Reactivity with Ethylene to Afford Silene Hydride Complexes. *Angew. Chem. Int. Ed.* **2017**, *56* (22), 6223–6227.

(49) Mukhopadhyay, T. K.; Flores, M.; Groy, T. L.; Trovitch, R. J. A β-Diketiminate Manganese Catalyst for Alkene Hydrosilylation: Substrate Scope, Silicone Preparation, and Mechanistic Insight. *Chem. Sci.* **2018**, *9* (39), 7673–7680.

(50) Chalk, A. J.; Harrod, J. F. Homogeneous Catalysis. II. The Mechanism of the Hydrosilation of Olefins Catalyzed by Group VIII Metal Complexes. *J. Am. Chem. Soc.* **1965**, *87* (1), 16–21.

(51) Yang, X.; Wang, C. Dichotomy of Manganese Catalysis via Organometallic or Radical Mechanism: Stereodivergent Hydrosilylation of Alkynes. *Angew. Chem.* **2018**, *130* (4), 935–940.

(52) Zhang, G.; Zeng, H.; Wu, J.; Yin, Z.; Zheng, S.; Fettinger, J. C. Highly Selective Hydroboration of Alkenes, Ketones and Aldehydes Catalyzed by a Well-Defined Manganese Complex. *Angew. Chem. Int. Ed.* **2016**, *55* (46), 14369–14372.

(53) Vasilenko, V.; Blasius, C. K.; Wadepohl, H.; Gade, L. H. Mechanism-Based Enantiodivergence in Manganese Reduction Catalysis: A Chiral Pincer Complex for the Highly Enantioselective Hydroboration of Ketones. *Angew. Chem. Int. Ed.* **2017**, *56* (29), 8393–8397.

(54) Vasilenko, V.; Blasius, C. K.; Gade, L. H. One-Pot Sequential Kinetic Profiling of a Highly Reactive Manganese Catalyst for Ketone Hydroboration: Leveraging σ-Bond Metathesis via Alkoxide Exchange Steps. *J. Am. Chem. Soc.* **2018**, *140* (29), 9244–9254.

(55) Erken, C.; Kaithal, A.; Sen, S.; Weyhermüller, T.; Hölscher, M.; Werlé, C.; Leitner, W. Manganese-Catalyzed Hydroboration of Carbon Dioxide and Other Challenging Carbonyl Groups. *Nat. Commun.* **2018**, *9* (1), 1–9.

(56) Schäffner, B.; Schäffner, F.; Verevkin, S. P.; Börner, A. Organic Carbonates as Solvents in Synthesis and Catalysis. *Chem. Rev.* **2010**, *110* (8), 4554–4581.

(57) Barman, M. K.; Das, K.; Maji, B. Selective Hydroboration of Carboxylic Acids with a Homogeneous Manganese Catalyst. *J. Org. Chem.* **2019**, *84* (3), 1570–1579.

(58) Macaulay, C. M.; Gustafson, S. J.; Fuller, J. T.; Kwon, D.-H.; Ogawa, T.; Ferguson, M. J.; McDonald, R.; Lumsden, M. D.; Bischof, S. M.; Sydora, O. L.; Ess, D. H.; Stradiotto, M.; Turculet, L. Alkene Isomerization–Hydroboration Catalyzed by First-Row Transition-Metal (Mn, Fe, Co, and Ni) N-Phosphinoamidinate Complexes: Origin of Reactivity and Selectivity. *ACS Catal.* **2018**, *8* (11), 9907–9925.

(59) Brzozowska, A.; Zubar, V.; Ganardi, R.-C.; Rueping, M. Chemoselective Hydroboration of Propargylic Alcohols and Amines Using a Manganese(II) Catalyst. *Org. Lett.* **2020**, *22* (10), 3765–3769.

Chapter 2

(1) Power, P. P. Stable Two-Coordinate, Open-Shell (d^1–d^9) Transition Metal Complexes. *Chem. Rev.* **2012**, *112* (6), 3482–3507.

(2) Power, P. P. Some Highlights from the Development and Use of Bulky Monodentate Ligands. *J. Org. Chem.* **2004**, *689* (24), 3904–3919.

(3) Holland, P. L. Electronic Structure and Reactivity of Three-Coordinate Iron Complexes. *Acc. Chem. Res.* **2008**, *41* (8), 905–914.

(4) Chen, C.; Bellows, S. M.; Holland, P. L. Tuning Steric and Electronic Effects in Transition-Metal β-Diketiminate Complexes. *Dalton Trans.* **2015**, *44* (38), 16654–16670.

(5) Webster, R. L. β-Diketiminate Complexes of the First Row Transition Metals: Applications in Catalysis. *Dalton Trans.* **2017**, *46* (14), 4483–4498.

(6) Basuli, F.; Aneetha, H.; Huffman, J. C.; Mindiola, D. J. A Fluorobenzene Adduct of Ti(IV), and Catalytic Carboamination to Prepare α,β-Unsaturated Imines and Triaryl-Substituted Quinolines. *J. Am. Chem. Soc.* **2005**, *127* (51), 17992–17993.

(7) Vela, J.; Smith, J. M.; Yu, Y.; Ketterer, N. A.; Flaschenriem, C. J.; Lachicotte, R. J.; Holland, P. L. Synthesis and Reactivity of Low-Coordinate Iron(II) Fluoride Complexes and Their Use in the Catalytic Hydrodefluorination of Fluorocarbons. *J. Am. Chem. Soc.* **2005**, *127* (21), 7857–7870.

(8) Mukhopadhyay, T. K.; Flores, M.; Groy, T. L.; Trovitch, R. J. A β-Diketiminate Manganese Catalyst for Alkene Hydrosilylation: Substrate Scope, Silicone Preparation, and Mechanistic Insight. *Chem. Sci.* **2018**, *9* (39), 7673–7680.

(9) Chai, J.; Zhu, H.; Fan, H.; Roesky, H. W.; Magull, J. Structurally Characterized Neutral Monoalkyl and -aryl Complexes of Manganese(II). *Organometallics*, 2004, **23**, 1177.

(10) Chai, J.; Zhu, H.; Stückl, A. C.; Roesky, H. W.; Magull, J.; Bencini, A.; Caneschi, A.; Gatteschi, D. Synthesis and Reaction of [{HC(CMeNAr)$_2$}Mn]$_2$ (Ar = 2,6-iPr$_2$C$_6$H$_3$): The Complex Containing Three-Coordinate Manganese(I) with a Mn−Mn Bond Exhibiting Unusual Magnetic Properties and Electronic Structure *J. Am. Chem. Soc.*, **2005**, *127*, 9201.

(11) Yao, S.; Xiong, Y.; Driess, M. Facile Metalation of Silicon and Germanium Analogues of Thiocarboxylic Acids with a Manganese (II) Hydride Precursor. *Chem. Eur. J.*, **2012**, *18*, 11356.

(12) Nguyen, T. T.; Kim, J.-H.; Kim, S.; Oh, C.; Flores, M.; Groy, T. L.; Baik, M.-H.; Trovitch, R. J. Scope and Mechanism of Nitrile Dihydroboration Mediated by a β-Diketiminate Manganese Hydride Catalyst. *Chem. Commun.* **2020**, *56*, 3959.

(13) Trovitch, R. J.; Nguyen, T. T.; Mukhopadhyay, T. K.; Glazier, B. M. Beta-Diketiminate Manganese Catalysts for Hydrosilylation, Hydroboration, and Dehydrogenative Pnictogen-Silicon and Pnictogen-Boron Bond Formation. U.S. Patent 11,273,432, **2022**.

(14) Bianchi, R.; Gervasio, G.; Marabello, D. Experimental Electron Density Analysis of Mn$_2$(CO)$_{10}$: Metal−Metal and Metal−Ligand Bond Characterization. *Inorg. Chem.* **2000**, *39*, 11, 2360–2366.

(15) Bernal, I.; Korp, J. D.; Herrmann, W. A.; Serrano, R. Syntheses of Metal Carbonyls, XVI1). Metal-Metal Multiple Bonds: Synthesis, Crystal and Molecular Structure of Tri-μ-Carbonyl-Bis[(H$_5$-Pentamethylcyclopentadienyl)Manganese](Mn≡Mn) − The First Manganese-Manganese Triple Bond. *Chem. Ber.* **1984**, *117* (2), 434–444.

(16) Ashley, A. E.; Cooper, R. T.; Wildgoose, G. G.; Green, J. C.; O'Hare, D. Homoleptic Permethylpentalene Complexes: "Double Metallocenes" of the First-Row Transition Metals. *J. Am. Chem. Soc.* **2008**, *130* (46), 15662–15677.

(17) Chai, J.; Zhu, H.; Most, K.; Roesky, H. W.; Vidovic, D.; Schmidt, H.-G.; Noltemeyer, M. Synthesis and Reaction of Mn^{II} Iodides Bearing the β-Diketiminate Ligand: The First Divalent Manganese N-Heterocyclic Carbene Complexes [{HC(CMeNAr)$_2$}Mn^I{C[N(^{i}Pr)CMe]$_2$}] and [{HC(CMeNAr)$_2$}MnNHAr{C[N(^{i}Pr)CMe]$_2$}] (Ar = $^{2,6-i\text{Pr}_2}$C$_6$H$_3$). *Eur. J. Inorg. Chem.* **2003**, *2003* (24), 4332–4337.

217

(18) Hicks, J.; Hoyer, C. E.; Moubaraki, B.; Li Manni, G.; Carter, E.; Murphy, D. M.; Murray, K. S.; Gagliardi, L.; Jones, C. A Two-Coordinate Manganese(0) Complex with an Unsupported Mn–Mg Bond: Allowing Access to Low Coordinate Homo- and Heterobimetallic Compounds. *J. Am. Chem. Soc.* **2014**, *136* (14), 5283–5286.

(19) Azuah, R. T.; Kneller, L. R.; Qiu, Y.; Tregenna-Piggott, P. L. W.; Brown, C. M.; Copley, J. R. D.; Dimeo, R. M. DAVE: A Comprehensive Software Suite for the Reduction, Visualization, and Analysis of Low Energy Neutron Spectroscopic Data. *J. Res. Natl. Inst. Stand. Technol.* **2009**, *114* (6), 341–358.

(20) Bossek, U.; Nühlen, D.; Bill, E.; Glaser, T.; Krebs, C.; Weyhermüller, T.; Wieghardt, K.; Lengen, M.; Trautwein, A. X. Exchange Coupling in an Isostructural Series of Face-Sharing Bioctahedral Complexes [LM^{II}(μ-X)$_3$M^{II}L]BPh$_4$ (M = Mn, Fe, Co, Ni, Zn; X = Cl, Br; L = 1,4,7-Trimethyl-1,4,7-Triazacyclononane). *Inorg. Chem.* **1997**, *36* (13), 2834–2843.

Chapter 3

(1) Philipp, H. R. Optical Properties of Silicon Nitride. *J. Electrochem. Soc.* **1973**, *120* (2), 295.

(2) De Brito Mota, F.; Justo, J. F.; Fazzio, A. Structural Properties of Amorphous Silicon Nitride. *Phys. Rev. B* **1998**, *58* (13), 8323–8328.

(3) Kaloyeros, A. E.; Pan, Y.; Goff, J.; Arkles, B. Review—Silicon Nitride and Silicon Nitride-Rich Thin Film Technologies: State-of-the-Art Processing Technologies, Properties, and Applications. *ECS J. Solid-State Sci. Technol.* **2020**, *9* (6), 063006.

(4) Khomenkova, L.; Normand, P.; Gourbilleau, F.; Slaoui, A.; Bonafos, C. Optical, Structural and Electrical Characterizations of Stacked Hf-Based and Silicon Nitride Dielectrics. *Thin Solid Films* **2016**, *617*, 143–149.

(5) Kaga, Y.; Imamura, H.; Watanabe, J. Silicon Nitride Substrate Manufacturing Method, Silicon Nitride Substrate, Silicon Nitride Circuit Substrate, and Semiconductor Module. U.S. Patent No. 7,915,533 (2011).

(6) Kuo, Y. Plasma Enhanced Chemical Vapor Deposited Silicon Nitride as a Gate Dielectric Film for Amorphous Silicon Thin Film Transistors—a Critical Review. *Vacuum* **1998**, *51* (4), 741–745.

(7) El amrani, A.; Menous, I.; Mahiou, L.; Tadjine, R.; Touati, A.; Lefgoum, A. Silicon Nitride Film for Solar Cells. *Renewable Energy* **2008**, *33* (10), 2289–2293.

(8) van Assche, F. J. H.; Unnikrishnan, S.; Michels, J. J.; van Mol, A. M. B.; van de Weijer, P.; van de Sanden, M. C. M.; Creatore, M. On the Intrinsic Moisture

Permeation Rate of Remote Microwave Plasma-Deposited Silicon Nitride Layers. *Thin Solid Films* **2014**, *558*, 54–61.

(9)   Roenigk, K. F.; Jensen, K. F. Low Pressure CVD of Silicon Nitride. *J. Electrochem. Soc.* **1987**, *134* (7), 1777.

(10)   Niskanen, A. J.; Chen, S.; Pore, V.; Fukazawa, A.; Fukuda, H.; Haukka, S. P. Si Precursors for Deposition of SiN at Low Temperatures. U.S. Patent No. 9,564,309 (2017).

(11)   Yusup, L. L.; Park, J.-M.; Noh, Y.-H.; Kim, S.-J.; Lee, W.-J.; Park, S.; Kwon, Y.-K. Reactivity of Different Surface Sites with Silicon Chlorides during Atomic Layer Deposition of Silicon Nitride. *RSC Adv.* **2016**, *6* (72), 68515–68524.

(12)   Laxman, R. K.; Roberts, D. A.; Hochberg, A. K.; Hockenhull, H. G.; Kaminsky, F. D. Silicon Nitride from Bis(Tertiarybutylamino)Silane. U.S. Patent No. 5,874,368 (1999).

(13)   Kim, K.-H. Fabrication and Properties of Silicon-Nitride Films Deposited by Using PECVD with a Tris(Dimethylamino)Silane of Aminosilane Precursor. *J. Korean Phys. Soc.* **2015**, *67* (12), 2115–2119.

(14)   Aylett, B. J.; Emsley, J. The Preparation and Properties of Dimethylamino- and Diethylaminosilane. *J. Chem. Soc. A* **1967**, No. 0, 652–655.

(15)   Anderson, G. D.; Rankin, D. W. H. Isopropyldisilylamine and Disilyl-*t*-Butylamine: Preparation, Spectroscopic Properties, and Molecular Structure in the Gas Phase, Determined by Electron Diffraction. *Dalton Trans.* **1989**, *0* (5), 779–783.

(16)   Schwab, S. T.; Graef, R. C.; Blanchard, C. R.; Dec, S. F.; Maciel, G. G. The Pyrolytic Conversion of Perhydropolysilazane into Silicon Nitride. *Ceram. Int.* **1998**, *24* (6), 411–414.

(17)   Wang, K.; Zheng, X.; Ohuchi, F. S.; Bordia, R. K. The Conversion of Perhydropolysilazane into SiON Films Characterized by X-Ray Photoelectron Spectroscopy. *J. Am. Ceram. Soc.* **2012**, *95* (12), 3722–3725.

(18)   Zhang, Z.; Shao, Z.; Luo, Y.; An, P.; Zhang, M.; Xu, C. Hydrophobic, Transparent and Hard Silicon Oxynitride Coating from Perhydropolysilazane. *Polym. Int.* **2015**, *64* (8), 971–978.

(19)   Kang, Y. H.; Min, B. K.; Kim, S. K.; Bae, G.; Song, W.; Lee, C.; Cho, S. Y.; An, K.-S. Proton Conducting Perhydropolysilazane-Derived Gate Dielectric for Solution-Processed Metal Oxide-Based Thin-Film Transistors. *ACS Appl. Mater. Interfaces* **2020**, *12* (13), 15396–15405.

(20) Seyferth, D.; Wiseman, G. H.; Prud'homme, C. A Liquid Silazane Precursor to Silicon Nitride. *J. Am. Ceram. Soc.* **1983**, *66* (1), C-13-C–14.

(21) Schwab, S. T. Polysilazane Precursors for Silicon Nitride and Resultant Products. U.S. Patent No. 5,294,425 (1994).

(22) Liu, H. Q.; Harrod, J. F. Dehydrocoupling of Ammonia and Silanes Catalyzed by Dimethyltitanocene. *Organometallics* **1992**, *11* (2), 822–827.

(23) Reuter, M. B.; Hageman, K.; Waterman, R. Silicon–Nitrogen Bond Formation via Heterodehydrocoupling and Catalytic N-Silylation. *Chem. Eur. J.* **2021**, *27* (10), 3251–3261.

(24) Dunne, J. F.; Neal, S. R.; Engelkemier, J.; Ellern, A.; Sadow, A. D. Tris(Oxazolinyl)Boratomagnesium-Catalyzed Cross-Dehydrocoupling of Organosilanes with Amines, Hydrazine, and Ammonia. *J. Am. Chem. Soc.* **2011**, *133* (42), 16782–16785.

(25) Hill, M. S.; Liptrot, D. J.; MacDougall, D. J.; Mahon, M. F.; Robinson, T. P. Hetero-Dehydrocoupling of Silanes and Amines by Heavier Alkaline Earth Catalysis. *Chem. Sci.* **2013**, *4* (11), 4212–4222.

(26) Bellini, C.; Dorcet, V.; Carpentier, J.-F.; Tobisch, S.; Sarazin, Y. Alkaline-Earth-Catalysed Cross-Dehydrocoupling of Amines and Hydrosilanes: Reactivity Trends, Scope and Mechanism. *Chem. Eur. J.* **2016**, *22* (13), 4564–4583.

(27) Li, N.; Guan, B.-T. A Dialkyl Calcium Carbene Adduct: Synthesis, Structure, and Catalytic Cross-Dehydrocoupling of Silanes with Amines. *Eur. J. Inorg. Chem.* **2019**, *2019* (16), 2231–2235.

(28) Pindwal, A.; Ellern, A.; Sadow, A. D. Homoleptic Divalent Dialkyl Lanthanide-Catalyzed Cross-Dehydrocoupling of Silanes and Amines. *Organometallics* **2016**, *35* (11), 1674–1683.

(29) Yonekura, K.; Iketani, Y.; Sekine, M.; Tani, T.; Matsui, F.; Kamakura, D.; Tsuchimoto, T. Zinc-Catalyzed Dehydrogenative Silylation of Indoles. *Organometallics* **2017**, *36* (17), 3234–3249.

(30) Ríos, P.; Roselló-Merino, M.; Rivada-Wheelaghan, O.; Borge, J.; López-Serrano, J.; Conejero, S. Selective Catalytic Synthesis of Amino-Silanes at Part-per Million Catalyst Loadings. *Chem. Commun.* **2018**, *54* (6), 619–622.

(31) Allen, L. K.; García-Rodríguez, R.; Wright, D. S. Stoichiometric and Catalytic Si–N Bond Formation Using the p-Block Base Al(NMe$_2$)$_3$. *Dalton Trans.* **2015**, *44* (27), 12112–12118.

(32) Bellini, C.; Orione, C.; Carpentier, J.-F.; Sarazin, Y. Tailored Cyclic and Linear Polycarbosilazanes by Barium-Catalyzed N−H/H−Si Dehydrocoupling Reactions. *Angew. Chem. Int. Ed.* **2016**, *55* (11), 3744–3748.

(33) Bellini, C.; Roisnel, T.; Carpentier, J.-F.; Tobisch, S.; Sarazin, Y. Sequential Barium-Catalysed N−H/H−Si Dehydrogenative Cross-Couplings: Cyclodisilazanes versus Linear Oligosilazanes. *Chem. Eur. J.* **2016**, *22* (44), 15733–15743.

(34) Morris, L. J.; Whittell, G. R.; Eloi, J.-C.; Mahon, M. F.; Marken, F.; Manners, I.; Hill, M. S. Ferrocene-Containing Polycarbosilazanes via the Alkaline-Earth-Catalyzed Dehydrocoupling of Silanes and Amines. *Organometallics* **2019**, *38* (19), 3629–3648.

(35) Gasperini, D.; King, A. K.; Coles, N. T.; Mahon, M. F.; Webster, R. L. Seeking Heteroatom-Rich Compounds: Synthetic and Mechanistic Studies into Iron Catalyzed Dehydrocoupling of Silanes. *ACS Catal.* **2020**, *10* (11), 6102–6112.

(36) Barroso, G.; Döring, M.; Horcher, A.; Kienzle, A.; Motz, G. Polysilazane-Based Coatings with Anti-Adherent Properties for Easy Release of Plastics and Composites from Metal Molds. *Adv. Mater. Interfaces* **2020**, *7* (10), 1901952.

(37) Mukhopadhyay, T. K.; Flores, M.; Groy, T. L.; Trovitch, R. J. A β-Diketiminate Manganese Catalyst for Alkene Hydrosilylation: Substrate Scope, Silicone Preparation, and Mechanistic Insight. *Chem. Sci.* **2018**, *9* (39), 7673–7680.

(38) Oh, C.; Siewe, J.; Nguyen, T. T.; Kawamura, A.; Flores, M.; Groy, T. L.; Anderson, J. S.; Trovitch, R. J.; Baik, M.-H. The Electronic Structure of a β-Diketiminate Manganese Hydride Dimer. *Dalton Trans.* **2020**, *49* (41), 14463–14474.

(39) Sanchez, A.; Itov, G.; Zhang, P.; Stephens, M. D.; Khandelwal, M. Halogen Free Syntheses of Aminosilanes by Catalytic Dehydrogenative Coupling. U.S. Patent Application No. 2018/0230171 (2018).

(40) Levy, R. A.; Lin, X.; Grow, J. M.; Boeglin, H. J.; Shalvoy, R. Low Pressure Chemical Vapor Deposition of Silicon Nitride Using the Environmentally Friendly Tris(Dimethylamino)Silane Precursor. *J. Mater. Res.* **1996**, *11* (6), 1483–1488.

(41) Gumpher, J.; Bather, W.; Mehta, N.; Wedel, D. Characterization of Low-Temperature Silicon Nitride LPCVD from Bis(Tertiary-Butylamino)Silane and Ammonia. *J. Electrochem. Soc.* **2004**, *151* (5), G353.

(42) Smith, A. L. Infrared Spectra-Structure Correlations for Organosilicon Compounds. *Spectrochimica Acta* **1960**, *16* (1), 87–105.

(43) Abel, A. E.; Kruger, T. A.; Mouk, R. W.; Knasiak, G. J. Silazane and/or Polysilazane Compounds and Methods of Making. U.S. Patent No. 6,329,487 (2001).

(44) Iwamoto, Y.; Kikuta, K.; Hirano, S. Si_3N_4–TiN–Y_2O_3 Ceramics Derived from Chemically Modified Perhydropolysilazane. *J. Mater. Res.* **1999**, *14* (11), 4294–4301.

(45) Bauer, F.; Decker, U.; Dierdorf, A.; Ernst, H.; Heller, R.; Liebe, H.; Mehnert, R. Preparation of Moisture Curable Polysilazane Coatings: Part I. Elucidation of Low Temperature Curing Kinetics by FT-IR Spectroscopy. *Prog. Org. Coat.* **2005**, *53* (3), 183–190.

(46) Witanowski, M.; Stefaniak, I.; Webb, G. A. Nitrogen NMR Spectroscopy. In *Annual Reports on NMR Spectroscopy*; Webb, G. A., Ed.; Academic Press, 1978; Vol. 7, pp 117–244.

(47) Lewis, R. H.; Maciel, G. E. Magnetic Resonance Characterization of Solid-State Intermediates in the Generation of Ceramics by Pyrolysis of Hydridopolysilazane. *J. Mater. Sci.* **1995**, *30* (19), 5020–5030.

(48) Nguyen, T. T.; Kim, J.-H.; Kim, S.; Oh, C.; Flores, M.; Groy, T. L.; Baik, M.-H.; Trovitch, R. J. Scope and Mechanism of Nitrile Dihydroboration Mediated by a β-Diketiminate Manganese Hydride Catalyst. *Chem. Commun.* **2020**, *56*, 3959.

Chapter 4

(1) Khomenkova, L.; Normand, P.; Gourbilleau, F.; Slaoui, A.; Bonafos, C. Optical, Structural and Electrical Characterizations of Stacked Hf-Based and Silicon Nitride Dielectrics. *Thin Solid Films* **2016**, *617*, 143–149.

(2) Kuo, Y. Plasma Enhanced Chemical Vapor Deposited Silicon Nitride as a Gate Dielectric Film for Amorphous Silicon Thin Film Transistors—a Critical Review. *Vacuum* **1998**, *51* (4), 741–745.

(3) El amrani, A.; Menous, I.; Mahiou, L.; Tadjine, R.; Touati, A.; Lefgoum, A. Silicon Nitride Film for Solar Cells. *Renewable Energy* **2008**, *33* (10), 2289–2293.

(4) Colombo, P.; Mera, G.; Riedel, R.; Sorarù, G. D. Polymer-Derived Ceramics: 40 Years of Research and Innovation in Advanced Ceramics. In *Ceramics Science and Technology*; John Wiley & Sons, Ltd, 2013; pp 245–320.

(5) Slavov, S. V.; Sanger, A. R.; Chuang, K. T. Mechanism of Silation of Alumina with Hexamethyldisilazane. *J. Phys. Chem. B.* **1998**, *102* (28), 5475–5482.

(6)   Coan, T.; Barroso, G. S.; Machado, R. A. F.; de Souza, F. S.; Spinelli, A.; Motz, G. A Novel Organic-Inorganic PMMA/Polysilazane Hybrid Polymer for Corrosion Protection. *Prog. Org. Coat.* **2015**, *89*, 220–230.

(7)   Kozuka, H.; Fujita, M.; Tamoto, S. Polysilazane as the Source of Silica: The Formation of Dense Silica Coatings at Room Temperature and the New Route to Organic–Inorganic Hybrids. *J. Sol-Gel Sci. Technol.* **2008**, *48* (1), 148–155.

(8)   Sønderbæk-Jørgensen, R.; Meier, S.; Dam-Johansen, K.; Skov, A. L.; Daugaard, A. E. Reactivity of Polysilazanes Allows Catalyst-Free Curing of Silicones. *Macromol. Mater. Eng.* **2022**, *307*, 2200157

(9)   Marceaux, S.; Bressy, C.; Perrin, F.-X.; Martin, C.; Margaillan, A. Development of Polyorganosilazane–Silicone Marine Coatings. *Prog. Org. Coat.* **2014**, *77* (11), 1919–1928.

(10)   Nguyen, T. D. H.; Perrin, F.-X.; Nguyen, D. L. New Hybrid Materials Based on Poly(Ethyleneoxide)-Grafted Polysilazane by Hydrosilylation and Their Anti-Fouling Activities. *J. Nanotechnol.* **2013**, *4* (1), 671–677.

(11)   Krannich, H.; Mehnert, R.; Reiser, J.; Weseloh, S. Hydrophobic and Scratch-Resistant Paints for Metal Surfaces and Brake Dust-Repelling Wheel Coatings, WO2008135262, November 13, 2008.

(12)   Suzuki, K.; Okamura, T.; Okayasu, T.; Stein, T. vom. Polycarbosilazane, and Composition Comprising the Same, and Method for Producing Silicon-Containing Film Using the Same. Patent No. WO2022084022A1 (2022).

(13)   Quenard, S.; Laucournet, R.; Roumanie, M.; Flassayer, C.; Moreac-Njeim, G.; Abramczuk, M. Revêtement d'isolation thermique à base d'un Polymere PREcéramique pour améliorer les performances des moteurs thermiques. Patent No. FR3116823A1 (2022).

(14)   Bellini, C.; Roisnel, T.; Carpentier, J.-F.; Tobisch, S.; Sarazin, Y. Sequential Barium-Catalysed N−H/H−Si Dehydrogenative Cross-Couplings: Cyclodisilazanes versus Linear Oligosilazanes. *Chem. Eur. J.* **2016**, *22* (44), 15733–15743.

(15)   Bellini, C.; Orione, C.; Carpentier, J.-F.; Sarazin, Y. Tailored Cyclic and Linear Polycarbosilazanes by Barium-Catalyzed N-H/H-Si Dehydrocoupling Reactions. *Angew. Chem. Int. Ed.* **2016**, *55* (11), 3744–3748.

(16)   Morris, L. J.; Whittell, G. R.; Eloi, J.-C.; Mahon, M. F.; Marken, F.; Manners, I.; Hill, M. S. Ferrocene-Containing Polycarbosilazanes via the Alkaline-Earth-Catalyzed Dehydrocoupling of Silanes and Amines. *Organometallics* **2019**, *38* (19), 3629–3648.

(17) Gasperini, D.; King, A. K.; Coles, N. T.; Mahon, M. F.; Webster, R. L. Seeking Heteroatom-Rich Compounds: Synthetic and Mechanistic Studies into Iron Catalyzed Dehydrocoupling of Silanes. *ACS Catal.* **2020**, *10* (11), 6102–6112.

(18) Nguyen, T. T.; Mukhopadhyay, T. K.; MacMillan, S. N.; Janicke, M. T.; Trovitch, R. J. Synthesis of Aminosilane Chemical Vapor Deposition Precursors and Polycarbosilazanes through Manganese-Catalyzed Si–N Dehydrocoupling. *ACS Sustainable Chem. Eng.* **2022**, *10* (13), 4218–4226.

(19) Smith, A. L. Infrared Spectra-Structure Correlations for Organosilicon Compounds. *Spectrochimica Acta* **1960**, *16* (1), 87–105.

(20) Farcaș-Johnson, M. A.; Kyne, S. H.; Webster, R. L. Dehydrocoupling Polymerization: Poly(Silylether) Synthesis by Using an Iron β-Diketiminate Catalyst. *Chem. Eur. J.* **2022**, e202201.

(21) Ríos, P.; Roselló-Merino, M.; Rivada-Wheelaghan, O.; Borge, J.; López-Serrano, J.; Conejero, S. Selective Catalytic Synthesis of Amino-Silanes at Part-per Million Catalyst Loadings. *Chem. Commun.* **2018**, *54* (6), 619–622.

Chapter 5

(1) Suginome, M.; Uehlin, L.; Murakami, M. Aminoboranes as "Compatible" Iminium Ion Generators in Aminative C−C Bond Formations. *J. Am. Chem. Soc.* **2004**, *126* (41), 13196–13197.

(2) Khalimon, A. Y.; Farha, P. M.; Nikonov, G. I. Imido–Hydrido Complexes of Mo(IV): Catalysis and Mechanistic Aspects of Hydroboration Reactions. *Dalton Trans.* **2015**, *44* (43), 18945–18956.

(3) Kitano, T.; Komuro, T.; Tobita, H. Double and Single Hydroboration of Nitriles Catalyzed by a Ruthenium–Bis(Silyl)Xanthene Complex: Application to One-Pot Synthesis of Diarylamines and N-Arylimines. *Organometallics* **2019**, *38* (7), 1417–1420.

(4) Junor, G. P.; Romero, E. A.; Chen, X.; Jazzar, R.; Bertrand, G. Readily Available Primary Aminoboranes as Powerful Reagents for Aldimine Synthesis. *Angew. Chem. Int. Ed.* **2019**, *58* (9), 2875–2878.

(5) Ghosh, C.; Kim, S.; Mena, M. R.; Kim, J.-H.; Pal, R.; Rock, C. L.; Groy, T. L.; Baik, M.-H.; Trovitch, R. J. Efficient Cobalt Catalyst for Ambient-Temperature Nitrile Dihydroboration, the Elucidation of a Chelate-Assisted Borylation Mechanism, and a New Synthetic Route to Amides. *J. Am. Chem. Soc.* **2019**, *141* (38), 15327–15337.

(6)   Khalimon, A. Y.; Farha, P.; Kuzmina, L. G.; Nikonov, G. I. Catalytic Hydroboration by an Imido-Hydrido Complex of Mo(IV). *Chem. Commun.* **2011**, *48* (3), 455–457.

(7)   Geri, J. B.; Szymczak, N. K. A Proton-Switchable Bifunctional Ruthenium Complex That Catalyzes Nitrile Hydroboration. *J. Am. Chem. Soc.* **2015**, *137* (40), 12808–12814.

(8)   Kaithal, A.; Chatterjee, B.; Gunanathan, C. Ruthenium-Catalyzed Selective Hydroboration of Nitriles and Imines. *J. Org. Chem.* **2016**, *81* (22), 11153–11161.

(9)   Weetman, C.; Anker, M. D.; Arrowsmith, M.; Hill, M. S.; Kociok-Köhn, G.; Liptrot, D. J.; Mahon, M. F. Magnesium-Catalysed Nitrile Hydroboration. *Chem. Sci.* **2015**, *7* (1), 628–641.

(10)   Li, J.; Luo, M.; Sheng, X.; Hua, H.; Yao, W.; Pullarkat, S. A.; Xu, L.; Ma, M. Unsymmetrical β-Diketiminate Magnesium(I) Complexes: Syntheses and Application in Catalytic Hydroboration of Alkyne, Nitrile and Carbonyl Compounds. *Org. Chem. Front.* **2018**, *5* (24), 3538–3547.

(11)   Nakamura, G.; Nakajima, Y.; Matsumoto, K.; Srinivas, V.; Shimada, S. Nitrile Hydroboration Reactions Catalysed by Simple Nickel Salts, Bis(Acetylacetonato)Nickel(II) and Its Derivatives. *Catal. Sci. Technol.* **2017**, *7* (15), 3196–3199.

(12)   Ito, M.; Itazaki, M.; Nakazawa, H. Selective Double Hydroboration and Dihydroborylsilylation of Organonitriles by an Iron–Indium Cooperative Catalytic System. *Inorg. Chem.* **2017**, *56* (22), 13709–13714. .

(13)   Ibrahim, A. D.; Entsminger, S. W.; Fout, A. R. Insights into a Chemoselective Cobalt Catalyst for the Hydroboration of Alkenes and Nitriles. *ACS Catal.* **2017**, *7* (5), 3730–3734.

(14)   Huang, Z.; Wang, S.; Zhu, X.; Yuan, Q.; Wei, Y.; Zhou, S.; Mu, X. Well-Defined Amidate-Functionalized N-Heterocyclic Carbene -Supported Rare-Earth Metal Complexes as Catalysts for Efficient Hydroboration of Unactivated Imines and Nitriles. *Inorg. Chem.* **2018**, *57* (24), 15069–15078.

(15)   Harinath, A.; Bhattacharjee, J.; Panda, T. K. Catalytic Hydroboration of Organic Nitriles Promoted by Aluminum Complex. *Adv. Synth. Catal.* **2019**, *361* (4), 850–857.

(16)   Liu, W.; Ding, Y.; Jin, D.; Shen, Q.; Yan, B.; Ma, X.; Yang, Z. Organic Aluminum Hydrides Catalyze Nitrile Hydroboration. *Green Chem.* **2019**, *21* (14), 3812–3815.

(17) Ding, Y.; Ma, X.; Liu, Y.; Liu, W.; Yang, Z.; Roesky, H. W. Alkylaluminum Complexes as Precatalysts in Hydroboration of Nitriles and Carbodiimides. *Organometallics* **2019**, *38* (15), 3092–3097.

(18) Saha, S.; Eisen, M. S. Catalytic Recycling of a Th–H Bond via Single or Double Hydroboration of Inactivated Imines or Nitriles. *ACS Catal.* **2019**, *9* (7), 5947–5956.

(19) Banerjee, I.; Anga, S.; Bano, K.; Panda, T. K. Efficient and Chemoselective Hydroboration of Organic Nitriles Promoted by Ti(IV) Catalyst Supported by Unsymmetrical Acenaphthenequinonediimine Ligand. *J. Organomet. Chem.* **2019**, *902*, 120958.

(20) Das, S.; Bhattacharjee, J.; Panda, T. K. An Imidazolin-2-Iminato Ligand Organozinc Complex as a Catalyst for Hydroboration of Organic Nitriles. *New J. Chem.* **2019**, *43* (43), 16812–16818.

(21) Feng, X.; Ji, P.; Li, Z.; Drake, T.; Oliveres, P.; Chen, E. Y.; Song, Y.; Wang, C.; Lin, W. Aluminum Hydroxide Secondary Building Units in a Metal–Organic Framework Support Earth-Abundant Metal Catalysts for Broad-Scope Organic Transformations. *ACS Catal.* **2019**, *9* (4), 3327–3337.

(22) Ben-Daat, H.; Rock, C. L.; Flores, M.; Groy, T. L.; Bowman, A. C.; Trovitch, R. J. Hydroboration of Alkynes and Nitriles Using an α-Diimine Cobalt Hydride Catalyst. *Chem. Commun.* **2017**, *53* (53), 7333–7336.

(23) Trovitch, R. J. Comparing well-defined manganese, iron, cobalt, and nickel ketone hydrosilylation catalysts. *Synlett*, **2014**, *25*, 1638–1642.

(24) Garbe, M.; Junge, K.; Beller, M. Homogeneous catalysis by manganese-based pincer complexes. *Eur. J. Org. Chem.* **2017**, *2017*, 4344–4362.

(25) Trovitch, R. J. The emergence of manganese-based carbonyl hydrosilylation catalysts. *Acc. Chem. Res.* **2017**, *50*, 2842–2852.

(26) Yang, X.; Wang, C. Manganese-Catalyzed Hydrosilylation Reactions. *Chem. Asian J.* **2018**, *13*, 2307–2315.

(27) Mukhopadhyay, T. K.; Flores, M.; Groy, T. L.; Trovitch, R. J. A β-Diketiminate Manganese Catalyst for Alkene Hydrosilylation: Substrate Scope, Silicone Preparation, and Mechanistic Insight. *Chem. Sci.* **2018**, *9* (39), 7673–7680.

(28) Song, H.; Ye, K.; Geng, P.; Han, X.; Liao, R.; Tung, C.-H.; Wang, W. Activation of Epoxides by a Cooperative Iron–Thiolate Catalyst: Intermediacy of Ferrous Alkoxides in Catalytic Hydroboration. *ACS Catal.* **2017**, *7* (11), 7709–7717.

226

APPENDIX A

UNPUBLISHED - AN APPROACH TO MANGANESE CATALYZED

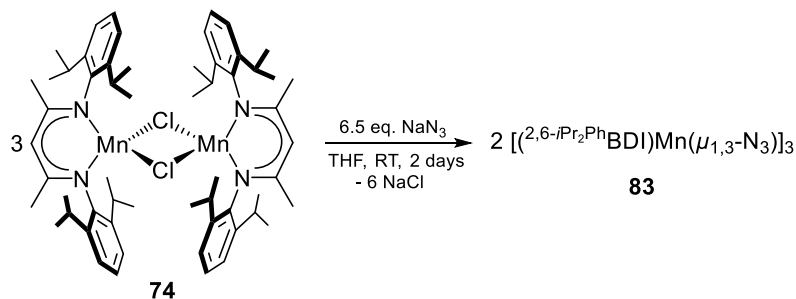AZIRIDINATION OF ORGANIC AZIDES AND ALKENES

A1. Introduction

Aziridines are known to possess biological activity and are important building blocks for organic synthesis.[1] The preparation of aziridines often involves the cyclization of 2-chloroalkylamine, epoxide amination or ylide addition to imines. A recent report from Guzei and Wickens demonstrated the synthesis of aziridines by dehydrogenative coupling of alkenes to amines via an electrogenerated dication, which can overcome the thermodynamic barrier ($\Delta G_0 > 30$ kcal mol^{-1}) of the strain-inducing oxidative reaction.[2] Another strategy to obtain aziridine is through nitrene transfer to C=C bonds, which involves the use of azides and (*N*-(*p*-tolylsulphonyl)imino)phenyl iodinane (PhI=NTs).[3] Several studies on metal-catalyzed aziridination have been reported. For example, the first demonstration involved using Cu powder to decompose benzenesulfonyl azide in hexene, where the aziridine was obtained along with C–H amination products through a radical mechanism.[4] Other porphyrin- and salen-based transition metal catalysts have been found to mediate the aziridination of olefins, including those based on Fe,[5] Mn,[6,7] Co[7] and Ru.[7] Although the use of Mn-catalysts for aziridination has been explored,[7] none of the examples demonstrated the use of organic azides as nitrene precursors for aziridination. Therefore, we hope to develop a more active Mn catalyst for aziridination using organic azides under mild conditions.

A2. Synthesis of [($^{2,6-iPr_2Ph}$BDI)Mn($\mu_{1,3}$-N$_3$)]$_3$ (83)

The idea and motivation for this project began from the preparation of **83** by a simple salt-metathesis of **74** with NaN$_3$ at room temperature to yield a yellow compound (Scheme A1). The ^{1}H NMR spectrum of this paramagnetic compound shows broad resonances over 70 ppm. The solid-state structure of this compound features an azido

228

bridging trimer with a pseudo-tetrahedral environment around each Mn center (Figure A1). The Mn–N bond distances of the trimer were found to range from 2.01 – 2.07 Å, which are a bit shorter than a normal Mn–N single bond.

$$3 \quad \text{74} \quad \xrightarrow[\substack{\text{THF, RT, 2 days} \\ \text{- 6 NaCl}}]{\text{6.5 eq. NaN}_3} \quad 2\ [(^{2,6\text{-}i\mathrm{Pr}_2\mathrm{Ph}}\mathrm{BDI})\mathrm{Mn}(\mu_{1,3}\text{-}N_3)]_3$$

83

Scheme A1. The synthesis of **83**.
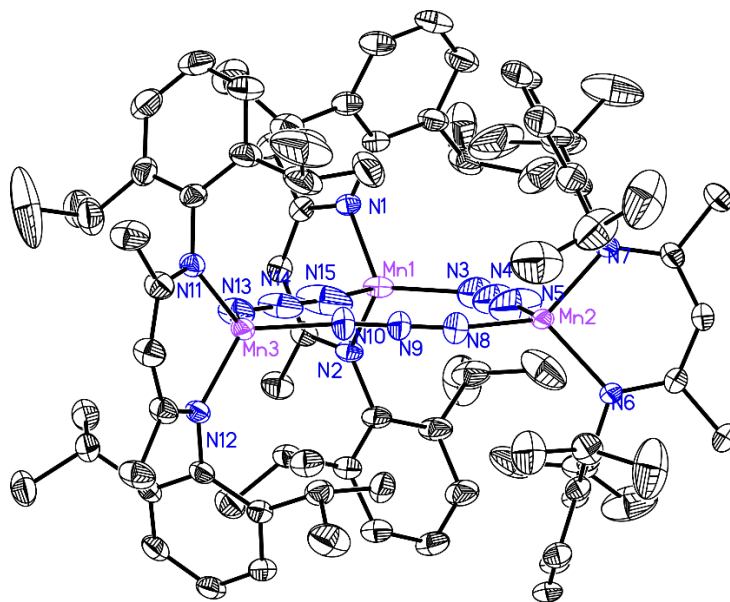
Figure A1. Solid-state structure of **83**.

Interestingly, reaction of **83** with KC$_8$ in the presence of 18-crown-6 did not result in a reduction of Mn but rather the cleavage of an ethylene moiety from the crown ether to afford a new Mn(II) species (**84**, Scheme A2-top). The solid-state structure of this compound was found to feature a Mn dimer with a Mn–O bond of 1.98 Å (Figure A2). This finding led us to question what the side products of this stoichiometric reaction might

be. Based on the observation of gas generation while conducting this reaction and isolation of an alkoxide compound, we hypothesize that the side product was aziridine and N_2 gas. The presence of aziridine salt was confirmed by GC-MS from the reaction liquor.

Scheme A2 demonstrates the proposed mechanism for this transformation, which began with reduction of the azido ligand by KC_8 to generate a Mn nitrene salt with an outer sphere potassium cation (**85**) and the elimination of N_2 gas, while the oxidation state of the Mn center remained +2. The next step is the the coordination, followed by the 1,2-addition of a C–O bond from the crown ether to Mn=N bond, which can result in the formation of cyclic compound **86**. Finally, intramolecular σ-metathesis of Mn–N and O–C bonds might release the aziridine salt and **84**.
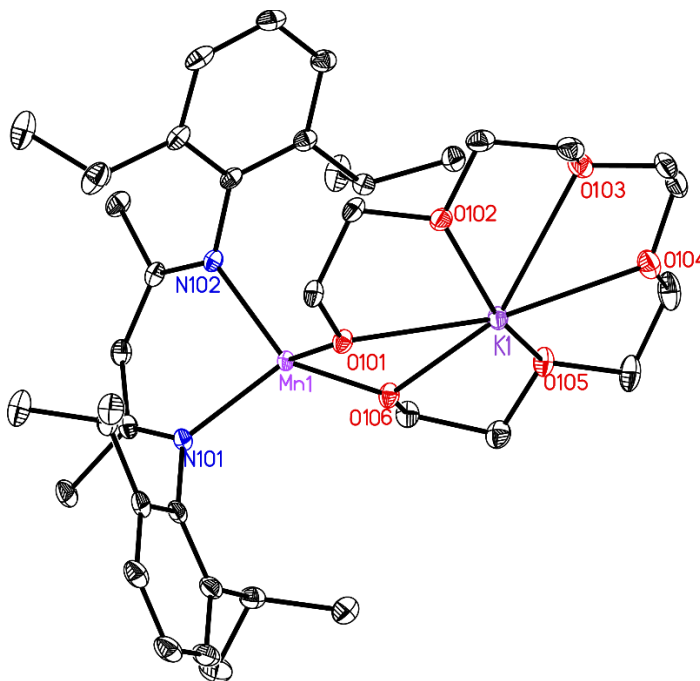
Figure A2. Solid-state structure of **84**.
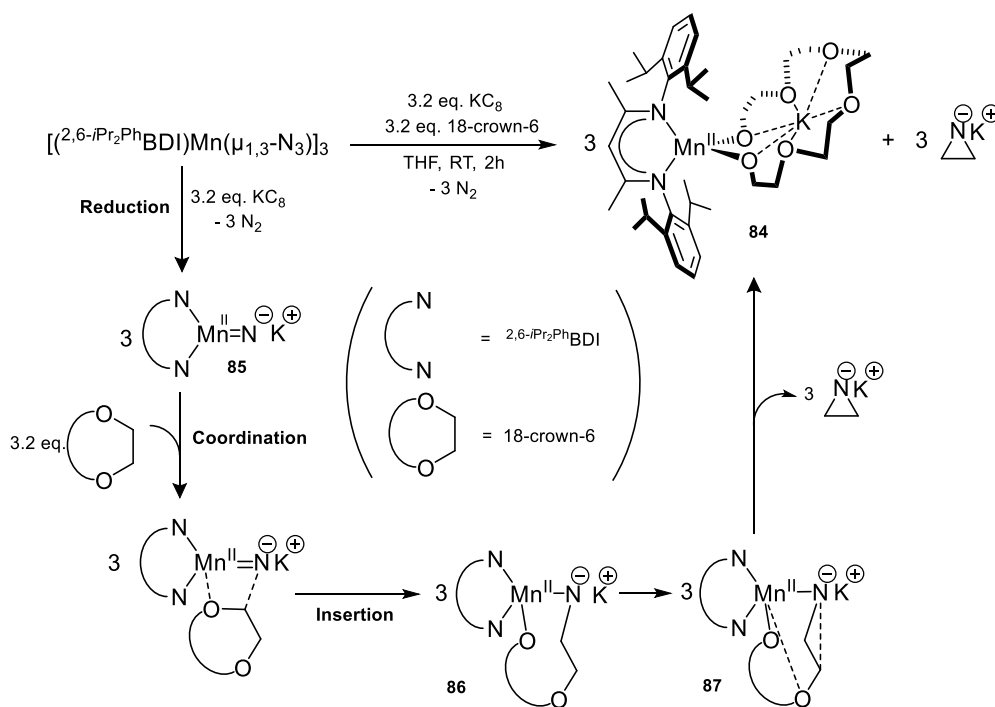
Scheme A2. The synthesis of **84** and a proposed mechanism for the formation of **84** and aziridination product.

A3. Synthesis of ($^{2,6\text{-}i\text{Pr}_2\text{Ph}}$BDI)Mn(THF)(Et₂O)

This data encouraged us to find a stategy to prepare aziridines catalytically using a Mn-catalyst from olefin and organic azides (Scheme A3, a). This might be possible if we have a Mn(I) catalyst in hand, which allows the oxidative addition of an azide to form the proposed Mn(III) species **88** (Scheme A3, b). In the presence of alkenes, coordination followed by [2+2] addition of the C=C bond to Mn=N can afford **89**. Next, the 4-membered ring might undergo reductive elimination to regenerate the catalyst along with the formation of the desired aziridine product.
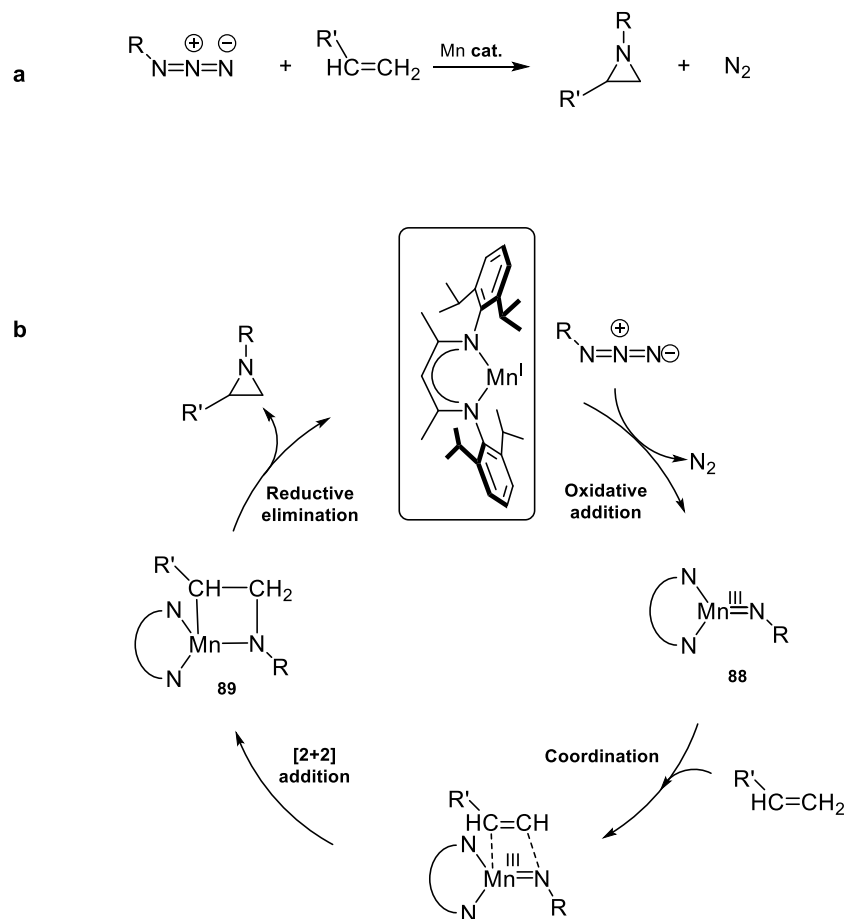
Scheme A3. a) Strategy for the Mn-catalyzed aziridination olefins. b) Proposed mechanism.
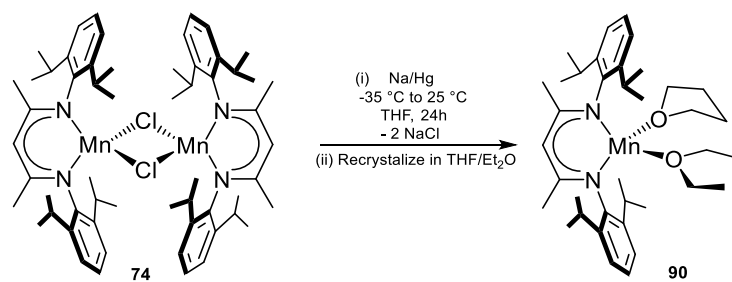
Scheme A4. The synthesis of **90**.
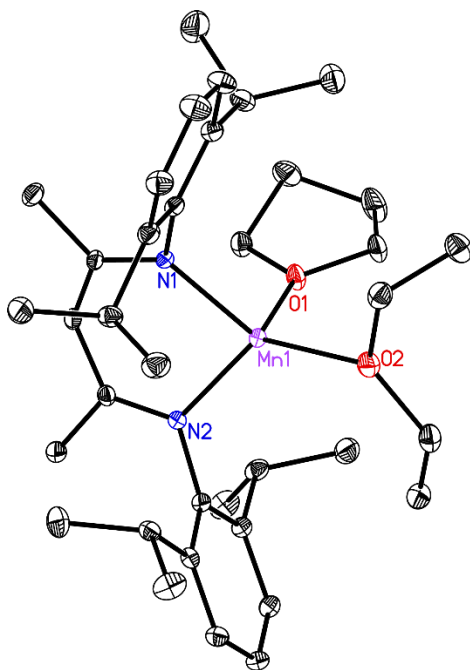
Figure A4. Solid-state structure of **90**.

This motivated us to synthesize a Mn(I) catalyst in order to evaluate the hypothesized catalysis. Reduction of $[(^{2,6-iPr_2Ph}BDI)Mn(\mu\text{-Cl})]_2$ with excess Na/Hg in THF, followed by recrystallization in THF/Et$_2$O yielded a greenish yellow compound which is identified as $(^{2,6-iPr_2Ph}BDI)Mn(THF)(Et_2O)$ (**90**, Scheme A4). The solid-state structure of this compound features a tetrahedral Mn(I) complex with a shortened Mn–N distance of 2.08 Å and elongated Mn–O bond of 2.2-2.49 Å (Figure A4). The electron deficient Mn(I) center is stabilized by THF and Et$_2$O L-type ligands.

A4. Experimental Procedures

Synthesis of $[(^{2,6-iPr_2Ph}BDI)Mn(\mu_{1,3}\text{-N}_3)]_3$ (83): Under inert atmosphere, a 20 mL scintillation vial was charged with 0.248 g of **74** (0.244 mmol) in 10 mL of THF. Next 0.035 g (0.54 mmol) of NaN$_3$ in 5 mL was added dropwise to the slurry while stirring. The reaction was kept at ambient temperature for 2 days. Then 3 mL of pentane was added to the mixture, and the solution was stored at -35 °C for 1 h. This step helps NaCl precipitate

out from the reaction solution, which improves the purity of the final product. The mixture was then filtered through Celite, the solvents were evacuated under vacuum to obtain 0.343 g (91% yield) of a yellow powder, which is further identified as **83**.

^{1}H NMR (benzene-d_6, 25 °C): 38.18, 19.12, 2.89, -19.01.
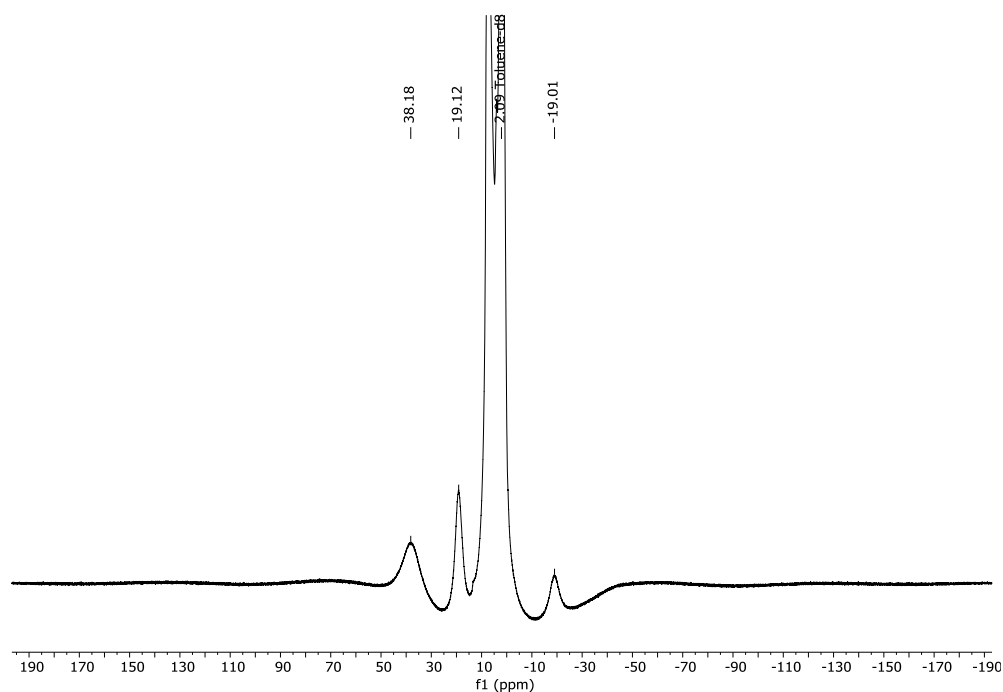
Figure A5. ^{1}H NMR spectrum of **83** in benzene-d_6 at 25 °C.

Synthesis of compound 84: Under inert atmosphere, a 20 mL scintillation vial was charged with 0.072 g of **83** (0.049 mmol) in 10 mL of THF. Next, a mixture containing 0.021 g (0.157 mmol) of KC$_8$ and 0.033 g (0.157 mmol) of 18-crown-6 in 5 mL was slowly added dropwise to the slurry while stirring. The reaction was kept at ambient temperature for 2 h. Then the mixture was then filtered through Celite, the solvents were evacuated under vacuum to obtain 0.022 g (62% yield) of a greenish yellow solid identified as **84**.

Synthesis of ($^{2,6-iPr_2Ph}$BDI)Mn(THF)(Et$_2$O) (90): In the glovebox, 2.52 g (12.6 mmol) of Hg was added to a vial, followed by 5 mL of THF. To the Hg mixture, 0.015 g (0.63 mmol)

of freshly cut Na was added. The solution turned grey and became cloudy. It was stirred for 45 min until the solution became clear. Then 0.064 g (0.063 mmol) of [($^{2,6-}$ ^{iPr_2Ph}BDI)Mn(μ-Cl)]$_2$ in 10 mL of THF was added to the Na/Hg amalgam while stirring. The reaction was kept at room temperature for 15 h. Next, the mixture was filtered through Celite, the solvent was evacuated under vacuum to yield 0.026 g (55% yield) of a yellow solid identified as **90**.

A5. Future development

The promising preliminary data shows potential to develop a strategy for the Mn-catalyzed aziridination of alkenes. I hope that the characterization and activity of **90** will be explored in the near future for this and related organic transformations. A large scope of organic azides and alkenes can be screened, and the aziridination can be examined with internal olefins.

A6. References

(1)   Sweeney, J. B. Aziridines: Epoxides' Ugly Cousins? *Chem. Soc. Rev.* **2002**, *31* (5), 247–258.

(2)   Holst, D. E.; Wang, D. J.; Kim, M. J.; Guzei, I. A.; Wickens, Z. K. Aziridine Synthesis by Coupling Amines and Alkenes via an Electrogenerated Dication. *Nature* **2021**, *596* (7870), 74–79.

(3)   Hennessy, J. Protection Not Included. *Nature Chem* **2014**, *6* (3), 168–168.

(4)   Kwart, Harold.; Kahn, A. A. Copper-Catalyzed Decomposition of Benzenesulfonyl Azide in Hydroxylic Media. *J. Am. Chem. Soc.* **1967**, *89* (8), 1950–1951.

(5)   Mahy, J.-P.; Bedi, G.; Battioni, P.; Mansuy, D. Aziridination of Alkenes Catalyzed by Porphyrinirons: Selection of Catalysts for Optimal Efficiency and Stereospecificity. *J. Chem. Soc., Perkin Trans. 2* **1988**, No. 8, 1517–1524.

(6)   Groves, J. T.; Takahashi, T. Activation and Transfer of Nitrogen from a Nitridomanganese(V) Porphyrin Complex. Aza Analog of Epoxidation. *J. Am. Chem. Soc.* **1983**, *105* (7), 2073–2074.

(7)   Müller, P.; Fruit, C. Enantioselective Catalytic Aziridinations and Asymmetric Nitrene Insertions into CH Bonds. *Chem. Rev.* **2003**, *103* (8), 2905–2920.

APPENDIX B

COPYRIGHT AND PERMISSIONS

Parts of Chapter 1 have been reproduced from: Nguyen, T. T.; Trovitch, R. J. Manganese-catalyzed Hydrosilylation and Hydroboration Reactions. In Manganese Catalysis in Organic Synthesis; Sortais, J. B., Ed; Wiley-VCH: Weinheim, Germany, **2021**; pp 101-135. *Reproduced with permission from the publisher and co-authors.*

Parts of Chapter 3 have been reproduced from Nguyen, T. T.; Mukhopadhyay, T. K.; MacMillan, S. N.; Janicke, M. T.; Trovitch, R. J., "Synthesis of aminosilane chemical vapor deposition precursors and polycarbosilazanes through manganese-catalyzed Si–N dehydrocoupling." *ACS Sustainable Chem. Eng.,* **2022***, 10*, 13, 4218 – 4226. Copyright 2022 American Chemical Society. *Reproduced with permission from co-authors.*

Parts of Chapter 5 have been taken from: Nguyen, T. T.; Kim, J. H.; Kim, S.; Oh, C.; Flores, M.; Groy, T. L.; Baik, M. H.; Trovitch, R. J., "Scope and mechanism of nitrile hydroboration mediated by a β-diketiminate manganese hydride catalyst." *Chem. Commun.*, **2020**, *56*, 3959, with permission from the Royal Society of Chemistry and co-authors.

BIOGRAPHICAL SKETCH

Thu Thao Nguyen was born June 27th, 1995, in Hanoi, Vietnam to Hien Van Nguyen and Lan Duy Thi Nguyen. She is the sibling to Huong and Phuong. She attended High School for Gifted Students of Science in Hanoi. She pursued a Bachelor of Science degree from Hanoi National University of Education and began working on synthesizing new platinum complexes containing derivatives of quinoline ligand under Dr. Hai Thi Hong Le. She graduated with an Honors B. Sc. in 2017. In 2018, she came to the U.S. to pursue a Ph.D at Arizona State University under Dr. Ryan J. Trovitch. She began studying the structure and reactivity of a manganese catalyst, publishing four papers on this work. She is a wife to Nguyen Dao and a mother to Celine Dao.